STRENGTHENING OF REINFORCED CONCRETE TWO-WAY SLABS

USAMA ALI ALI EBEAD

Strengthening of Reinforced Concrete Two–Way Slabs

by

©Usama Ali Ali Ebead, B.Sc., M.Sc.

A thesis submitted to the School of Graduate Studies in conformity with the requirements for the Degree of Doctor of Philosophy

Faculty of Engineering and Applied Science
Memorial University of Newfoundland
May 2002

St. John's Newfoundland Canada

Abstract

Strengthening of existing concrete structural elements is a viable means for improving the performance of such elements. Plenty of strengthening–related research work on beams and columns has been conducted. However, research work related to two–way slab strengthening is very scarce. Hence, there are academic and industrial needs to investigate such an issue experimentally and theoretically. This thesis is an attempt to fill the need for an experimental and theoretical research work on the punching shear and flexural strengthening of two–way slab system.

The experimental phase of this research work includes testing of three groups of specimens. The first and second groups are composed of specimens strengthened using steel plates and steel bolts. The specimens of the first group are loaded centrally only. The second group of specimens is loaded centrally combined with lateral static or cyclic moment. The specimens of the third group are loaded centrally and strengthened with either Carbon Fibre Reinforced Polymer (CFRP) strips or Glass Fibre Reinforced Polymer (GFRP) laminates.

The first group of specimens is used to develop and optimize a strengthening technique using the integration of steel plates and steel bolts. The effectiveness of four different configurations of steel plates and steel bolts are evaluated. The steel plates are assumed to act as horizontal flexural reinforcement representing an equivalent concrete drop panel. Moreover, the steel bolts are designed to act as vertical shear reinforcement, to transfer the horizontal forces between steel plates and concrete slab, and to confine the concrete between the steel plates. An average increase in the load capacity of 50% is achieved over that of the unstrengthened specimens.

The second group of specimens is intended to evaluate the performance of recommended steel strengthening technique for specimens subjected to static or cyclic moments. The ultimate load capacity is increased by an average of 122% for specimens subjected to static moment compared to the unstrengthened specimens. For the specimens subjected to cyclic moment, the lateral drift is increased by 76% compared to the unstrengthened specimens.

The third group includes specimens strengthened using CFRP strips and GFRP laminates for flexural-strengthening. In addition, This group includes specimens strengthened with CFRP strips and steel bolts for punching-shear strengthening. Utilizing CFRP strips and GFRP laminates contribute to an average increase of the flexural capacity of two-way slabs by an average of 36% compared to that of the unstrengthened specimens. However, a small average increase within 9% is achieved for the CFRP punching shear-strengthening.

The theoretical work is composed of two parts: mechanical model and Finite Element Analysis (FEA). In the first part, a mechanical model is developed to analyze centrally loaded two-way slabs strengthened using steel plates. A concrete model that considers the biaxial state of stress of concrete as well as the confinement effect of steel plates is introduced. An iterative incremental mechanical model is used to determine the load carrying capacity and to evaluate the deformation characteristics of strengthened slabs at each load increment until failure.

In the finite element analysis part, a full bond assumption is made between the concrete and both reinforcing steel bars and the strengthening FRP material. The comparison between the FEA and the experimental results showed an acceptable agreement. A tension-stiffening model is recommended for the concrete constitutive model taking into consideration the effect of strengthening material on the concrete behaviour in tension. In addition a regression equation based on the statistical approach of the Response Surface Methodology is recommended. The tension stiffening model is useful as an input in finite element packages and useful for classical approaches. In addition, The regression design equations can be used to provide simple design guide for engineers to predict the ultimate load carrying capacity of CFRP and GFRP strengthened two-way slabs.

Acknowledgements

Praise be to Allah Almighty and Peace be upon His Prophet Muhammad.

Many thanks to my mother for her prayer, love, and support. Without her, this work would never have come into existence. Thanks to my father with whom I wish I could share these moments. I am sure that his spirit is always with me. Also thanks to my brother Hesham for taking care of my mother and my sisters. I am also grateful to my sisters for their love and support.

Many thanks to my supervisor Dr. H. Marzouk for his support, guidance, and patience during the course of the program. I appreciate his commitment to help me doing this work in this shape. Also I would like to thank Dr. and Mrs. Marzouk for the great attention they devoted during my initial settlement in Canada.

I would like to thank Dr. L. Lye for his advice regarding the statistical work in the thesis. Many thanks to Dr. A. Hussein for his valuable comments for improving the final thesis. Also, I am very thankful to Dr. K. El-Rayas for his advice when preparing the initial proposal. I am indebted to Dr. A. Swamidas, Dr. M. Haddara, and Dr. J. Quaicoe for their support, help, and precious advice.

I had the pleasure of work with A. Bursey and C. Ward, Structures and Concrete laboratories technicians. Their assistance made research like this possible. I should also Thank Mr. M. Wrinch and Mr. C. Wight for their help.

Many thanks to Ms. D. Gill for her suggestions on the matters of wording of the thesis. I wish to thank Dr. S. Helmy, Dr. A. Awad, Mr. D. Toshack, Dr. Y. El-Sayed, Dr. A. Osman, Dr. A. Abdel-Razek, Mr. M. Andrews, Dr. A. Zubaydi, Dr. S. Awadallah, Mr. A. El-Aneed, Dr. M. Stavely, Mr. G. Cook, Mr. T. Dyer, and Mr. F. Poland for their friendship.

I appreciate and thank the School of Graduate Studies at Memorial University of Newfoundland for the financial support of this doctoral study.

St. John's, Newfoundland
May 30, 2002

Usama Ebead

Contents

List of Figures

List of Tables

Notation and List of Abbreviations

The following notations were used in the thesis.

a	:	support to support distance
a_1	:	a factor
a_2	:	a factor
A	:	constant
A_c	:	shear area at the critical section of the slab
A_s	:	Steel reinforcement cross sectional area
b	:	side dimension of the square loaded area
b_0	:	a factor used defines the ratio between the biaxial and uniaxial tensile strengths
b_1	:	width of the critical section for shear measured in the direction of the span for which moments are determined
b_2	:	width of the critical section for shear measured in the direction perpendicular to b_1
b_{cr}	:	critical perimeter for shear in slabs and footings
c	:	side length of the square column
c_0	:	a constant that determines the ratio between the plastic strain in a monotonically loaded biaxial compression test and the plastic strain in a monotonically loaded uniaxial test
c_1	:	constant
c_2	:	constant
c_3	:	a factor or constant
d	:	depth
d'	:	distance from the compression fiber to the centeroid compression reinforcement of the slab
dh	:	thickness of the subdivision of the concrete section
$d\varepsilon_c$	:	total compressive strain rate
$d\varepsilon_c^{el}$	:	elastic compressive strain rate
$d\varepsilon_c^{pl}$	:	plastic compressive strain rate
$d\varepsilon_{ij}^{pl}$	:	plastic–strain increment vector
$d\varepsilon_t$	:	total tensile strain rate for the crack detection problem
$d\varepsilon_t^{el}$	:	tensile elastic strain rate

$d\varepsilon_t^{pl}$	:	tensile plastic strain rate associated with the crack detection surface
e	:	distance from centroid of section for critical shear to point where shear stress is being calculated
E_c	:	Initial modulus of elasticity of concrete
E_s	:	initial modulus of elasticity of steel
f	:	concrete compressive stress or the yield function
$f_{bc}^{'}$	:	the equal biaxial compressive strength
$\overline{f}_{bc}^{'}$	:	a factor
$f_c^{'}$	:	characteristic strength of concrete, uniaxial compressive strength of concrete, or uniaxial compressive cylinder strength
$f_{ci,j}$	:	concrete stress at iteration$i$ on the location$j$ of the section
f_{cm}	:	mean concrete strength
f_{cu}	:	cube strength of concrete
f_l	:	confining pressure
f_{res}	:	concrete residual compressive stress
$f_t^{'}$	:	tensile stress of concrete
f_y	:	yield stress of the slab reinforcement
f_{yp}	:	yield stress of the steel plate
$F_{ci,j}$	:	concrete force at iteration$i$ on the location$j$ of the section
$F_{si,c}$	:	force of the compression reinforcement at iteration,i
$F_{spi,c}$	:	force of the steel plate located at the compression side of the slab at iteration,i
$F_{si,t}$	:	force of the tensile reinforcement at iteration,i
$F_{spi,t}$	:	force of the steel plate located at the tension side of the slab at iteration,i
g	:	the plastic-potential function
G_0	:	the shear modulus of the un-cracked concrete
G_f	:	fracture energy
h	:	thickness of the slab
h''	:	width of the concrete core
H	:	static or cyclic or Lateral load
i	:	iteration number
j	:	location level on the concrete cross section
J	:	property of the critical shear section analogous to the polar moment of inertia
J_{cs}	:	polar moment of inertia of the slab critical section about its centroid
K	:	confinement coeffecient
K_a	:	0.13 for normal concrete and .105 for lightweight concrete
K_{sc}	:	$1.15/[4\pi$ (column area)/(column perimeter)$^2]^1/_2$
l_p	:	side length of the steel plate
l_r	:	normalized slab length or the length ratio

L	:	side distance between supports of the square slab or the slab length
M	:	number of divisions of the upper fiber concrete strain range
M_0	:	nominal slam moment capacity when at zero shear
M_i	:	moment at interior support resisted by elements above and below the slab
M_{ri}	:	internal moment at iteration,i
M_u	:	un-balanced moment transferred between slab and column
n	:	modular ratio between steel and concrete
N	:	number of divisions of the concrete section
N_B	:	number of steel bolts
p	:	effective pressure stress
P_{cal}	:	calculated Load carrying capacity
P_{exp}	:	experimental load carrying capacity
P_{fi}	:	flexural load, at iteration,i
P_{fi_1}	:	flexural load, at iteration,i when the maximum tensile strain in tension reinforcement reach 0.01
P_{fi_2}	:	flexural load, at iteration,i when the maximum compression strain in concrete extreme fiber reach 0.035
P_{max}	:	maximum load
q	:	Mises equivalent deviatoric stress
Q	:	number of divisions of the lower concrete strain range
R^2	:	correlation coefficient
s	:	spacing between stirrups or vertical shear reinforcement
S_1	:	a principal stress deviation
S_2	:	a principal stress deviation
S_3	:	a principal stress deviation
S_{ij}	:	deviatoric stress components
t_p	:	thickness of the steel plate, mm
t_r	:	normalized slab thickness, or the thickness ratio
u	:	perimeter of the loaded area
u_t	:	crack opening displacement
$v_{1,2}$	:	shear stresses on faces of the critical section
v_c	:	nominal shear strength of concrete or concrete shear strength
v_u	:	ultimate shear stress or shear strength
V	:	shear force
V_c	:	nominal punching shear capacity at zero moment
V_{cal}	:	calculated ultimate load carrying capacity
$V_{cal,corr}$	:	corrected ultimate load carrying capacity for the number of bolts
V_f	:	load carrying capacity at flexural failure
V_r	:	load carrying capacity of the slab, the least betweenV_f andV_s
V_s	:	load carrying capacity at shear failure

V_u	:	ultimate shear force
w_r	:	strengthening material fraction area, or the width ratio
W_f	:	the strengthening energy
x_1	:	a principal axis of the critical section
y_1	:	a principal axis of the critical section perpendicular to x_1
y_j	:	the distance from the an arbitrary location to centriod of the compression concrete fiber.
$y_{s,c}$	:	the distance from the centriod of the compression reinforcement to the compression concrete fiber.
$y_{s,t}$	:	distance from extreme compression fiber to the center of tension reinforcement
$y_{tp,t}$	:	distance from extreme compression fiber to the center of tension steel plate
$y_{sp,c}$	:	distance from centriod of the compression steel reinforcement to the center of tension steel plate
Z_m	:	descending line slope in concrete stress strain relationship
α	:	constant
α_s	:	factor adjusts v_c for support dimensions and equals 4 for interior columns and 3 for edge columns
β	:	factor or constant
β_c	:	ratio of the long side to the short side of the column, concentrated load, or reaction area
δ_{fi_1}	:	deflection associated to P_{fi_1}
δ_{fi_2}	:	deflection associated to P_{fi_2}
δ_s	:	deflection associated to V_s
δ_u	:	drift at the ultimate unbalanced cyclic moment
δ_y	:	drift at the yield unbalanced cyclic moment
λ_c	:	compressive hardening parameter
ϕ	:	diameter of a steel bolt or linear degradation function of shear modulus
Φ_0	:	ratio of the ultimate shear capacity and the ultimate flexural capacity of the slab
ρ	:	tension reinforcement ratio of the slab
ρ'	:	compression reinforcement ratio of the slab
ρ_{sh}	:	volumetric ratio of the hooks to the concrete core
ρ_x	:	reinforcement ratio in the X direction
ρ_y	:	reinforcement ratio in the Y direction
σ_1	:	a principal normal stress
σ_{11}	:	a principal stress
σ_{12}	:	a principal stress

σ_2	:	a principal normal stress
σ_{22}	:	a principal stress
σ_3	:	a principal normal stress
σ_{bc}	:	stress magnitude in case of biaxial stress state
σ_c	:	stress magnitude in case of uniaxial stress state
σ_I	:	first in-plane concrete compressive stress
σ_{II}	:	second in-plane concrete compressive stress
σ_{ij}	:	normal stresses components
σ_t	:	uniaxial concrete tensile stress
σ_t^u	:	uniaxial concrete tensile strength (cracking strength
τ_c	:	yield stress in a state of pure shear stress when all the components of σ_{ij} vanish except $\sigma_{12} = \sigma_{21} = \tau_c$ or it is the size of the yield surface on the q axis at zero value of p in Figure 8.1
ε	:	strain
ε_{11}	:	a principal strain
ε_{12}	:	a principal strain
ε_{22}	:	a principal strain
ε_{bolt}	:	axial strain of a steel bolt after tightening up
$\varepsilon_{bot,i}$	:	strain at the tension fiber of concrete section at iteration,i
ε_c	:	concrete compressive strain at an arbitrary location of the section
ε_{ci}	:	concrete compressive strain at an arbitrary location of the section at iteration i
ε_p	:	tensile strain at maximum concrete tensile stress
$\varepsilon_{si,c}$	:	strain at the centriod of the compression reinforcement at iteration,i
$\varepsilon_{si,t}$	:	strain at the centriod of the tensile reinforcement at iteration,i
$\varepsilon_{spi,c}$	:	strain at the middle of the steel plate's thickness at the compression side at iteration,i
$\varepsilon_{spi,t}$	:	strain at the middle of the steel plate's thickness at the tension side at iteration,i
ε_{sr}	:	total average shear effective strain at which concrete shear stiffness vanishes
$\bar{\varepsilon}_{sr}$	:	total ultimate shear effective strain at which concrete shear stiffness vanishes
ε_t	:	tensile strain of concrete
$\varepsilon_{t,max}$	:	concrete tensile strain at zero tensile stress
$\varepsilon_{top,i}$	:	strain at the compression fiber of concrete section at iteration,i
$\bar{\varepsilon}_t$	:	average crack opening strain across the crack
ε_{t0}	:	concrete tensile strain at $\sigma_t = \sigma_t^u$
ξ	:	size-effect coefficient

ACI	:	American Concrete Institute
AFRP	:	Aramid Fiber Reinforced Plastic
ASTM	:	American Society for Testing and Materials
CEB	:	Comité Euro–Internationale de Beton
BS	:	British Standards
CFRP	:	Carbon Fiber Reinforced Plastic
CSA	:	Canadian Standards Association
FEA	:	Finite Element Analysis
FIP	:	Federation Internationale de la Procontrainte
FOS	:	Fiber Optic Sensor
FRP	:	Fiber Reinforced Plastic
GFRP	:	Glass Fiber Reinforced Plastic
LVDT	:	Linear Variable Displacement Transformer
MPC	:	Multi Point Constraint
NSM	:	Near Surface Mounted
RSM	:	Response Surface Methodology

Chapter 1

Introduction

1.1 General

The two–way slab is an economical and popular structural system that consists of a plate of a uniform thickness cast monolithically with columns. Slabs have been used in different structural applications, such as floors and roofs of buildings; walls of tanks and offshore structures; and bridges. One of the major drawbacks of the two–way slab system is the susceptibility to "punching" failure. Punching failure is a type of failure in which a column together with a portion of the slab punches through the slab. The sudden nature of this type of failure is a major shortcoming of two–way slab structures.

The two–way slab as a structural system is an optimum solution for building constructions in countries located in low or moderate seismic zones. Moreover, this structural system can be used efficiently in high seismic zones, if an appropriate lateral bracing system is provided to resist lateral loads induced from earthquakes.

Strengthening of existing concrete structural elements is a viable means of improving the load carrying capacity and the serviceability performance of such elements. Strengthening is vital when altering the usage of the structure, overloading,

or meeting necessary structural code changes or upgrades. Plenty of research works have been carried out to investigate the structural behaviour of two–way slabs. On the other hand, there is an academic/industrial need for research on two–way slabs strengthening.

Extensive applications of the Fibre reinforced polymer (FRP) composites as structural materials have been accomplished recently. It is deemed one of the most promising technological advances in materials science and structural engineering. FRP composites are lightweight, high strength, non-corrosive and non-magnetic materials. The excellent properties of FRP composite materials are due to the superior properties of very small diameter fibres embedded in a ductile polymeric matrix. These fibres enable a good transfer of internal forces from one fibre to another. The most common types of FRPs are the Carbon Fibre Reinforced Polymer (CFRP) and the Glass Fibre Reinforced Polymer (GFRP). Typical CFRPs used in the construction industry have tensile strengths exceed six times those of steel. The stiffness of CFRPs is within the range of that of steel. GFRPs have lower strengths and considerable lower stiffness than CFRPs. However, GFRP materials attract attentions due to the reduced cost compared to CFRP materials.

Due to the advantages of FRP composites, there is a wide range of current and potential applications of these composites for new and existing structures. The most common application of FRP materials is strengthening and rehabilitating reinforced concrete beams, columns, and deck bridges. The ease of handling FRP laminates and sheets provides the means to extend their applications to other structural elements. Applications of FRP materials for two–way slabs strengthening are scarce. Investigating the effectiveness of FRP materials in two–way slabs strengthening is an

interesting subject to engineers and researchers.

1.2 Scope

There is a lack of research on strengthening or rehabilitation of two–way slabs. Most of the published research related to slab strengthening addressed one way slabs. This initiate the need for this research work to investigate experimentally and theoretically the issue of two–way slabs strengthening. The current research is aimed at enriching the literature with a comprehensive study on strengthening two–way slabs.

The scope of this work includes investigating experimentally the effectiveness of using steel, as a traditional material, and FRPs, as modern or advanced materials for two–way slabs strengthening. It is intended to develop different strengthening techniques to suit each type of these materials and the purpose of strengthening whether for punching–shear or flexure. In addition, it is intended to investigate experimentally the effectiveness of the developed strengthening techniques for enhancing the behaviour of two–way slabs subjected to different load combinations and reinforced with different reinforcement ratios.

The scope of this work is extended to include theoretical investigation of two–way slab strengthening. The theoretical investigation includes developing a mechanical model for steel strengthened two–way slabs. Such a model is needed for researchers and engineers to design steel strengthened two slabs. In addition, a finite element analysis, as a powerful tool, is to be carried out to investigate the behaviour of FRP–strengthened slabs. Results of the extensive finite element analysis will be used to develop a tension stiffening model for FRP strengthened concrete using the statistical approach of the Response Surface Methodology (RSM). In addition, the finite element

analysis results will be used to develop a simple design equation for FRP strengthened slabs using the RSM. Such a design equation is of a great value to practicing engineers and researchers.

1.3 Research Objectives

The current study includes experimental and theoretical investigations on strengthening reinforced concrete two–way slabs. The experimental phase of the study includes evaluation of a traditional strengthening technique, using steel plates, and a modern strengthening technique, using CFRP strips and GFRP laminates. The theoretical phase of the investigation includes numerical modelling of the strengthened two–way slabs using either closed form iterative technique or finite element analysis.

The experimental phase is a comprehensive study on strengthening two–way slabs subjected to different types of loading. The slabs are reinforced with different reinforcement ratios and strengthened using different strengthening techniques and materials. The objectives of the experimental investigation are summarized as follows:

1. Developing and evaluating a new strengthening technique by testing different configurations of steel plates and steel bolts for strengthening two–way slabs subjected to central monotonic loads.

2. Optimizing the strengthening technique with regard to the minimum number of steel bolts so that the technique contributes to a reasonable improvement of the load carrying capacity and the deformational characteristics of the strengthened two–way slabs.

3. Generalizing the optimized technique by investigating its viability in strengthening two–way slabs originally reinforced with different reinforcement ratios and subjected to central monotonic loads combined with either static or cyclic moments.

4. Investigating the applicability and the effectiveness of using CFRP strips and GFRP laminates for flexural–strengthening of two–way slabs.

5. Investigating the effectiveness of using CFRP strips for punching shear–strengthening of two–way slabs.

The theoretical investigation includes developing a mechanical model that is intended to analyze two–way slabs strengthened with steel plates. In addition, the theoretical work includes a finite element analysis of two–way slabs strengthened with CFRP strips or GFRP laminates. The objectives of theoretical investigation are summarized as follows:

1. Developing an iterative incremental mechanical model to analyze centrally loaded two–way slabs strengthened with steel plates and steel bolts. The model takes into consideration the confinement effect and the bi-axial state of stress on the overall behaviour of two–way slabs strengthened with steel plates.

2. Finite element analysis of the behaviour of two–way slabs strengthened in flexural with CFRP strips and GFRP strips.

3. Developing a tension stiffening model for FRP–strengthened concrete.

4. Developing a simplified model that evaluates the ultimate load carrying capacity of FRP–strengthened two–way slabs using a reliable statistical method, the

Response Surface Methodology (RSM). The RSM will be used to develop a simplified expression that can help the researchers as well as practicing engineers as a guide for the design of two–way slabs strengthened with FRP materials.

1.4 Thesis Outline

Chapter 2 is divided into four parts intended to survey relevant research work. The first part surveys research work related to the design and code requirements of shear in two–way slabs. The second part surveys experimental research work on the enhancement of shear behaviour of slabs using different types of concrete or shear reinforcement. The third part reviews research work on FRP materials highlighting the properties and applications of these materials as construction materials. The fourth part surveys research work on strengthening different reinforced concrete elements using either FRP or steel.

In Chapter 3, details of the test set up, the loading frame, and specimens preparation are given. In addition, the different strengthening techniques are described in terms of the methodology and the sequence of installing the strengthening components of each technique. Finally, a description of the instrumentation and the data acquisition system is provided.

Chapter 4 introduces the results of the steel strengthening technique of centrally loaded two–way slabs. The effectiveness of two configurations of steel plates and four different arrangements of steel bolts are evaluated. The load carrying capacity as well as the deformational characteristics of the tested specimens are discussed. In addition, Chapter 4 includes a simple approach that is based on yield line theory to estimate the load carrying capacity of the strengthened specimens.

In Chapter 5, the most effective configuration of steel plates and steel bolts introduced in Chapter 4 is investigated further for specimens of the same dimensions but of different reinforcement ratios and subjected to different load combinations. The tested specimens are subjected to a combination of central load and either static or cyclic moment. A detailed analysis of the test results of these specimens in terms of the load carrying capacity and deformational characteristics is presented.

Chapter 6 presents test results of strengthened two–way slabs with CFRP strips and GFRP laminates. It represents the results of two different strengthening schemes: flexural strengthening and punching–shear strengthening. A detailed analysis of the test results of these specimens in terms of the load carrying capacity and deformational characteristics is presented.

Chapter 7 introduces a mechanical model developed to analyze centrally loaded two–way slabs strengthened with steel plates and bolts. The model can be used for unstrengthened two–way slabs. Predicted results are included for strengthened and unstrengthened cases and are compared to available experimental data.

Chapter 8 presents a finite element study on the FRP–strengthened two–way slabs. A comparison between the finite element analysis and available test results is presented. In addition, Chapter 8 includes a numerical analysis based on the statistical approach of the RSM. Developed tension stiffening model and regression design equations for FRP strengthened two–way slabs are presented.

The last chapter, Chapter 9, summarizes and concludes the findings of the experimental work presented in Chapters 4,5, and 6, and of the theoretical work presented in Chapters 7 and 8. Chapter 9 includes also recommendations for future work.

Chapter 2

Literature Survey

2.1 General

Reinforced concrete two–way slab system is a popular structural system. This system has contributed to the development of reinforced concrete as a construction material since the construction of the first two–way slab in 1906 in the USA by Turner, as reported (Sozen and Seiss, 1963). In the same year, 1906, Maillart of Europe built a two–way slab system in Switzerland. A considerable amount of research has been conducted to investigate the behaviour of reinforced concrete two–way slabs since that time.

Failure of two–way slabs may occur in a form of flexural failure, punching–shear failure, or a combination of both flexure and punching–shear failure modes. Punching–shear failure is of more concern to design engineers than flexural failure. It is sudden and has a catastrophic nature unlike flexural failure.

In this chapter, it is intended to survey research work related to the design of shear in slabs including several codes' revisions and theoretical approaches of evaluating shear strength of two–way slabs. In addition, the survey includes experimental

research work on using different concrete types and using different shear reinforcement types in slabs. Furthermore, this chapter introduces FRP materials through research works that highlights some of the properties and the construction applications of these materials. Concluding this chapter is a survey of some of the research work completed on strengthening of different reinforced concrete structural elements.

2.2 Shear Strength of Two–Way Slabs

One of the early outstanding investigations on the two–way slab system was conducted by Kinnunen and Nylander in 1960. Tests were conducted on circular concrete slabs without shear reinforcement. The specimens were subjected to a uniformly distributed load along the circumference of the slabs. The study contained measurements of deflections, strains, and loads at the appearance of the first shear crack and ultimate shear loads. The mechanical model presented by Kinnunen and Nylander's has been the basis of many subsequent rationale models of analyzing two–way slabs (Kinnunen and Nylander, 1960).

In another early investigation on slabs, Elstner and Hognested tested thirty-nine square specimens that were loaded up to failure through a centrally located column stub (Elstner and Hognested, 1956). The test results indicated that eccentric loading had a negligible effect on shear strength compared to that of concentric loading. In addition, it was concluded that compression reinforcement had no contribution on increasing the ultimate shear strength of slabs. A total of 198 laboratory specimens were constructed in a very extensive research on two–way slabs (Moe, 1961). It is worth mentioning that the shear design methods of slabs of the American Concrete Institute Code, ACI–1963 were based on Moe's work. Moe suggested the following

equation to evaluate the shear capacity of slabs loaded with square area without shear reinforcement:

$$v_u = \left[15\left(1 - .075\frac{b}{d}\right) - 5.25\Phi_0\right]\sqrt{f_c'} \tag{2.2.1}$$

where:

v_u = the ultimate shear stress, MPa,

b = the side dimension of the square loaded area, mm,

d = the effective depth of the slab, mm,

f_c' = the compressive strength of the concrete, MPa, and

Φ_0 = the ratio of the ultimate shear capacity and the ultimate flexural capacity of the slab.

A large research investigation was conducted to study the behaviour of two–way slabs of statically indeterminate arrangements (Regan, 1981). It was noticed that shear forces could continue to increase after the formation of local yield lines. These yield lines had limited the moments transferred to the column. The design equations of shear in two–way slabs in the British code (BS 8110, 1985) was based primarily on Regan's investigation.

Some other theoretical studies on concrete slabs were focused on the design of pre-stressed and reinforced concrete two–way slab structures (Brotchie, 1978). In Brotchie's study, the interaction of shear and moment is treated as an independent variable.

2.3 Shear Design Equations of Two–Way Slabs

The shear design equations of the Canadian Standards Association Code (CSA–A23.3, 1994) and that of ACI building code (ACI–318, 1999) are based on Moe's work (Moe,

1961). The design methods in these two codes are based on an assumption that the ultimate shear strength is proportional to the square root of the compressive strength of concrete. The shear strength of slabs without shear reinforcement in the CSA A23.3-94, v_c in the S.I. units is the smallest of:

$$v_c = \left(1 + \frac{2}{\beta_c}\right) 0.2\sqrt{f'_c} \tag{2.3.1}$$

$$v_c = \left(\frac{\alpha_s d}{b_{cr}} + 0.2\right) \sqrt{f'_c} \tag{2.3.2}$$

$$v_c = 0.4\sqrt{f'_c} \tag{2.3.3}$$

where:

v_c = concrete shear strength, MPa,

α_s = factor is used to adjust v_c for support dimensions and equals 4 for interior columns and 3 for edge columns,

β_c = the ratio of the long side to the short side of the column, concentrated load, or reaction area,

d = the slab depth, mm

b_{cr} = critical perimeter for shear in slabs and footings, mm, and

f'_c = specified compressive strength of concrete, MPa.

The shear strength of slabs without shear reinforcement in the ACI Code (ACI-318, 1999) in the imperial units, v_c, is the smallest of:

$$v_c = \left(2 + \frac{4}{\beta_c}\right) \sqrt{f'_c} \tag{2.3.4}$$

$$v_c = \left(\frac{\alpha_s d}{b_{cr}} + 2\right) \sqrt{f'_c} \tag{2.3.5}$$

$$v_c = 4\sqrt{f'_c} \tag{2.3.6}$$

where:

v_c = concrete shear strength, psi,

α_s = 40 for interior columns, 30 for edge columns, and 20 for corner columns,

d = the effective depth of the slab, inch,

b_{cr} = perimeter of critical section for shear in slabs and footings, inch, and

f_c' = specified compressive strength of concrete, psi.

The shear design equation of the British code (BS 8110, 1985) is based on Regan's results (Regan, 1981) and differs from the North American codes. The discrepancy of the British code approach is in the proportionality of the concrete shear strength to the cubic root of concrete compressive strength rather than the square root. The shear design equation of the British code (S.I. units) is: (BS 8110, 1985)

$$v_c = 0.79\ (100\ \rho)^{1/3}(f_c'/25)^{1/3}\ (400/d)^{1/4} \tag{2.3.7}$$

The notations are the same as those in the CSA equations.

Another difference between the British code and the North American codes for slab shear design is the location of shear critical section of slabs. The CSA building code and the ACI code assume that two–way shear is critical at a vertical section through slabs and never less than $d/2$ from the column face (CSA–A23.3, 1994; ACI–318, 1999). On the other hand, critical shear perimeter is assumed located at 1.5 d around column faces in the British code (BS 8110, 1985).

Also in the European code (CEB–FIP, 1990), the punching shear resistance, v_c is proportional to $\left(f_c'\right)^{\frac{1}{3}}$. However, the critical section is considered at $2d$ from the column edge. The highest concrete grade considered in the European code corresponds to concrete compressive strength of to 80 MPa. The effect of steel reinforcement and the slab size effect are considered in the European code where the shear equation is

expressed as (CEB–FIP, 1990):

$$v_c = 0.12\ \xi \left(100\rho\, f_c^{'}\right)^{\frac{1}{3}} b_{cr}\, d \tag{2.3.8}$$

and

$$\rho = \sqrt{\rho_x\, \rho_y} \tag{2.3.9}$$

where:

$\xi = 1 + \sqrt{\frac{200}{d}}$ is a size-effect coefficient

b_{cr} is the length of the control perimeter at 2d from the column

ρ_x and ρ_y are the reinforcement ratios in the X and Y, respectively.

It was found that the shear design equation of the British code can be used accurately for high strength concrete. It was concluded from the results of an experimental work conducted on both high strength and normal strength concrete slabs that concrete shear strength is proportional to the cubic root of the concrete compressive strength (Marzouk and Hussein, 1991a; Marzouk and Hussein, 1991b). These findings were supported and confirmed by another research work (Gardner and Shao, 1996) for high strength concrete.

2.4 Slabs Subjected to Central Loads and Moments

The two–way slab system is an efficient system for multistory buildings located at low and moderate seismic zones and for those subjected to moderate wind loads. Many researchers carried out experimental investigations to estimate the capability of a two–way slab system to resist a simulated earthquake drift routine or unbalanced moment caused by wind or unsymmetrical structural and/or loading distribution (Pan and Moehle, 1989; Ghali et al., 1976; Islam and Park, 1976).

Building codes set clear statements of the limitations of the shear stress level carried by slab-to-column connections (CSA–A23.3, 1994; ACI–318, 1999). Revisions of the code limitations were presented to overview cases of utilizing vertical shear reinforcement and cases of corner and edge columns (Elgabry and Ghali, 1996b; Elgabry and Ghali, 1996a).

Canadian Standards Association stated, "Shear forces and unbalanced moments to be transferred to the support shall be resolved into a single shear force" (CSA–A23.3, 1994). This single shear force is acting at the centroid of a critical section. The fraction of the unbalanced moment transferred by eccentricity of the load, γ_v, is calculated using the following equation:

$$\gamma_v = 1 - \frac{1}{1 + \frac{2}{3}\sqrt{\frac{b_1}{b_2}}} \tag{2.4.1}$$

where:

b_1 = width of the critical section for shear measured in the direction of the span for which moments are determined and

b_2 = width of the critical section for shear measured in the direction perpendicular to b_1.

The resulting shear stress due to applied load combination is calculated from the following equation:

$$v = \frac{V}{b_{cr}d} + \left[\frac{\gamma_v M_i\, e}{J}\right]_{x_1} + \left[\frac{\gamma_v M_i\, e}{J}\right]_{y_1} \tag{2.4.2}$$

where:

V = the shear force, N,

b_{cr} = perimeter of the critical section for shear in slabs and footings, mm,

d = the effective depth of the slab, mm,

M_i = moment at interior support resisted by elements above and below the slab, N.mm,

e = distance from centroid of section for critical shear to point where shear stress is being calculated, mm,

J = property of the critical shear section analogous to the polar moment of inertia, mm^4, and

x_1, y_1 = the two perpendicular principal axes of the critical section.

Equations 2.4.1 and 2.4.2 are based on earlier research work (Di Stasio and Van Buren, 1960). These equations are adopted by both Canadian and American codes (CSA–A23.3, 1994; ACI–318, 1999).

Shear stresses are increased near the column at the location of the slab-column connection due to the lateral loading caused by an earthquake, wind, or eccentric loading. The excessive shear stresses causes punching–shear failure that is brittle in nature and is not desirable. The displacement ductility of a two–way slab is defined as the ratio between the displacement at the ultimate load and that at the yield load. The displacement ductility is a good indicator on the slab performance and the type of failure. The shear stress acting on the slab critical section should not exceed $0.15\ \sqrt{f_c'}$ MPa, to ensure adequate displacement ductility under severe earthquake loading (Pan and Moehle, 1989). Hence, enhancing the shear strength of a two–way slab is a key issue to achieve a better resistance to lateral and seismic loading. An increase of the shear strength of about 20% was achieved when high strength concrete in two–way slabs was used (Emam et al., 1997). Higher moments to central load ratio may significantly reduce the stiffness and the strength of two–way slabs, especially with openings (El-Salakawy et al., 1998)

A comprehensive test program was carried out to investigate the behaviour of two–way slabs subjected to both direct shear and moment (Hawkins and Corley, 1989). That program investigated the effect of slab thickness, concrete compressive strength, stirrups shear reinforcement, column rectangularity, slab reinforcement, and the ratio of moment to shear on the behaviour of the slab. The high moment loading was referred to a case of loading, when the ratio between the applied moment and the shear force at any loading increment was equal to 584 mm. On the other hand, low moment loading was referred to when the same ratio was 130 mm.

The column moment transfer was investigated recently using finite element analysis (Megally and Ghali, 2000). In this finite element analysis of punching of concrete slabs due to column moment transfer, it was concluded that ACI code equation calculates γ_v adequately.

2.5 High Strength Concrete Two–Way Slabs

A continuous series of research projects on slabs was conducted using high strength concrete at Memorial University of Newfoundland, starting from 1988. Seventeen reinforced concrete slabs were tested to investigate the behaviour of slabs in terms of deformations and punching–shear capacities (Marzouk and Hussein, 1991a). The tested slabs had different depths and reinforcement ratios that varied between 0.50% and 2.50%. The test results revealed that high strength concrete slabs exhibited more brittle failure than normal strength concrete slabs. Two more important findings were achieved. First, there is a direct proportionality of the level of the steel reinforcement and the punching–shear strength of the tested slabs. The second finding is that using the cubic root of concrete compressive strength to predict punching–shear strength of

the concrete slabs generally yielded a better result than that when using the square root expression.

On the theoretical level, a mechanical model was developed to predict punching shear capacity of high strength concrete two–way slabs (Marzouk and Hussein, 1991b). This model was adopted for high strength concrete applications. The formulation of the model included an idealization of the actual behaviour of high strength concrete and steel reinforcement. A modified mechanical model considering crack size and slab size effects was developed to predict punching–shear capacity of high strength light weight concrete two–way slabs (Osman et al., 1998).

In addition, the effect of high strength concrete columns on the behaviour of two–way slabs was investigated (Marzouk et al., 1996). The variables selected for that study were concrete strength, flexural steel reinforcement ratio, and moment to shear ratio. It was noticed that the connection performance was greatly enhanced by the use of high strength concrete columns. Also, it was concluded that: using high strength concrete for columns led to an increase in the connection strength by about 5% in the case of no moment and 17% in the case of high moment.

In another research work, tests were conducted to investigate the effect of concrete strength on the behaviour of two–way slabs (Marzouk et al., 1998a). Specimens were tested under combinations of gravity and lateral loads to investigate the effect of concrete strength on the entire behaviour of two–way slabs. The same parameters as those in the aforementioned work were considered. It was concluded that as concrete compressive strength of a slab increased from 35 to 75 MPa the shear strength increased by 15% for specimens subjected to moment. It was uneconomical to use high strength concrete for building slabs subjected to gravity loads only. However,

high strength concrete slabs and plates of 70 MPa are commonly used for offshore applications. The results showed that only 7% increase in punching–shear strength was achieved if the concrete compressive strength increased from 35 MPa to 75 MPa. It was found that the use of high strength concrete had a significant effect on the load–deflection characteristics for specimens subjected to high moment. The ductility of the tested slabs was greatly improved due to using high strength concrete. The results indicated that deflection values at failure loads for high strength concrete specimens were greater than those for normal strength concrete specimens, with the same reinforcement ratio. In addition, the extensions of the yielding radii were larger than those in cases of normal strength concrete specimens. This means more efficiency of flexural reinforcement was achieved when high strength concrete was used. In general, the yielding of specimens constructed with high strength concrete slabs occurs at lower load values than those of specimens constructed with normal strength concrete.

Moreover, tests were conducted to investigate the seismic response of two–way slabs constructed with high strength concrete (Emam et al., 1997). One half of the specimens was constructed using high strength concrete and the other half was constructed with normal strength concrete. The compressive strengths of concrete were 35 MPa and 75 MPa for normal and high strength concrete, respectively. It was concluded that as the concrete slab strength increased from 35 to 75 MPa, the displacement ductility was increased by a 100%. Also, the rotation ductility was increased by 125%. Moreover, shear strength, moment capacity, drift percent, and rotation capacity were increased by 20, 31, 37, and 50% respectively, when high strength concrete was used for the slabs.

2.6 Shear Reinforcement of Two–Way Slabs

Many researchers have investigated the pure behaviour of two–way slabs and/or two–way slab to column connections (Hewitt and Batchelor, 1975; Kinnunen and Nylander, 1960; Marzouk and Hussein, 1991a; Marzouk and Hussein, 1991b; Broms, 1990; Dilger and Ghali, 1981; Rankin and Long, 1987). The major problem of the two–way slab system is the sensitivity of slabs to the punching–shear failure. The following alternatives can be used in case of the inadequate punching–shear capacity:

- Increasing the slab thickness in the whole floor,
- Increasing the slab thickness in the vicinity of the column by providing a drop panel,
- Flaring the top of a column by providing a column capital,
- Constructing the slab using high strength concrete, and/or
- Providing shear reinforcement.

These solutions are applicable during the construction of the building. It is practically difficult to introduce one of those solutions as a strengthening technique for existing two–way slabs of inadequate punching–shear strength. It was proven that the most effective technique for enhancing the shear strength of a two–way slab is to provide vertical shear reinforcement in the form of shear studs around the column (Seible et al., 1980; Dilger and Ghali, 1981; Marzouk and Jiang, 1997; Yamada et al., 1992).

Researchers have paid special attention to the enhancement of two–way slab to column connections during construction against punching–shear failure by adding vertical shear reinforcement. There have been several research works to investigate the effectiveness of different types of shear reinforcement used in two–way slabs. These types of shear reinforcement include bent bars, stirrups (closed or U typed), shear-heads (C or I sections steel channels placed in the slab around the column), welded

wire fabric, studs, hat-shaped shear reinforcement, and hooked bars. These types of shear reinforcement are summarized in a number of research papers (Corley and Hawkins, 1968; Seible et al., 1980; Dilger and Ghali, 1981; Broms, 2000; Broms, 1990; Mortin and Ghali, 1991; Yamada et al., 1992).

The so-called shear studs were developed at Calgary University and reviewed in several research works (Seible et al., 1980; Mokhtar et al., 1986; Mortin and Ghali, 1991). Shear studs are mechanically anchored studs with a plate or a head at each end that is capable of developing the yield strength of the studs. Some of the early developed types of the shear studs are shown in Figure 2.1. The stems of these studs intersect the shear cracks preventing their widening (Ghali and Megally, 1999). In addition, the heads of the shear studs provide mechanical anchorage at both ends.

The use of five different types of shear reinforcement was investigated at Memorial University of Newfoundland to enhance the punching shear capacity of high strength concrete slabs (Marzouk and Jiang, 1997). The types of the shear reinforcement used in the study were single bent, U-stirrup, double bent, shear stud, and T-headed shear reinforcement. The structural behaviour was evaluated in terms of the deformational characteristics, load capacity, and post-failure behaviour. It was found that double bent, shear studs, and T–headed shear reinforcement types were adequate shear reinforcement. The enhancement technique eliminated punching shear failure and transferred it to flexure failure. It was noticed that the ductility and energy absorption were significantly increased by using shear reinforcement.

The Canadian code states that shear reinforcement consisting of headed shear reinforcement, stirrups, or shear–heads may be used to increase the shear capacity of slabs (CSA–A23.3, 1994). Headed shear reinforcement are vertical bars, which

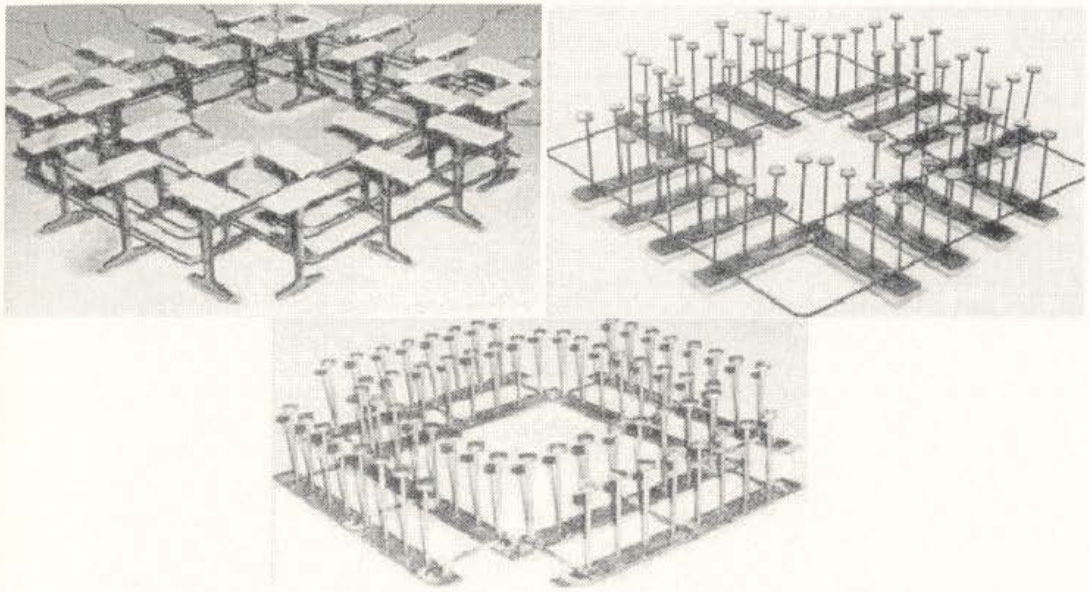

Figure 2.1: Different early kinds of shear reinforcement (Seible et al., 1980)

are anchored at each end by a plate or a head bearing against the concrete. It is recommended that the area of these plates should be 10 times the cross sectional area of the bar. The headed shear reinforcement is to be aligned concentrally around the column. The first line is to be located at a distance $s/2$ from the column face, where s is the spacing of such reinforcement. The value of s is determined according to the shear stress requirement as provided by the Canadian code (CSA–A23.3, 1994). The reinforcement is to be extended to the section where the factored shear stress is not greater than $0.2\sqrt{f'_c}$ for normal concrete. The current code permits the usage of shear reinforcement consisting of bars or wires. In addition, shear reinforcement consisting of steel I or channel-shape sections (shear-heads) can be used. It is stated in the ACI code that when bars or wires are provided as shear reinforcement, the shear strength may be increased to a maximum shear stress of $6\sqrt{f'_c}$. However, shear

reinforcement must be designed to carry all shear in excess of stress of $6\sqrt{f_c'}$, where f_c' is the concrete compressive strength, psi (ACI–318, 1999).

2.7 Finite Element Analysis of Two–Way Slabs

Few investigations have dealt with the finite element analysis of two–way slabs. Some of the published research in this regard is presented in this section.

An analytical study was aimed at validating the adequacy of the code equations of the fraction of moment transferred by slab shear stresses (Megally and Ghali, 2000). The analytical study was a 3-D finite element analysis in which both the longitudinal reinforcement and vertical shear reinforcement were defined. It was concluded that the fraction of moment transferred to the slabs is in concordance with the results of previous research work on which the ACI code is based on (ACI–318, 1999).

A finite element analysis was conducted to investigate the behaviour of high strength concrete slabs. A plasticity based concrete model was used to define concrete behaviour under compression (Marzouk and Chen, 1993). A suitable post cracking tensile model of reinforced high strength concrete was utilized. This model was based on the fracture energy of high strength concrete. An eight–node quadrilateral shell element with reduced 2×2 Gaussian integration was used. It was concluded that post-cracking behaviour of high strength concrete had a significant effect on the deformational characteristics of two–way slabs. A similar research work was completed on the behaviour of two–way slabs with a special emphasis on the sensitivity of shear strength to fracture energy of high strength concrete slabs (Marzouk et al., 1998a). A more accurate expression for the shear stresses in slabs than that used in the CSA and ACI codes was derived and verified against experimental results.

A finite element evaluation of the shear enhancement of high strength concrete plates was conducted using a nonlinear analysis of reinforced concrete structures using three-dimensional solid finite elements (Marzouk and Jiang, 1996). The purpose of this research was to demonstrate a proper way of representing vertical shear reinforcement in slabs as an "out of plane" three-dimensional bar elements. A three-dimensional 20–node brick elements with $2 \times 2 \times 2$ Gaussian integration rule over the element faces, and a plasticity–based concrete model were employed.

2.8 Fibre Reinforced Plastics (FRP)

The use of FRP composites, as reinforcement for concrete members, has become a new trend during the last decade. These materials are non-corrosive and non-magnetic composites. One of the most common types of the FRP composites is the Carbon FRP (CFRP). CFRP is up to six times stronger than steel and one fifth lighter. Two other common types of the FRPs are the Glass FRP (GFRP), and Aramid (AFRP). CFRPs are of highest stiffness and cost among all other types. The cost of AFRPs is in between those of CFRPs and GFRPs (Demers et al., 1996). Aramid fibres are of lower strength and modulus of elasticity compared to carbon fibres.

The overall properties of any of the FRPs depend, at large, on the properties of the fibres component. The superior properties of FRP materials are due to the excellent properties of the fibres embedded in a ductile polymeric matrix. The function of the ductile polymeric matrix is to enable good transfer of the load from one fibre to another. The advantages of using FRP composites as construction materials especially for strengthening, are summarized in a research work (Ballinger, 1997). The main advantage of the FRP composites is their relatively high tensile strength to weight

ratio, compared to steel for instance. Hence, these composites as strengthening materials do not cause an increase in the dimensions of existing structural members. These materials are not subject to corrosion and can be used instead of steel in reinforcing structural elements.

The use of FRP composites was relatively limited to the field of airspace industry due to the high cost of these products (Nanni, 1993). Nowadays, FRP composites, as construction materials, have a wide range of applications for both new and existing structures, especially for strengthening. FRP composites are considered excellent strengthening materials for existing structural elements like beams and columns.

2.8.1 FRP Reinforcement for Concrete Structures

Extensive research work has been conducted on FRP as reinforcement for structural elements. The attraction of FRP reinforcing bars as an alternative to steel reinforcement is to overcome the corrosion related problems in structural elements. Typical applications for FRP reinforcement are reinforcing bridge decks, parking garages, water and wastewater treatment facilities, marine structures, and chemical plants.

A comprehensive research work has been conducted at Sherbrooke University in Québec, to investigate the behaviour of concrete structures reinforced with FRP. Test results of concrete beams reinforced with FRP and conventional steel reinforcement were presented emphasizing the deformational and cracking characteristics. Theoretical correlations for the prediction of crack width, maximum deflection, and ultimate load-carrying capacity were proposed (Masmoudi et al., 1998; Theriault and Benmokrane, 1997; Theriault and Benmokrane, 2001).

In another research work, the effect of the reinforcement ratio of the FRP carbon rods known as C-bars on cracking, deflection, ultimate capacities and modes of

failure of beams were investigated. The results of the beams reinforced with C-bars were compared to those reinforced with conventional steel reinforcement (Benmokrane et al., 1997a).

The interaction between GFRP reinforcement bars and concrete is one of the main issues that attracts the attention of researchers. It was concluded that a modification factor of 1.29 is recommended for computing the development length for the case of the GFRP rebars to obtain an equivalent steel reinforcement development length (Benmokrane et al., 1997b).

Carbon Fibre Reinforced Polymer (CFRP) was used as deck slab reinforcement for bridge applications in Sherbrooke (Québec, Canada), as reported (Benmokrane et al., 1998). The advanced technology used in the construction of a section of the bridge was the use of integrated Fibre Optic Sensors (FOS) into the FRP reinforcement allowing continuous tracking of the strains in the FRP reinforcement and hence, the bridge structural behaviour.

Another research work reported the test results of one-way concrete slabs reinforced with glass fibre, carbon fibre and conventional steel reinforcement. The slabs were tested under static loading conditions to determine their flexural and shear limit states, including the behaviour prior to cracking, cracking, ultimate capacities and modes of failure (Michaluk et al., 1998).

Other researchers dealt with slabs reinforced with FRP grids. The structural behaviour in one-way bending is investigated for different types of FRP grid reinforcement (Matthys and Taerwe, 2000a). In addition, The punching shear behaviour of two-way slabs reinforced with FRP grids was investigated in a continuing research (Matthys and Taerwe, 2000b).

2.8.2 Flexural Strengthening of Beams

The behaviour of reinforced concrete beams externally reinforced with advanced composite materials has been studied by a large number of researchers.

An experimental and theoretical research program was conducted to investigate the effectiveness of using FRP plates as external reinforcement to strengthen reinforced concrete beams (Ritchie et al., 1991). Carbon, glass, and aramid FRPs were used in the study for strengthening. Also, mild steel plates were used as a traditional and reference strengthening technique. The mechanical properties, in terms of modulus of elasticity and ultimate tensile strength were altered from one material to another according to the fibre orientation angle. All of the plates were bonded to the tension side of the beams using a two-parts epoxy. It was observed the ultimate strength of the beams strengthened with FRP plates increased from 40% to 97%. The serviceability conditions of the strengthened beams, in terms of crack patterns, were noticeably improved. Although the behaviour of FRP plates was brittle at failure unlike the steel plates, it was concluded that beams strengthened with FRP plates showed enough ductility required for some of the existing cases.

The performance of conventionally reinforced concrete beams strengthened with externally bonded advanced composite materials (ACM) has been studied by analyzing an experimental database compiled from ten separate studies (Bonacci, 1996). The strengthening FRP composites included carbon, glass, aramid, and mixed FRP. More than 95% of the selected beams were strengthened with carbon or glass FRPs. More precisely, 52% of the selected beams were strengthened with CFRP, and 45% were strengthened with GFRP. It was clear from these experimental studies that the

procedures were most representative to external reinforcing rather than rehabilitation. Premature debonding failure was prevalent in 64% of the tests reviewed in this database.

Further research was carried out to investigate the effectiveness of external FRP reinforcement to strengthen reinforced concrete beams (Chajes et al., 1995). A series of reinforced concrete beams were tested to determine the ability of externally bonded CFRP reinforcement to improve the flexural and shear capacities of beams. CFRP sheets were bonded to the beams using a two-parts resin and cured at the ambient temperature. The studied parameters included the variation of number of layers and fibre orientation. It was concluded that the flexural stiffness and the ultimate capacity of the beams were noticeably increased. The reinforcing CFRP sheets led to an increase in flexural stiffness up to 178%, and increases in ultimate beam capacity up to 292% over that of the control beams. It was noticed in that study that failure was initiated by either tensile failure of the composite or shear failure of the concrete. E-glass and graphite FRP were used as external reinforcement for the reinforced concrete beams (Chajes et al., 1994; Chajes et al., 1995).

GangaRao and Vijay investigated experimentally and analytically the increase in flexural strength of reinforced concrete beams after wrapping them with carbon fabrics (GangaRao and Vijay, 1998). In this study, 24 reinforced concrete beams were tested to determine the effectiveness of using carbon fibre wraps in strengthening concrete beams. The tested specimens were not subjected to any level of damage prior to repair. Four different carbon wrap configurations were used for rehabilitation. It was concluded that high strength and stiffness properties of carbon sheets resulted in improving the performance of rehabilitated concrete members.

2.8.3 Shear Strengthening of Beams

Fewer research investigations are reported in the literature on the FRP beam-shear–strengthening using FRP composites than those reported on the flexural–strengthening. Triantafillou investigated the application of FRP as shear–strengthening materials for reinforced concrete beams by analyzing experimental data of seven different investigations together with his own investigation (Triantafillou, 1998). In addition, this research included developing an analytical model for design of beams based on the ultimate limit states design method. The experimental part of the study included testing of eleven concrete beams strengthened in shear with CFRP at various area fractions and fibre configurations. The analytical investigation contained a model that calculated the gain in shear capacity due to adding FRP composites in analogy with steel stirrups. It was shown that the use of FRP is effective in improving the shear capacity of tested specimens.

A comprehensive design approach for reinforced concrete beams and one–way slabs strengthened with externally bonded FRP plates was investigated (Chaallal et al., 1998). The research was divided into two main parts, namely flexural–strengthening and shear–strengthening. In the first part, analytical models were presented for two modes of failure, namely classical modes, such as crushing of concrete in compression or tensile failure of the laminate, and premature modes such as debonding of plates. The models were based on common principles of compatibility of deformations and equilibrium of forces that could be used to predict the ultimate strength in flexure. In the second part, design equations were derived to enable the calculation of required cross-sectional area of different patterns of FRP shear plates or strips.

Another research was conducted to investigate the effectiveness of glass fibre reinforced polymer laminates (in the form of plates or strips) as a shear–strengthening of reinforced concrete beams (Al-Sulaimani et al., 1994). In this investigation, it was assumed that the GFRP–concrete interfaces carry average shear stresses of 0.8 MPa and 1.2 MPa for the case of plates and strips, respectively, before peeling-off occurred.

2.8.4 Failure Criteria of FRP Strengthened Beams

Generally, the modes of failure of FRP–strengthened beams may be classified as two main categories, namely, the flexural failure and the local bond or shear failure (Malek et al., 1998). The flexural failure includes the concrete crushing and reinforcement yielding. The local failure category includes any other sudden failure such as debonding, peeling-off, and shear failures (Maalej and Bonacci, 1998). Local failure modes are more difficult to be characterized than flexural failure modes as they depend on factors that are difficult to be included in conventional analysis. These factors may include the thickness of bonding agent and concrete surface preparation level.

A summary of the possible modes of failure that occurred or could occur during some of experimental investigations of strengthening reinforced concrete beams with CFRP were presented (Meier et al., 1993). It was implied that the calculation of flexure in reinforced concrete elements post-strengthened with carbon fibre reinforced epoxy resin sheets can be performed analogous to conventional reinforced concrete elements. Generally, strengthening sheets lead to a much finer cracking distribution of the strengthened beams compared to that of the unstrengthened beams. The following failure modes were observed in the tests, as shown in Figure 2.2:

- Tensile failure of the CFRP sheet. CFRP sheets failed more or less suddenly,(1).

- Classical concrete failure in the compressive zone of the beam,(2).
- Continuous peeling-off of the CFRP sheets due to an uneven concrete surface,(3).
- Shearing of the concrete in the tensile zone,(3).
- Interlaminar shear within the CFRP sheet, (4).
- Failure of the reinforcing steel in the tensile zone, (5).

The following failure modes are theoretically possible:

- Cohesive failure within the adhesive, (6).
- Adhesive failure at the interface CFRP sheet/adhesive, (7).
- Adhesive failure at the interface CFRP concrete/adhesive, (8).

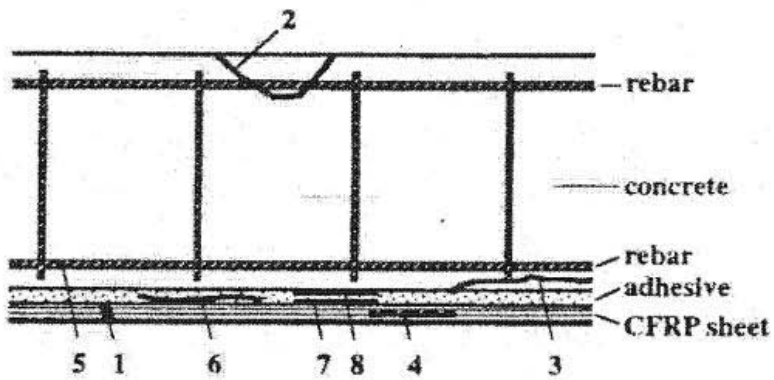

Figure 2.2: Longitudinal section of a repaired beam (Meier et al., 1993)

The main failure mechanisms were classified into three different collapse mechanisms of strengthened concrete beams, namely, plate-peeling, concrete shear cracking at plate ends, and concrete tensile cracking at mid-span (Arduini et al., 1994). An experimental and analytical investigation on stress mechanism between concrete and FRP plates through the epoxy-resin was conducted (Arduini et al., 1994). It was

concluded that when using FRP plates, the flexural carrying capacity increases considerably. Relevant increases of stiffness can be obtained only using very thick plates. Moreover, it was recommended that the adhesive must be of a good viscosity to avoid air binds formation during the bonding phase. It is crucial to prepare interface surfaces to obtain desired reinforcing strength. In addition, it was concluded that shear failure modes in concrete occurred at the ends of the plates due to the tangential stress concentration in these regions.

2.8.5 Near Surface Mounted FRP Rods

An innovative use of FRP bars was introduced (De Lorenzis et al., 2000). This technique was referred to as the Near Surface Mounted (NSM) that is a kind of external flexural or shear reinforcement. This reinforcement may be located in the specified direction to serve as shear or flexural reinforcement. The method used in applying the rods was as follows: a groove was cut in the desired direction into the concrete surface. The groove was then filled halfway with epoxy paste; the FRP rod was placed in the groove and lightly pressed to force the paste to flow around the rod and fill completely between the rod and the sides of the groove. The groove was then filled with more paste and the surface was leveled. Carbon and Glass FRP rods of different sizes were used for flexural strengthening. Carbon FRP deformed rods were used for shear strengthening. The variables examined in the shear tests were spacing of the rods, strengthening pattern, end anchorage of the rods and presence of internal steel shear reinforcement. The test results confirm that NSM FRP rods could be used to increase the flexural and the shear capacity of reinforced concrete elements significantly, with efficiency that varies depending on the tested variables. However, bond slip was considered the main drawback of the NSM technique. Deformed rods were

more efficient than sandblasted rods from the standpoint of the bond performance. In addition, increasing the groove size, and thus the cover thickness, could lead to higher bond strength (Lorenzis and Nanni, 2001; Lorenzis and Nanni, 2002)

2.8.6 Strengthening of Columns

In literature there are research works on rehabilitation or strengthening reinforced concrete columns (Aboutaha et al., 1999; Saatcioglu and Baingo, 1999; Toutanji, 1999; Jin et al., 1994; Soudki and Green, 1996). Generally, the use of CFRP sheets for columns repair is quick and simple to implement.

The effectiveness of rectangular steel jackets for seismic strengthening of non-ductile reinforced concrete frame columns with inadequate shear strength was experimentally investigated (Aboutaha et al., 1999). Eleven large-scale columns were tested to examine the effectiveness of steel jackets on improving ductility and strength of columns. The test results indicated that the use of thin rectangular steel jackets could be an effective strengthening technique of reinforced concrete columns with inadequate shear strength.

Another experimental study on strengthening reinforced concrete columns using carbon fibre reinforced polymer (CFRP) wraps, with a focus on corrosion-related issues was carried out (Bonacci et al., 1998). The initial work concentrated on establishing improved techniques for laboratory simulation of field corrosion in reinforced concrete columns. Various aspects of accelerated corrosion testing were discussed. Considerations in designing FRP wraps for column repair were also presented. The results showed that using CFRP led to an increase in the load carrying capacity of corroded columns by about 28% compared to reference specimens. In addition, strengthening has increased the ductility significantly. Axial deformations at failure

were about six times those of corroded specimens.

The performance of circular columns strengthened with CFRP in cold weather was investigated (Soudki and Green, 1996). The experimental program contained testing of forty-two circular plain and reinforced concrete columns of different reinforcement ratios, number of CFRP layers, and environmental exposure conditions. It was concluded that CFRP sheets were effective for strengthening concrete columns exposed to repeated freeze/thaw cycles.

A seismic strengthening technique to enhance flexural strengths, ductility, and shear strength of existing reinforced concrete bridge columns, using advanced composite materials as external reinforcement was presented (Jin et al., 1994). Test results indicated that the confinement induced by E-glass FRP straps significantly increased the shear strength. The ductility capacity and the flexural behaviour of reinforced concrete columns under simulated earthquake load were increased as well due to the additional materials.

Experimental and analytical investigations were presented on the performance of concrete columns externally wrapped with carbon and glass fibre reinforced polymer sheets (Toutanji, 1999). The experimental results showed a significant enhancement of strength, ductility, and energy absorption of wrapped columns.

2.8.7 Strengthening of Beam-Column Connections

Many of the existing reinforced concrete frame structures, such as non-ductile reinforced concrete frame structures designed and constructed during the 1950s through 1970s do not meet current seismic design requirements. Many researchers have investigated the problem of the rehabilitation of beam to column connections using steel plates and FRP wrapping (Geng et al., 1998; Alcocer and Jirsa, 1993; Priestley et al.,

1994; Chai et al., 1990).

Four large-scale beam column connections under cyclic loading were tested, which represented existing frame connection (Ghobarah et al., 1997). Two strengthening techniques for connections using corrugated steel jacketing were investigated. The variables of the test included the reinforcement of the joint, and transverse reinforcement of the column. One group of the specimens had jacketing of column only and the other group had jacketing of both column and beam. The corrugated steel jackets were found efficient in the rehabilitation of the existing connections that were not meeting the current seismic codes.

In another research on column strengthening, CFRP was introduced as an alternative strengthening material to steel plates (Geng et al., 1998). It was used to improve the ductility and the development length sufficiency. CFRP sheets were wrapped around the column near the joint region for ductility strengthening, and were longitudinally bonded to and/or wrapped around the column near the joint with a set of steel angles and rods for development strengthening. Repeated loading, unloading, and reloading were applied on ductility specimens to simulate seismic loads. Development specimens were tested under monotonic loading. It was shown that ductility strengthening had contributed to a significant enhancement of the connection ductility.

2.8.8 Strengthening of Slabs

There is a lack of research on rehabilitation of the two–way slabs. Generally, research on slabs is considerably less than that on beams and columns. Published research related to slab strengthening addressed slabs as one-dimensional structures, or in other words, as one way slabs or beams in the way the load was applied or in the way

the supports were located. To the best of the author's knowledge, limited research has been conducted on the strengthening of slab to column connections (Farhey et al., 1995). Four specimens were loaded until a complete failure. Then, the specimens were fully repaired externally using screwed steel plates before applying quasi-static loads until a second failure. There is no specific conclusion can be drawn from the study due to the limited number of specimens. In addition, the specimens were completely failed before repair. This is not the case of strengthening existing slabs in a building where the slabs are suffering a certain level of damage not a complete failure. Hence, further applications on strengthening existing two–way slabs are needed. Moreover, there is a lack of design of the strengthening technique presented (Farhey et al., 1995).

A few research works have been conducted on FRP–strengthened two–way slabs. Some research works dealt with the strengthening of one-way slabs using FRP materials in which slabs were treated in a similar way to beams (Karbhari et al., 1994; Kikukawa et al., 1998; Seim et al., 2001; Paramasivam et al., 1995; Hormann et al., 1999). On the other hand, investigations on FRP two–way slabs strengthening are scarce. To the best of the author's knowledge, there has been only one attempt to investigate the effectiveness of FRP materials in the strengthening of 1.0 m width and 0.05 m thickness two–way slabs or plates (Erki and Hehhernan, 1995). It is the author's belief that those dimensions are not realistic enough to be counted on when drawing conclusions regarding the effectiveness of FRP materials for strengthening two–way slabs in field.

The failure mode of the two–way slabs of low and medium reinforcement ratios is flexural failure mode rather punching shear failure mode. Using FRP materials to enhance two-way slabs in flexure is desirable from the applicability point of view

due to the easiness of handling and installing FRP materials. FRP materials are not subject to either corrosion or rust in the long term. A drawback of using FRP materials in strengthening of flexural structural members is the brittleness of such materials that may result in a decrease of the overall structural member ductility.

2.9 Pre-Loading Effect Prior to Strengthening

In almost all of the surveyed research work, original reinforced concrete beams were not subjected to certain level of damage before strengthening process took place. This is clearly is in contrast with the real life cases in which strengthening structures takes place after some signs of damage due to structural service loads.

A loading frame for testing beams was developed that can be used not just to apply loads prior to strengthening but also to maintain part of the load during strengthening process (Ebead, 1998). This research was an attempt to simulate the actual field situation of strengthened concrete beams using ferrocement.

Maalej and Bonacci in their laboratory study, investigated the effect of pre-loading levels on the behaviour of strengthened beams with FRP (Maalej and Bonacci, 1998). The status of beams during strengthening, whether loaded or unloaded, was investigated. The study consisted of testing of seven reinforced concrete beams. It was concluded from the results that the pre-loading level and the status of beams during the strengthening processes had a slight effect on the results.

The strengthening of the initially loaded reinforced concrete beams using fibre glass-reinforced polymer sheets was investigated (Sharif et al., 1994). Despite the low tensile strength and low modulus of elasticity of the GFRP compared to the conventional steel, it was selected as a strengthening material for beams in this study.

GFRP used consisted of three layers of woven roving embedded in a plastic matrix with a thickness of 0.5 mm and a maximum tensile strength of about 1700 MPa. The studied parameters were the plate thickness and the anchoring schemes. The strengthened beams were subjected to a pre-load of 85% of a control beam capacity. In fact, this percent is deemed a very high pre-loading level, since working loads that are generally about 0.67 of the ultimate loads are recommended for pre-loading. Besides, applying this level of damage to original beams before rehabilitation may cause the beams to fail to satisfy the serviceability conditions. Generally, the test results indicated that flexural strengths of the strengthened beams were increased. In addition, the ductile behaviour of the strengthened beams was inversely proportional to the plate thickness. The research investigation also showed that the use of I-jacket plate provided a proper anchorage at plate ends and improved the ductility of beams with plates of greater thickness.

Chapter 3

The Experimental Program

3.1 General

This chapter gives a detailed description of the experimental program. It includes sections describing the preparation of the formwork and the steel cages; mixing concrete; and strengthening techniques and procedures. The different strengthening techniques are described in terms of the methodology of each technique, the sequence of installing the strengthening components, and the dimensions of the strengthening materials. Moreover, a detailed description of the tested specimens is provided that includes the dimensions and title convention of each specimen.

The test set–up is described in detail in this chapter. The components of the test set–up include the loading test frame, the different actuators by which different kinds of loads are applied, and the supports. In addition, a description of the data acquisition system is also provided in this chapter.

Detailed description of the material properties utilized in this investigation is given. These materials are the concrete; steel reinforcement; CFRP strips and GFRP laminates; and the epoxy adhesives.

3.2 Properties of Materials

In the next sections, the properties of the materials utilized are detailed.

3.2.1 Concrete and Steel Reinforcement Properties

Concrete mix was designed to obtain a target compressive strength equal to 35 MPa after 28 days of 152–mm diameter by 304–mm height cylinder. The unit weight of the concrete mix was 2480 Kg/m^3. The concrete mix proportions for one cubic meter of the concrete used in the entire test program are given in Table 3.1.

Table 3.1: Mix proportions for one cubic meter of concrete

Coarse aggregate (granite 19–mm max. size)	1160 kg
Fine aggregate (graded sand)	690 kg
Cement content	350 kg
Water content	175 litre
Water/cement ratio	0.5

The type of cement utilized was normal Portland cement type 10, as specified by the Canadian Standards Association (CSA). The surface area of the cement is approximately 4000 cm^2/gm as per the supplier. The cement content was kept to 350 kg/m^3. The mixing water was clear and about 4–10 °C. The water content per one cubic meter was 175 liter resulting a water to cement ratio of 0.5. Normal weight local coarse aggregate was utilized in the mix. That coarse aggregate was mostly crushed granite with a maximum nominal size of 19 mm. A minimum number of three standard cylinders were cast at the day of casting and tested at the day of testing. The steel reinforcement bars were deformed CSA grade 400 bars. The actual yield strength varied from 435 MPa to 450 MPa. Detailed properties of the steel reinforcement are listed in Table 3.2.

Table 3.2: Properties of the steel reinforcement bars

Size, mm	Diameter, mm	Area, mm^2	Yield strain,	Yield stress, MPa	Max. stress, MPa	Elastic modulus, GPa
10	11.3	100	0.00236	450	660	191
15	16.0	200	0.00225	435	670	193
20	19.5	300	0.00226	440	665	195

3.2.2 Strengthening Materials Properties

For specimens strengthened using steel plates, ASTM–A36 steel plates were utilized. The nominal thickness of steel plates was 6 mm and the actual thickness was 6.35 mm. The minimum yield strength of this type of steel was 248 MPa and the ultimate tensile strength was 400 MPa. For the same group of specimens, steel bolts, ASTM–A325 19 mm–diameter bolts were used. The ultimate tensile strength of each bolt was 235 kN (ASTM, 1995). These bolts were used to ensure full interaction between the concrete and the steel plates and to apply a confinement pressure of the plates on the concrete slab (when the nuts of these bolts were tightened). Epoxy adhesive was used to ensure, along with the steel bolts, full interaction between the steel plates and the concrete. Moreover, it was used to fill the gaps around the bolts in the holes. The properties of the steel plates are summarized in Table 3.3. In addition, the properties of the epoxy adhesive utilized for the steel plates strengthening specimens are given in Table 3.4 as per the manufacturer specifications.

For specimens strengthened using FRP materials, unidirectional Glass Fibre Reinforced Polymer (GFRP) laminates and unidirectional Carbon Fibre Reinforced Polymer (CFRP) strips were utilized as strengthening materials. The thickness of one layer of a cured GFRP laminate and CFRP strips was 1.0 mm and 1.2 mm, respectively.The Sika CarboDur was used for the CFRP strips. Also, the glass fibre fabric,

SikaWrap Hex 100G, was used for the GFRP laminate. Two types of two-component paste adhesive epoxy resin were utilized for each type of the FRP material as per the manufacturer's specifications. For CFRP strips, the Sikadur 30 was used and for GFRP laminates, the Sikadur Hex 300 was used. Properties of FRP materials are given in Table 3.5. In addition, the properties of the used epoxy for the FRP–strengthening are given in Table 3.6.

Table 3.3: Properties of the strengthening steel plates

Thickness, mm	Weight, kN/m^3	Yield strain	Yield stress, MPa	Ultimate strength, MPa	Young's modulus, GPa
6.35	77	0.00130	248	400	191

Table 3.4: Properties of the epoxy adhesive for steel strengthening specimens*

Compressive strength, MPa	100
Adhesive strength on concrete, MPa	2
Adhesive strength on steel, MPa	26
Elastic modulus, GPa	12.8

* (As per the manufacturer's specifications)

Table 3.5: Properties of a layer of the FRP materials

FRP	Cured thickness, mm	Tensile strength, MPa	Elastic modulus, GPa	Elongation at break ,%
CFRP strips*	1.2	2800	170	>1.7
GRFP laminates *	1.0	600	26.13	2.24

* (Sika CarboDur)

* (Sika Wrap)

Table 3.6: Properties of the epoxy adhesive for FRP strengthening

Property	Epoxy for strips*	Epoxy for laminates*
Tensile strength, MPa	24.8	72.4
Elongation at break,%	1.00	4.8
Elastic modulus, GPa	4.5	3.1

* (Sikadur 30)
* (Sikadur Hex 300)

3.3 The Formwork of the Specimens

Steel formwork was used for preparing the specimens as shown in Figure 3.1. As it will be explained in the following sections, the specimens have two different geometrical configurations. Some specimens have one column stub and some others have two column stubs. For the former, both the panel and the column stub were cast monolithically. The specimens that have two column stubs were cast in two stages. In the first stage, the panel and one column stub were cast first and one day later an additional mold of the other column stub was placed and rested on the concrete surface for casting the second column stub. The additional mold used for casting the second (upper) column stub as shown in Figure 3.1.

3.4 Preparing Steel Cages

Steel reinforcement rods were cut in the required lengths and arranged together to form the cage of the tested specimens. The steel reinforcement cage was prepared according to whether the slab has one column stub or two.

For the panel reinforcement, rods of diameters 10 mm and 15 mm were used as main (tension) reinforcement based on the reinforcement ratio of the prepared specimen. For all specimens, 10 mm diameter steel rods were used as secondary

Figure 3.1: The formwork with a cast specimen

(compression) reinforcement for the panel. Steel wires were used to tie the steel rods of each layer of the slabs together and to keep the spacing and orientation of steel rods as required.

In order to ensure an efficient utilization of the steel rods, the upper and lower cages were welded together using connecting pieces of rods. These pieces of rods were necessary to keep the distance between both the tension and compression reinforcement of the panel. This method of ensuring the developing of the tension bars was adopted based on an earlier research work (Marzouk and Hussein, 1991a).

All tension and compression rods of the panels had the same length of 1800 mm that allowed for a distance of 50 mm from each side of the panel edge. Details of the reinforcement of the panels are shown in Figure 3.2.

The column stub bars had two configurations based on whether a second column stub was used or not. For specimens with only one column stub, the rods were bent at a right angle and extended to 400 mm horizontally inside the panel. For specimens with two column stubs, column bars were straight and of 1750–mm length allowing for a distance of 50 mm between the ends of the rods and the concrete column surface. For the column stubs, 20–mm diameter steel rods were used as the longitudinal reinforcement, while 10–mm diameter mild steel ties were used as transverse reinforcement spaced at 160 mm.

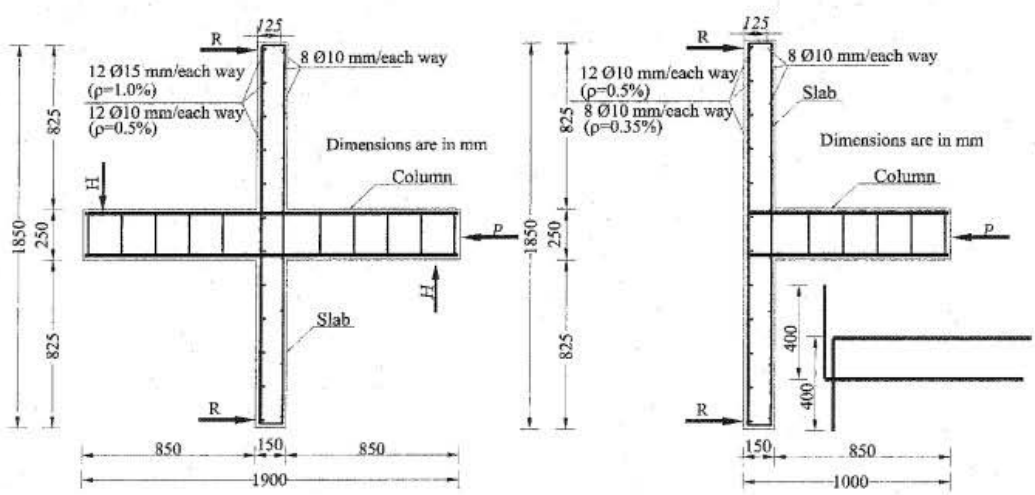

(a) Specimens with two column stubs

(b) Specimens with one column stub

Figure 3.2: Reinforcement details of tested specimens

3.5 Mixing Concrete

The specimens were cast after appropriate placing of the steel cages inside the form allowing for a minimum concrete cover of 25 mm. Concrete was mixed mechanically at a rate of 18 rpm in the concrete laboratory at Memorial University of Newfoundland. The mixer had a capacity of 0.12 m^3 and allowed casting batches of 0.1 m^3 each. It took six batches to cast the panel and one column stub of each specimen. An extra batch was needed for the second column stub for specimens with two column stubs.

A minimum of three 150 mm diameter by 300 mm height plastic cylinders, as per the ASTM standards (ASTM-C192-88, 1993), were cast with each specimen to determine the compressive strength of concrete at the day of the test. Polyethylene sheets were placed on the top surface of the cast specimens for at least three days. Then the specimens were left in the mold for four more days during which the concrete surface was sprayed with water twice a day. Afterwards, the specimens were removed from the form and kept in the ambient temperature until testing.

3.6 Test Slabs

3.6.1 General

Tests were conducted on a model of a two–way slab part enclosed by contra-flexure lines on which bending moment values vanish as shown in Figure 3.3. All specimens were square with 1900–mm side length and 150–mm thickness. The corners of the slabs subjected to central loads only were free to lift. The span of 1830 mm represents 0.4 of the total span of two–way slabs in an actual building in field (Rankin and Long, 1987). Hence, the selected dimensions represent a slab of full scale with an actual span of about 4575 mm. A slab of 150–mm thickness and a span of 4575–mm is commonly

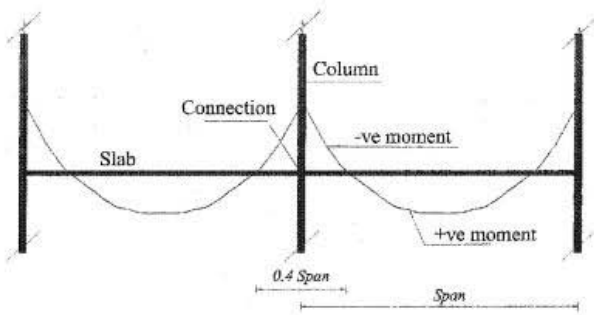

Figure 3.3: The simulated part of the building (0.4 the Span)

used in multistory buildings. The test specimens were simply supported along four sides with corners free to lift except for specimens subjected to moment or lateral cyclic loading. Two configurations of specimens were manufactured. Specimens of the first configuration have one column stub and those of the other configuration have two column stubs as will be explained in Section 3.6.2 and Section 3.6.3. Column stubs were located at the slab center and were of 250–mm square cross section dimensions. The columns stubs were extended to a distance of 850 mm from each slab surface.

The tested specimens are divided into three main groups; Group 1: slabs strengthened using steel plates under central monotonic loads; Group 2: slabs strengthened using steel plates under either combination of monotonic central load and moment load or cyclic load; and Group 3: specimens strengthened using CFRP strips or GFRP laminates and loaded using central monotonic loading. All of the three groups include reference (unstrengthened) specimens.

Figure 3.4 shows a layout of specimens with two column stubs and loaded centrally only. Figure 3.5 shows a layout of specimens with two column stubs and loaded with a combination of central load, P, and lateral load, H (static or cyclic). Figure 3.6

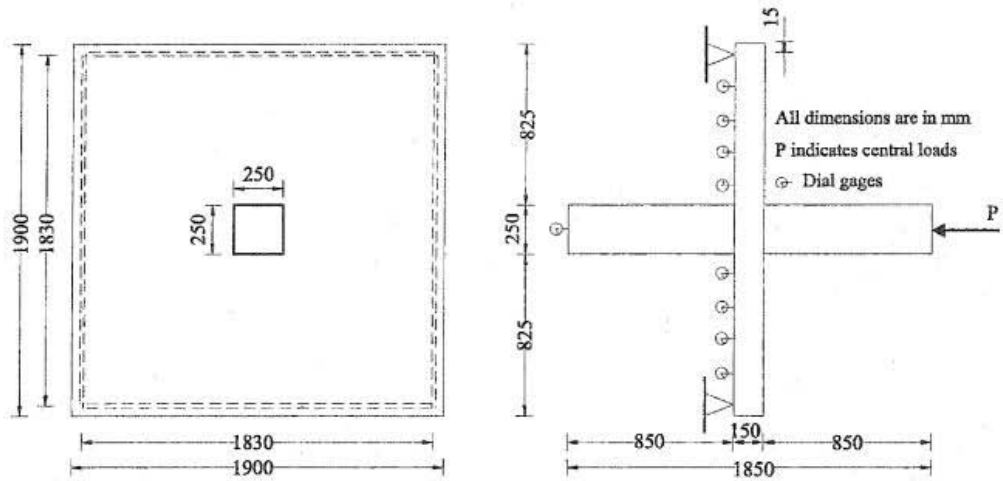

Figure 3.4: Layout of specimens with two column stubs and loaded centrally

shows a layout of specimens with one column stub and loaded centrally.

3.6.2 Specimens of Group 1

For Group 1, the specimens were simply supported along four edges with corners free to lift as shown in figure 3.4. This group was composed of specimens subjected to central loading and strengthened using steel plates and steel bolts. This group includes two unstrengthened specimens, Ref–P–1.0% and Ref–P–0.5%; and six strengthened specimens, Steel–P1–1.0%, Steel–P2–1.0%, Steel–P3–1.0%, Steel–P4–1.0%, Steel–P5–1.0%, and Steel–P–0.5%.

The specimens in this group were used to investigate the effectiveness of the strengthening technique. Particularly, specimens Steel–P1–1.0% through Steel–P4–1.0% were designed to optimize the strengthening system in terms of the number of steel bolts used and the steel plates' configuration.

Figure 3.7 shows the different configurations of steel plates and bolts. The pattern

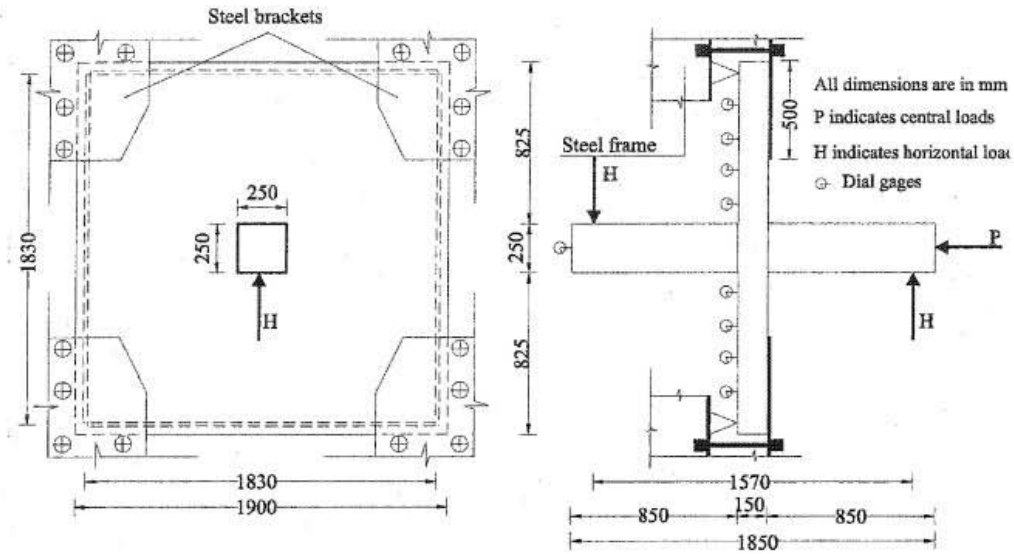

Figure 3.5: Layout of specimens with two column stubs and loaded centrally and laterally

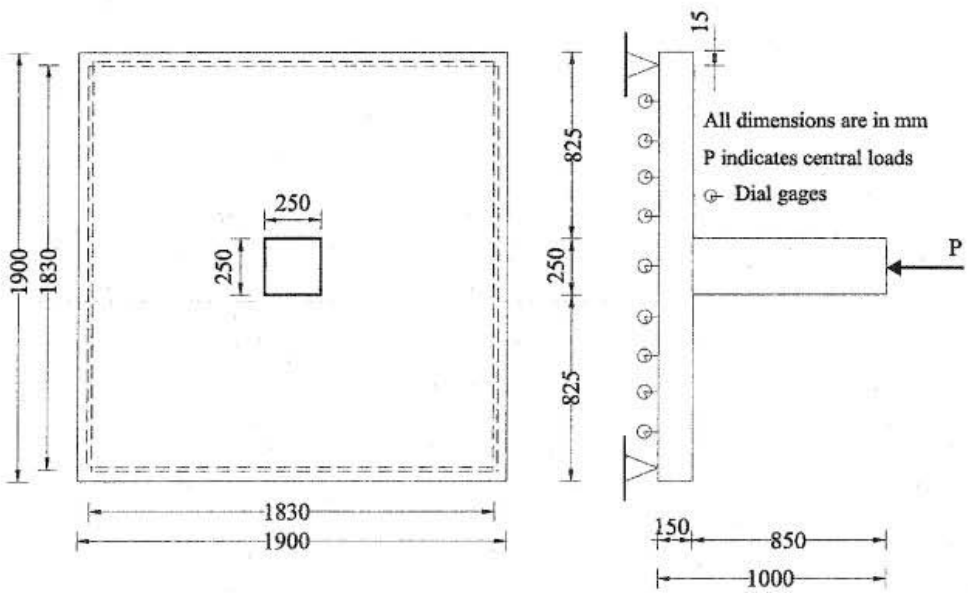

Figure 3.6: Layout of specimens with one column stub and loaded centrally

of specimen Steel–P1–1.0% is referred to as Pattern 1 in Figure 3.7.a. Specimen Steel–P1–1.0% utilized eight steel bolts and four separate steel plates at each side of the panel. Each plate's dimensions were 250 mm by 240 mm, that means it was extended to twice the slab depth from the column face. Bolts were placed at the locations shown on Figure 3.7.a

The pattern of specimen Steel–P2–1.0% is referred to as Pattern 2 as shown in figure 3.7.b. This specimen utilized the same number of steel bolts as used in Pattern 1 but with different arrangements and different dimensions of steel plates. Pattern 2 utilized two L–shaped steel plates welded together and located at each side of the concrete panel. The overall dimensions of each steel plate were 730 mm by 730 mm. These dimensions are equal to the column side dimension plus four times the slab depth.

The pattern of specimen Steel–P3–1.0% is referred to as Pattern 3 in Figure 3.7.c. This pattern adopts the same steel plate's configuration as used in Pattern 2. However, an additional steel bolts were added in between the outer four bolts to investigate the impact of increasing the steel bolts from 8 bolts to 12 bolts on the overall behaviour of the slabs.

The final pattern is Pattern 4 for specimen Steel–P4–1.0% in Figure 3.7.d. It is the same as Patterns 2 and 3 with respect to the configuration and dimensions of the steel plates but utilizes 16 steel bolts distributed as shown in Figure 3.7.

Based on some preliminary results, Pattern 2 was found to be the preferable and recommended pattern. Consequently, an additional specimen adopting the same steel bolts and plates configuration, was manufactured and tested (specimen Steel–P5–1.0%). This specimen was prepared to record the values of strain in the steel bolts

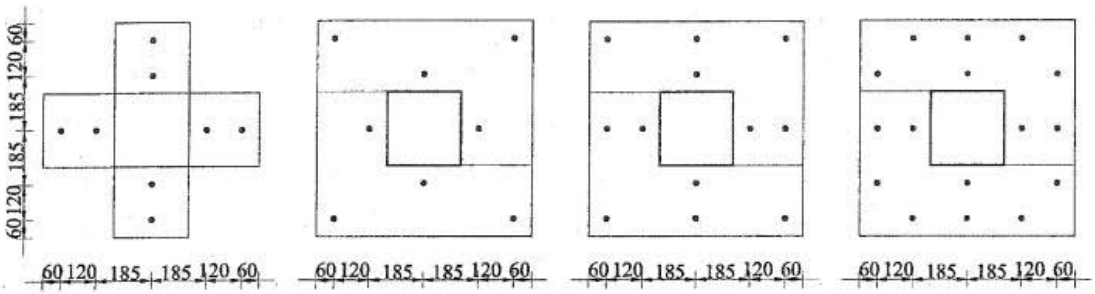

(a) Pattern 1 (b) Pattern 2 (c) Pattern 3 (d) Pattern 4

Figure 3.7: Steel plates and bolts configuration (dimension are in mm)

and at different locations on the steel plates. Table 3.7 summarizes the specimens' parameters of Group 1.

Table 3.7: Specimens of Group 1

Specimen title	Concrete strength, MPa	No of steel bolts	Pattern type
Ref–P–0.5%	35	—	—
Ref–P–1.0%	36	—	—
Steel–P–0.5%	34	8	Pattern 2
Steel–P1–1.0%	33	8	Pattern 1
Steel–P2–1.0%	37	8	Pattern 2
Steel–P3–1.0%	33	12	Pattern 3
Steel–P4–1.0%	30	16	Pattern 4
Steel–P5–1.0%	34	8	Pattern 2

3.6.3 Specimens of Group 2

The tested specimens in this group are divided into two main divisions: slabs subjected to combined central load and static moment, and slabs subjected to combined

central and cyclic moment. It is emphasized that for the specimens of this group additional steel brackets were placed at slabs' corners to prevent the lateral movement. These brackets will cause a fixation at the corners of these specimens. The specimens subjected to central loading associated with unbalanced monotonic moment included two reference specimens, Ref–M–0.5% and Ref–M–1.0%, and two strengthened specimens, Steel–M–0.5% and Steel–M–1.0%. In addition, the specimens of this group, that were subjected to a central loading associated to a cyclic moment, were composed of two reference specimens, Ref–C–0.5% and Ref–C–1.0% and two strengthened specimens, Steel–C–0.5% and Steel–C–1.0%.

The second letters M and C indicate specimens subjected to static moment and cyclic moment, respectively. The specimens of this group have the configuration of Pattern 2 in Figure 3.7. As shown in Figure 3.5, specimens of Group 2 are subjected to lateral load, H, that is either static or cyclic. The parameters of Group 2 are summarized in Table 3.8.

Table 3.8: Specimens of Group 2

Specimen title	Concrete strength, MPa	Pattern type	Load type
Ref–M–0.5%	32	Reference	Moment
*Ref–M–1.0%	33	Reference	Moment
*Ref–C–0.5%	31	Reference	Cyclic
*Ref–C–1.0%	36	Reference	Cyclic
Steel–M–0.5%	33	Pattern 2	Moment
Steel–M–1.0%	34	Pattern 2	Moment
Steel–C–0.5%	32	Pattern 2	Cyclic
Steel–C–1.0%	31	Pattern 2	Cyclic

* (Marzouk et al., 2000a)
* (Marzouk et al., 2001)

3.6.4 Specimens of Group 3

The third group is composed of specimens subjected to central monotonic loads and were used to evaluate two–way slabs strengthening techniques using CFRP strips and GFRP laminates.

The specimens of this group were reinforced with three different reinforcement ratios. The selection of the reinforcement ratios was based on the purpose of the strengthening. Studies on slabs at Memorial University of Newfoundland showed that slabs with a reinforcement ratio less than or equal to 0.5% are subject to flexural failure. Those slabs with a reinforcement ratio of more than 1.0% are subject to punching–shear failure (Marzouk and Hussein, 1991a).

It was intended to investigate the effectiveness of CFRP strips and GFRP laminates in strengthening two–way slabs against flexural and punching–shear deficiencies. The specimens in this group are classified as FRP flexural–strengthening specimens and FRP punching–shear–strengthening specimens. The latter will be called "FRP shear–strengthening" specimens for convenience. It is already expected that FRP materials are not the proper materials for shear–strengthening however two specimens were tested to confirm this expectation and to compare the test results with those for specimens utilized the steel plates system in Group 1.

Specimens Ref–P–0.35% and Ref–P$'$–0.5% are used as reference specimens for FRP flexural–strengthening, while specimen Ref–P–1.0% is used as reference specimen for the shear–strengthening. The rest of the specimens were strengthened using either CFRP strips or GFRP laminates. The author would like to emphasize that specimen Ref–P$'$–0.5% has one column stub and specimen Ref–P–0.5% has two column stubs.

Specimens CFRP–F–0.35% and CFRP–F–0.5% had reinforcement ratios of 0.35%

and 0.5%, respectively, and were strengthened using CFRP strips. Similarly specimens GFRP–F–0.35% and GFRP–F–0.5% had reinforcement ratios of 0.35% and 0.5%, respectively, and were strengthened using GFRP laminates. Specimens CFRP–F–0.35%, CFRP–F–0.5%, GFRP–F–0.35% and GFRP–F–0.5% are referred to as FRP flexural–strengthening specimens. The FRP shear–strengthening specimens are represented by specimens CFRP1–S–1.0% and CFRP2–S–1.0% having a reinforcement ratio of 1.0%. In the title conventions, S and F in the middle of each specimen's title refers to shear or flexure strengthening, respectively.

For FRP flexural–strengthening-specimens, columns were located at the compression side only and extended to 850 mm from the panel surface as shown in Figure 3.6. However, for FRP shear–strengthening, both column stubs were extended to a distance of 850 mm from each side for a possible comparison with steel strengthened specimens. All the test specimens of this group were simply supported along the four edges with corners free to lift. Table 3.9 summarizes the parameters of specimens in Group 3.

Table 3.9: Specimens of Group 3

Specimen title	$f_c^{'}$,MPa	ρ,%	Strengthening material	Column stubs
Ref–P–0.35%	30	0.35	Reference	Single
Ref–P'-0.5%	34	0.50	Reference	Single
CFRP–F–0.35%	35	0.35	CFRP strips	Single
GFRP–F–0.35%	29	0.35	GFRP laminates	Single
CFRP–F–0.5%	34	0.5	CFRP strips	Single
GFRP–F–0.5%	38	0.5	GFRP laminates	Single
CFRP1–S–1.0%	29	1.0	CFRP strips	Double
CFRP2–S–1.0%	36	0.5	CFRP strips	Double

3.7 Test Set–up and Instrumentation

A 10-ton capacity crane was used to lift and install the specimens vertically inside the loading frame and to remove the specimens after testing as shown in Figure 3.8. The loading frame used for testing the specimen was a large reaction steel frame as shown in Figure 3.9. Pieces of rubber were placed between the back surface of the slab and the supporting edges of the frame. The centrally loaded specimens were simply supported along the four sides as shown in Figures 3.4 and 3.6. For specimens of Group 2, four brackets were placed at the corners to prevent lateral movement of specimens as shown in Figure 3.5.

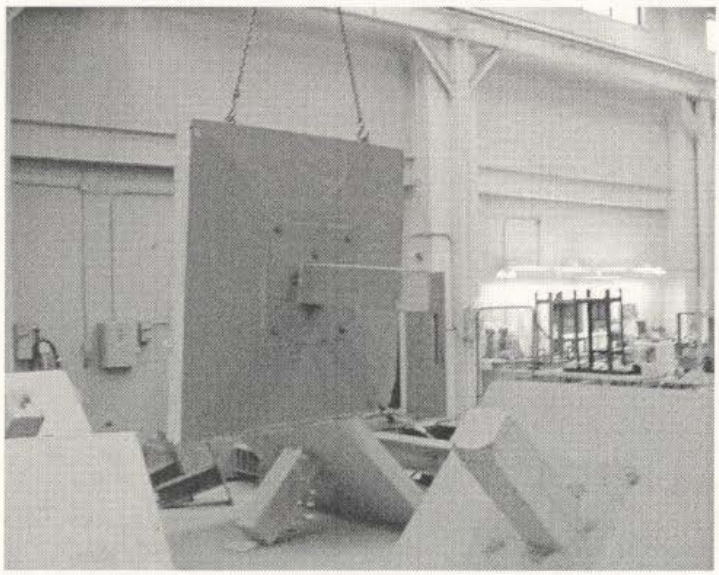

Figure 3.8: A specimen carried using the 10-ton capacity crane

A central and two side hydraulic actuators were fixed to the frame. The central actuator was facing the specimens and was used to apply central load, P, through the inside column stub. The two side actuators were fixed to wide flange steel columns

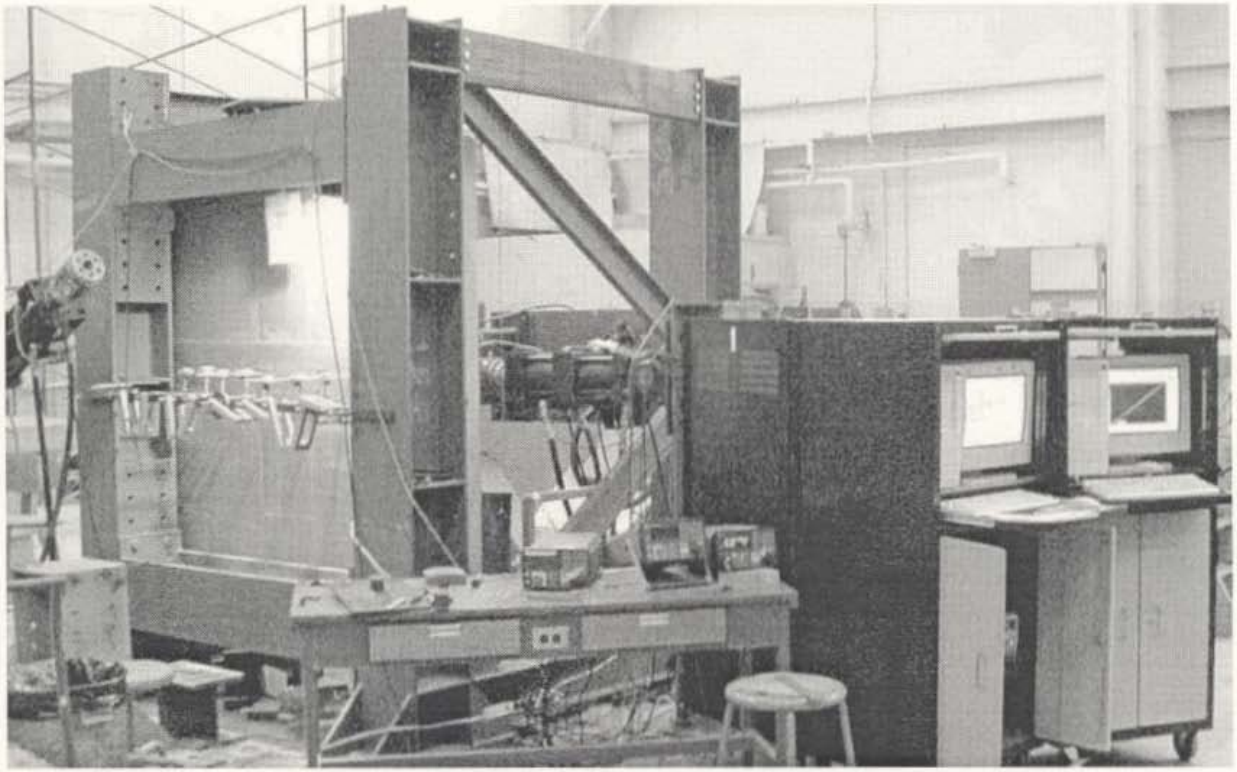

Figure 3.9: Layout of the test set–up with a centrally loaded specimen mounted in place

that were located next to the frame. These side actuators were used to apply a couple of equal and opposite monotonic (static) or cyclic lateral load, H, for specimens of Group 2 subjected to static moment or cyclic moment, respectively. The lever arm of that couple was kept at a distance of 1570–mm measured along the column stubs' axis. In the case of the cyclic moment, the two side actuators were clamped to the column stubs as shown in Figure 3.10 to allow for reversal application of the quasi–static lateral load. The maximum capacity of the central actuator was 700 kN and the maximum stroke (displacement) was 150 mm. For any of the side actuators, the maximum load capacity was about 133 kN and the maximum stroke was 150 mm.

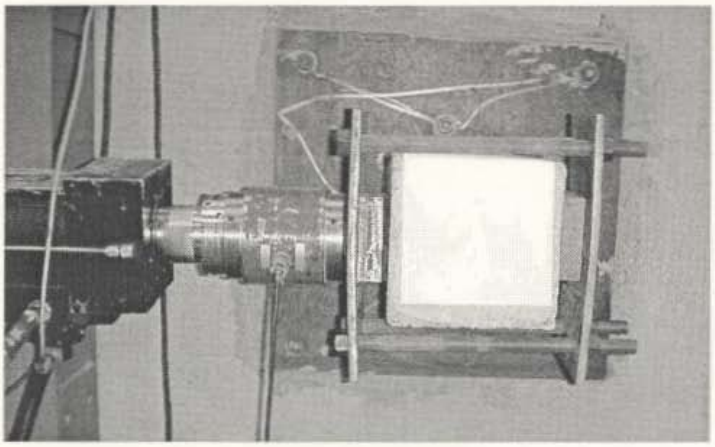

Figure 3.10: Clamping of specimens subjected to reversal lateral loads

A load cell in each actuator was used to record the load using four calibrated electrical resistance stain gages fixed to the inner cylinder of each load cell. Linear Variable Displacement Transformers (LVDTs) were built in the actuators to measure the central deflection of the slabs associated with the loads. Hydraulic pumps of maximum pressure of 20 MPa were used to supply the actuators with the pressure.

The load can be applied under either *load* or *displacement* control. In case of load control the actuator tries to maintain the most recent load value and build more loads based on a predefined load rate that cannot be exceeded irrespective of the displacement changes. Under displacement control; however, the actuator tries to maintain the recent displacement value and build more displacements based on a predefined displacement rate that cannot be exceeded irrespective to the load changes. For the central load application, it was decided to apply the load under the displacement control to prevent the sudden and uncontrolled failure at the maximum load. The rate of applying the displacement for the central actuator ranged from 0.25 to 0.50 mm/min. In case of the side actuators, the main concern was to apply equal and opposite lateral loads by each actuator at the same time. Hence, it was decided that the loads of the side actuators be applied using a load control. The rate of applying the load for each of the side actuators ranged from 0.75 to 1.25 kN/min provided that each actuator would apply the same load.

Electrical resistance strain gages, 8-mm long with a nominal resistance of 120 Ω and a gage factor of 2.070 $\pm$ 0.50% were used to measure the strains in selected locations of steel reinforcement, steel bolts, and steel plates. Figure 3.11 shows the locations of strain gages on tension and compression steel reinforcement for all specimens. The locations of the strain gages for steel bolts and steel plates are shown in Figure 3.12.

The LVDTs and the electrical strain gages were connected to a data acquisition system. The data acquisition system was programmed using the G language to apply the load and/or displacement using predefined functions. For the specimens of Group 2, two computers were used to define both the central and lateral movements of the

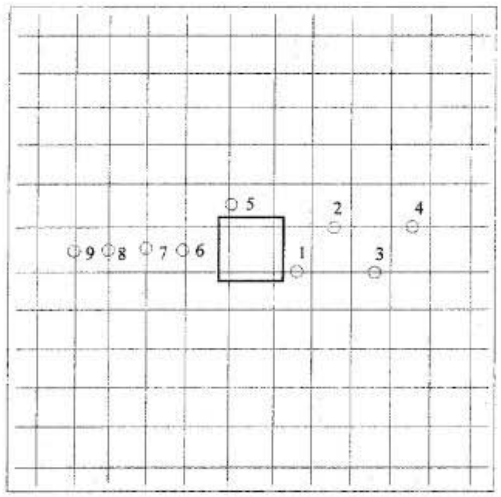

(a) Tension steel, $\rho = 0.5\%$ or 1.0%, subjected to central loading only

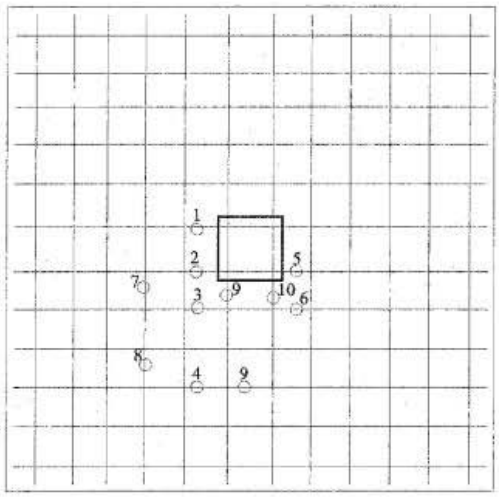

(b) Tension steel, $\rho = 0.5\%$ or 1.0%, subjected to central and lateral loading.

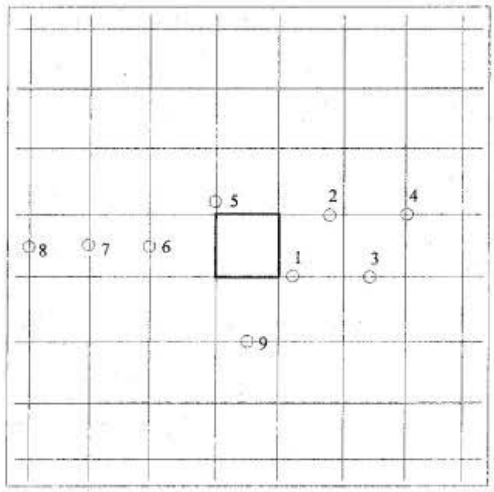

(c) Tension steel, $\rho = 0.35\%$

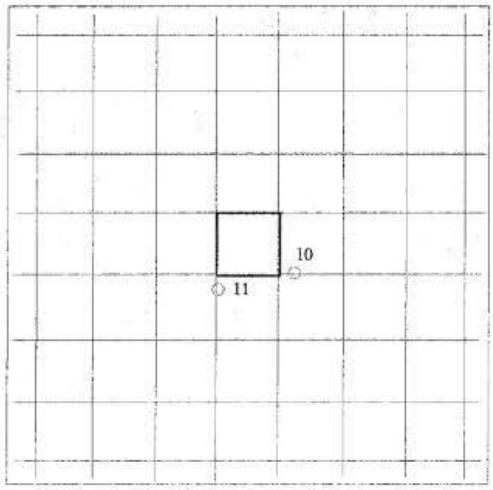

(d) Compression steel for all specimens.

Figure 3.11: Steel gages locations on tension or compression steel reinforcement for different reinforcement ratios and cases of loading.

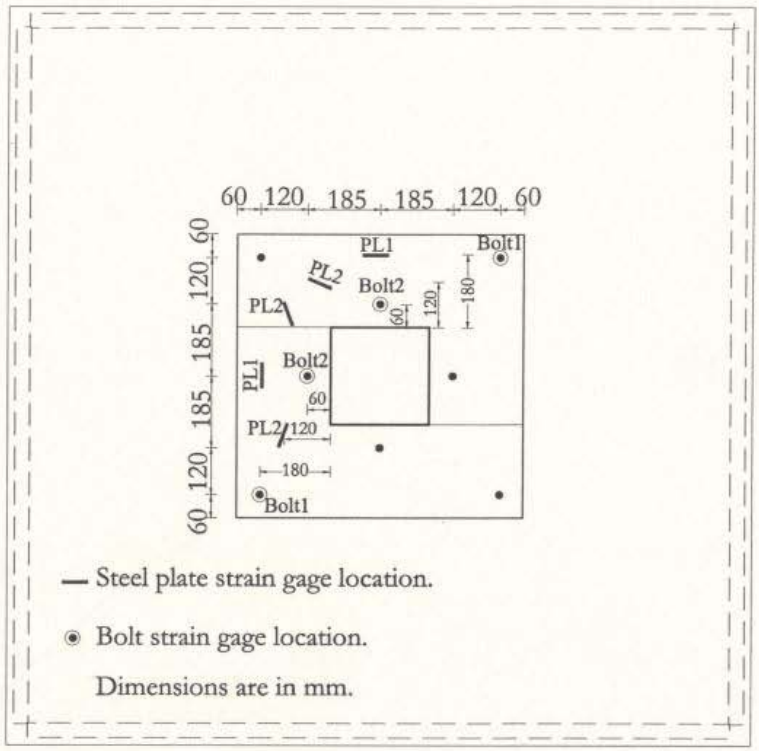

(a) Schematic locations of the gages

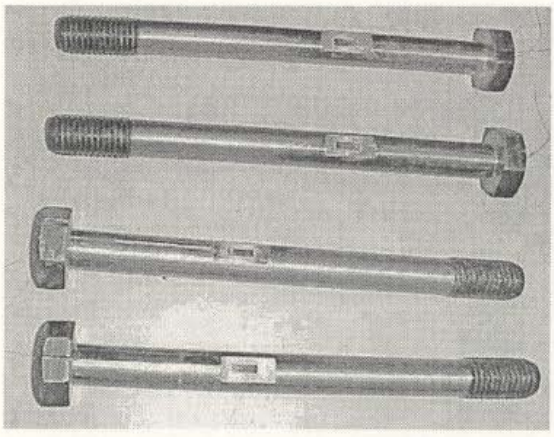

(b) Steel bolts

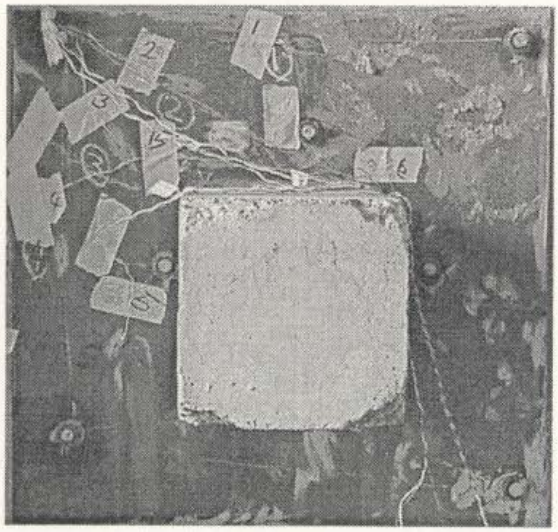

(c) Steel plates

Figure 3.12: Locations of strain gages on Pattern 2 steel plates and bolts

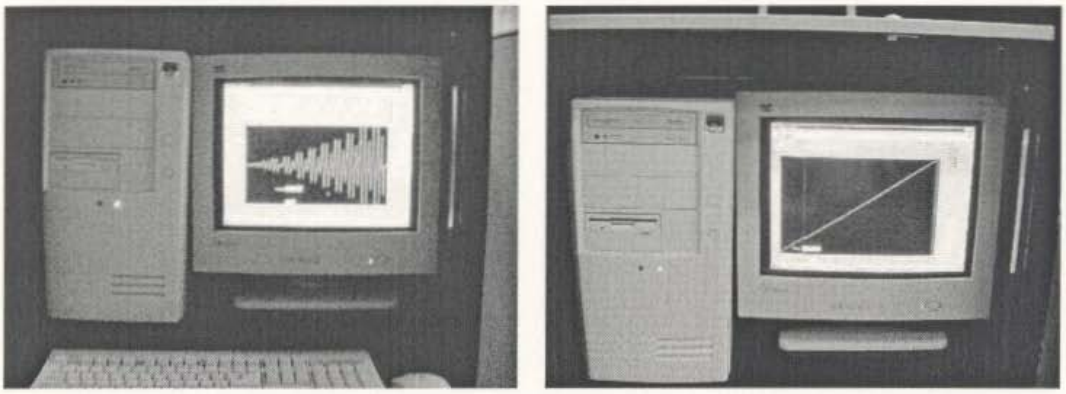

(a) Cyclic loads (b) Static loads

Figure 3.13: Computer monitors showing the type of loading

actuators simultaneously as shown in Figure 3.13. The values of load, deflection, and strains in the form of analog electrical signals, were converted through the data acquisition system to digital signals and were saved in digital computer files. One set of readings was scanned and saved every two seconds.

Nine equi–spaced dial gages were placed along the width of slabs to record the deflection profiles of specimens except for those subjected to cyclic loading as shown in Figure 3.5.

For specimens subjected to cyclic loading, a drift-routine that was limited to 22 cycles (Robertson and Durrani, 1992) was adopted. This drift routine was modified by increasing the number of cycles to 29 as shown in Figure 3.15. The increased number of cycles was necessary to accommodate possible expected improvement in the behaviour of the strengthened specimens subjected to cyclic loading.

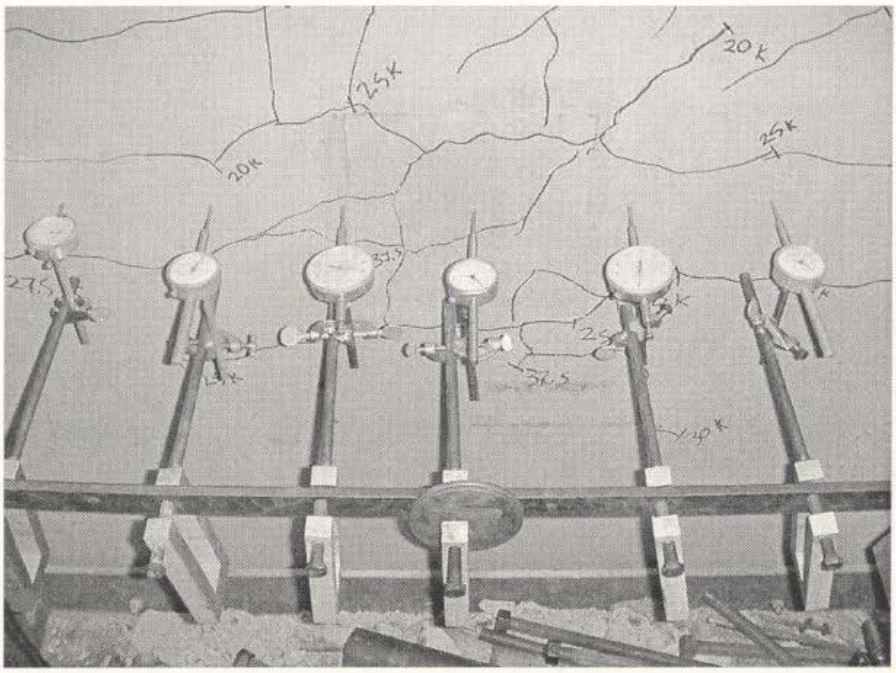

Figure 3.14: A close up of the dial gages

3.8 Test Procedure and Load Sequence

All specimens were subjected to a central load 50% of the ultimate central failure load for a reference specimen with the same reinforcement ratio as the specimen considered. This level of pre–loading represents the service loads. Specimens with reinforcement ratios of 0.35%, 0.50%, and 1.0% were initially loaded to 125 kN, 159 kN, and 210 kN; respectively. Then, the load was released and the specimens were removed from the loading frame for strengthening. This stage simulates the state of a slab in the field shored during the strengthening process. After strengthening and curing, specimens were placed in the loading frame for reloading.

For specimens of Group 1 and Group 3, the central load was applied gradually

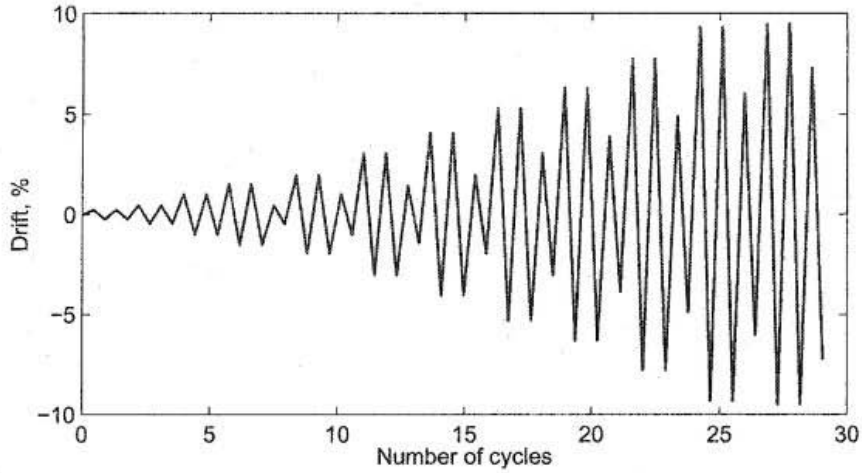

Figure 3.15: The drift routine used for specimens subjected to cyclic loading

using a ramp function until failure. For the specimens of Group 2, a central load of 90 kN was applied. This value of load (90 kN) represents the dead load subjected to a two–way slab in the field. For specimens subjected to static moment, the static lateral loads were applied simultaneously using the two side actuators, as the central load was kept constant. The maximum value of the lateral load at both sides was kept at 56 kN that produced an unbalanced static moment of 88 kN.m. As the lateral load was kept constant, the central load was increased gradually until failure. For specimens subjected to unbalanced cyclic moment, the predefined drift routine, as shown in Figure 3.16, was applied using the side actuators. The cyclic moment was applied as the central load was kept constant.

3.9 Strengthening Techniques and Procedure

3.9.1 Steel Plates and Bolts Strengthening Technique

Both the Canadian and American structural concrete codes state that the location of the critical shear perimeter in two–way slabs is at 0.5 of the effective depth of the slab (CSA–A23.3, 1994; ACI–318, 1999). However, the British code limits this value to 1.5 times the effective depth of the slab (BS 8110, 1985). A three dimensional finite element analysis of concrete slabs revealed that the critical punching–shear perimeter is located at a distance that is twice the slab depth around the column (Marzouk and Jiang, 1996). The finite element analysis findings were also supported by an experimental evidence (Marzouk and Jiang, 1997).

Based on the aforementioned research work and code provisions (CSA–A23.3, 1994; ACI–318, 1999; BS 8110, 1985), the strengthening steel plates were square with a side length of that of the column plus four times the slab depth. The thickness of the steel plates was chosen so that a reasonable equivalent increase of the slab thickness is achieved. Specimens of Group 1 were used to optimize the strengthening technique utilizing steel plates and steel bolts. The optimized system is based on bonding two L–shaped steel plates welded together to the concrete panel followed by inserting the steel bolts.

The strengthening steel plates are of nominal thickness of 6–mm and bonded to the upper and the lower surfaces of the slab using epoxy resign. The dimensions of the bonded steel plate were chosen so that it surrounds the column with a minimum distance of twice the depth from the column face. The steel plates compose a rigid zone at the position of maximum shear and flexural stresses. This rigid zone acts as a new drop panel of equivalent concrete depth equal to 2 n times the steel plate

thickness, where n is the modular ratio between steel and concrete.

Holes were pre–drilled all the way through the slab thickness and 19–mm diameter bolts were inserted immediately after bonding the steel plates. Then, the nuts were subjected to a specified torque using a calibrated torque wrench. The functions of the steel bolts were threefold: 1) to transfer the horizontal forces generated between the steel plates and concrete panels, 2) to improve the punching–shear strength since steel bolts act, with the aid of the steel plates, as vertical shear reinforcement, and 3) to improve the concrete behaviour by confining the concrete sandwiched between the steel plates due to the pre–applied torque.

3.9.2 Steel Plates and Bolts Strengthening Procedure

The reference specimens were tested to estimate the ultimate load and deflection characteristics. Each slab was loaded up to 50% of the ultimate load of the reference specimen before strengthening. The slabs were pre-drilled according to a specified distribution of bolts using a hammer drill. The drilling process was followed by roughening the slab surface using a vibrating hammer as shown in Figure 3.16. Soon after, the surface of the slab and the holes were carefully cleaned by removing the dust and fine materials using a vacuum cleaner. The 2–L–shaped steel plates are aligned and welded together. The two-part epoxy adhesive was ready to be applied on the concrete surfaces and steel plates. The surface of the steel plates was ensured to be free from oil and dust by using suitable solvent. Then, the steel plates were bonded to the concrete surfaces at both sides. Afterwards, the steel bolts were immersed in the epoxy adhesive before they were inserted inside the holes. The bolts were subjected to a torque of 441 kN.mm using a calibrated torque wrench. The strengthened specimens were left for curing one week before testing. Figure 3.17 shows a schematic of the

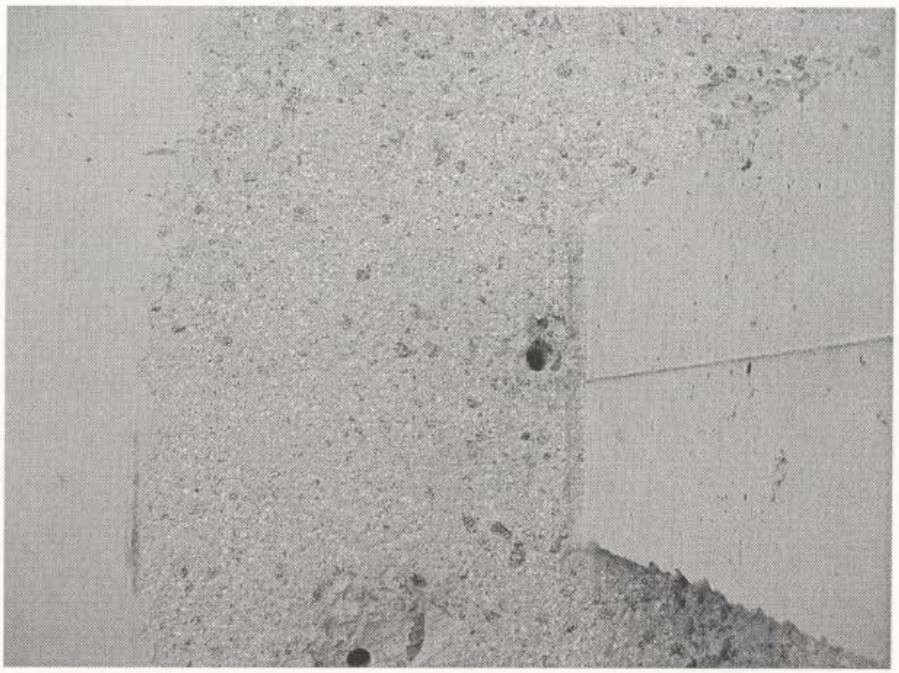

Figure 3.16: Roughening and drilling a specimen to be strengthened

different components of strengthening technique using steel plates.

3.9.3 FRP–strengthening Techniques and Procedure

The reference specimens of Group 3 were tested to estimate the capacity and the deformational characteristics of typical unstrengthened specimens. The strengthened specimens were loaded up to 50 percent of the ultimate load of the corresponding reference specimen. The surface of the specimens to be strengthened and those of the strengthening materials were carefully cleaned by removing the dust and fine materials as per the supplier's specifications. The two-part epoxy adhesive was applied on both the concrete surfaces and the strengthening materials. Then, the strengthening materials were bonded to the concrete surfaces according to the specified scheme as

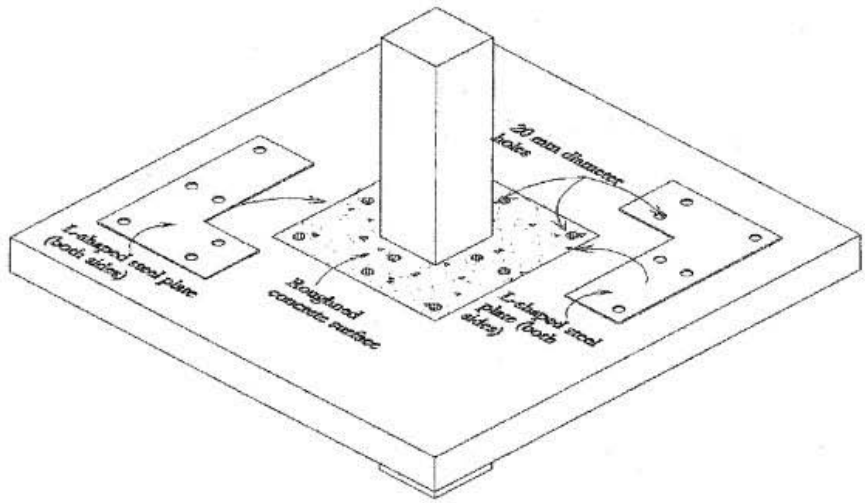

Figure 3.17: Part of the procedure of strengthening using steel plates

follows:

FRP flexural–strengthening specimens

The strengthening materials were bonded at the bottom (tension) side and extended to 50 mm before the support locations. For specimens GFRP–F–0.35% and GFRP–F–0.5%, two layers of GFRP laminates of 300–mm width were bonded to the slab surface in both directions. Specimens CFRP–F–0.35% and CFRP–F–0.5% were strengthened using CFRP strips with the same configuration as those strengthened using GFRP laminates. Transverse layers of CFRP strips were bonded at the end of the FRP strips or laminates to improve the FRP-concrete bond. Figure 3.18.a shows details of the FRP flexural–strengthening specimens

FRP Shear–Strengthening Specimens

In case of FRP shear–strengthening specimens, the CFRP strips were placed around the column to a distance of twice the concrete slab depth. Steel bolts were inserted in the slab to achieve full interaction between the strengthening material and concrete. Holes were pre-drilled all the way through the slab thickness and 19–mm diameter bolts were immersed in the epoxy adhesive before installation. The bolts nuts were subjected to a specified torque of 441 kN.mm using a calibrated torque wrench. Details of the CFRP punching–shear–strengthening specimens are shown in Figure 3.18.b.

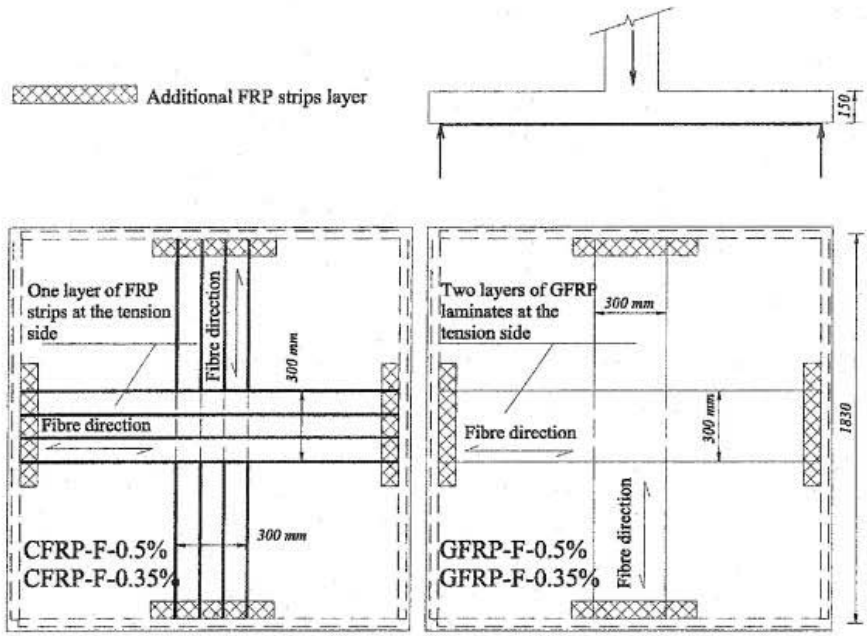

(a) FRP flexural–strengthening

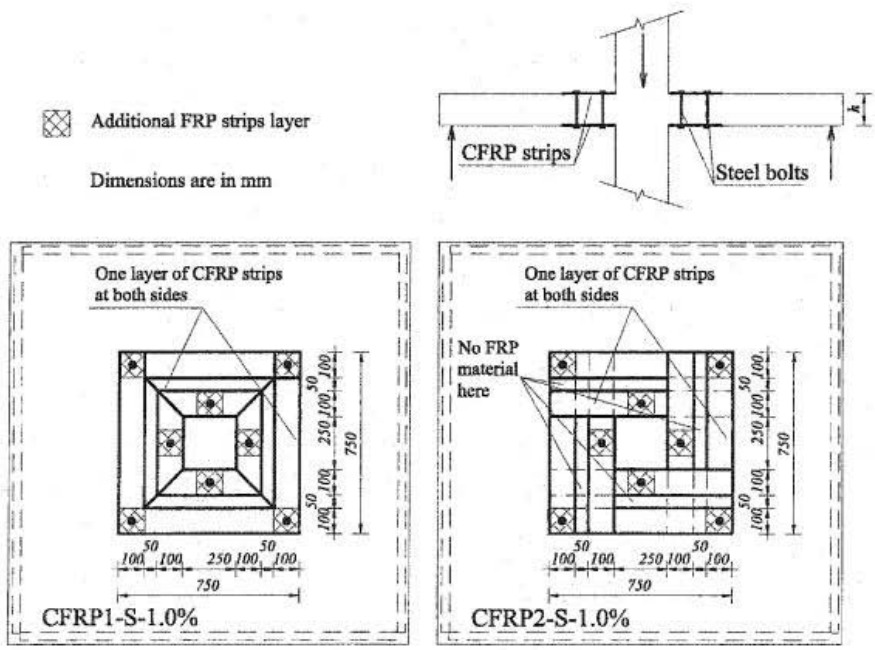

(b) CFRP shear–strengthening

Figure 3.18: Strengthening techniques using FRP materials

Chapter 4

Behaviour of Centrally Loaded Two–Way Slabs Strengthened Using Steel Plates

4.1 Introduction

In this chapter the results of centrally loaded two–way slabs strengthened using steel plates and steel bolts are introduced. Steel bolts were intended to serve as vertical shear reinforcement, since these bolts were distributed in a similar way to the shear studs in the aforementioned references.

Steel bolts were inserted in the concrete slab around the column; while steel plates were bonded to the concrete surface at the upper and lower sides of the slab using the epoxy and the tightened nuts. Hence, the functions of the steel bolts, in addition to being vertical shear reinforcement, is to ensure a complete interaction between steel plates and concrete slab. The steel bolts transmit the horizontal force between steel plates and concrete, and apply a confinement pressure on concrete. Therefore, the integration of steel plates, steel bolts, and the confining pressure on the slab make up the suggested strengthening technique. The number of steel bolts was altered to

obtain an optimum number of bolts capable of functioning as explained.

4.2 Test Results of Specimens of Group 1

The results of specimens of Group 1 are discussed in detail. This group contained specimens Ref–P–0.5%, Ref–P–1.0%, Steel–P–0.5%, Steel–P1–1.0%, Steel–P2–1.0%, Steel–P3–1.0%, Steel–P4–1.0%, and Steel–P5–1.0%.

These specimens were loaded using the central actuator of 700 kN load capacity and 150–mm stroke capacity. It was decided to apply the load under the displacement control to prevent the sudden and uncontrolled failure at maximum load as explained in Section 3.7. The rate of applying the displacement for the central actuator ranged from 0.25 to 0.50 mm/min.

The discussion of results is in terms of the central load–deflection characteristics, deflection profiles, first crack loads, yield loads, ultimate load carrying capacity, ductility, stiffness, steel reinforcement strains, steel plates and bolts strains, and failure characteristics. In addition, a verification of the design code equations is introduced in this chapter.

4.2.1 Central Load–Central Deflection Characteristics

The values of the central load and the associated central deflection were automatically stored in computer digital files during the application of the load as explained in Section 3.7. Moreover, the deflection profiles at nine different locations were arranged, as shown in Figure 3.4, along each slab's width and recorded using dial gages. Figures 4.1 and 4.2 show the complete central load–deflection curves for Group 1 specimens.

The load–deflection relationships for specimen Steel–P–0.5% and specimens Steel–P1–1.0% to Steel–P5–1.0% are presented in three stages. The first stage is the loading stage up to 50% of the associated unstrengthened reference specimen's failure load. The second stage is the unloading to zero load. Finally, the third stage is the reloading stage as specimens are loaded again until failure occurs.

The first crack of each specimen in this group was visually inspected and the corresponding load was recorded as the first crack load. Points on the central load–steel strain curves that correspond to a location of 2000 μstrain were considered yield points. This strain was measured at a location 170 mm from the center of the slab. The value of 2000 μstrain was suggested based on experimental observations of the stress–strain curve of a single rebar. Locations of the first crack loads are shown on the load–deflection relationships in Figures 4.1 and 4.2.

Central load–central deflection curves of all the specimens of Group 1 combined together are shown in Figure 4.3.a. Figure 4.3.b shows a comparison between specimens with a reinforcement ratio of 0.5% and those with a reinforcement ratio of 1.0%. Specimen Steel–P3–1.0% was used to represent the specimens with 1.0% reinforcement ratio. In these figures, only the relationships at the reloading stage, the loading after strengthening, was shown for the purpose of clarity of the results.

With regard to the central load–central deflection relationships, the slopes of the curves within the pre-cracking stage were steeper than the slopes within later stages. At the same load level, the central deflection was increased as the reinforcement ratio was decreased. The variation of the deflection values against the load was largely dependent on the reinforcement ratio. The deflection values at the first crack load varied according to the original reinforcement ratios. The average first crack

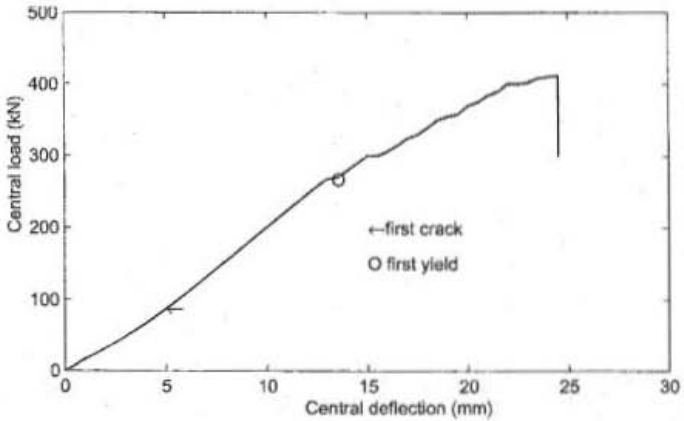

(a) Ref–P–1.0%, P_{max} =420 kN

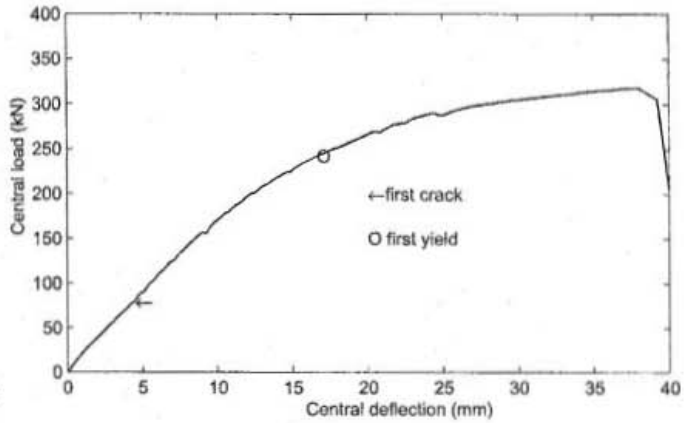

(b) Ref–P–0.5%, P_{max} =312 kN

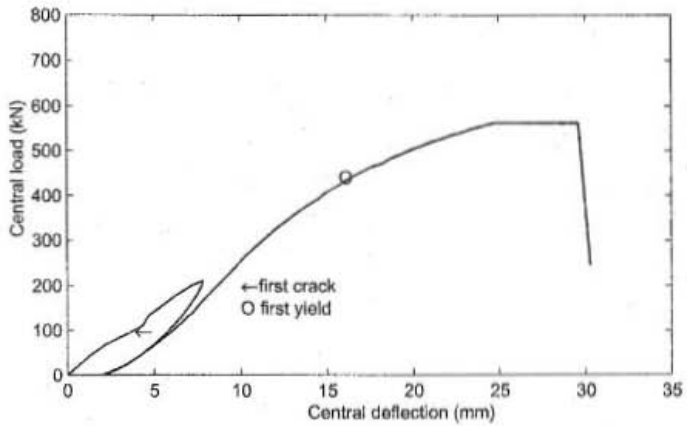

(c) Steel–P1-1.0%, P_{max} =560 kN

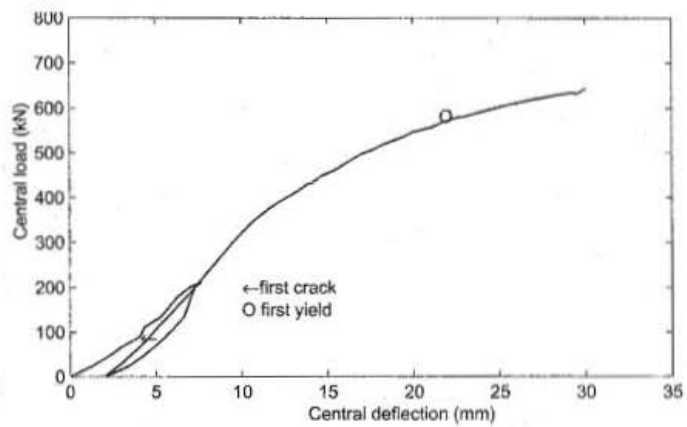

(d) Steel–P2–1.0%, P_{max} =645 kN

Figure 4.1: Load–deflection relationships for Ref–P–1.0%, Ref–P–0.5%, Steel–P1–1.0%, and Steel–P2–1.0%

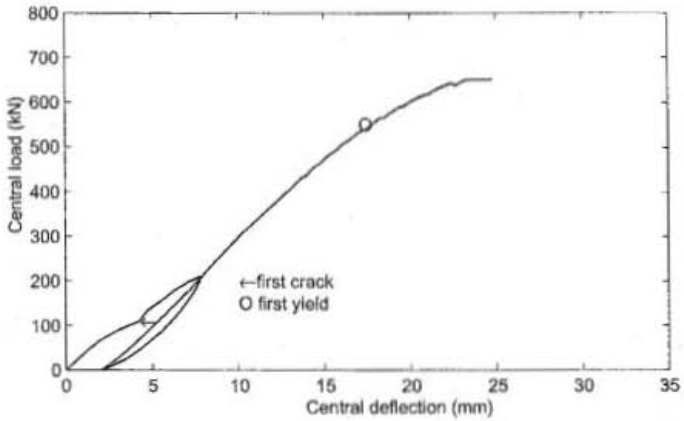

(a) Steel–P3–1.0%, P_{max} =650 kN

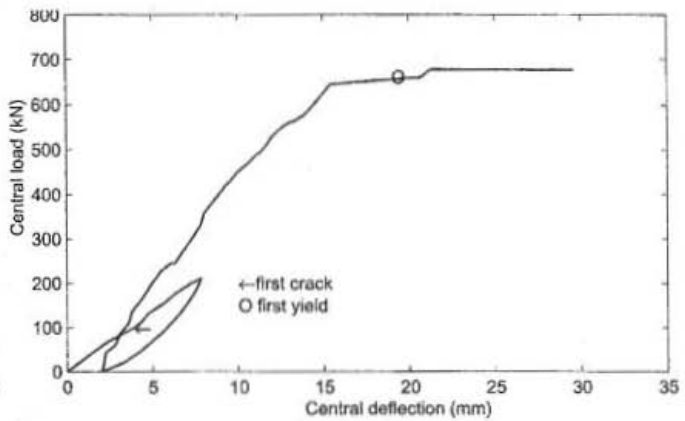

(b) Steel–P4–1.0%, P_{max} =678 kN

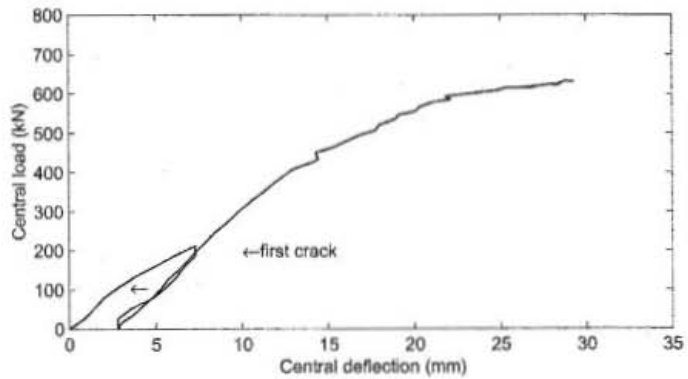

(c) Steel–P5-1.0%, P_{max} =634 kN

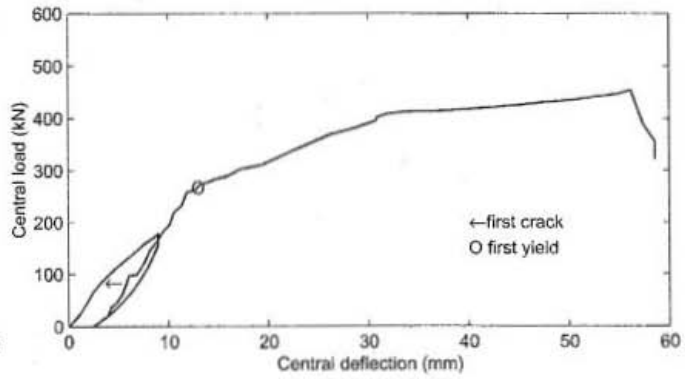

(d) Steel–P–0.5%, P_{max} =453 kN

Figure 4.2: Load–deflection relationships for Steel–P3–1.0%, Steel–P4–1.0%, Steel–P5–1.0%, and Steel–P–0.5%

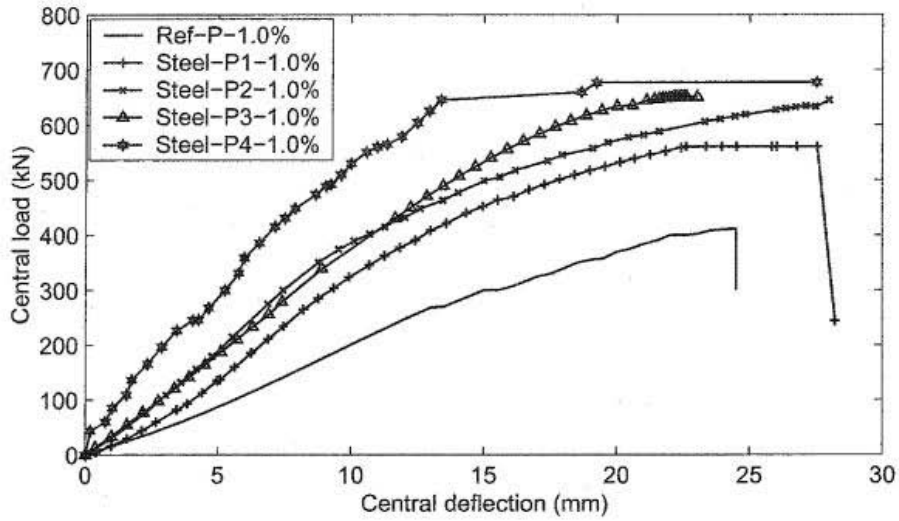

(a) Load–deflection curves for specimens with ρ =1.0%

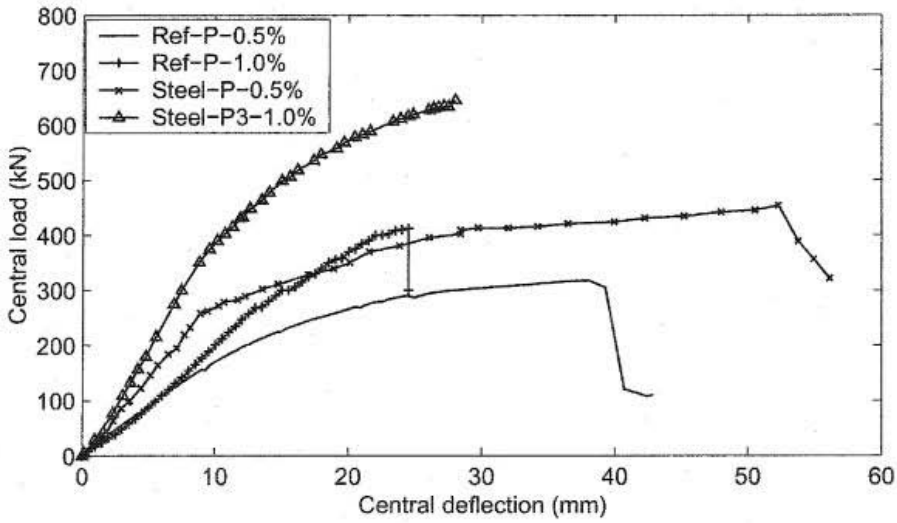

(b) Comparison between specimens with $\rho = 0.5$ % and ρ =1.0%

Figure 4.3: Load–deflection relationships of specimens of Group 1

deflection for specimens with a reinforcement ratio of 0.5% was 22.86% more than that for specimens with a reinforcement ratio 1.0%.

4.2.2 Deflection Profiles

Measuring the deflection at equal spaced locations along a specimen's width is used to construct the deflection profile for such a specimen. Deflection profiles give a global indication of the deformational response to the application of load not just at the location of the application of load but also along the slab width. In addition, using the deflection profiles, the rotational response of the slabs can be specified.

The deflection values at nine equi–spaced locations along the slabs width versus the central load were recorded as shown in Figure 3.4. Values of the central deflection at each load increment were recorded and used to determine the deflection profile at that increment. Figures 4.4 and 4.5 show the deflection profiles of the specimens of this group.

Figures 4.4.a and 4.4.b indicate that specimen Ref–P–1.0% required more load to reach the same level of deformation as that of specimen Ref–P–0.5%. It is also clear that the zone of high deformation of specimen Ref–P–0.5% is extended over a higher distance from the center of the slab than that of specimen Ref–P–1.0%. This is a clear indication that specimen Ref–P–0.5% tends to deform due to flexure unlike specimen Ref–P–1.0% that deforms due to local punching–shear at the location of the application of load.

The deflection profile of specimen Steel–P–0.5% in Figure 4.4.c showed that a stiffer behaviour was achieved due to strengthening. This stronger behaviour was represented by lower deflection values than that of associated with specimen Ref–P–0.5% at the same load level. Strengthened specimens with a reinforcement ratio

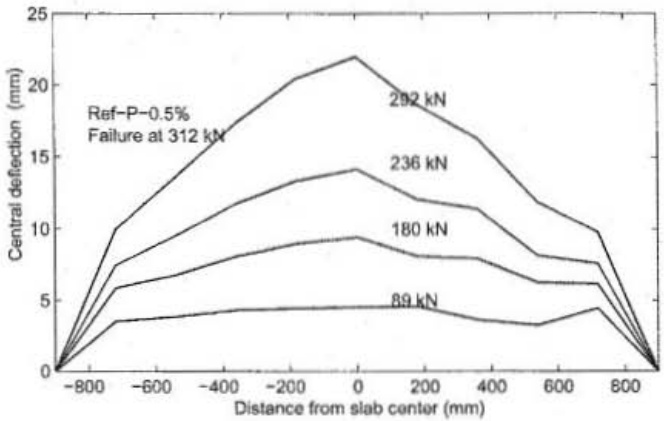

(a) Ref-P-0.5%, P_{max} =312 kN

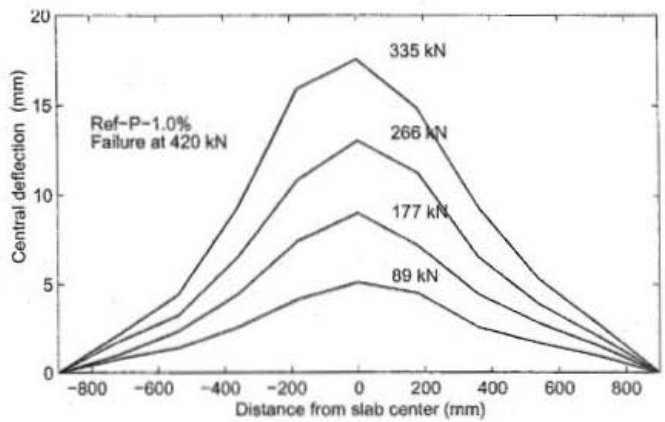

(b) Ref-P-1.0%, P_{max} =420 kN

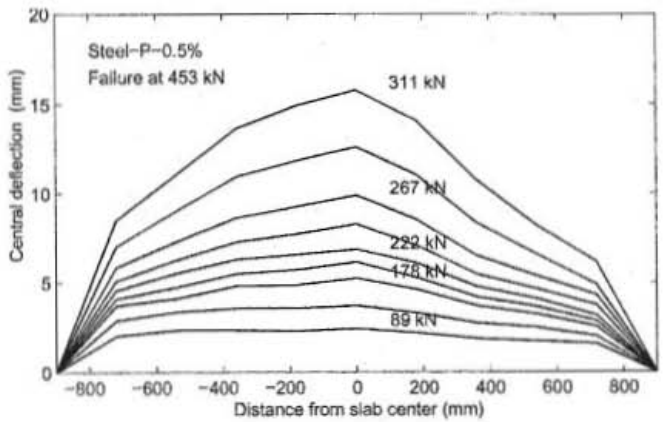

(c) Steel-P-0.5%, P_{max} =453 kN

Figure 4.4: Deflection profiles for Ref-P-0.5%, Ref-P-1.0%, and Steel-P-0.5%

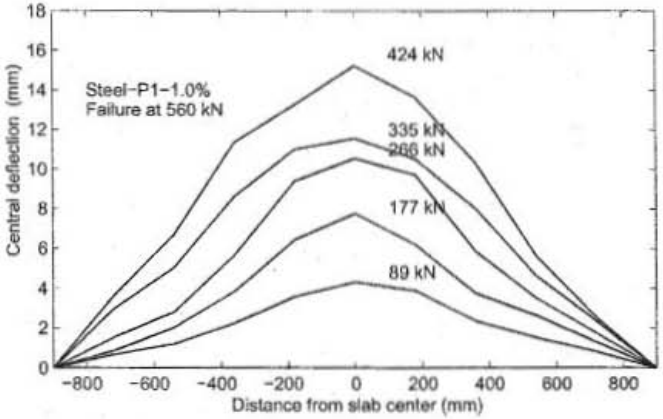

(a) Steel–P1–1.0%, P_{max} =560 kN

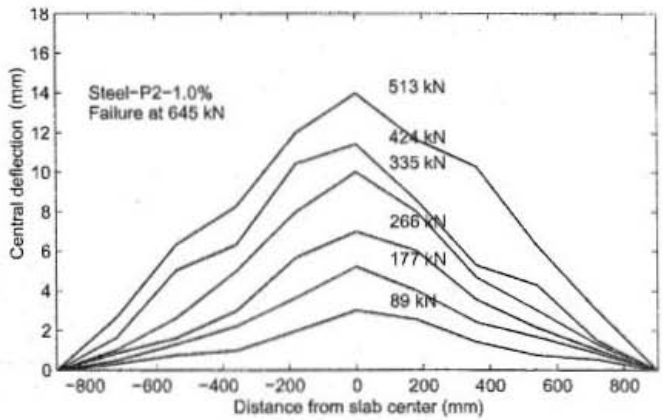

(b) Steel–P2–1.0%, P_{max} =645 kN

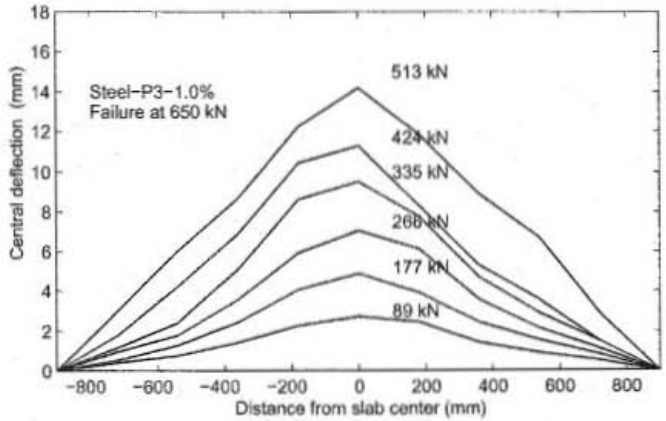

(c) Steel–P3–1.0%, P_{max} =650 kN

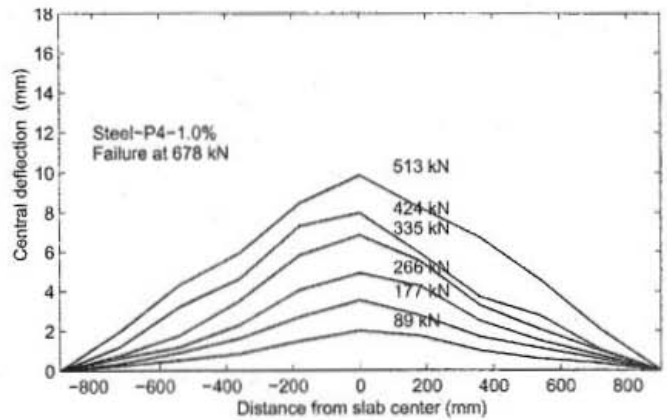

(d) Steel–P4–1.0%, P_{max} =678 kN

Figure 4.5: Deflection profiles for Steel–P1–1.0%, Steel–P2–1.0%, Steel–P3–1.0%, and Steel–P4–1.0%

of 1.0% in Figure 4.5 showed lower deflection values compared to the associated unstrengthened reference specimen, Ref–P–1.0% in Figure 4.4.b. This indicates that the strengthening technique improved the deformational response of specimens. There was not a clear effect of altering the number of steel bolts on the deflection profile of strengthened specimens with a reinforcement ratio of 1.0%.

4.2.3 Crack and Yield Loads

The crack propagation for all specimens, prior to strengthening, was traced as the load was applied. Load values that caused the first crack of tested specimens before strengthening were recorded. Specimens with a reinforcement ratio of 1.0% showed higher first crack loads compared to those with a reinforcement ratio of 0.5%. The average first crack load of specimens with a reinforcement ratio of 1.0% was 22% higher than that of specimens with a reinforcement ratio of 0.5%. The first crack loads and the associated central deflection values for all specimens prior to strengthening are shown in Table 4.1.

The yield load of the unstrengthened specimen Ref–P–1.0% was 1.53 times that of the unstrengthened specimen Ref–P–0.5%. Moreover, the yield load of the strengthened specimen Steel–P–0.5% was 1.1 times that of the unstrengthened reference specimen, Ref–P–0.5%.

The average first crack load of specimens to be strengthened using two L–shaped steel plates was 1.37 times that of the strengthened specimen with four separate steel plates. It is clear from Table 4.1 that the specimen utilized 16 bolts showed higher yield load than the others. Moreover, the average yield load of the specimens utilized 8 bolts with 2-L–shaped steel plates, Steel–P2–1.0%, showed about 32% increase in the yield load compared to that utilizes the same number of steel bolts with four

separate plates, Steel–P1–1.0%. The yield loads and the associated central deflection values for all specimens are shown in Table 4.1.

4.2.4 Ultimate Load Carrying Capacity

Regarding the influence of the reinforcement ratio on the ultimate load carrying capacity of the unstrengthened reference specimens, an increase of 27.3% was observed for specimen Ref–P–1.0% over that of specimen Ref–P–0.5% due to the increase in the reinforcement ratio from 0.5% to 1.0%.

In general, strengthened specimens showed higher ultimate load carrying capacities than the unstrengthened reference specimens. The average increase in the ultimate load carrying capacity of specimens Steel–P2–1.0%, Steel–P3–1.0%, and Steel–P4–1.0% (with Patterns 2, 3, 4, respectively in Figure 3.7) was about 56.59% higher than the ultimate load carrying capacity of the associated unstrengthened reference specimen, Ref–P–1.0%. Even specimen Steel–P1–1.0% with a different steel plates configuration (Pattern 1 in Figure 3.7) and had of the lowest gain in ultimate load carrying capacity showed 33.33% increase over that of the unstrengthened reference specimen Ref–P–1.0%. In addition, specimen Steel–P–0.5% (Pattern 2 in Figure 3.7) showed 37.5% increase in the ultimate load carrying capacity over that of the associated unstrengthened reference specimen Ref–P–0.5%.

With regard to the strengthening components' effect on the ultimate load carrying capacity of the strengthened specimens, it was observed that the steel plates had more impact on the gain of ultimate load carrying capacity than that of the steel bolts. In other words, the system was sufficient if a minimum number of bolts of eight is used. As it can be seen from Table 4.1, for specimen Steel–P2–1.0% where 8 bolts were used (Pattern 2 in Figure 3.7), an increase of the ultimate load carrying capacity of 56.55%

over the ultimate load carrying capacity of the unstrengthened reference specimen, Ref–P–1.0% was achieved. For specimen Steel–P4–1.0% (Pattern 4 in Figure 3.7), where 16 bolts were used, the gain in load carrying capacity was 64.56% compared to the associated unstrengthened specimen. Hence, a minor increase in the ultimate load carrying capacity was observed due to doubling the number of the steel bolts from 8 to 16 bolts. Hence, utilizing the eight bolts was sufficient to provide concrete confinement and complete interaction with the steel plates. Value of the ultimate load carrying capacity of each specimen of Group 1 are shown in Table 4.1.

4.2.5 Stiffness

The stiffness of a slab at any loading point is the slope of the load–deflection curve at that point. The initial stiffness, hence, is the tangent to the central load–central deflection curves. For the unstrengthened specimens, the initial stiffness was calculated at the uncracked loading. It could be expected that the effect of the reinforcement ratio to be minor. In this analysis the stiffness was calculated based on early readings of the load and deflection values at which specimens were in the pre-cracked stage. In case of the strengthened specimens, the initial stiffness were calculated at early stages of the re-loading stage. The initial stiffness values of all the tested slabs as well as the initial stiffness values of the strengthened specimens are tabulated in Table 4.1.

As expected, a clear difference was not recognized in the initial stiffness of specimens with 1.0% reinforcement ratio and that of those with reinforcement ratio of 0.5% since the concrete is in the pre–cracking stage. However, it was evident that the strengthened slabs showed an increase of the stiffness over that of the associated unstrengthened specimens. Specimen Steel–P–0.5% showed an increase of 46% of the initial stiffness over that of the associated unstrengthened reference specimen,

Ref–P–0.5%. Specimen Steel–P1–1.0% with four separate steel plates showed an increase in the initial stiffness of 33% compared to specimen Ref–P–1.0%. There was a noticeable effect of the steel plates configuration on the initial stiffness of specimens Steel–P2–1.0%, Steel–P3–1.0%, and Steel–P4–1.0%. The increase in the initial stiffness for these specimens was 98%, 109%, and 209%, respectively, over that of the unstrengthened specimen, Ref–P–1.0%.

This indicates that as the number of steel bolts was increased, the stiffness of the slabs was increased although this increase wasn't linear. The increased stiffness was attributed to the increased confinement pressure on the concrete mass around the column and the increased cross sectional area of the steel bolts as vertical shear reinforcement. That confinement pressure was due to the applied torque on each steel bolt.

4.2.6 Steel Reinforcement Strain

Measurements were made to determine the steel strain distribution at selected radii from the center of slabs. The locations of the strain gages were selected to track the variation of the steel strain with the distance from the center of the slab panel. Strain gage locations differed according to the slab reinforcement ratios and the type of the applied loads. These locations were adopted according to previous research work on slabs carried out at Memorial University of Newfoundland with the same concrete dimensions for any possible comparison (Marzouk and Hussein, 1991a; Marzouk et al., 2000a). Figure 3.11.a shows the reinforcement strain gages distribution for Group 1. The closest location of measuring the steel strain was at a location (1) that was 170 mm from the center of the slab. Measurements of the strain at that location were of a special importance since these measurements were used to define the ductility

of tested specimens as discussed in Section 4.2.8. Figure 4.6 shows samples of the typical steel strain distribution at different locations (for specimens Ref–P–0.5% and Steel–P–0.5%). As the distance from the location of a strain gage to the center of the slab was increased, the strain gages readings were decreased.

Strain readings at location (1) for all slabs of Group 1 were combined together and shown in Figure 4.7. It is clear that a stiffer behaviour is shown for specimens of higher reinforcement ratios. In addition, strengthened specimens showed stiffer behaviour compared to the associated unstrengthened specimens.

Typical steel strain profiles at different radial distances from panels centers are shown in Figure 4.8. Strain profiles of specimens Ref–P–0.5% and specimen Steel–P3–1.0% are presented in Figure 4.8 to represent the specimens of Group 1. It is clear from Figure 4.8 that the flexural strains are inversely proportional to the radial distance between the center of the slab and the position on the steel strain gage.

4.2.7 Strains in Steel Plates and Steel Bolts

Due to the restrictions on the number of channels in the data acquisition system, specimen Steel–P5–1.0% was fabricated and tested mainly to measure the strain values of steel plates and steel bolts for specimens that used Pattern 2 for strengthening as shown in Figure 3.7. It was shown in previous sections that Pattern 2 was considered the optimized pattern among the other four introduced strengthening patterns. Hence, it was important to investigate the effectiveness of that strengthening pattern further by providing extra data related to the strain distribution at locations on the steel plates and bolts. The average measured strain in the steel bolts of the specimen Steel–P5–1.0%, was estimated as 1500 μstrain due to the application of the 441 kN.m torque as a part of the strengthening technique as explained in Section 3.9. Locations

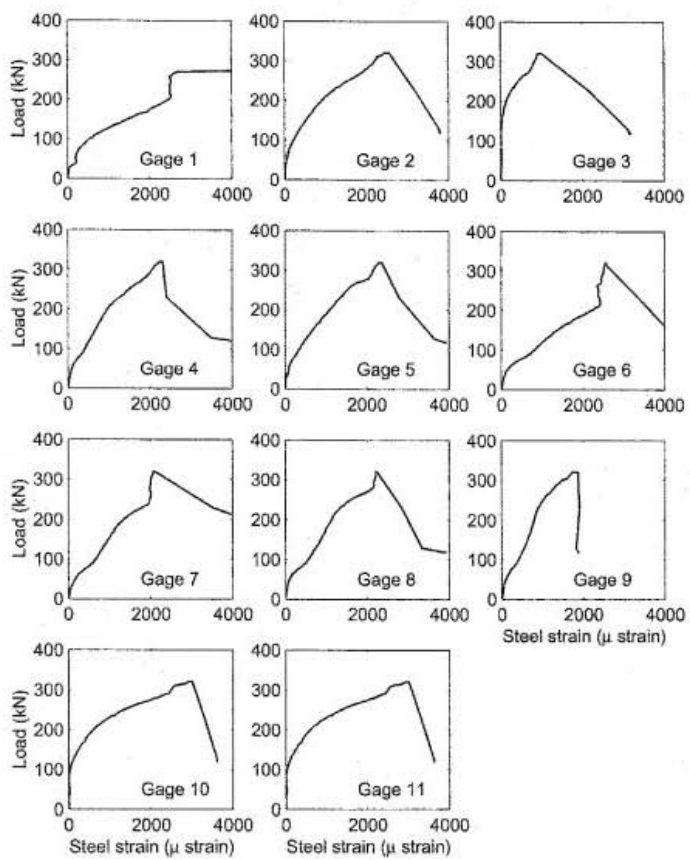

(a) Ref–P–0.5%

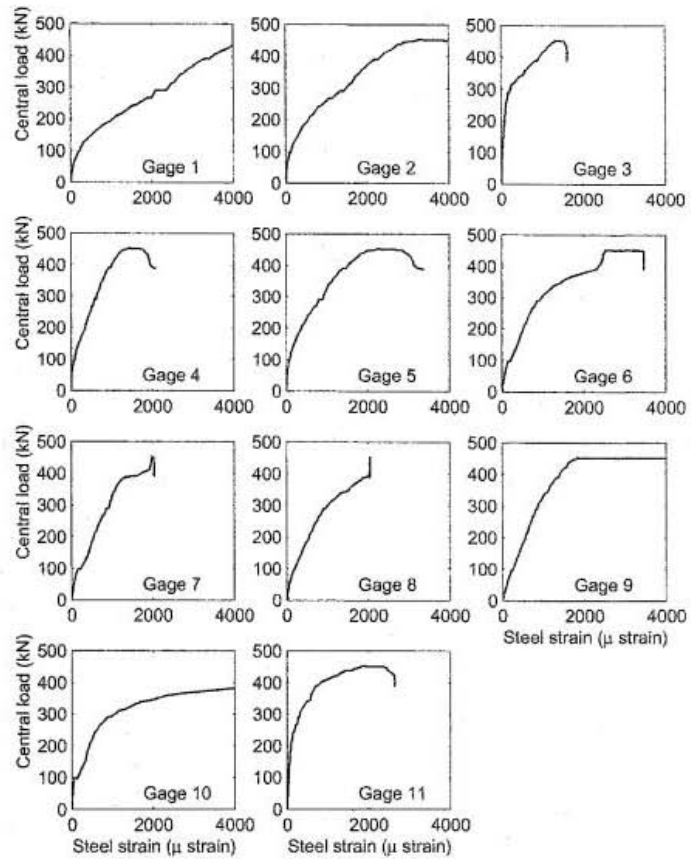

(b) Steel–P–0.5%

Figure 4.6: Samples of the typical load–steel reinforcement strain relationships

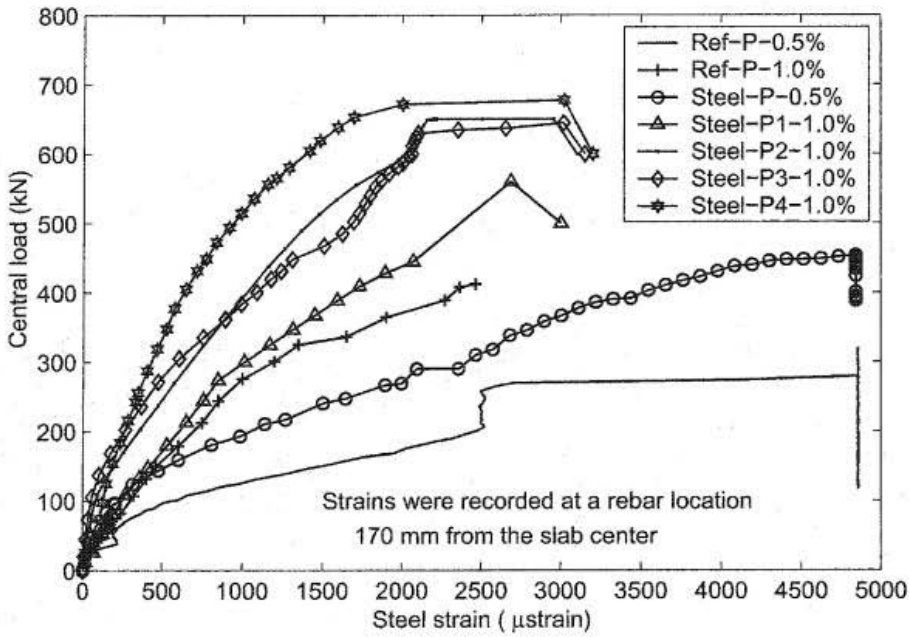

Figure 4.7: Load–steel reinforcement strain at location (1) relationships for the specimens of Group 1

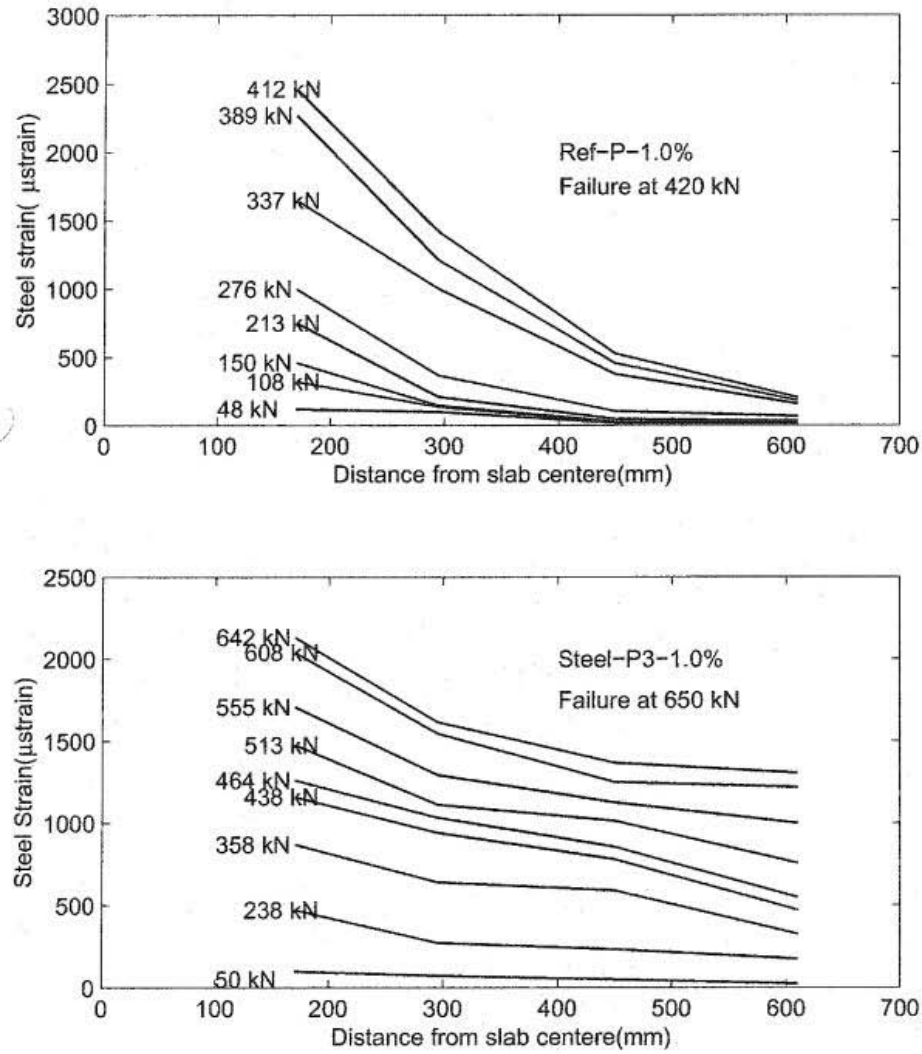

Figure 4.8: Strain profiles of specimens Ref-P-1.0% and Steel-P3-1.0%

of the strain gages placed on the steel plates and bolts are shown in Figure 3.12.

Yielding of the steel plates and steel bolts indicates an efficient utilization of the strengthening components. The average strain of bolts Bolt1 and Bolt2 versus the load is shown in Figure 4.9. Regarding the strains in the steel plates, as the load was increased the outer perimeter strain, at location PL1, was increased. In addition, the strain at a location midway the distance between inner and outer bolts, location PL2, was increased as the central load increased. The strain at location PL1 was slightly less than that at the location PL2. This result implies that the locations on the steel plate in the direction from inner to outer bolts were utilized more efficiently that those located along the outer perimeter. The steel strains in the plates at locations PL1 and PL2 are shown in Figure 4.9. Hence, the suggested dimensions of the steel plates and the configuration of steel bolts of Pattern 2, that was utilized in specimens Steel–P2–1.0% and Steel–P5–1.0%, ensures enhancement of the overall behaviour of slabs by complete functioning of the steel plates and steel bolts.

4.2.8 Ductility and Energy Absorption

Displacement ductility is defined as the ratio between the deflection at the ultimate load and that at the yield load (Geng et al., 1998; Marzouk and Hussein, 1991a; Marzouk et al., 1996). Steel reinforcement strain gages were used to record steel strain values versus the central loads. Figure 4.7 shows the steel strain distribution for tested specimens at location (1) in Figure 3.11.a. Points on the load–steel strain relationships in Figure 4.7 that correspond to a load at which steel strain reaches a value of 2000 μstrain are considered yield points for each specimen.

The displacement ductility of the strengthened specimen Steel–P–0.5% was 73% higher than that of the associated unstrengthened reference specimen, Ref–P–0.5%.

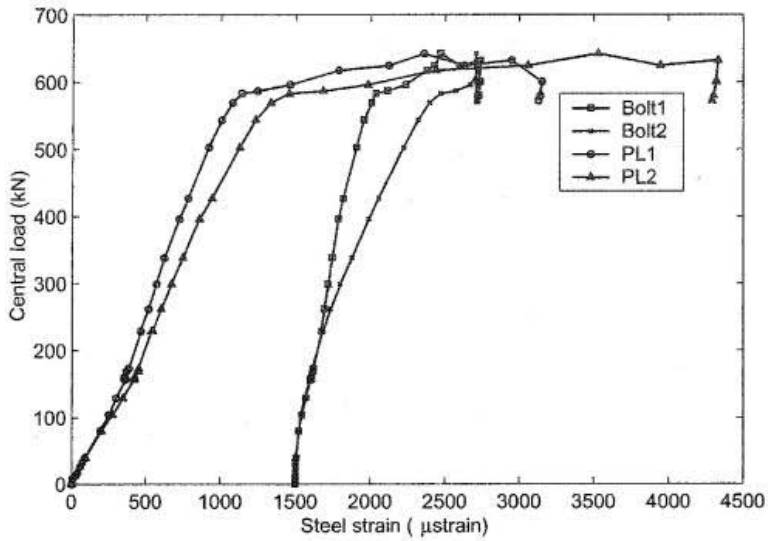

Figure 4.9: Load–strain distribution of steel bolts and plates

On the other hand, the average ductility of strengthened specimens, that have a reinforcement ratio of 1.0 %, specimens Steel–P1–1.0%, Steel–P2–1.0%, Steel–P3–1.0%, and Steel–P4–1.0%, was about 29% of that of the associated unstrengthened reference specimen Ref–P–1.0%. The displacement ductility indices are summarized in Table 4.1.

Energy absorption is one of the important deformational characteristics of two–way slabs. The definition of the energy absorption is the area under the load–deflection curve of a tested specimen. The integration of the area under the load–deflection relationships was carried out numerically of the data of the load versus deflection. For the unstrengthened specimens, Ref–P–0.5% and Ref–P–1.0%, the numerical integration was made along the whole load history. However, for the strengthened specimens, the integration was made for the part of the curve at the reloading

stage neglecting the first two loading stages, the initial loading and unloading stages. A considerable increase in the energy absorption values was observed due to the strengthening. The energy absorption of the strengthened specimen Steel–P–0.5% was 2.04 times that of the reference unstrengthened specimen Ref–P–0.5%. In addition, the average of the values of the energy absorption for specimens Steel–P1–1.0% to Steel–P5–1.0% was 2.07 times the value of the energy absorption of the reference unstrengthened specimen Ref–P–1.0%. Table 4.1 shows the values of the energy absorption of the entire number of specimens of this group.

4.2.9 Failure Characteristics

The tension reinforcement of a specimen may reach the yield point at locations around the column and far from the center of the specimen and extended to a certain distance called "punching radius". Larger punching radii are associated with the flexural failure mode than those associated with punching–shear failure mode (Marzouk et al., 2001).

The mode of failure of the unstrengthened reference specimen, Ref–P–1.0% was classified as ductile punching–shear failure where the failure mode was not either bending (flexural) failure or punching–shear failure. However, for the unstrengthened reference specimen with reinforcement ratio of 0.5%, Ref–P–0.5%, the mode of failure was classified as flexural mode of failure. The strengthened specimens with a reinforcement ratio of 1.0%, more precisely those with L–shaped steel plates, had a better utilization of the flexural steel reinforcement than the associated unstrengthened reference specimen, Ref–P–1.0%. The strengthening technique contributed to transferring the mode of failure from a punching–shear mode of failure to a flexural mode of failure. The utilization of the reinforcement was represented by a larger crack

Table 4.1: Test results of Group 1 specimens

Title	Crack load, P_{cr}, kN	Deflection at crack load, δ_{cr}, mm	Yield load, P_y kN	Deflection at yield load, δ_y, mm	Ultimate load, P_u, kN	Deflection at ultimate load, δ_u, mm	Energy Absorption, ψ, kN.mm	Stiffness, K, kN/mm	Ductility index	Steel strain, $\varepsilon_{su}(10^6)$
Ref–P–0.5%	79	5.30	242	16.63	312	38.08	9473	18.50	2.29	3286
Ref–P–1.0%	89	4.85	370	20.09	420	24.50	5950	20.08	1.22	2463
Steel–P–0.5%	82	5.02	267	13.21	453	52.27	19414	27.00	3.96	4841
Steel–P1–1.0%	100	3.85	440	15.70	560	27.00	10424	24.10	1.72	2684
Steel–P2–1.0%	85	4.80	582	21.70	645	28.00	11711	35.90	1.30	2950
Steel–P3–1.0%	111	4.25	560	17.0	650	23.00	11722	37.80	1.35	3015
Steel–P4–1.0%	100	3.90	670	19.0	678	27.50	14521	55.90	1.45	3020
Steel–P5–1.0%	106	3.65	—	—	634	28.84	11570	40.24	1.72	2684

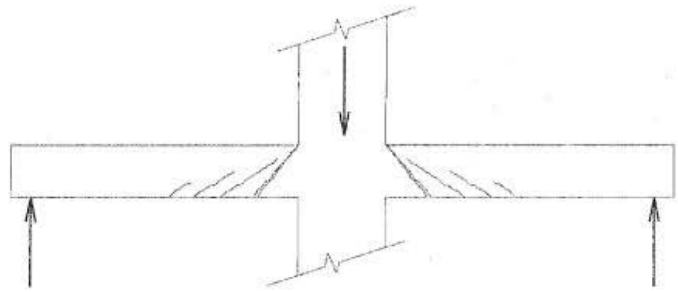

(a) Unstrengthened with ρ=1.0%

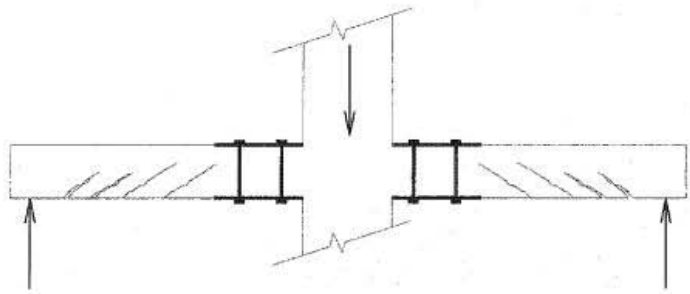

(b) Strengthened with ρ=1.0% using 2-L shaped steel plates.

Figure 4.10: Schematic illustration of the difference in the failure mode due to the strengthening

radius due to straining and utilizing of the steel reinforcement.

The difference in the failure modes of the unstrengthened specimen, Ref–P–1.0%, and that of the strengthened specimens, Steel–P1–1.0%, Steel–P2–1.0%, and Steel–P3–1.0% is shown schematically in Figure 4.10 based on the observed crack pattern.

This was clearly observed for specimen Steel–P3–1.0%. Comparing the mode of failure of specimen Ref–P–1.0% (Figure 4.11) and that of specimen Steel–P3–1.0% (Figure 4.15), it is evident that the steel reinforcement was mobilized up to the slab edge as the interfacial contact with concrete was failed. Reaching such a level of

mobilization was noticed for the strengthened specimens rather than the unstrengthened reference specimens. For the strengthened specimen Steel–P–0.5%, more ductile behaviour was noticed compared to the associated unstrengthened specimen, Ref–P–0.5%. Figures 4.11 to 4.17 show specimens of this group at failure.

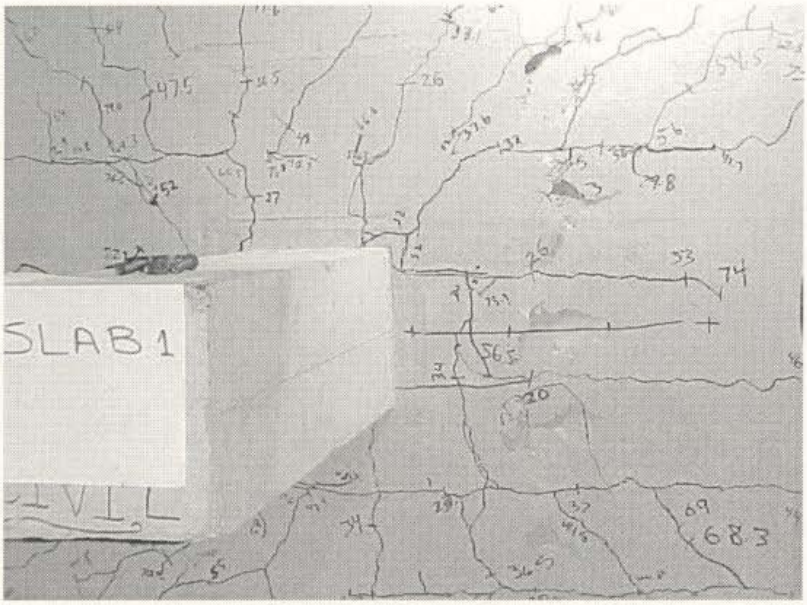

Figure 4.11: Specimen Ref–P–1.0% after final testing

4.3 Evaluation of the Ultimate Load Carrying Capacity

Theoretically, two possible modes of failure are expected, the punching–shear mode and the flexural mode. However, the strengthening technique changed the mode of failure from punching–shear failure to a flexural failure. The rigid zone created by the steel plates eliminated the punching–shear failure; therefore, the flexural reinforcement was fully utilized as shown in Figure 4.16. To verify the codes' provisions

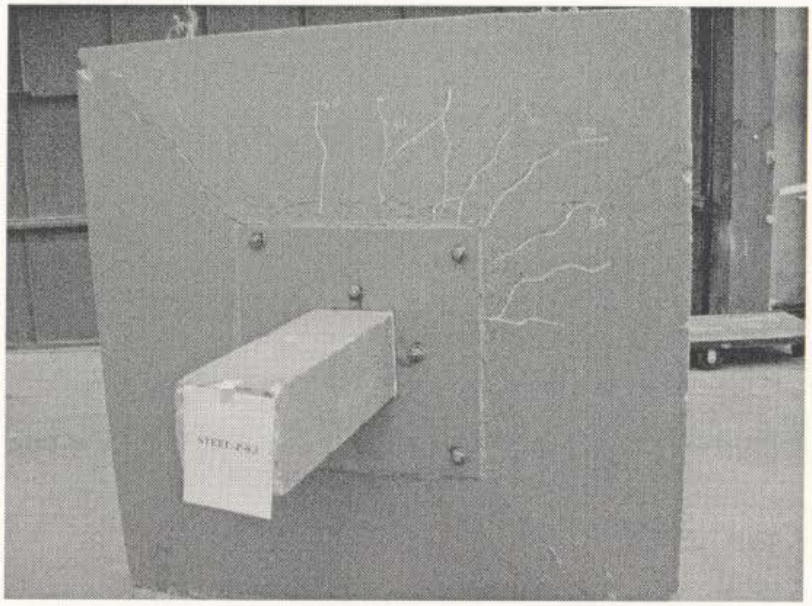

Figure 4.12: Specimen Steel–P–0.5% after final testing

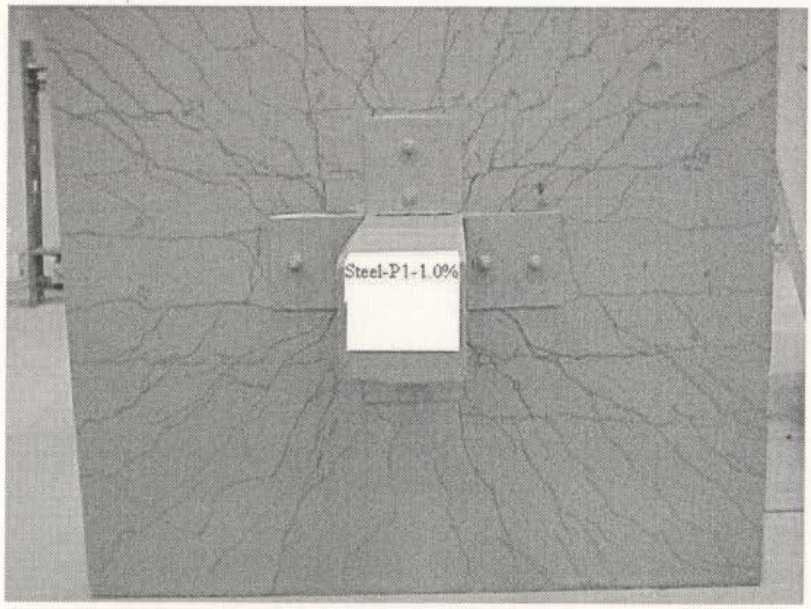

Figure 4.13: Specimen Steel–P1–1.0% after final testing

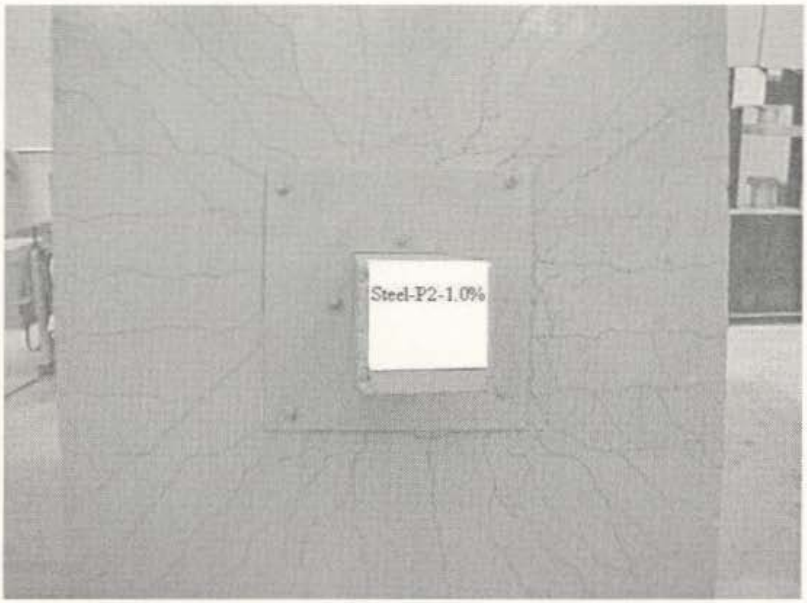

Figure 4.14: Specimen Steel–P2–1.0% after final testing

with the experimental work, both the flexural and punching–shear capacities are to be evaluated. The ultimate capacity of the centrally loaded slabs can be calculated using available design equations in both the CSA and ACI codes (CSA–A23.3, 1994; ACI–318, 1999). Both punching–shear capacity and the flexural capacity can be evaluated at the critical section and the least of both determines the ultimate capacity of the slabs.

For the calculation of the punching–shear capacity, the critical shear perimeter is calculated assuming that the critical section is located at a distance $l_p/2$ from the center of the slab for the strengthened specimens rather than $(c + d)/2$. The critical section at $(c + d)/2$ determines the location of the critical section for the unstrengthened specimens.

Hence; the punching–shear capacity can be evaluated using the following formula:

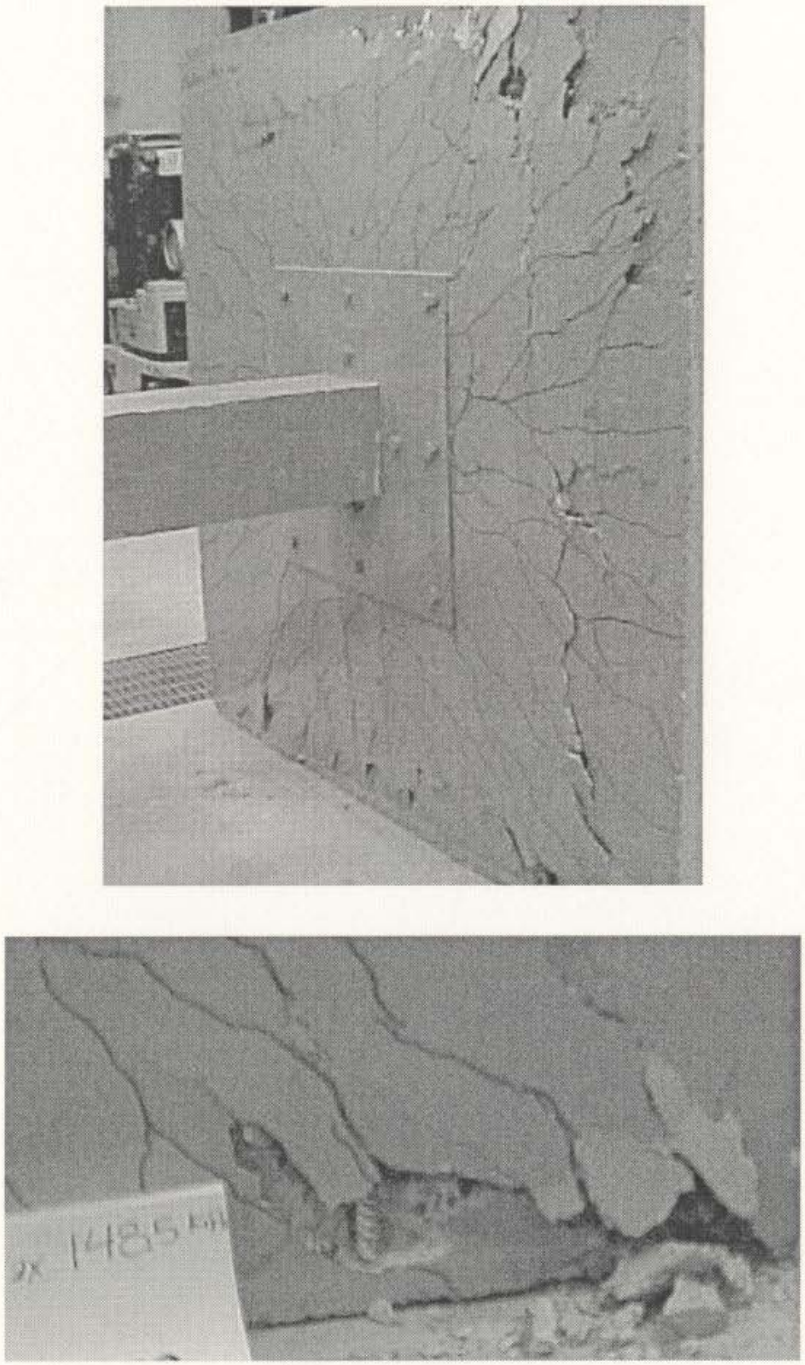

Figure 4.15: Specimen Steel–P3–1.0% after final testing

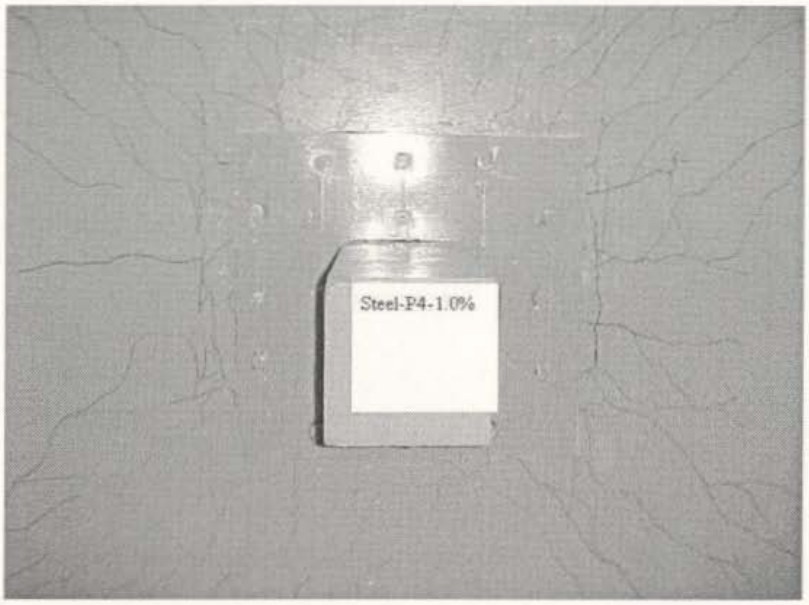

Figure 4.16: Specimen Steel–P4–1.0% after final testing

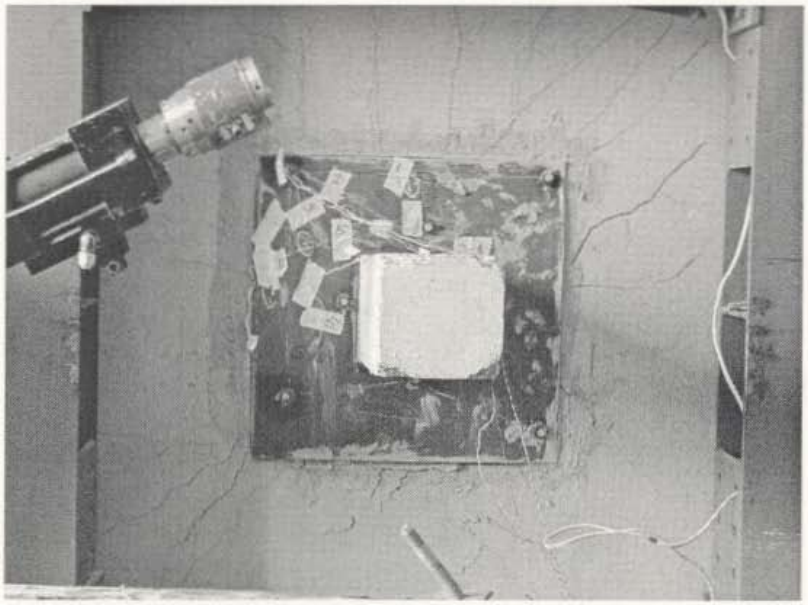

Figure 4.17: Specimen Steel–P5–1.0% after final testing.

$$V_c = v_c A_c \tag{4.3.1}$$

Where: $A_c = 4\,d\,l_p$ and $4\,d\,(c + d)$ in case of strengthened and unstrengthened specimens, respectively.

The flexural capacity of the tested slabs can be evaluated using the yield line theory. A modification is made to the original equation presented by Rankin and Long in which the flexural capacity was evaluated using the following equation and considering (Rankin and Long, 1987);

$$P_{flex} = 8\,M_b \left(\frac{L}{a-c} - 0.172 \right) \tag{4.3.2}$$

Where L and a are the length and support–to–support distance of the slab. Equation 4.3.2 is based on the virtual work done by the actions of the yield lines. For the present case, the column size dimension c is replaced by the width of the steel plate, l_p. This effective width could be assumed as shown in Figure 4.11. Therefore, the yield line flexural capacity of the strengthened slabs can be written as follows:

$$P_{flex} = 8\,M_b \left(\frac{s}{a-l_p} - 0.172 \right) \tag{4.3.3}$$

M_b is calculated at the unstrengthened section of the slab as follows:

$$M_b = M_{b1} + M_{b2} \tag{4.3.4}$$

$$M_{b1} = b\,d^2 \left(\rho - \rho' \right) f_y \left[1 - 0.59\,\frac{\left(\rho - \rho' \right) f_y}{f'_c} \right] \tag{4.3.5}$$

$$M_{b2} = \rho'\,f_y\,d \left(d - d' \right) \tag{4.3.6}$$

Results of this approach, in terms of the flexural and punching–shear capacities are compared with the experimental work results in Table 4.2. It is indicated in this

table that there is a good agreement between the experimental results and the simple prediction of the CSA and ACI codes regarding the ultimate load carrying capacity of specimens with 1.0% reinforcement ratio and the mode of failure of the slabs (CSA–A23.3, 1994; ACI–318, 1999). The predicted values of the ultimate load carrying capacities for specimens that have a reinforcement ratio 0.5% was underestimated by the codes' prediction. The contribution of the steel bolts is introduced using an empirical equation that modifies the ultimate load capacity calculated using the codes' provisions. It is assumed that a minimum number of 8 bolts are sufficient to achieve the solid part around the column and therefore the critical section can be shifted to the steel plate edge as explained earlier. Hence, any steel bolts in excess of the 8 bolts can contribute to increase the load capacity. An empirical equation based on the experimental test results is derived to consider the effect of the number of bolts. In this equation N_B is the number of bolts that should not be less than 8 bolts. The corrected shear force due to the steel bolts is:

$$V_{cal,corr} = 0.9392\, e^{0.0073\, N_B}\, V_{cal} \tag{4.3.7}$$

4.4 Summary and Conclusions

The effectiveness of two different configurations of steel plates and four different arrangements of steel bolts were evaluated. The following conclusions are drawn for the strengthened two–way slabs.

1. The suggested dimensions of the rehabilitating steel plates and the number of the steel bolts were efficient as a strengthening technique. The steel plate side

Table 4.2: Code evaluation of the load capacity of centrally loaded specimens

Specimen	f_c', MPa	N_B	V_{test}, kN	V_{cal}, kN		$V_{cal,corr}$, kN		$V_{test}/V_{cal0,corr}$		Mode of failure
				ACI	CSA	ACI	CSA	ACI	CSA	
Ref–P–0.5%	34	—	312	225	225	225	225	0.72	0.72	Flexure
Ref–P–1.0%	33	—	420	357	430	357	430	0.85	1.02	Punching–shear
Steel–P–0.5%	34	8	453	335	335	333	333	0.74	0.74	Flexure
Steel–P2–1.0%	37	8	645	704	699	700	695	1.09	1.08	Flexure
Steel–P3–1.0%	33	12	650	704	699	721	716	1.11	1.10	Flexure
Steel–P4–1.0%	30	16	678	704	699	743	737	1.10	1.09	Flexure
Steel–P5–1.0%	34	12	634	704	699	700	695	1.10	1.10	Flexure

dimension should equal the column size plus four times the slab depth. A minimum of 6 mm is recommended for the plate thickness for efficient strengthening. A minimum of eight bolts is recommended with four bolts on the outer perimeter of the steel plate and four bolts on the inner perimeter of the steel plate near the column.

2. Both of the yield load and the ultimate load carrying capacity were increased due to the strengthening process. For specimens with 1.0% reinforcement ratio, the average increase of the yield load is 50 % of the yield load of the unstrengthened reference specimen. Moreover, the average increase of the ultimate load of the strengthened specimens over that of the unstrengthened specimen is 53%. However, the increase of the ultimate load of the specimens with separate steel plates, Steel-P1–1.0%, is evaluated at 36%. The use of separate steel plates is not recommended for the strengthening of two–way slabs.

3. For the specimen with a reinforcement ratio of 0.5%, the strengthening contributed to increase the yield load and the ultimate load by 10.33% and 45.19%, respectively.

4. The minimum number of steel bolts that is needed to ensure full interaction between steel plates and slab is eight bolts. However, an increase in the ultimate capacity of about 5% was recorded due to increasing the bolts from eight to 16 bolts.

5. The steel plates with the suggested dimensions and steel bolts with the suggested configuration were well utilized. The strain in the steel plates and bolts indicated a complete composite action and interaction between concrete and

steel plates.

6. The strengthened specimens were stiffer than the unstrengthened reference specimen. Moreover, the average ductility of the strengthened specimens was about 29% more than the ductility of the unstrengthened reference specimen.

7. The energy absorption of the strengthened specimens is greatly increased due to the strengthening process. The average increasing of the energy absorption of the strengthened specimens over that of the unstrengthened reference specimen was about 100%.

8. A simple expression based on the equivalent concrete depth can be used to estimate the shear capacity of the strengthened slabs. The yield line theory shows a good agreement with the experimental results in terms of the ultimate flexural capacity of the strengthened specimens.

Chapter 5

Behaviour of Steel Strengthened Two–Way Slabs under Different Types of Loading

5.1 Introduction

In this chapter the results of a further application of the proposed strengthening technique are presented for the case of specimens subjected to different loading conditions are provided. The strengthening technique is composed of the integration of steel plates and steel bolts that work as a unit to enhance the performance of two–way slabs against excessive flexural and shear stresses due to the combination of either central loads plus static or cyclic moments. The strengthening technique could be adopted in multistory buildings that are subjected to unbalanced static or cyclic moments in addition to the central gravity loads.

This chapter provides further details on the application of a strengthening technique using steel plates and steel bolts of specimens of Group 2. The tested slabs of this group were subjected to a combination of either central load and unbalanced

static or cyclic moments. This group contains specimens the unstrengthened specimens Ref–M–0.5%, Ref–M–1.0%, Ref–C–0.5%, and Ref–C–1.0% and the strengthened specimens, Steel–M–0.5%, Steel–M–1.0%, Steel–C–0.5%, Steel–C–1.0%. The discussion is divided into two main parts. The first part is a discussion on specimens subjected to a combination of central load and unbalanced static moments and the second part is a discussion of specimens subjected to a combination of central loads and unbalanced cyclic moments.

5.2 Specimens Subjected to Static Moment

In the following discussion, the results of specimens in Group 2 that were subjected to a combination of central loads and unbalanced static moment are discussed in detail. This group contains specimens Ref–M–0.5%, Ref–M–1.0%, Steel–M–0.5%, and Steel–M–1.0%. For the central load application, it was decided to apply the load under the displacement control to prevent the sudden and uncontrolled failure at the maximum load. The rate of applying the displacement for the central actuator was ranged from 0.25 to 0.50 mm/min. In case of the side actuators, the main concern was to apply equal and opposite lateral loads by each actuator at the same time. Hence, it was decided that the loads of the side actuators be applied using a load control. The rate of applying the load for each of the side actuators ranged from 0.75 to 1.25 kN/min provided that each actuator would apply the same load.The discussion is focused on the load–deflection characteristics, ductility, stiffness, steel reinforcement details, and failure characteristics.

5.2.1 Load–Deflection Relationships and Deflection Profiles

The values of the central load and central deflection were automatically stored in computer digital files during the application of load using the LVDT's. Moreover, the deflection profiles at nine different locations arranged as shown in Figure 3.5 along each slab's width were recorded using dial gages. Figure 5.1 shows the complete load–deflection curves for specimens Ref–M–0.5%, Steel–M–0.5%, and Steel–M–1.0%. Figure 5.2 combines the load–deflection curves for those three specimens as well as specimens from Group 1 for comparison.

The load–deflection relationships for specimens Steel–M–0.5% and Steel–M–1.0% are presented within five stages. The first stage is the initial central loading stage until 50% of ultimate load carrying capacity of the associated unstrengthened reference specimen while the second stage is the unloading of the central load to zero. The third stage is the central reloading until a value of the central load of 97 kN. Stage 4 starts by maintaining the central load level while applying the lateral load that causes a pre-specified unbalanced moment. Finally, stage five starts by maintaining the lateral load level while increasing the central load gradually until failure occurs.

The first crack of each specimen in this group was visually inspected and the corresponding load was recorded as the first crack load. Points on the central load–steel strain curves that correspond load values at which steel strains at a certain location reach a value of 2000 μ strain were considered yield points. The location at which the steel strain was measured was 170 mm from the center of the slab and the value of 2000 μ strain was suggested based on experimental observations of the load-strain curve of a single rebar. Locations of the first crack loads are shown on the load–deflection relationships in Figure 5.1. The load–deflection curves of the

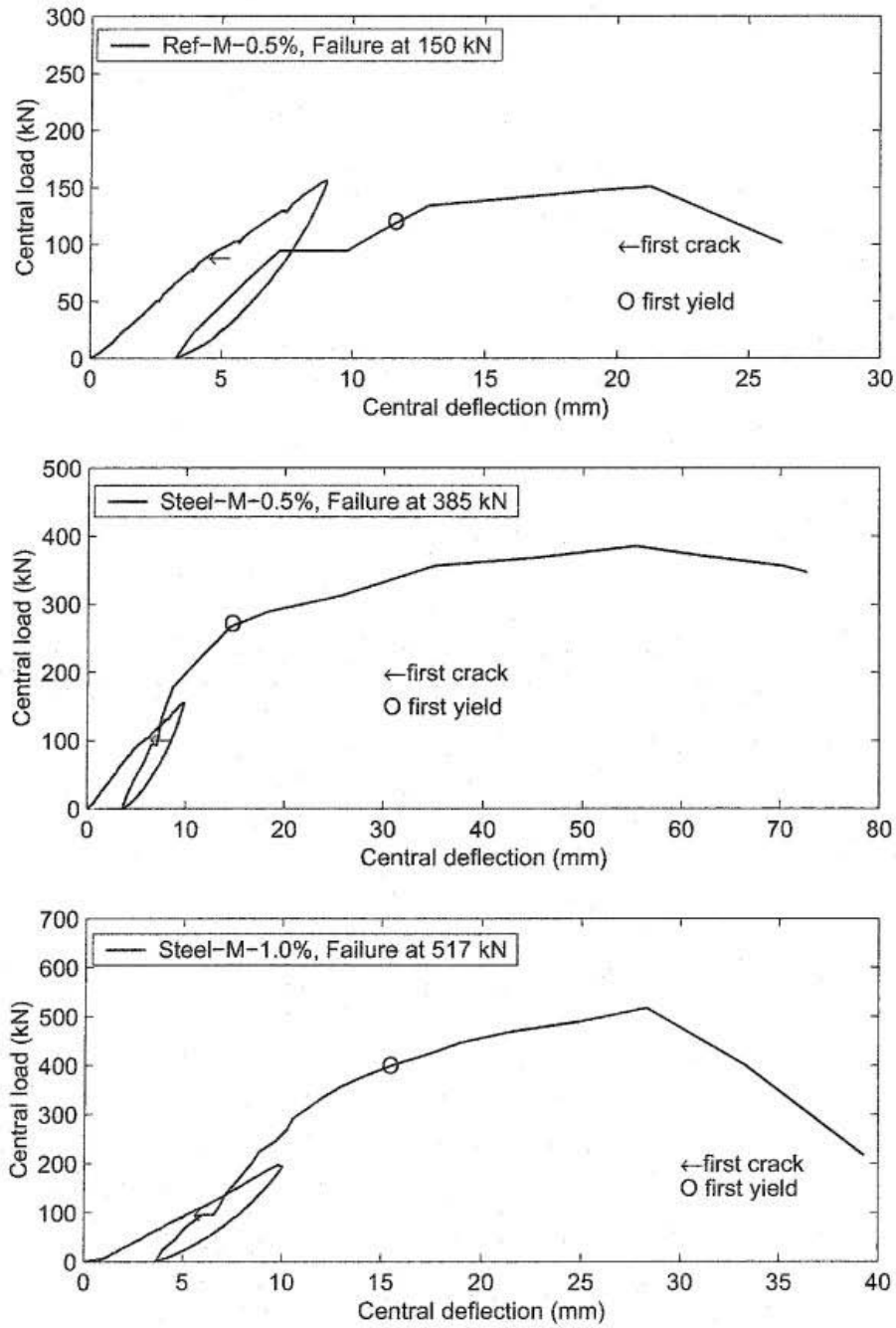

Figure 5.1: Load–deflection relationships of specimens Ref-M-0.50%, Steel–M–0.5%, and Steel–M–1.0%

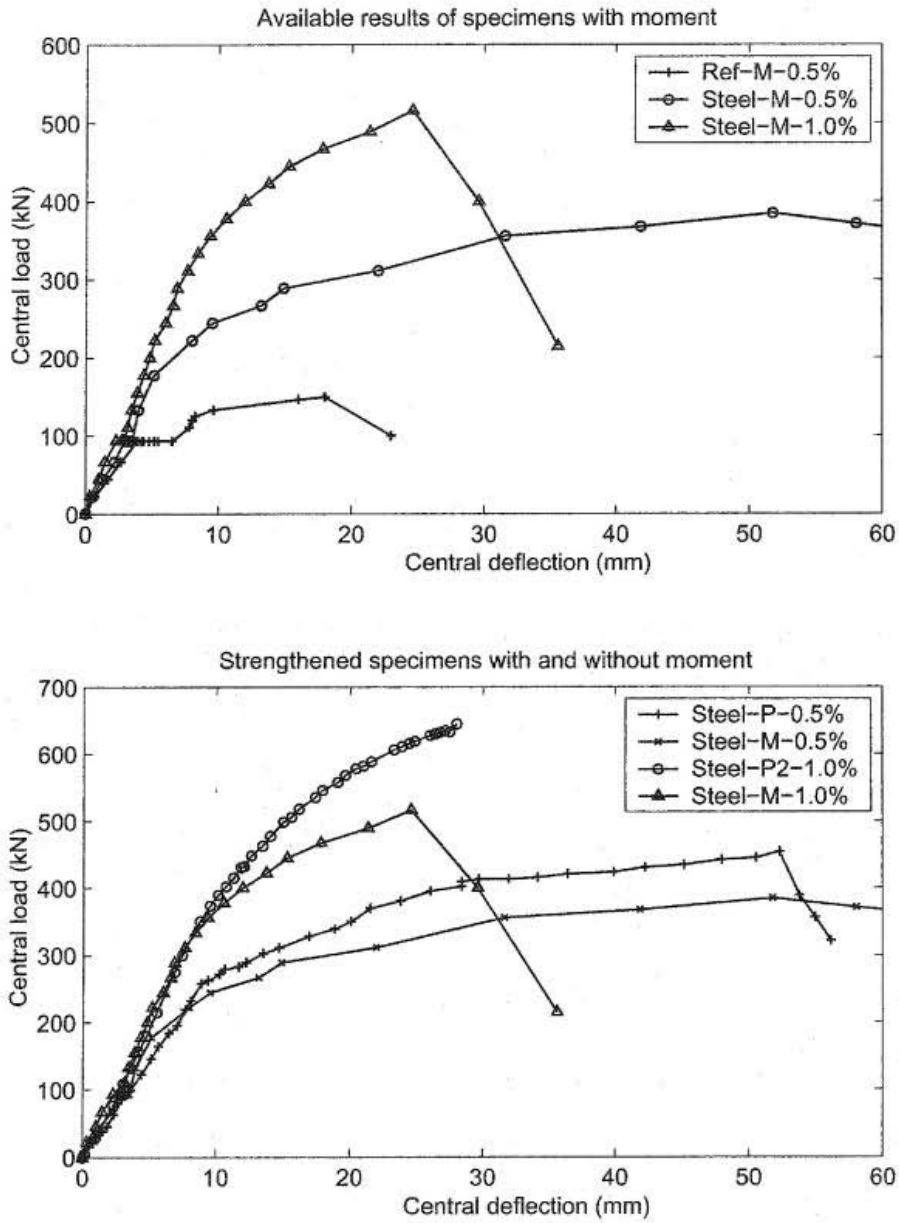

Figure 5.2: Combined load–deflection relationships of specimens subjected to static moment and a comparison with specimens of Group 1 and the reloading stage

specimens of Group 2 are combined together in Figure 5.2.

With regard to the load–deflection relationships, the slopes of the load–deflection relationships within the pre-cracking stage are flatter than the slopes of those of later stages. For the unstrengthened reference specimens, Ref–M–0.5% and Ref–M–1.0%, as the load was increased, the central deflection of a slab was increased. At the same load level, the central deflection was increased as the reinforcement ratio was decreased.

The first crack was observed in the first stage of loading of the strengthened specimens Steel–M–0.5% and Steel–M–1.0% at loads 90 kN and 85 kN, respectively. It is clear from Table 5.1 and Figure 5.2 that the deflection values at the same load levels are decreased due to the strengthening process. A strengthened specimen requires higher load compared to the unstrengthened specimen to achieve the same deflection.

Comparing the specimens subjected to static moment, combined with central load, and those subjected to central loads of Group 1, at the ultimate load, the strengthened specimens Steel–M–1.0% and Steel–M–0.5% showed average deflection values of about 5 % less than the average of those of specimens Steel–P2–1.0% and Steel–P–0.5%. The deflection values that correspond to first crack, yield, and ultimate load carrying capacity for each specimen are summarized in Table 5.1.

The deflection values at equi-spaced nine locations along the slabs width were recorded at each load increment. The values of the deflection at each load increment determine the deflection profile at that increment. Figure 5.3 shows the deflection profiles of specimen Steel–M–0.5% and specimen Steel–M–1.0%. It is shown in Figure 5.3 that the specimen Steel–M–1.0% has less deformation at the same load compared to specimen Steel–M–0.5%.

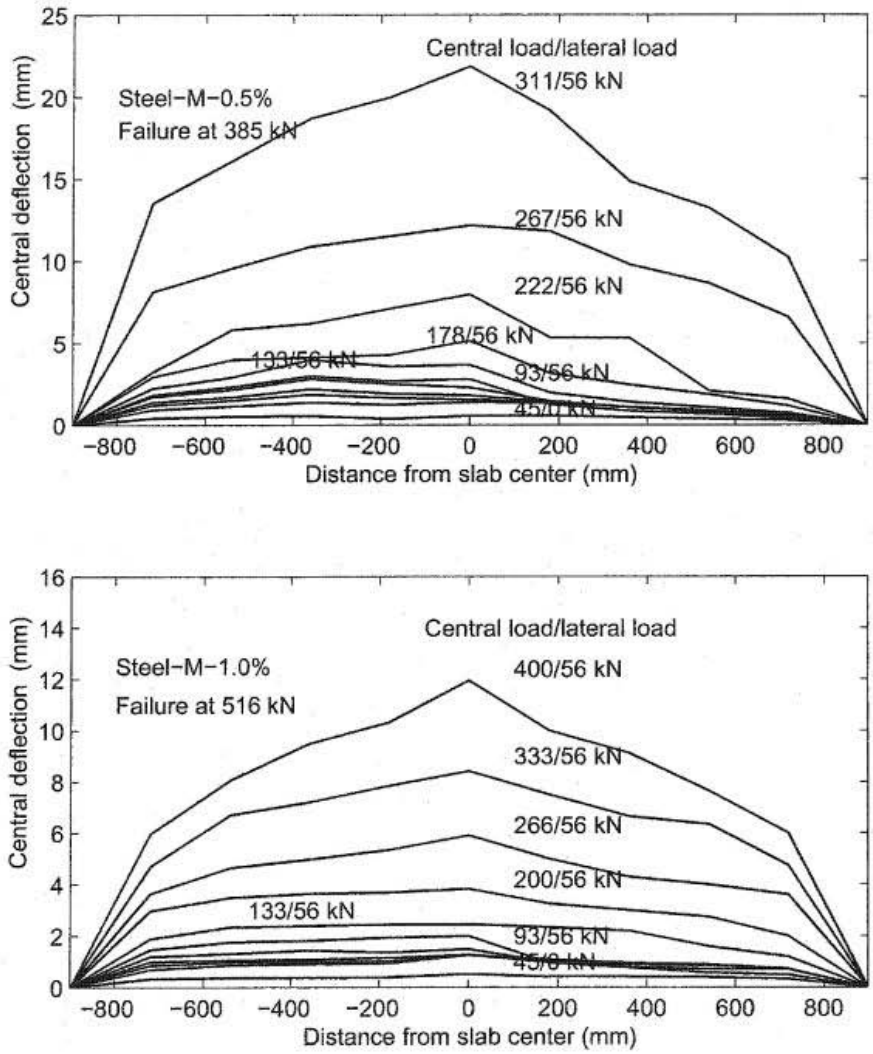

Figure 5.3: Deflection profiles of strengthened specimens subjected to central load and static moment

5.2.2 Crack and Yield Loads

The cracks for all specimens before strengthening were traced as the load was applied. Load values that caused the first crack of tested specimens before strengthening were recorded. The first crack loads and the associated central deflection values for all specimens before strengthening are shown in Table 5.1. Specimens with a reinforcement ratio of 1.0% showed higher average first crack loads compared to those with a reinforcement ratio of 0.5%.

Yield loads and the associated central deflection values for all specimens are summarized in Table 5.1. The effect of the applied static moment was clear on the value of the yield load of specimen Steel–M–1.0%. This specimen showed lower yield load compared to the specimen strengthened using the same steel plates and bolts configuration but loaded centrally only, specimen Steel–P2–1.0%. Specimen Steel–P2–1.0% showed a yield load value that was 1.45 times that of specimen Steel–M–1.0%. The yield load of specimens Steel–M–0.5% and Steel–P–0.5% that was subjected to central load only was almost the same.

5.2.3 Ultimate Load Capacity

As explained earlier in Chapter 4, due to the strengthening process, specimens Steel–P3–1.0% and Steel–P–0.5% showed an increase of about 54% and 36.5% in the ultimate load carrying capacity over that of the associated unstrengthened reference specimens, Ref–P–1.0% and Ref–P–0.5%, respectively. For specimens subjected to static moment as well as central load, the increase of the ultimate capacity was more noticeable. Due to the strengthening process, specimen Steel–M–0.5% showed more than twice the ultimate capacity of the reference specimen Ref–M–0.5%. Results of a

previous investigation indicated that the strengthened specimen Steel–M–1.0% gained an increase in the ultimate capacity of 88% over that of an unstrengthened reference specimen with the same dimensions and reinforcement ratio (Marzouk et al., 2000a).

Regarding the influence of the reinforcement ratio on the ultimate load carrying capacity of the unstrengthened reference specimens, an increase of 83% was observed for specimen Ref–M–1.0% over that of specimen Ref–M–0.5% due to the increase in the reinforcement ratio from 0.5% to 1.0%. Moreover, the strengthened specimen Steel–M–1.0% showed about 52% increase in the ultimate load carrying capacity over that of the strengthened specimen Steel–M–0.5%.

The ultimate load carrying capacities of the strengthened specimens were affected by the applied unbalanced static moment. As shown in Chapter 4, the strengthened specimens Steel–P2–1.0% and Steel–P–0.5% showed load carrying capacities of about 1.25 and 1.18 time those of the specimens Steel–M–1.0% and Steel–M–0.5%, respectively.

5.2.4 Stiffness

As explained in Section 4.2.5, the stiffness of a slab at any loading point is the slope of the load–deflection curve at that point. The initial stiffness, hence, is the tangent to the central load–central deflection curves. The initial stiffness is calculated at the uncracked stage of loading, i.e. at the first stage of central loading and before applying the lateral load that causes the unbalanced static moment. It could be expected that the effect of the reinforcement ratio to be minor. The stiffness was calculated based on early readings of the load and deflection values at which specimens is in the pre-cracked stage.

The initial stiffness values of all the tested slabs as well as the initial stiffness

values of the strengthened specimens are tabulated in Table 5.1. It was evident that the strengthened slabs showed an increase of the stiffness over that of the unstrengthened slabs. Also it was shown that the variation of the reinforcement ratio of the unstrengthened specimens did not have a profound effect on the stiffness of the slabs. On the other hand, the strengthening improved the stiffness of the specimens. Specimen Steel–M–0.5% showed an increase of 73% of the initial stiffness over that of the associated unstrengthened reference specimen, Ref–M–0.5%.

The application of the unbalanced static moment had an effect on the stiffness of specimens. Due to the application of the unbalanced static moment, the stiffness of specimens subjected to static moment was lower than those of the central loads only at the same load levels as may be recognized from Figure 5.2.

5.2.5 Steel Reinforcement Strain

Measurements were made to determine the steel strain distribution at selected radii from slabs centers. The locations of the strain gages were selected to track the variation of the steel strain with the distance from the center of the slab. Figure 3.11.b shows the main reinforcement strain gages distribution for specimens subjected to a combination of central load and static moment. Figure 3.11.d shows the distribution of the compression reinforcement strain gages. The closest location of measuring the steel strain is at a location (1) that is 170 mm from the center of the slab. Measurements of the strain at that location is of a special importance since it was used to define the ductility of tested specimens as discussed in Section 5.2.6. Figure 5.4 shows samples of the typical steel strain distribution at different locations (for specimens Steel–M–0.5% and Steel–M–1.0%). The values of the strains are recorded at locations shown in Figure 3.11.b and 3.11.d. As the distance from the location of

a strain gage to the center of the slab was increased, the strain gages readings were decreased.

Strain distributions at location (1) for specimens Ref–M–0.5%, Steel–M–0.5%, and Steel–M–1.0% were combines together and shown in Figure 5.5. It is clear that a stiffer behaviour is shown for specimens of higher reinforcement ratios. In addition, strengthened specimens showed stiffer behaviour compared to the associated unstrengthened specimens. The effect of the unbalanced static moment was noticeable on the strain distribution at Location (1) for Specimen Ref–M–0.5%. The location of strain gage (1) is shown in Figure 3.11.b. Table 5.1 shows the steel strain values at location (1) for the tested specimens subjected to static moment at the ultimate load.

5.2.6 Ductility and Energy Absorption

As explained earlier, displacement ductility is defined as the ratio between the deflection at the ultimate load and that at the yield load (Geng et al., 1998; Marzouk and Hussein, 1991a; Marzouk et al., 1996). The ductility indices are summarized in Table 5.1. Strengthened specimens showed more ductile behaviour than unstrengthened specimens. The ductility of the strengthened specimen Steel–M–0.5% was about 2.25 times that of the associated unstrengthened reference specimen, Ref–M–0.5%.

The definition of the energy absorption is the area under the load–deflection curve of a tested specimen. A considerable increase in the energy absorption values was observed due to the strengthening. Specimen Steel–M–0.5% showed energy absorption of about 8.4 times that of the associated unstrengthened specimen, Ref-M-0.5. It was noticed that specimens subjected to unbalanced static moment gained more energy absorption values than those subjected to central loads only. Table 5.1 shows the

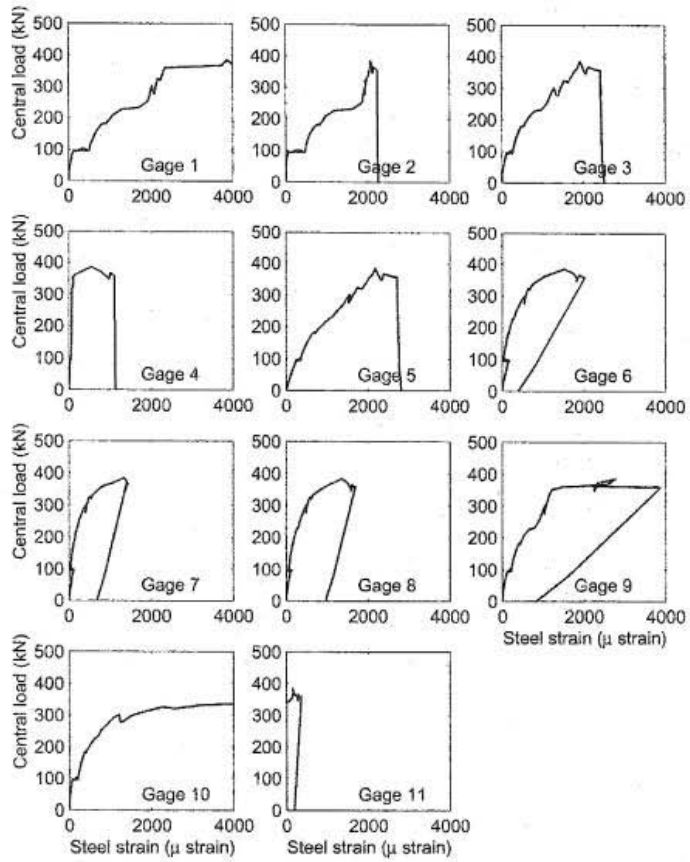

(a) Steel–M–0.5%

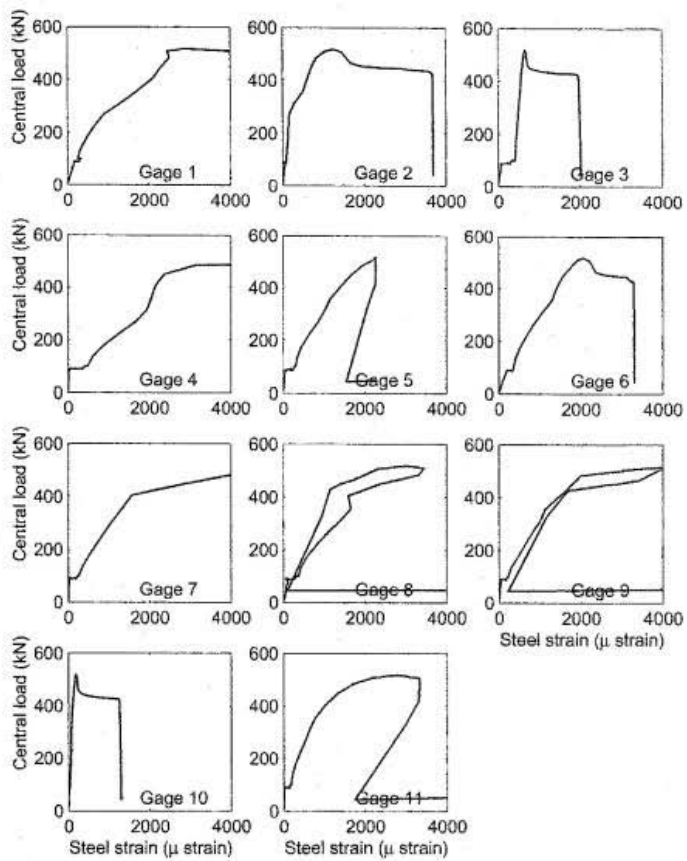

(b) Steel–M–1.0%

Figure 5.4: Typical load–steel reinforcement strain relationships for tested specimens (Steel–M–0.5% and Steel–M–1.0%)

Table 5.1: Test results of specimens of Group 2 subjected to static moment, including references from Group 1

Title	Crack load, P_{cr}, kN	Deflection at crack load, δ_{cr}, mm	Yield load, P_y kN	Deflection at yield load, δ_y, mm	Ultimate load, P_u, kN	Deflection at ultimate load, δ_u, mm	Energy Absorption, ψ, kN.mm	Stiffness, K, kN/mm	Ductility index	Steel strain, $\varepsilon_{su}(10^6)$
Ref–P–0.5%	79	5.30	242	16.63	312	38.08	9473	18.50	2.29	3286
Ref–P–1.0%	89	4.85	370	20.09	420	24.50	5950	20.08	1.22	2463
Ref–M–0.5%	86	4.99	120	8.03	150	18.00	2607	27.00	2.24	3399
Steel–M–0.5%	97	6.04	272	10.24	385	51.77	21924	32.00	5.06	3870
Steel–M–1.0%	100	5.50	400	11.96	517	24.60	12767	34.70	2.06	2884
Steel–P–0.5%	82	5.02	267	13.21	453	52.27	19414	27.00	3.96	4841
Steel–P2–1.0%	85	4.80	582	21.70	645	28.00	11711	35.90	1.30	2950

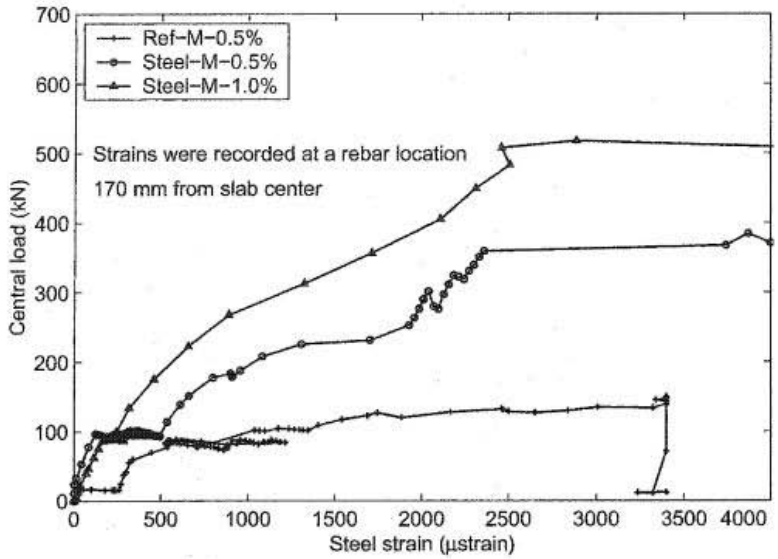

Figure 5.5: Load–steel reinforcement strain relationships at location (1)

values of the energy absorption for specimens subjected to static moment.

5.3 Specimens Subjected to Cyclic Moment

The following discussion focuses on the unbalanced cyclic moment-drift relationship, cyclic ductility characteristics, and cyclic stiffness characteristic of specimens subjected to a combination of central load and cyclic moment.

5.3.1 Cyclic Moment-Drift Relationship

Figure 5.6 shows the relationships between the cyclic moment and the associated drift for the strengthened specimens subjected to a combination of central loads and cyclic moments.

Specimen Steel–C–1.0% achieved unbalanced cyclic moments of 190 kN.m and

–160 kN.m that corresponded to lateral drift of 7.92 % and 7.93%, respectively, after 26 cycles. The unbalanced cyclic moment drops to 74 kN.m and 49 kN.m when the drift ratios reached 6.08% and 5.56%, respectively. Those values of lateral drifts were the maximum drift that could be reached by the testing actuator.

Specimen Steel–C–0.5% achieved a value of unbalanced cyclic moments of 145 kN.m and 134 kN.m that corresponded to lateral drift of 7.83 % and 7.94 %, respectively, after 26 cycles. The unbalanced cyclic moment drops to 143 kN.m and 108 kN.m when the drift ratios reached 9.30% and 8.66%, respectively, at which the specimen failed.

No distinct points on the unbalanced cyclic moment-drift relationship to define the yield point. It was noticed that the slope of the unbalanced cyclic moment–drift envelope was gradually decreased indicating the weakening of the tested specimens until failure.

In comparison with the unstrengthened reference specimens that were tested in the same laboratory with the same conditions and material properties (Marzouk et al., 2001), the unbalanced cyclic moment resistance of a strengthened specimen was about 15% higher than that of the corresponding unstrengthened specimen regardless the reinforcement ratio. It has been reported that the unstrengthened specimens with reinforcement ratio of 1.0%, Ref–C–1.0% showed higher unbalanced cyclic moment resistance of about 25.5% than that of specimens with reinforcement ratio of 0.5%, Ref–C–0.5% (Marzouk et al., 2001).

The most significant finding is that a strengthened slab can undergo a lateral drift as high as 76% more than the associated unstrengthened specimen. Moreover, the strengthened specimens had more drift cycles after reaching the ultimate capacity

than that of the unstrengthened specimens. The unstrengthened slab to column connections can resist a lateral drift ratio of about 4 to 5% before failure (Marzouk et al., 2001). On the other hand, the strengthened specimens resist a drift ratio of almost 8% before failure. Considering the actual building dimensions and safety consideration, most of the building codes limit the inter-story lateral drift ratio to 2% for most of structures except for hospitals. For a slab to column connection strengthened using the suggested technique, the limit of 2% could be safely increased to 3.5% if all other circumstances and factors remain the same.

5.3.2 Cyclic Ductility Characteristics

The lateral displacement ductility of a slab-column connection is defined as the ratio of lateral displacement at failure to that at the yield of the connection. The maximum peak values of the cyclic moment for the tested slabs are clear on the cyclic moment-drift relationship. The yield point of the slab-to column connection subjected to cyclic moment is not that straightforward to be identified since it depends on the overall behaviour of the connection. The lateral load-drift relationship is not unique since yield spreads across the slab width gradually (Pan and Moehle, 1989). An approximate method was developed to overcome the uncertainty of identifying the yield point of slab-column connections subjected to reversal lateral cyclic drift (Pan and Moehle, 1989). The procedure of the determination of the yield and the displacement ductility of a slab to column connection is shown in Figure 5.7. It is based on constructing a secant through $^2/_3$ the ultimate unbalanced cyclic moments that intersects the unbalanced cyclic moment-drift envelope with origin point (O) at (A). Denoting the intersection of line (OA) and the horizontal line at the ultimate unbalanced cyclic moment level as (B). The intersection of the vertical line from (B) and the drift axis

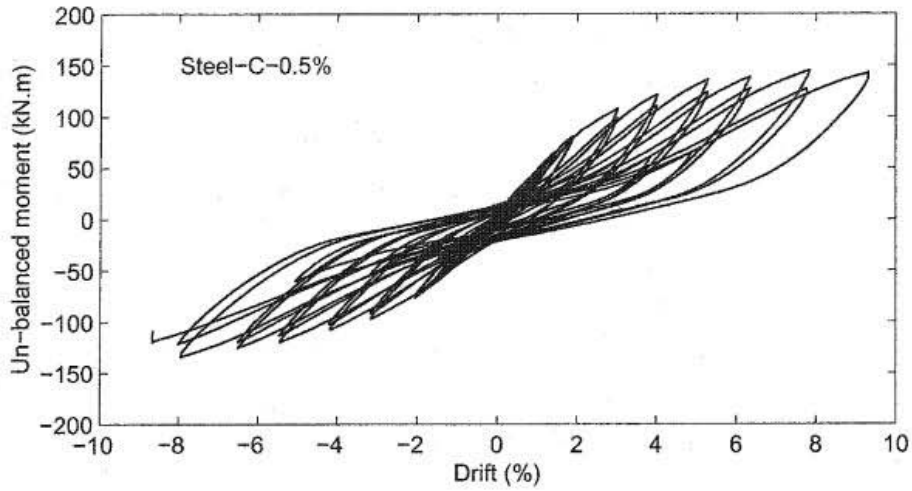

(a) Specimen Steel–C–0.5%

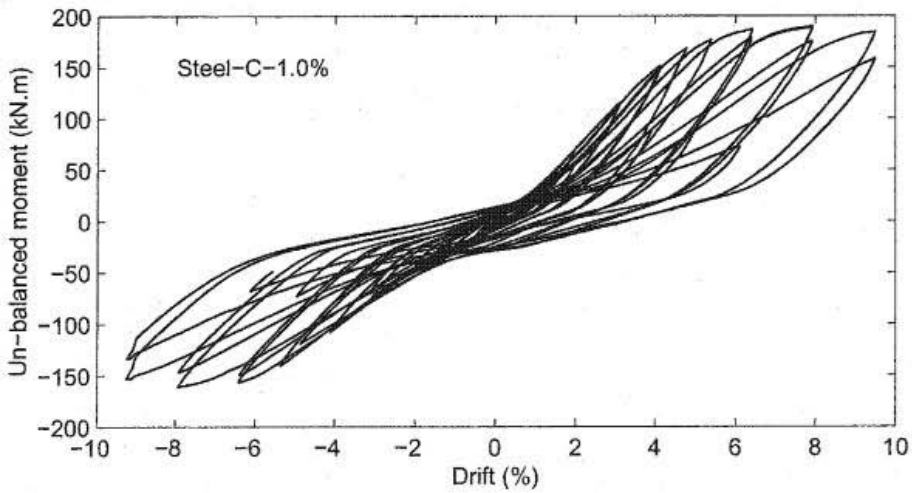

(b) Specimen Steel–C–1.0%

Figure 5.6: Unbalanced cyclic moment-drift relationship for strengthened specimens

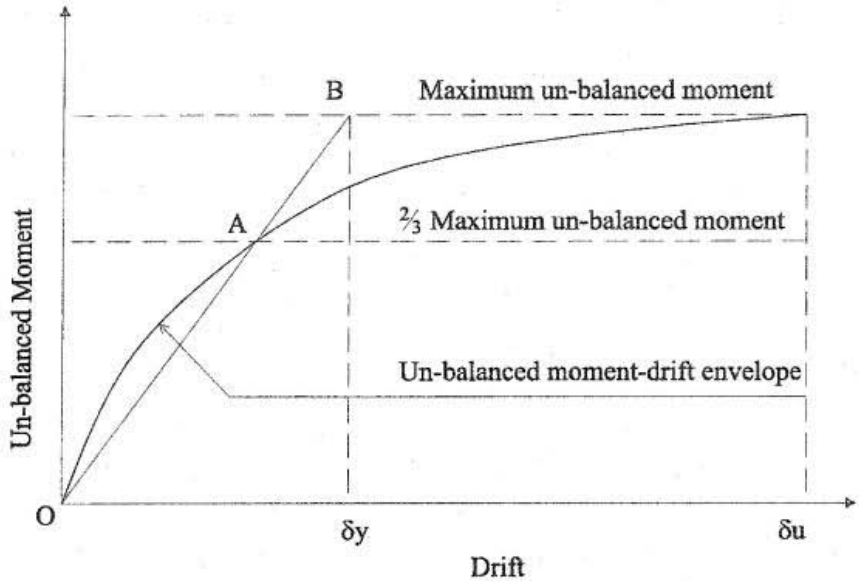

Figure 5.7: Evaluation of the displacement ductility for specimens subjected to cyclic moment

defines the drift at the yield of the connection.

As shown in Table 5.2, specimens with reinforcement ratio of 0.5 %, Ref–C–0.5% and Steel–C–0.5%, showed 57% and 24 % higher ductility values than specimens Ref–C–1.0% and Steel–C–1.0%, respectively. In addition, the strengthened specimen, Steel–C–0.5% showed 21% less ductility than that of the associated unstrengthened reference specimen, Ref–C–0.5%. Also, the ductility of the strengthened specimen, Steel–C–1.0% and that of the unstrengthened reference specimen, Ref–C–1.0% were almost the same.

5.3.3 Cyclic Stiffness Characteristics

The peak-to-peak connection stiffness is well defined as the slope of the line connecting the peak-to-peak unbalanced cyclic moment points at a load cycle of the unbalanced

cyclic moment–drift relationship (Emam et al., 1997). The ratio of stiffness at a drift corresponding to the ultimate unbalanced cyclic moment and that at a drift of 0.5% indicates the stiffness degradation as shown in Table 5.2. The average value of stiffness of the strengthened specimens was 25% lower than that of the unstrengthened reference specimens.

5.3.4 Reinforcement Steel Strain

Measurements were made to determine the steel strain distribution at selected radii from slabs centers of specimens Steel–C–0.5% and Steel–C–1.0%. The locations of the strain gages are shown in Figure 3.11.b and 3.11.d. Figure 5.8 shows a typical stress–strain distribution at different locations for a strengthened specimen (Specimen Steel–C–0.5%). Generally, as the unbalanced cyclic moment is increased, the strain in steel reinforcement is increased with accumulated irrecoverable strain. This indicates the plastic irrecoverable strains due to the increasingly repeated cyclic moment.

5.4 Failure Characteristics of Tested Specimens

The tension reinforcement of a specimen may reach the yield point at locations around the column and far from the center of the specimen with what is so called "punching radius". Larger punching radii are associated with the flexural failure mode than those associated with punching–shear failure mode (Marzouk et al., 2001; Osman et al., 1998).

Figures 5.9 to 5.13 show pictures of tested specimens at failure. It is shown in Figure 5.9 that the mode of failure of the unstrengthened Ref–P–0.5% was classified

Table 5.2: Test results of specimens of Group 2 subjected to cyclic moment

Title	M_{ub}	Δ_u,%	Δ_y,%	D	K at $\Delta = 0.5\%$ drift	K at M_{ub}	Stiffness degradation
Ref–C–0.5%	132	5.00	1.4	3.57	—	24.20	—
	-110	-4.00					
Ref–C–1.0%	176	5.00	2.2	2.27	—	28.30	—
	-128	-4.00					
Steel–C–0.5%	145	7.83	2.8	2.80	44.03	22.55	0.512
	-134	-7.94					
Steel–C–0.5%	190	7.92	3.5	2.26	43.05	16.65	0.397
	-160	-7.93					

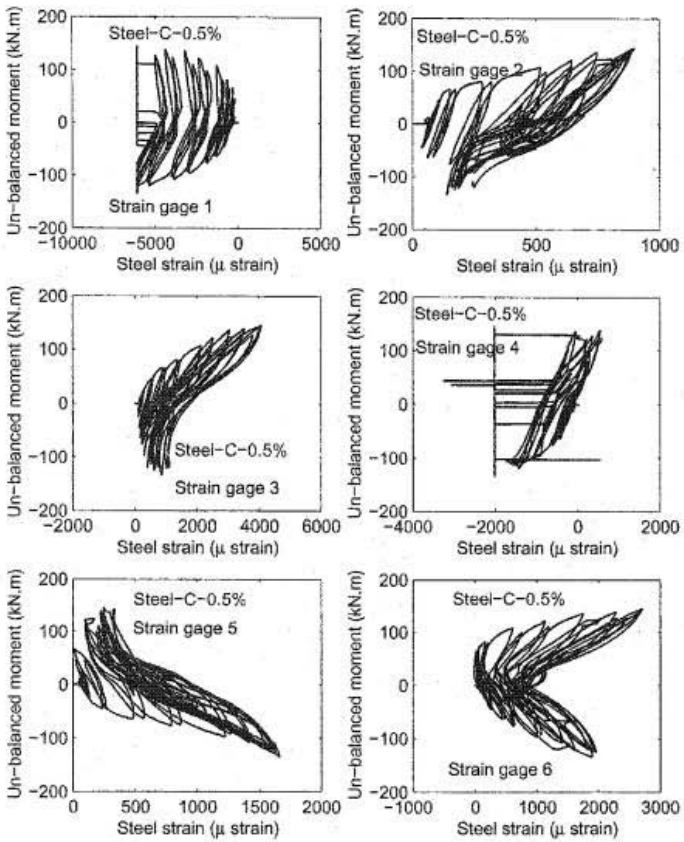

(a) Locations 1,2,3,4,5,and 6

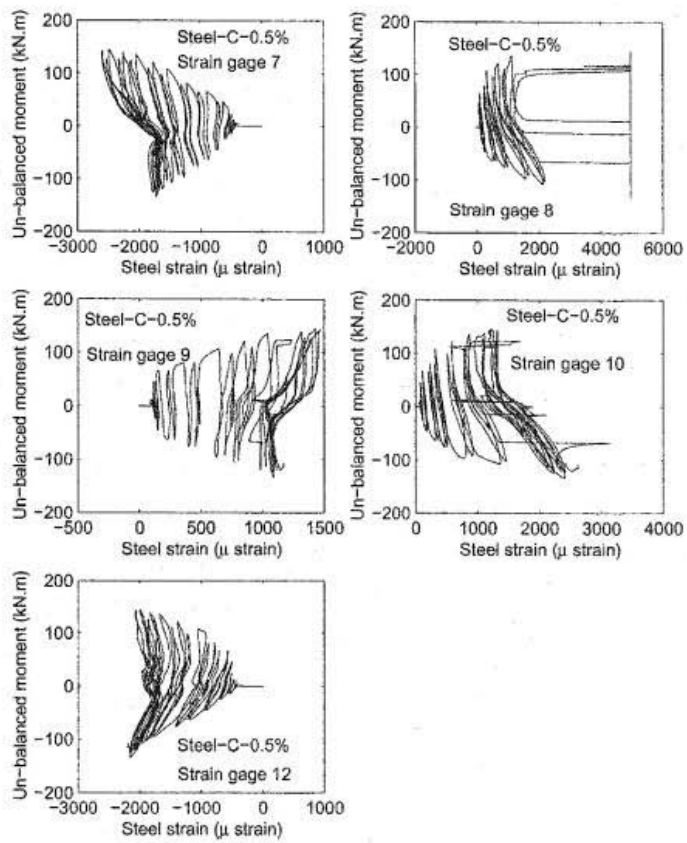

(b) Locations 7,8,9,10, and 12

Figure 5.8: Load–steel reinforcement strain relationships for specimen Steel–C–0.5%

as flexural ductile failure. Due to the strengthening process both specimens Steel–M–0.5% and Steel–M–1.0% showed more flexural ductile behaviour compared to the associated unstrengthened reference specimens. The punching radius was increased due to the contribution of the steel plates. Failure modes of specimens Steel–M–1.0% and Steel–M–0.5% are shown in Figures 5.10 and 5.11, respectively.

The strengthened specimens subjected to cyclic moment in this group, specimens Steel–C–1.0% and Steel–C–0.5% failed in the column portion as shown in Figures 5.12 and 5.13. The strengthening process improved the slab part of the connection forcing the failure to occur in the column unlike the failure mode experienced in the reference specimens Ref–C–1.0% and Ref–C–0.5% (Marzouk et al., 2001). It is essential when designing slab–column/beam–column connections that plastic hinges be formed in the slab/beam rather than the column. This fact does not contradict with the finding that the slab in the present work was strengthened to a limit that a plastic hinge, or failure, occurred in the column. In fact this is an indication of the successful strengthening technique, especially when emphasizing the finding that the column drift was increased by 76%.

5.5 Code Verification of Static Moment Specimens' Results

For two–way slabs subjected to central load and static moment, the shear perimeter is assumed that the perimeter of critical section be located at distance $l_p/2$ for strengthened specimen rather than $(c + d)/2$. Verification of several cases of the unstrengthened specimens was reported in previous research work (Marzouk et al., 2000a).

The fraction γ_v can be calculated as follows;

$$\gamma_v = 1 - \frac{1}{1 + 2/3\sqrt{\frac{l_p}{l_p}}} = 0.4 \tag{5.5.1}$$

Under combined load and moment transfer, the shear stresses on the critical slab sections are computed according to the equation;

$$v_{1,2} = \frac{V}{A_{cs}} \pm \frac{\gamma_v M_u}{J_{cs}}, \tag{5.5.2}$$

where; $A_{cs} = 4\,d\,l_p$ in case of strengthened specimen. According to CSA and the ACI codes' provisions (CSA–A23.3 1994, ACI–318 1999), the larger shear stress v_1 must not exceed the nominal shear stress, v_c. The flexural capacity M_r in this case is calculated at the unstrengthened section of the slab within slab width equals l_p which value is almost the same as $c + 3\,h$ as used in as follows;

$$M_r = \rho\, f_y\, l_p\, d^2 \left(1 - 0.59\,\rho\, f_y \Big/ f_c^{'}\right) + \left[\left(f_y - 0.85\, f_c^{'}\right)\, \rho^{'}\, l_p\, d\, \left(d - d^{'}\right)\right] \tag{5.5.3}$$

Values of M_r and the portion of ultimate measured moment $(1 - \gamma_v)\, M_u$ divided by flexural capacity M_r are listed in Table 5.3. The maximum shear and moment transferred to the column achieved in the tests simultaneously prior to failure, V_{test} and M_u are compared with the ACI/CSA codes prediction. V_c is the ultimate strength for shear transfer only, and M_0 is the ultimate strength for moment transfer only. The value of M_0 is calculated as follows (CSA–A23.3, 1994; ACI–318, 1999);

$$M_0 = \frac{v_c\, J_{cs}}{\gamma_v \frac{l_p}{2}} \tag{5.5.4}$$

The sum of the two non–dimensional quantities, V_{test}/V_c and M_u/M_0, represents the non–dimensional shear strength $V_{T(test)}/V_{T(calc)}$ as summarized in Table 5.3. Both

specimens Steel–M–0.5% and Steel–M–1.0% failed in flexure. The calculated ratio $V_{T(test)}/V_{T(calc.)}$ in Table 5.3 is less than 1.0 for both specimens Steel–M–0.5% and Steel–M–1.0% indicating that these two specimens in flexure. Hence the code prediction of the failure mode matches the experimental findings for strengthened specimens Steel–M–0.5% and Steel–M–1.0%.

The ratio $(1 - \gamma_v)\ M_u$ shown in Table 5.3 exceeds unity for specimen Steel–M–0.5% that confirms the codes for that specimen to fail in flexure. However, the ratio $(1 - \gamma_v)\ M_u$ for specimen Steel–M–1.0% is lower than one. The difference between test results and code requirements could be attributed to that the code shear stress model overestimates the portion of moment transferred by flexure. ACI and CSA codes' calculation of the shear force carried by concrete, V_c should be similar. Yet since the material and load factors are omitted, the calculations showed minor discrepancy.

5.6 Summary and Conclusions

The following conclusions are applied for two–way slabs strengthened with steel plates and steel bolts using the described technique.

1. The strengthened specimens subjected to central load plus static moment with reinforcement ratios of 0.5% and 1.0% showed ultimate capacities of 2 and 1.88, respectively, times those of the associated unstrengthened reference specimens.

2. The strengthening technique in the case of central loads and static moment was more efficient than in case of central loads only. The gain in ultimate load carrying capacity in case of central loads plus static moment was about 3 times that in case of central loading only.

Table 5.3: Code verification for strengthened specimens subjected to central load plus static moment

Specimen	f_c', MPa	V_{test}, kN	V_0, kN		M_0, kN.m	M_u, kN.m	V_{test}/V_c		M_u/M_0	$V_{T(test)}/V_{T(calc.)}$		M_r, kN.m	$(1-\gamma_v)\ M_u/M_r$
			ACI	CSA			ACI	CSA		ACI	CSA		
Steel–M–0.5%	33	385	696	838	436	88	0.55	0.46	0.2	0.75	0.66	36.8	1.43
Steel–M–1.0%	34	517	706	851	436	88	0.73	0.61	0.2	0.93	0.81	58.9	0.90

3. The strengthened specimens showed an average of 72% increase in the initial stiffness over that of the unstrengthened reference specimens.

4. A considerable increase in the energy absorption values was observed due to the strengthening for specimens subjected central load plus static moment over that of the unstrengthened reference specimens. Specimen with reinforcement ratio of 0.5% showed energy absorption of about 8.4 times that of the unstrengthened reference specimen.

5. For specimens subjected to a combination of central load and cyclic moment, the cyclic moment resistance of the strengthened slabs was about 15% higher than that of the unstrengthened reference specimen regardless the reinforcement ratio.

6. For specimens subjected to a combination of central load and cyclic moment, a strengthened slab can undergo a lateral drift capacity 76% higher than that of the associated unstrengthened reference specimen. Moreover, the strengthened specimens had more drift cycles after reaching the ultimate load carrying capacity than that of the unstrengthened reference specimens.

7. A simple approach based on the CSA and ACI codes is proposed to predict the mode of failure of strengthened specimens subjected to central loads and static moments.

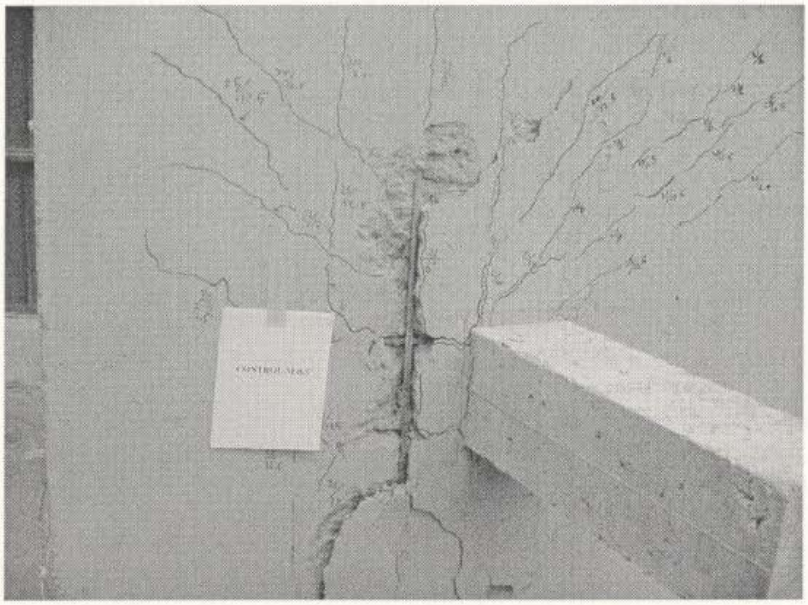

Figure 5.9: Specimen Ref–M–0.5% after final testing.

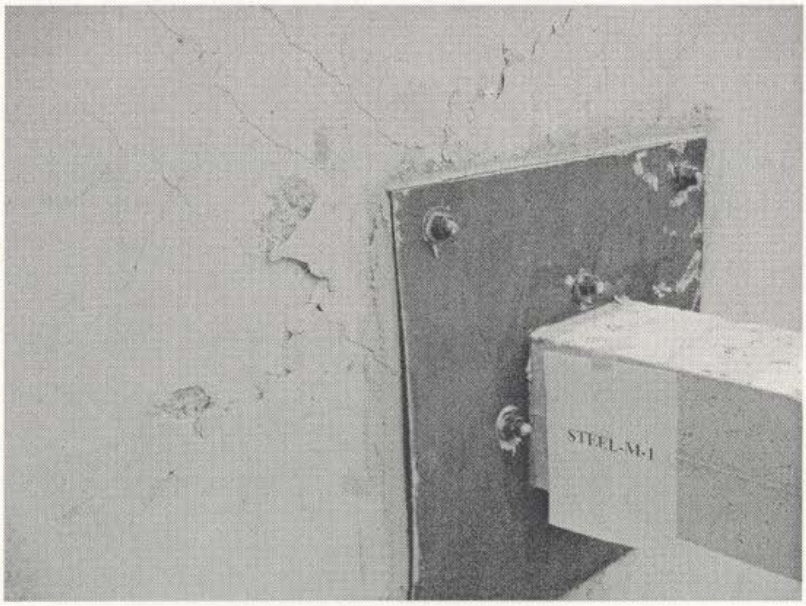

Figure 5.10: Specimen Steel–M–1.0% after final testing.

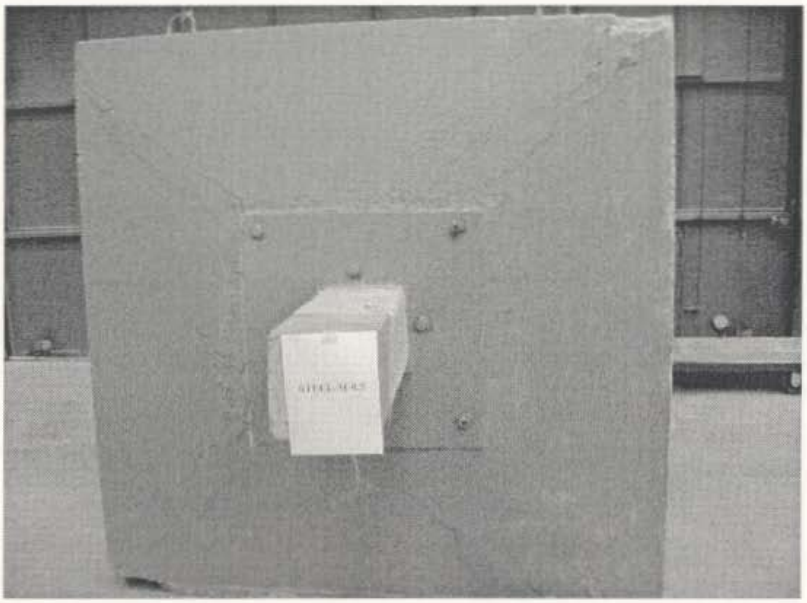

Figure 5.11: Specimen Steel–M–0.5% after final testing.

Figure 5.12: Specimen Steel–C–1.0% after final testing.

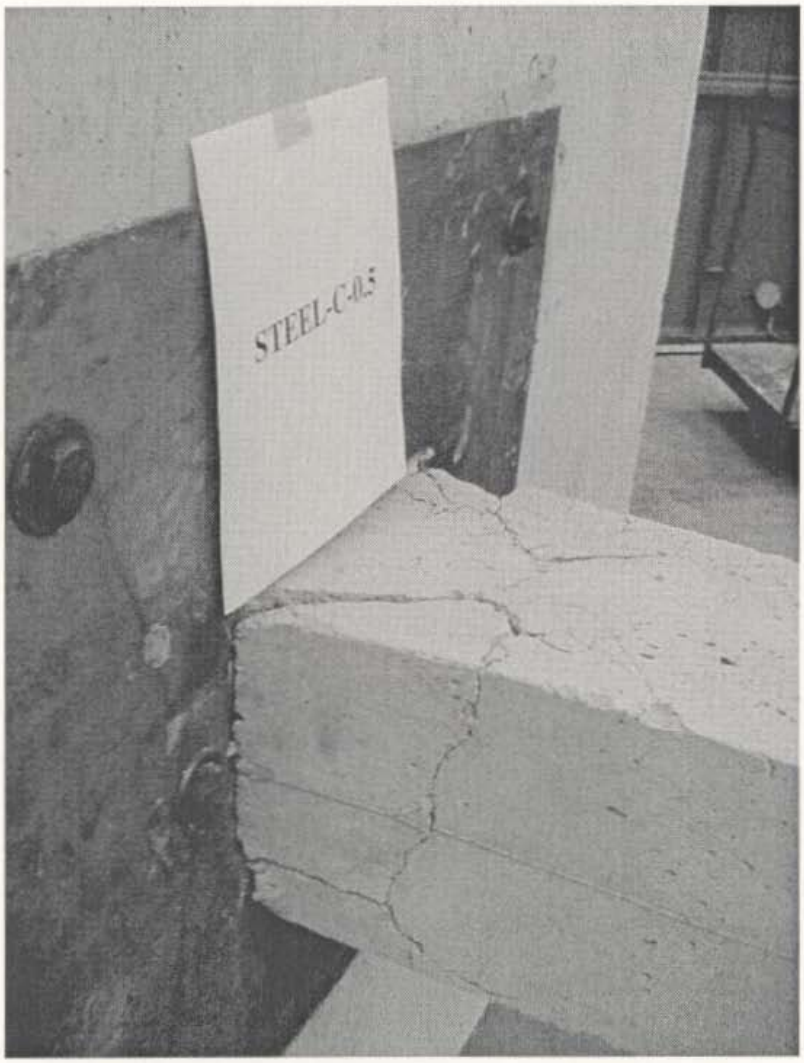

Figure 5.13: Specimen Steel–C–0.5% after final testing.

Chapter 6

Behaviour of Two–Way Slabs Using FRP Materials

6.1 Introduction

Increasing attention has been placed to the applications of the advanced composite materials especially glass fibre reinforced polymer (GFRP) laminates and carbon fibre reinforced polymer (CFRP) strips in the structural engineering field. Extensive applications of the FRP materials as new construction materials have been accomplished recently. FRP materials are lightweight, high strength, non-corrosive and non-magnetic materials. By virtue of the advantages of these materials, there is a wide range of recent, current and potential applications of these materials that cover both new and existing structures.

FRP materials have been used in many of the structural projects and strengthening applications. These composites have been used for strengthening reinforced concrete beams, columns, and one-way slabs. The flexural capacity of concrete beams is proven to be increased by bonding FRP sheets, strips or laminates to the tension side. The ease of handling FRP materials provides the means to the extension of their applications for strengthening other structural element.

In this chapter the results of FRP–strengthened two–way slabs are introduced. the specimens of this group are divided into flexural–strengthened slabs, and punching shear–strengthened specimen.

6.2 Test Results of Specimens of Group 3

The results of specimens of Group 3 are discussed in detail. This group is divided according to the purpose of the strengthening into two divisions. These divisions are FRP flexural–strengthening specimens and FRP shear–strengthening specimens. In the following sections, the latter will be referred to as FRP shear–strengthening specimens. For each set of specimens, there are associated unstrengthened reference specimens. The FRP flexural–strengthening set of specimens contains specimens Ref–P–0.35% and Ref–P'–0.5% that represent the unstrengthened reference specimens. Also, this set includes specimens GFRP–F–0.35%, GFRP–F–0.5%, CFRP–F–0.35%, and CFRP–F–0.5% that represent the strengthened specimens. The FRP shear–strengthening set of specimens contains specimen Ref–P–1.0% that represents the unstrengthened reference specimens and specimens CFRP1–S–1.0%, and CFRP2–S–1.0% that represent the strengthened specimens. A complete description of the specimens title conventions are introduced in Chapter 3. The following discussion is related to the structural behaviour in terms of the crack, yield, and ultimate loads; load–deflection characteristics; ductility; stiffness; reinforcement steel strains; and failure characteristics. In the following section of this chapter, the ultimate load carrying capacity will be referred to as the load capacity.

6.2.1 Crack, Yield, and Ultimate Loads

The cracks for all specimens before strengthening were traced as the load was applied. Cracks of each specimen in this group were visually inspected and the corresponding loads were recorded. Specimens with a reinforcement ratio of 0.35% showed the lowest first crack loads. The first crack loads and the associated central deflection values for all specimens before strengthening are shown in Table 6.1. The highest load causing the first crack was observed for specimens with reinforcement ratios of 1.0%. The average first crack load of specimens with a reinforcement ratio of 0.5% was higher than that of specimens with a reinforcement ratio of 0.35% by about 17%.

Due to flexural–strengthening, specimens GFRP–F–0.35% and CFRP–F–0.35% showed yield loads that were 1.96 and 1.91 times that of the unstrengthened reference specimen, Ref–P–0.35%. In addition, specimens GFRP–F–0.5% and CFRP–F–0.5% showed yield loads that were 1.88 and 2.47 times that of the unstrengthened reference specimen Ref–P$'$–0.5%. On the other hand, there was not a clear effect of the shear–strengthening on the values of yield load of specimens CFRP1–S–1.0% and CFRP2–S–1.0%. The yield loads and the associated central deflection values for all specimens are shown in Table 6.1.

The FRP flexural–strengthening specimens showed higher load capacity over that of the corresponding unstrengthened reference specimens. Specimens CFRP–F–0.35% and GFRP–F–0.35% showed an increase of 44.4% and 38%, respectively, in the load capacity over that of the unstrengthened reference specimen, Ref–P–0.35%. Moreover, Specimens CFRP–F–0.5% and GFRP–F–0.5% showed an increase of 36.4% and 25.8%, respectively, in the load capacity over that of the unstrengthened reference specimen, Ref–P$'$–0.5%. The load capacity of specimen Ref–P$'$–0.5% was 1.32 times

that of specimen Ref–P–0.35%.

FRP shear–strengthening specimens CFRP1–S–1.0% and CFRP2–S–1.0% gained an average increase in the load capacity of 9.0% over that of the unstrengthened reference specimen, Ref–P–1.0%. Consequently, FRP materials are not efficient in shear–strengthening for two–way slabs as much as in FRP flexural–strengthening. This could be attributed to the fact that FRP materials have a weak out–of–plane resistance compared to that of the in–plane. Comparing specimens strengthened using FRP materials and those strengthened using steel plates as presented in Chapter 4 and 5, specimens strengthened with steel plates significantly gained higher loads than the FRP shear–strengthening specimens. Specimen Steel-P2–1.0% gained an increase of 31.36% and 51.76%, as presented in Chapter 4, over that of the FRP shear–strengthening specimens CFRP1–S–1.0% and CFRP2–S–1.0%, respectively. Table 6.1 summarizes the ultimate load carrying capacity of all specimens.

6.2.2 Deformational Characteristics

The central load–central deflection relationships were stored using the data acquisition system described in Chapter 3. Moreover, the deflection profiles at nine different positions along each slab's width as shown in Figures 3.4, 3.6, and 3.14 were recorded using dial gages.

Complete load–deflection relationships of all the tested specimens in this group are shown in Figures 6.1 and 6.2. For the strengthened specimens of this group, the load–deflection relationships are presented within the initial central loading, unloading, and reloading stages. Locations of the first crack and yield loads are shown in Figures 6.1 and 6.2 using the symbols (←) and (O), respectively.

Points on the central load–steel strain curves that correspond to load values at

which steel strains at a certain location reach a value of 2000 μstrain were considered yield points. The location at which the steel strain was measured was 170 mm from the center of the slab as explained earlier in Chapter 4 and Chapter 5. All of the central load–central deflection curves of the specimens of Group 3 are combined together and shown in Figure 6.3. The load–deflection curve of specimen Steel-P2-1.0% is included in Figure 6.3.c for comparison purposes.

The deflection values at nine equi–spaced locations along the slabs width were recorded versus the load. Figures 6.4 and 6.5 show the deflection profiles of the specimens of Group 3. The deflection values that correspond to first crack, yield, and ultimate load for each specimen are summarized in Table 6.1.

Load–Deflection Relationships

The variation of the deflection values against the load is largely dependent on the reinforcement ratio. The average value of the deflection at first crack loads for specimens with reinforcement ratio of 0.35% is 1.18 times that of specimens with reinforcement ratio 0.5% and 1.52 times that of specimens with reinforcement ratio 1.0%.

For the FRP flexural–strengthening specimens, at the same load level the tangents to the load–deflection curves were higher than those of the associated unstrengthened specimens Ref–P–0.35% and Ref–P$'$–0.5%, respectively. Moreover, due to the brittle nature of the FRP materials (strips or laminates), the overall load–deflection relationships of the FRP flexural–strengthening specimens showed stiffer behaviour.

The deflection values at the ultimate load of strengthened specimens GFRP–F–0.35% and CFRP–F–0.35% were 0.76 and 0.50 that of the associated unstrengthened reference specimen Ref–P–0.35%. In addition, the deflection values at the ultimate load of strengthened specimens GFRP–F–0.5% and CFRP–F–0.5% were 0.83 and 0.64

times that of the associated unstrengthened reference specimen Ref–P′–0.5%. These findings agree with the fact that FRP flexural–strengthening reduces the deformations of the strengthened specimens. This behaviour is more obvious when the results of the ductility of the tested specimens are discussed.

The deflection values at yield of strengthened specimens GFRP–F–0.35% and CFRP–F–0.35% were about 1.84 and 1.4 times that the associated unstrengthened reference specimen Ref–P–0.35%. This result may be in contrast, at the first look, the fact that FRP–strengthened specimens show lower deflection values compared to the associated unstrengthened specimens. Actually, this fact is satisfied since at the same load level the unstrengthened specimen Ref–P–0.35% showed more deformation than any of the strengthened specimens GFRP–F–0.35% or CFRP–F–0.35%. These specimens showed higher deflection values at the their yield load since these values of the yield loads are increased due to the strengthening. Also, the deflection values at yield of strengthened specimens GFRP–F–0.5% and CFRP–F–0.5% were about 1.14 and 0.88 times those of the associated unstrengthened reference specimen, Ref–P′–0.5%.

Regarding the FRP shear–strengthening specimens, specimens CFRP1–S–1.0% and CFRP2–S–1.0% had deflection at yield 0.78 and 0.7, respectively, times that of the associated unstrengthened reference specimen Ref–P–1.0%. At ultimate load, specimens CFRP1–S–1.0% and CFRP2–S–1.0% had deflection at the ultimate load 1.09 and 0.99, respectively, times that of the associated unstrengthened reference specimen Ref–P–1.0%. This indicated that the contribution of CFRP strips and GFRP laminates for shear–strengthening was random and not effective. It is clear that FRP materials are more effective for flexural–strengthening than for shear–strengthening.

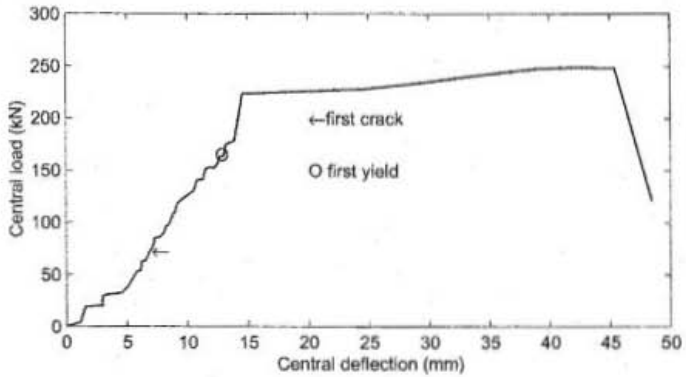

(a) Ref–P–0.35%, P_{max} =250 kN

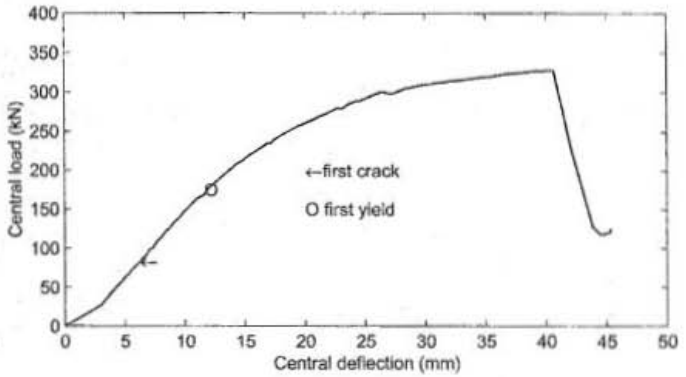

(b) Ref–P$'$–0.5%, P_{max} =330 kN

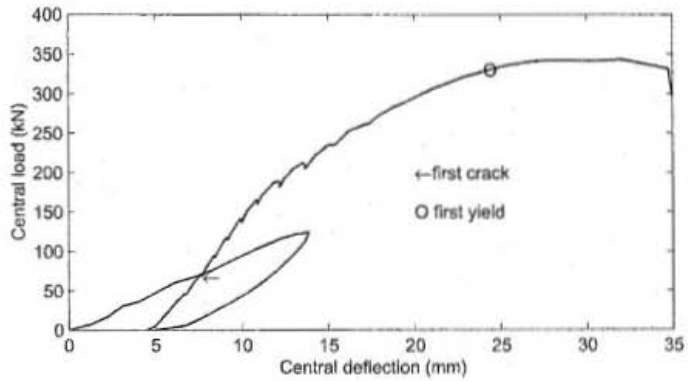

(c) GFRP–F–0.35%, P_{max} =345 kN

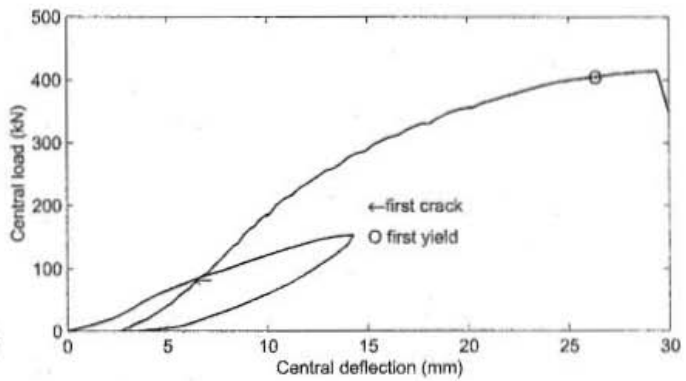

(d) GFRP–F–0.5%, P_{max} =415 kN

Figure 6.1: Load–deflection relationships for Ref–P–0.35%, Ref–P$'$–0.5%, GFRP–F–0.35%, and GFRP–F–0.5%

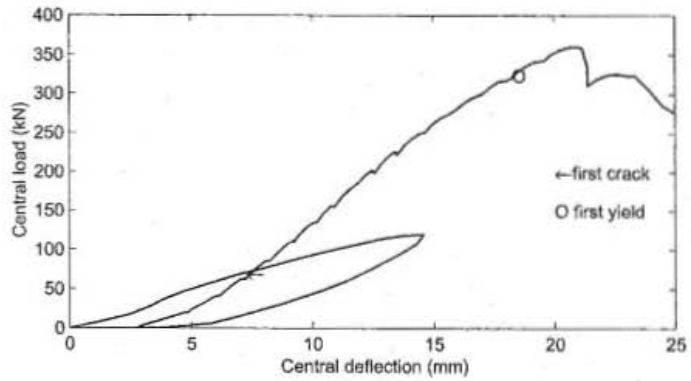

(a) CFRP–F–0.35%, P_{max} =361 kN

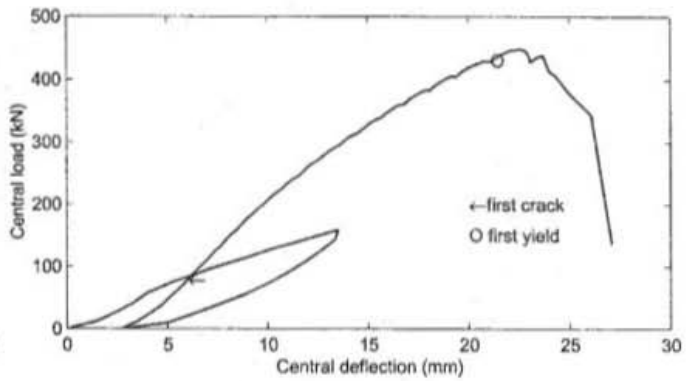

(b) CFRP–F–0.50%, P_{max} =450 kN

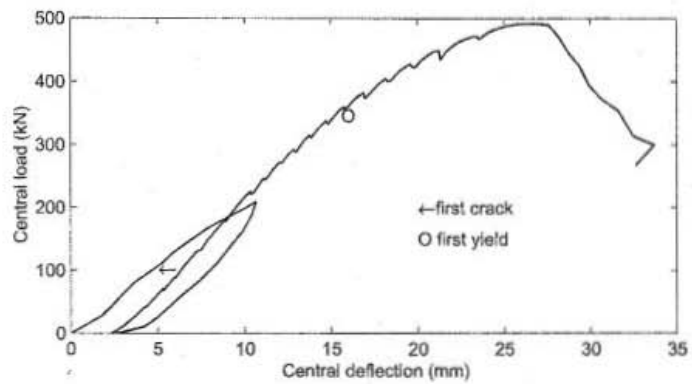

(c) CFRP1–S–1.0%, P_{max} =491 kN

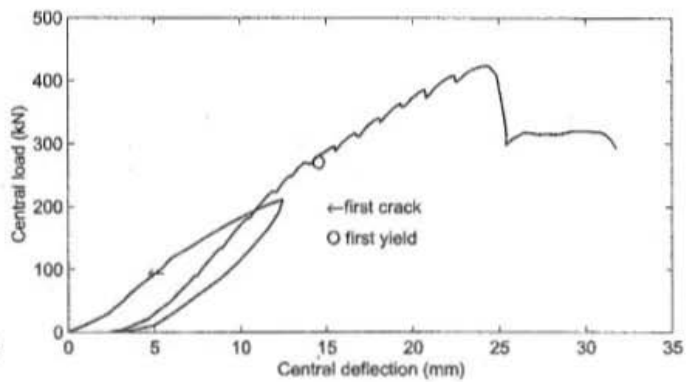

(d) CFRP2–S–1.0%, P_{max} =425 kN

Figure 6.2: Load–deflection relationships for CFRP–F–0.35%, CFRP–F–0.35%, CFRP1–S–1.0%, and CFRP2–S–1.0%

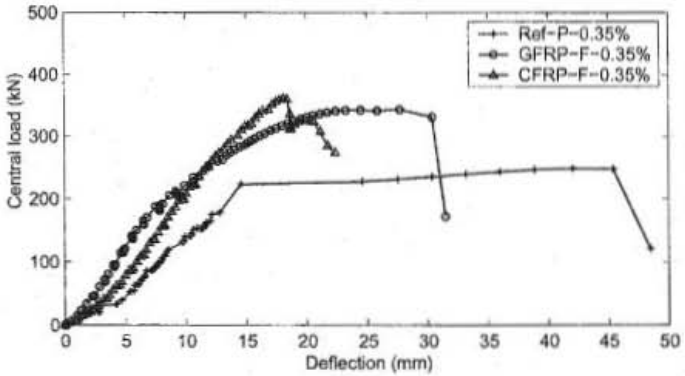

(a) Flexural–strengthening, ρ= 0.35%

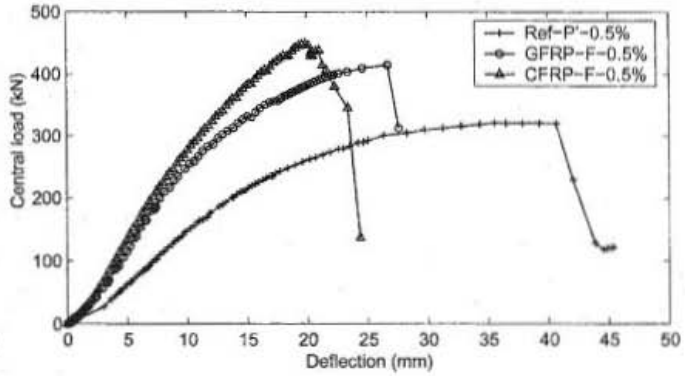

(b) Flexural–strengthening, ρ= 0.50%

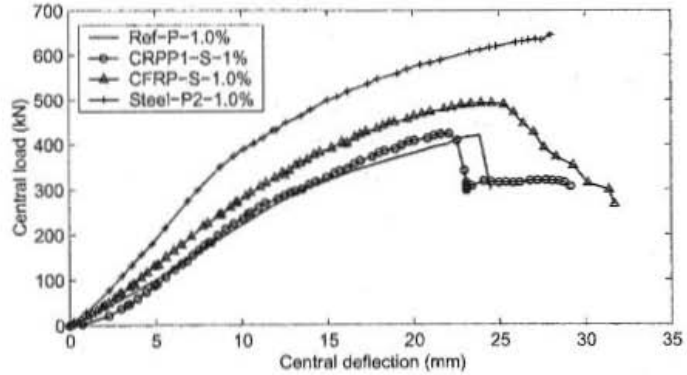

(c) Shear–strengthening, ρ= 1.0%

Figure 6.3: Load–deflection relationships for flexural and shear–strengthening specimens

Deflection Profiles

Figures 6.4 and 6.5 show the deflection profiles of all the specimens of Group 3 at nine equi–spaced locations along each slab's width. The variation of the deflection profile was largely dependent on the original reinforcement ratios of the slabs as well as on whether the slabs were strengthened or not. Specimen Ref–P′-0.50% needs more load to reach the same level of deformation as that of specimen Ref–P–0.35% as shown in Figures 6.4.a and 6.4.b.

For the FRP flexural–strengthening specimens, there was a clear influence of the presence of the strengthening FRP material on the deflection profiles of the strengthened specimens compared to that of the associated unstrengthened reference specimens. The brittle nature of FRP materials restrains the overall deflection profile of the strengthened specimens. This results in a stiffer and less deformable behaviour of the FRP flexural–strengthening specimens, GFRP–F–0.35%, GFRP-F0.5%, CFRP–F–0.35%, and CFRP–F–0.5% compared to specimens Ref–P–0.35% and Ref–P′–0.5%. Comparing the FRP flexural–strengthening specimens with reinforcement ratio of 0.35% and those of reinforcement ratio 0.5%, it is shown that specimens with reinforcement ratio 0.5% need more load to reach the same deflection level as those of specimens with reinforcement ratio 0.35% as shown in Figures 6.4 and 6.5.

For the FRP shear–strengthening specimens, there was not a clear effect of the contribution of the strengthening materials on the overall deflection profile of the strengthened specimens compared to that of the associated unstrengthened reference specimens as shown in Figures 6.5.c and 6.5.d. This indicates that it is ineffective to use FRP materials in shear–strengthening of the two–way slab system.

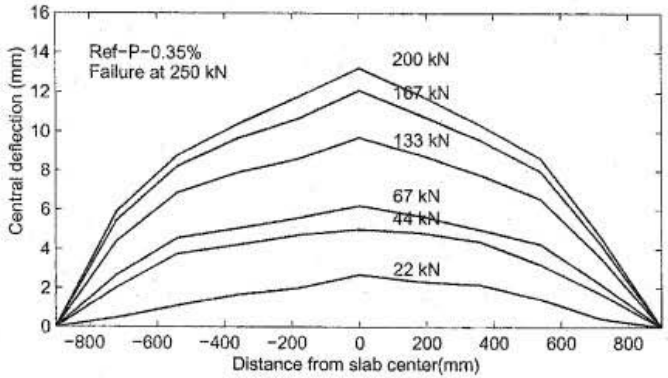

(a) Ref–P–0.35%, P_{max} =250 kN

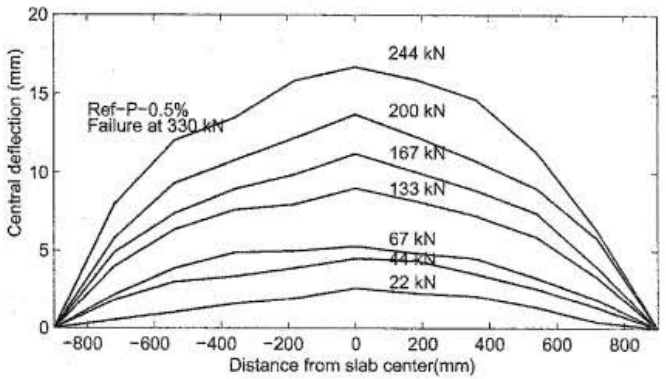

(b) Ref–P$'$–0.5%, P_{max} =330 kN

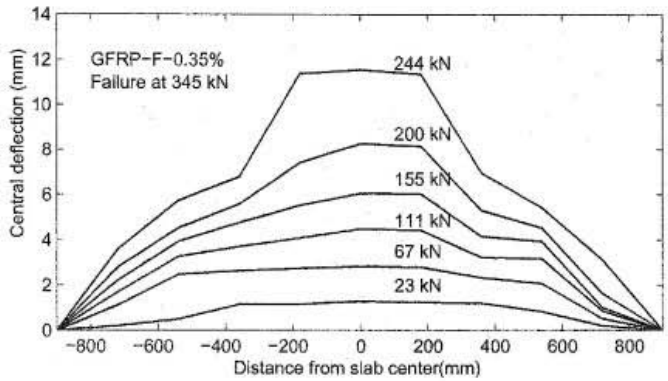

(c) GFRP–F–0.35%, P_{max} =345 kN

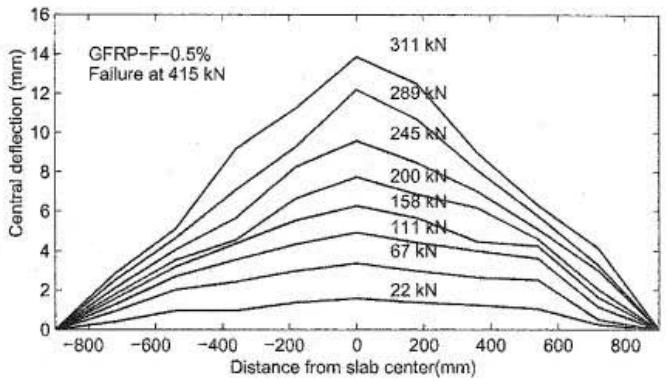

(d) GFRP–F–0.5%, P_{max} =415 kN

Figure 6.4: Deflection profiles for Ref–P–0.35%, Ref–P$'$–0.5%, GFRP–F–0.35%, and GFRP–F–0.5%

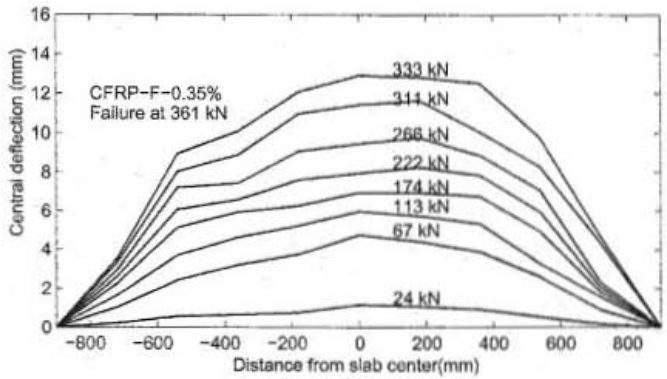

(a) CFRP–F–0.35%, P_{max} =361 kN

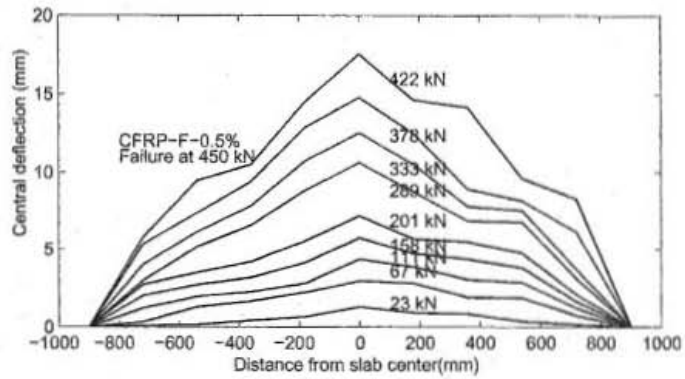

(b) CFRP–F–0.35%, P_{max} =450 kN

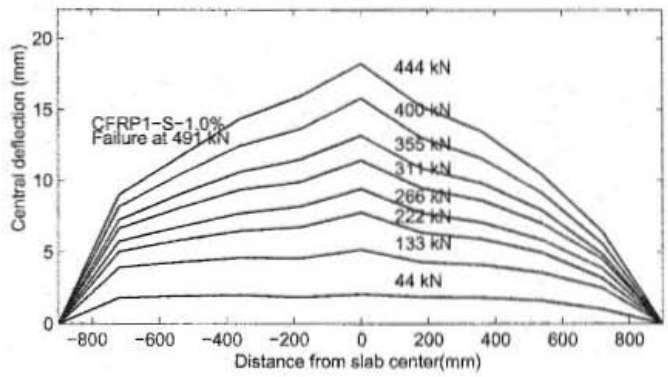

(c) CFRP1–S–1.0%, P_{max} =491 kN

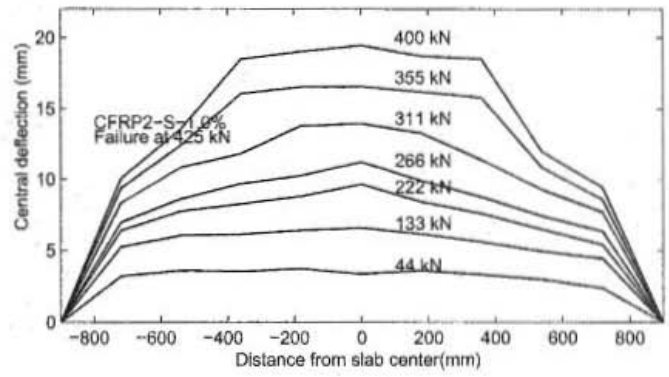

(d) CFRP2–S–1.0%, P_{max} =425 kN

Figure 6.5: Deflection profiles for CFRP–F–0.35%, CFRP–F–0.35%, CFRP1–S–1.0%, and CFRP2–S–1.0%

6.2.3 Stiffness Characteristics

As explained in Chapters 4 and 5, the stiffness of a slab at any loading point is the slope of the load–deflection curve at that point. Table 6.1 shows the initial stiffness values of all specimens.

The FRP flexural–strengthening specimens showed higher initial stiffness over that of the unstrengthened reference specimens. The flexural–strengthening specimens showed higher initial stiffness over that of the reference specimens. The average initial stiffness of specimens CFRP–F–0.35% and GFRP–F–0.35% was about 2.37 times that of the reference specimen, Ref–P–0.35%. Moreover, the average initial stiffness of specimens CFRP–F–0.5% and GFRP–F–0.5% was about 1.99 times that of the reference specimen, Ref–P′–0.5%.

Punching–shear–strengthening specimens CFRP1–S–1.0% and CFRP2–S–1.0% gained an average increase in the initial stiffness of 9% over that of the reference specimen, Ref–P–1.0%. The specimens strengthened using L–shaped steel plates gained an average increase in the initial stiffness of 70 % over the average of that of the FRP shear–strengthening specimens.

6.2.4 Steel Strain

Measurements were made to determine the steel strain distribution at selected radii from centers of the slabs. The locations of the strain gages were selected to track the variation of the steel strain with the distance from the center of the panel. Figures 3.11.a and 3.11.c show the main reinforcement strain gages distribution for specimens subjected to central load with reinforcement ratios 0.5% and 0.35%, respectively. Figure 3.11.d shows the distribution of the compression reinforcement strain gages.

As explained earlier in Chapters 4 and 5, locations of the strain gages were adopted according to previous research works on slabs carried at Memorial University of Newfoundland with the same concrete dimensions for any possible comparison (Marzouk et al., 2000a; Marzouk et al., 1998a). The closest location of measuring the steel strain is at a location (1) that is 170 mm from the center of the slab. Measurements of the strain at that location is of a special importance since it was used to define the ductility of tested specimens as discussed in Section 6.2.6.

Figure 6.6 show samples of a typical strain distribution at different locations for a specimens of flexural and punching shear strengthening. Obviously, strain gages readings reflected the locations of the gages from the panel center. As the distance from the strain gages location to the panel center was increased, the strain gages readings were decreased.

Figure 6.7 that combines the steel strain distribution for all specimens of Group 3 at location (1) of Figures 3.11.a. and 3.11.c. as shown in Figure 6.7.a, a stiffer behaviour was shown for the strengthened specimens compared to the associated unstrengthened specimens for flexural–strengthening specimens. In addition, specimens with higher reinforcement ratios showed stiffer behaviour compared to the equivalent specimens of lower reinforcement ratios. On the other hand, The punching shear–strengthening specimens showed a different observation as shown in Figure 6.7.b. The punching shear strengthened specimens showed lower stiffness compared to the reference unstrengthened specimens. This is due to the stress concentration effect around the locations of bolts. In addition, there was not much confinement to enhance the behaviour of these specimens and hence stiffer load–steel strain distribution.

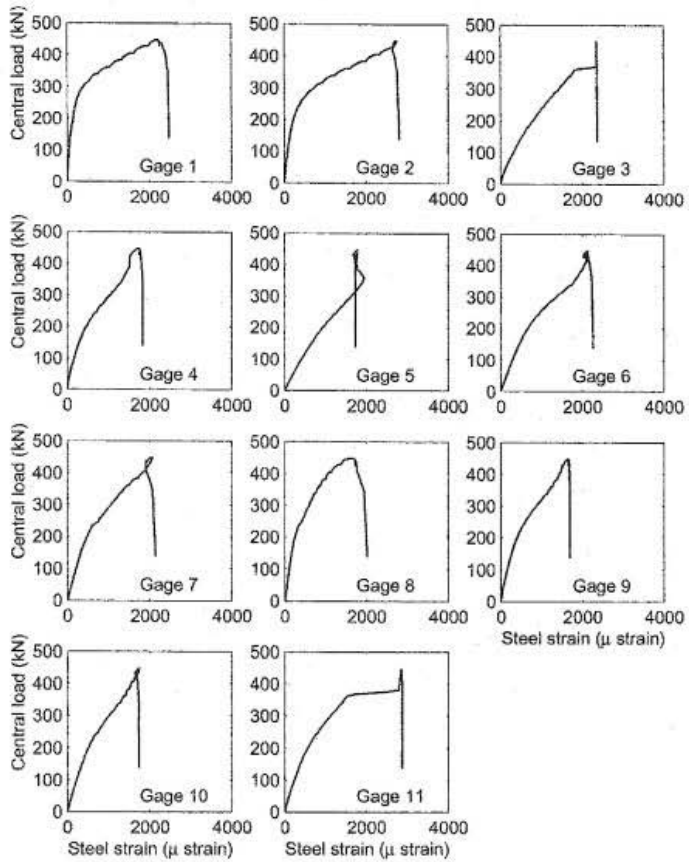

(a) CFRP–F–0.5%

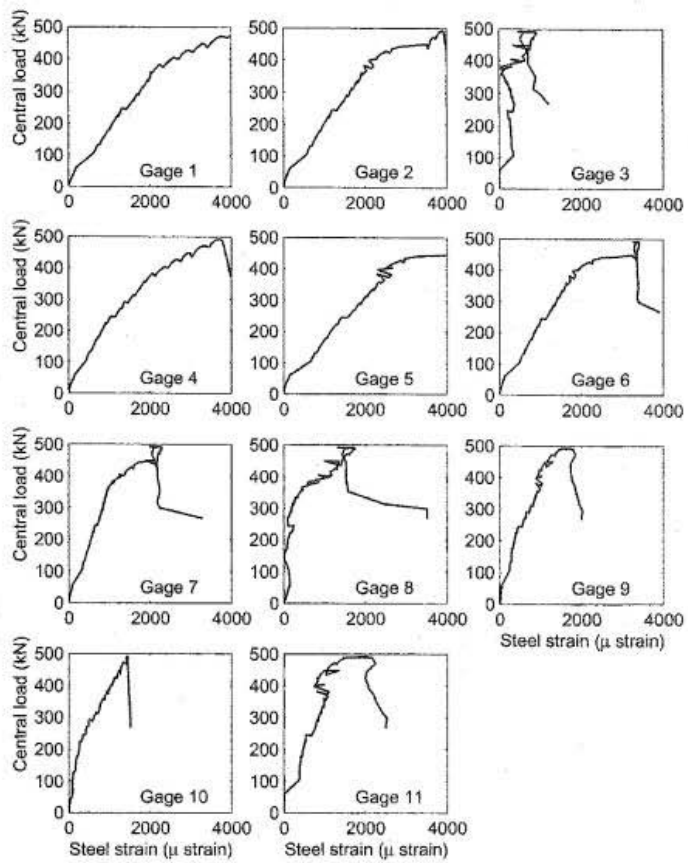

(b) CFRP1–S–1.0%

Figure 6.6: Typical Load–steel reinforcement strain relationships for flexural–strengthening specimens (CFRP–F–0.5%) and punching shear–strengthening specimens (CFRP1–S–1.0%)

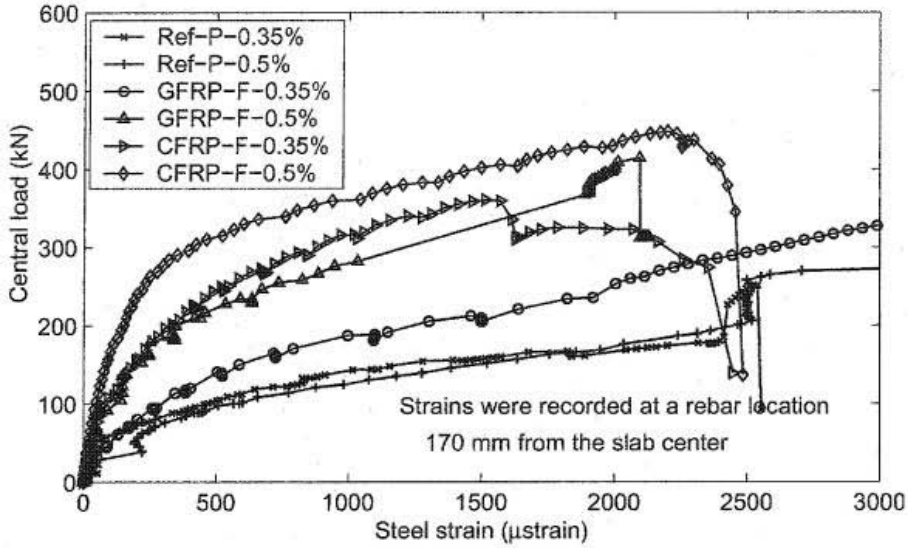

(a) Flexural-strengthening specimens

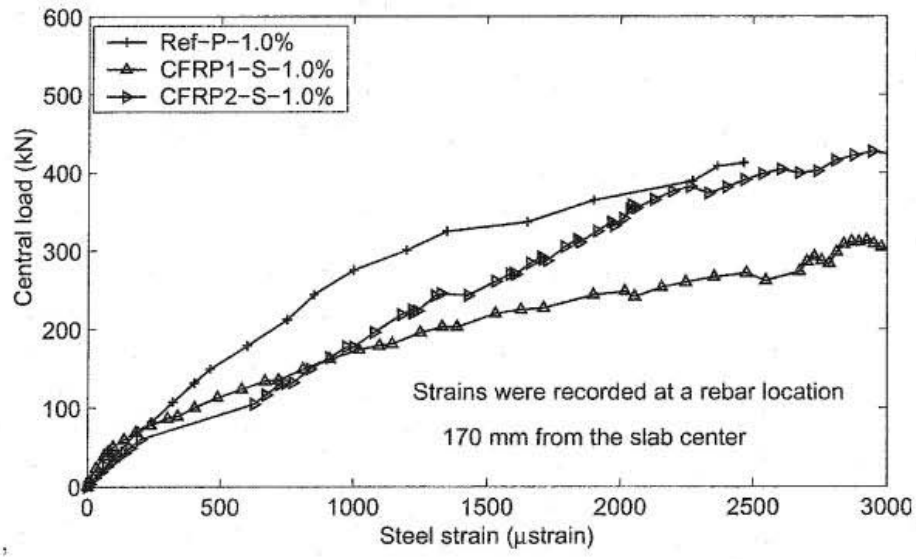

(b) Shear-strengthening specimens

Figure 6.7: Load-steel reinforcement strain relationships for all specimens of Group 3 at location (1)

6.2.5 Ductility and Energy Absorption Characteristics

Displacement ductility of a specimen, as defined in Chapters 4 and 5, is the ratio between the deflection at the ultimate load and the yield load. Regarding the unstrengthened specimens, as the reinforcement ratio was increased, the ductility was decreased. Specimen Ref–P′–0.5% showed ductility about 0.55 times that of the specimen Ref–P–0.35%, as shown in Table 6.1.

The effect of flexural–strengthening was noticeable on the ductility of the FRP flexural–strengthening specimen. Specimens GFRP–F–0.35% and CFRP–F–0.35% showed ductility 0.41 and 0.35, respectively, times that of unstrengthened reference specimen Ref–P–0.35%. Also, both specimens GFRP–F–0.5% and CFRP–F–0.5% showed ductility 0.39 times that of unstrengthened reference specimen Ref–P′–0.5%. On the other hand, the ductility of the FRP shear–strengthening specimens was randomly varied without a clear indication of the effect of the FRP shear–strengthening on the ductility.

The energy absorption is the area under the load–deflection curve for a tested specimen. It was clearly noticed that strengthening contributed to a decrease in the energy absorption of the FRP flexural–strengthening specimens. An average decrease in the values of the energy absorption of about 30% for FRP flexural–strengthening specimens was observed. On the other hand, an average increase of about 31% was recorded for the energy absorption for FRP shear–strengthening specimens. Values of the energy absorption for each slab are summarized in Table. 6.1.

Table 6.1: Test results of specimens of Group 3 including references from Group 1

Title	Crack load, P_{cr}, kN	Deflection at crack load, δ_{cr}, mm	Yield load, P_y kN	Deflection at yield load, δ_y, mm	Ultimate load, P_u, kN	Deflection at ultimate load, δ_u, mm	Energy Absorption, ψ, kN.mm	Stiffness, K, kN/mm	Ductility index	Steel strain, $\varepsilon_{su}(10^6)$
Ref–P–0.35%	73	7.00	169.0	13.05	250	42.01	9346	8.42	3.22	2540
Ref–P′–0.5%	84	6.25	175.6	12.35	330	38.08	9473	18.50	2.88	3065
Ref–P–1.0%	89	4.85	370.0	20.09	420	24.50	5950	20.08	1.22	2463
CFRP–F–0.35%	70	7.25	323.3	18.25	361	20.82	7821	15.54	1.14	2107
GFRP–F–0.35%	68	7.69	330.7	24.10	345	32.10	4597	24.42	1.33	2816
CFRP–F–0.5%	80	6.03	436.0	20.17	450	22.59	6686	26.76	1.12	2199
GFRP–F–0.5%	83	6.35	403.9	26.05	415	29.41	7475	23.15	1.13	2093
CFRP1–S–1.0%	103	5.02	341.0	15.60	491	26.91	10090	26.10	1.73	4377
CFRP2–S–1.0%	96	4.59	270.0	14.15	425	24.44	7501	17.68	1.73	3948

6.2.6 Failure Characteristics

For unstrengthened reference specimens, Ref–P–0.35% and Ref–P–0.5%, failure mode was classified as flexural–ductile. Flexural reinforcement yielded and these two specimens showed relatively large deflection values before reaching the ultimate load. On the other hand, as explained earlier in Chapter 4, specimen Ref–P–1.0% showed brittle failure due to punching–shear. Figures 6.11 and 6.12 show the failure of unstrengthened reference specimens Ref–P–0.35% and Ref–P$'$–0.5%.

Considering the failure characteristics of the FRP flexural–strengthening specimens as shown in Figures 6.13, 6.14, 6.15, and 6.16, the strengthening materials contributed to strengthening the specimen by increasing the capacity until the bond between the FRP material and concrete failed. Debonding cracks appeared at late stage of loading resulting in separation of the strengthening materials. These specimens failed due to accelerated flexural failure after the FRP–concrete debonding.

CFRP shear–strengthening specimens failed in a similar mode of failure as the associated unstrengthened reference specimens. There was not much contribution of CFRP strips on the failure characteristics of the specimens due to the lack of the confinement effect and the low out of plane stiffness of the CFRP strips. For specimens strengthened using CFRP strips, a local failure at bolt locations as shown in Figures 6.17 and 6.18 occurred at late stages of the application of load followed by a sudden punching–shear failure. As shown in Chapter 4, for the steel strengthened specimen, Steel-P2–1.0% that the punching failure was eliminated and transferred to a flexural ductile failure shown in Figure 4.15.

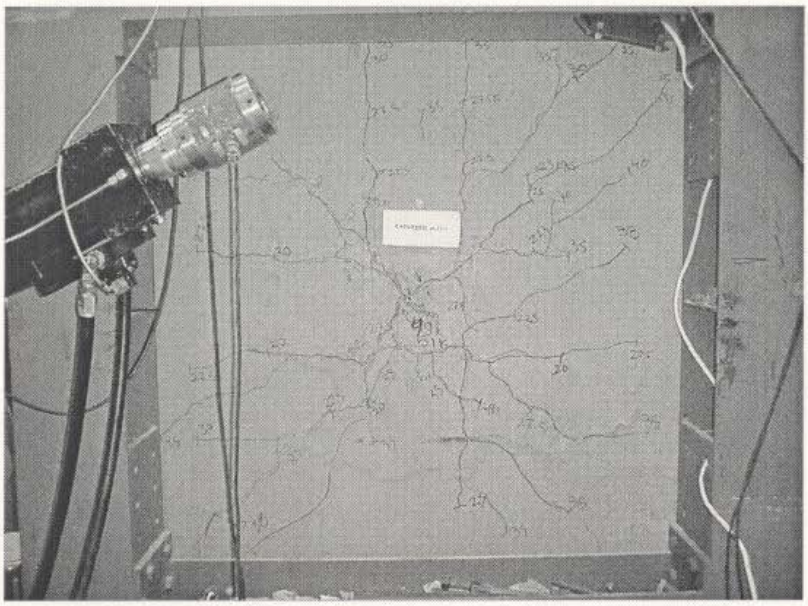

(a) Layout

(b) Close up

Figure 6.8: Specimen Ref–P–0.35% after final testing

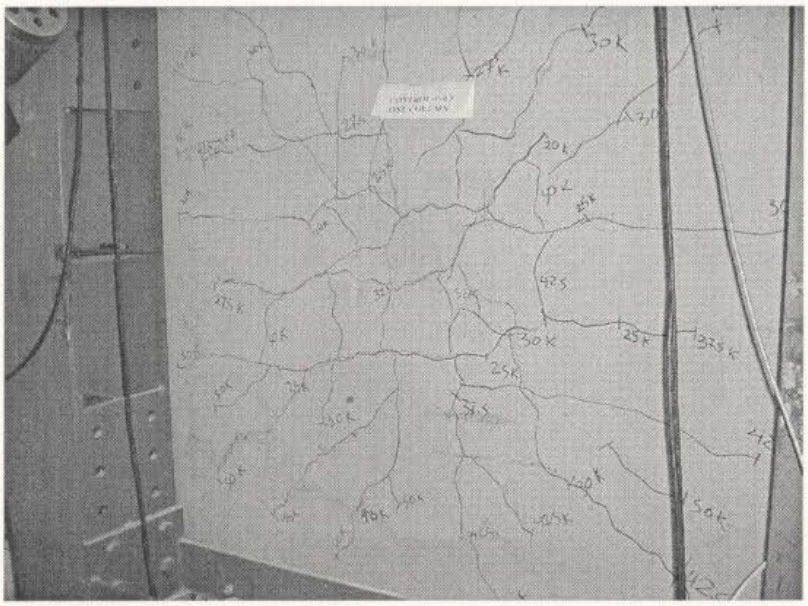

(a) Layout

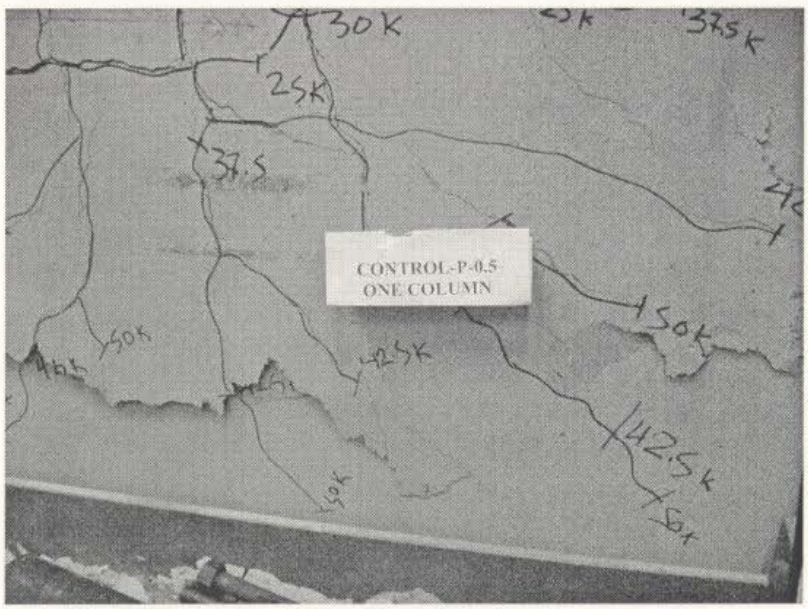

(b) Close up

Figure 6.9: Specimen Ref–P′ –0.5% after final testing

(a) Layout

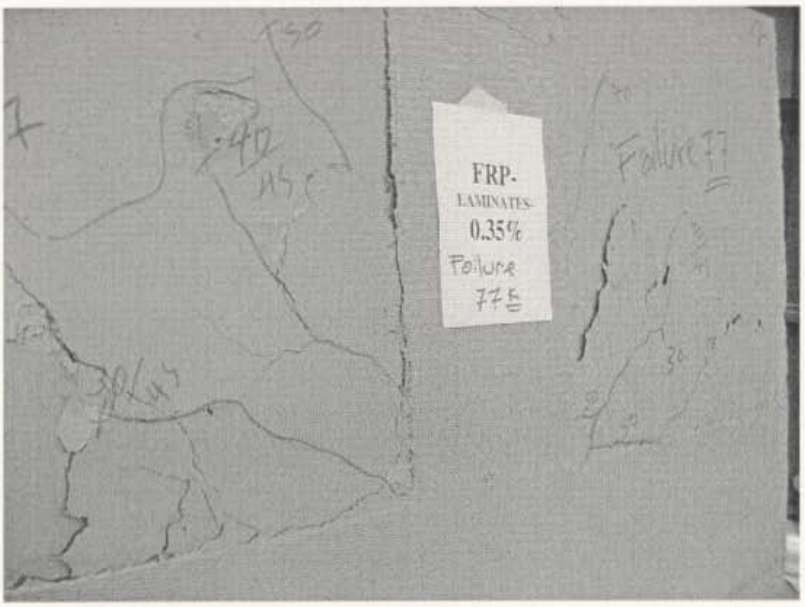

(b) Close up

Figure 6.10: Specimen GFRP–F–0.35% after final testing

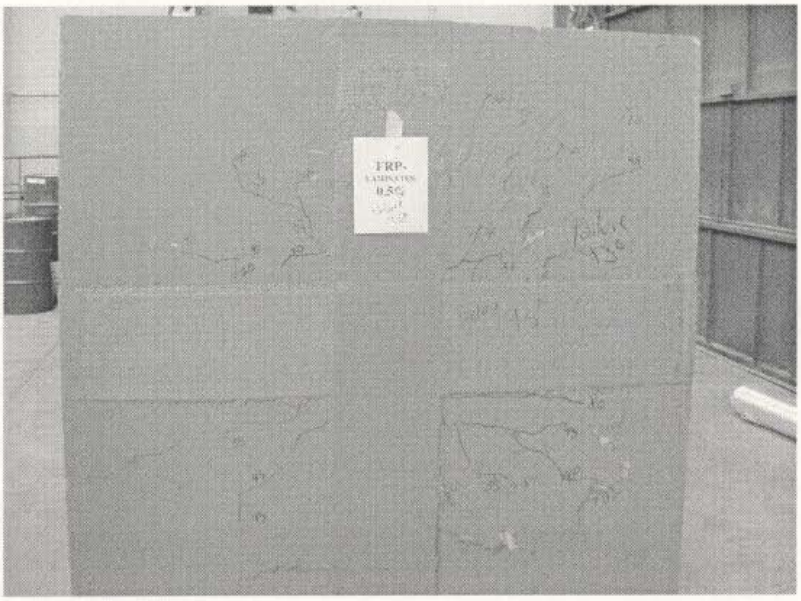

(a) Layout

(b) Close up

Figure 6.11: Specimen GFRP–F–0.5% after final testing

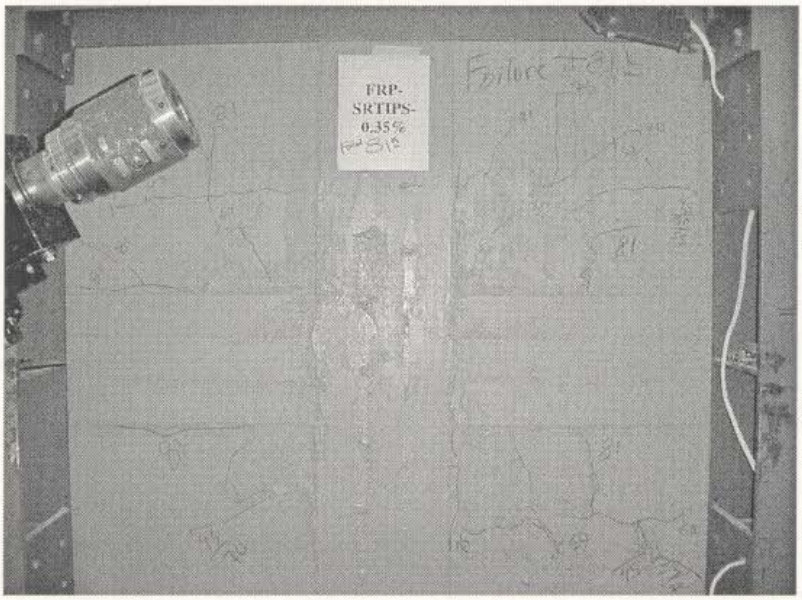

(a) Layout

(b) Close up

Figure 6.12: Specimen CFRP–F–0.35% after final testing

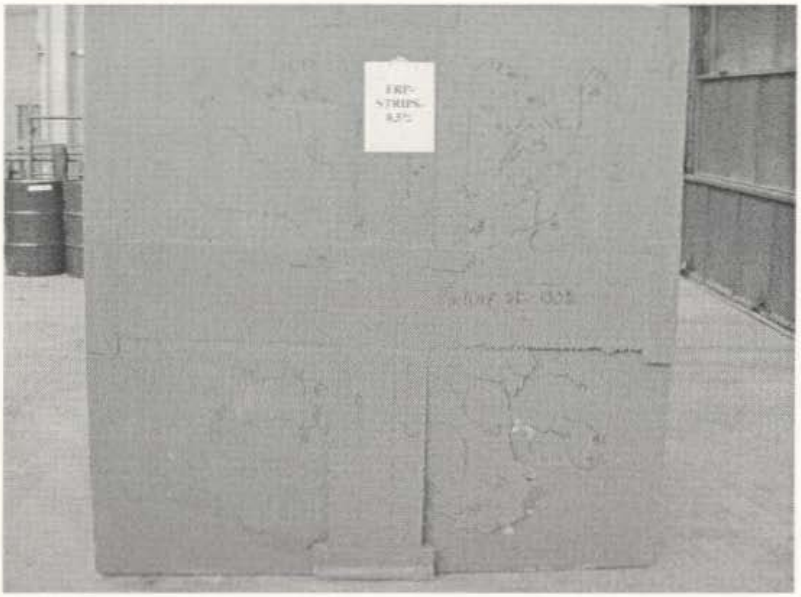

(a) Layout

(b) Close up

Figure 6.13: Specimen CFRP–F–0.5% after final testing

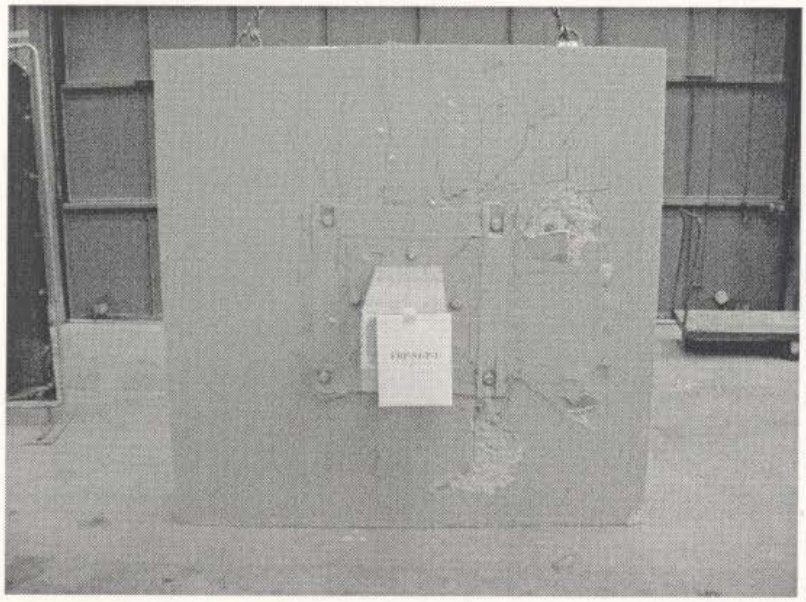

(a) Layout

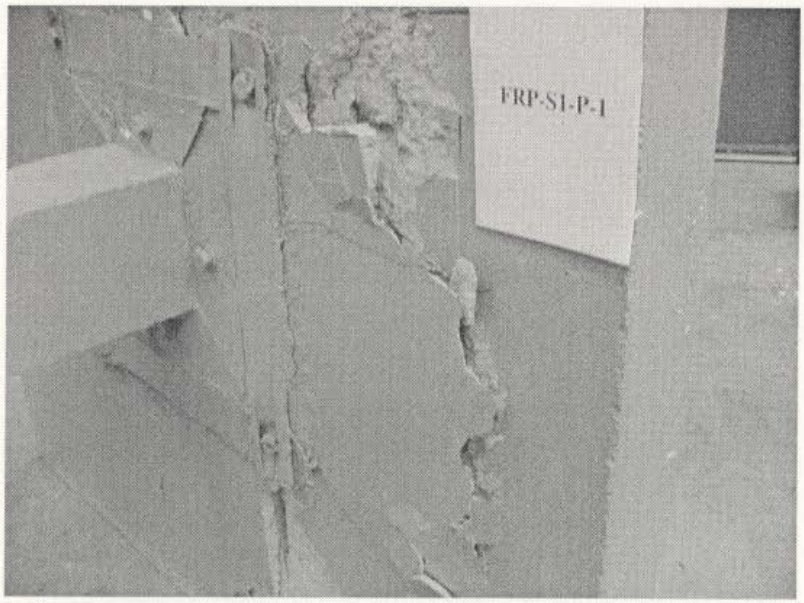

(b) Close up

Figure 6.14: Specimen CFRP1–S–1.0% after final testing

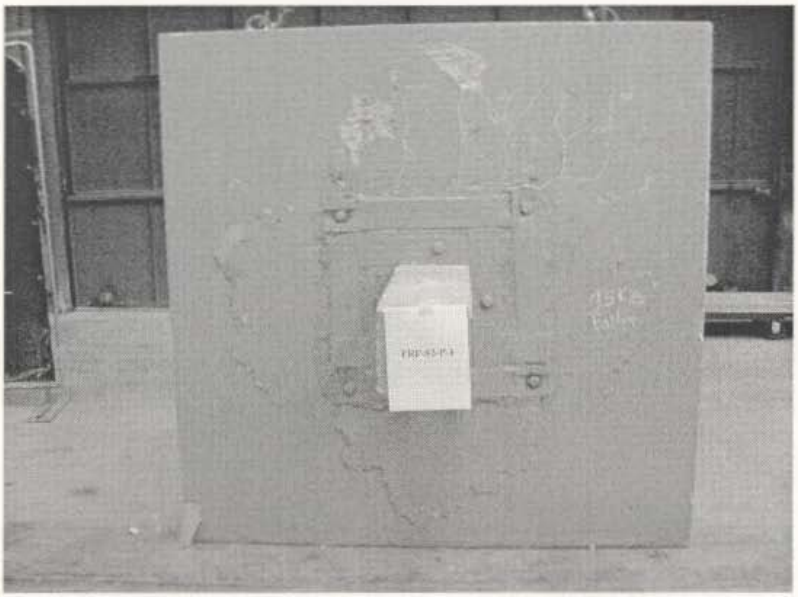

(a) Layout

(b) Close up

Figure 6.15: Specimen CFRP2–S–1.0% after final testing

6.3 Summary and Conclusions

The following conclusions were drawn for the strengthened two-way slabs using GFRP laminates and CFRP strips.

1. The use of the CFRP strips and GFRP laminates with the suggested dimensions were sufficient to achieve positive results for the flexural-strengthening specimens.

2. Flexural-strengthening specimens using CFRP strips showed an average gain in load capacity of about 40% over that of the unstrengthened reference specimens.

3. Flexural-strengthening specimens using GFRP laminates showed an average gain in load capacity of about 31% over that of the unstrengthened reference specimens.

4. The flexural-strengthening specimens showed a stiffer behaviour than that of the reference specimens. However, a decrease in ductility and energy absorption was recorded due to the brittle nature of the strengthening of the FRP materials. The average ductility of the strengthened specimens using CFRP strips and GFRP laminates were 0.37 and 0.40, respectively, of that of the reference specimens. In addition, the average energy absorption of the strengthened specimens using CFRP strips and GFRP laminates were 0.77 and 0.64, respectively, of that of the reference specimens.

5. For the suggested flexural-strengthening technique, debonding between FRP materials and concrete was the main cause of failure. Slabs failed soon after

debonding occurred due to exceeding flexural capacity. None of the strengthening material type experienced rupture or failure.

6. A small average increase within 9% was achieved for the CFRP strips and GFRP laminates punching–shear–strengthening specimens. In addition, the strengthened specimens failed under sudden undesirable punching shear failure mode. Therefore, it is not recommended to use CFRP strips or GFRP laminates for strengthening two–way slab system for specimens with a steel reinforcement ratio of 1.0% and more due to the nature of the punching–shear failure mode.

Chapter 7

Mechanical Model of Centrally Loaded Steel Strengthened Two–Way Slabs

7.1 Introduction

A mechanical model is developed to analyze strengthened and unstrengthened two–way reinforced concrete slabs. Details of this model are presented in this chapter. The developed model is intended to analyze steel plates strengthened two–way slabs using the strengthening technique presented and discussed in Chapters 3 and 4, respectively. Inclusively, the model analyzes the unstrengthened two–way slabs made of normal or high strength concrete. A uniaxial concrete constitutive model of concrete is developed considering the biaxial state of stress of concrete in a two–way slab as well as the confinement effect of the steel plates. The constitutive model of concrete includes defining the concrete properties in tension including pre–peak and post–peak properties of concrete. The mechanical model is iterative and incremental in nature. With this model, the deformation characteristics of a slab can be evaluated at each load increment until failure.

The strategy of the suggested model is based on evaluating the internal moment corresponding to a certain strain distribution at the column face section. The evaluated internal moment in the radial direction is correlated to the flexural central concentrated load, from which a value of a flexural central concentrated load, P_{fi}, is evaluated. A central deflection of the concrete slab, δ_i, due to the flexural central concentrated load, P_{fi}, is evaluated at each load increment i. Punching–shear capacity of the slab, V_c, is evaluated in accordance with the CSA code (CSA–A23.3, 1994). A failure criteria is set to differentiate between the flexural failure and punching–shear failure for the evaluation of the governing failure load and mode.

Unlike most of the available mechanical models, the model presented in this chapter evaluates not only the load carrying capacity of two–way slab but also the deformational characteristics during the application of flexural central concentrated load. In addition, the model considers the biaxial state of stress of the concrete that was ignored in most of the mechanical models in two–way slabs. This model includes the confining effect, which takes into consideration the effect of the initial strain in steel bolts due to the tightening torque. With such a treatment, the effect of steel bolts is included. A comparison between the suggested mechanical model and some of the available experimental data of strengthened and unstrengthened normal and high strength concrete two–way slabs is presented.

7.2 Rational Mechanical Models

Kinnunen and Nylander developed an early rational mechanical model for the analysis of circular concrete slabs based on the theory of plates (Kinnunen and Nylander, 1960). Further models adopted and modified the original model of Kinnunen and

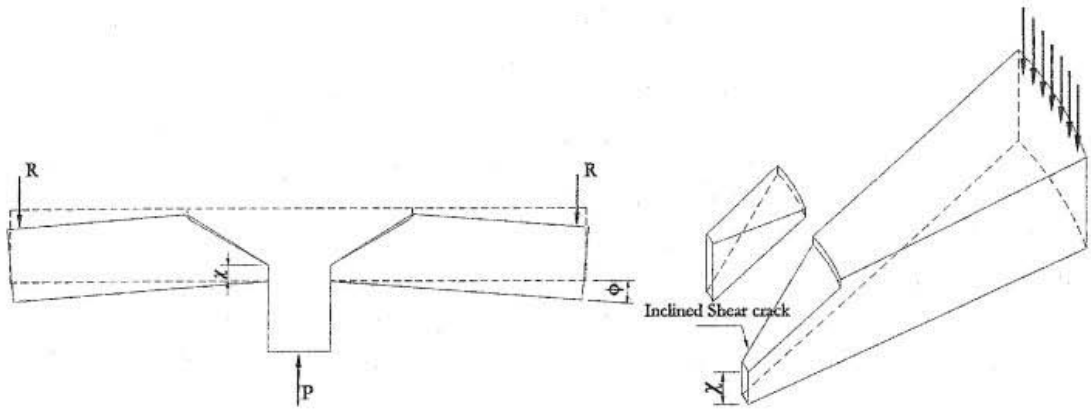

(a) Punching–shear mechanism (b) A radial sector of the slab

Figure 7.1: The original concept of rational mechanical model

Nylander (Hewitt and Batchelor, 1975; Regan, 1981; Broms, 1990; Marzouk and Hussein, 1991b; Marzouk et al., 2000b). The main approach of these models was based on dividing the slab into sectors then formulating equilibrium equations to obtain the ultimate load carrying capacity of the slab. Under the action of the central load, the column punches the slab and tends to separate its central part from the rest of it. This action of separation is well known as "punching–shear" that is caused by the creation of radial cracks that initiate at a distance x from the slab face measured along the column axis as shown in Figure 7.1. The distance x determines the height of the compression zone beyond which is the tension zone.

Some of the models ignored the tensile forces in concrete (Kinnunen and Nylander, 1960; Broms, 1990; Marzouk and Hussein, 1991b). The tensile properties of concrete were considered using the concept of the non-linear fracture mechanics. This concept was implemented through introducing the term characteristic length (Marzouk et al., 2000b). The characteristic length is defined through the relationship between the

pre-fracture and post-fracture properties of concrete and considered as a material property. The definition of the characteristic length is expressed as a function of the modulus of elasticity, E_c, tensile strength, σ_t, and the fracture energy, G_f, of concrete using the formula:

$$L_{ch} = \frac{E_c G_f}{\sigma_t^2} \tag{7.2.1}$$

The inclusion of the tensile forces when evaluating the concrete forces is demonstrated in Figure 7.2.

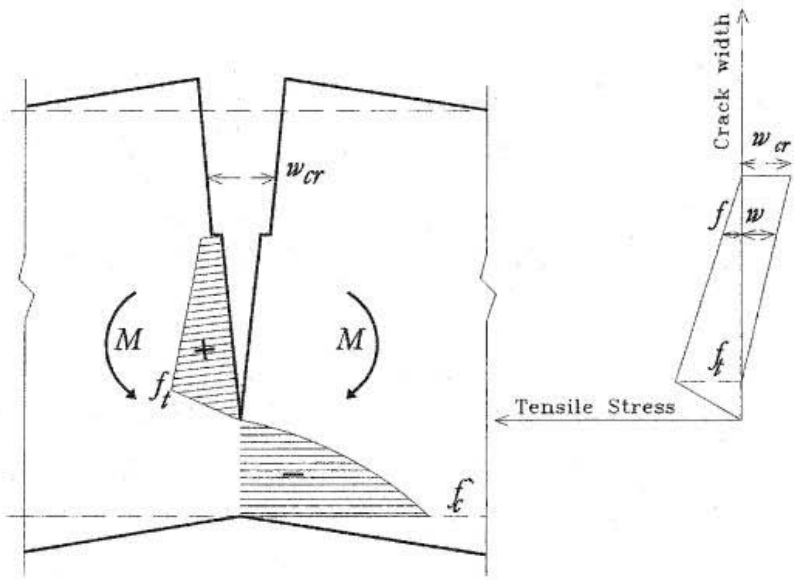

Figure 7.2: Inclusion of the tensile properties of concrete in a mechanical model.

The size effect was taken into consideration in a number of mechanical models (Broms, 1990; Zdenek and Shen, 1985; Marzouk et al., 2000b). In Broms work, a correction for the size effect was made by considering the height of the compression zone of concrete with respect to the diameter of standard test cylinder specimen. In turn, the compression zone height was a function of the total depth of the concrete

slab (Broms, 1990).

A truss-model-based design procedure was introduced for transversely reinforced slabs by Marti. In this model, the transverse shear reinforcement was adequately modeled (Marti, 1990). That approach was modified to fit slabs problems; however, it was originally intended for beams in earlier research work (Marti, 1986; Cerruti and Marti, 1987).

In some other surveyed work, a three-dimensional axi-symmetrical numerical solution for the punching–shear strength of concrete slabs was developed based on the theory of plasticity (Bortolotti, 1990). A modified Coulomb yield criterion was used in that model considering utilizing the concrete in tension. The theory of plasticity was applied to evaluate the load carrying capacity of concrete slabs in punching–shear by other researchers (Jiang and Shen, 1986).

In the aforementioned mechanical models, the state of stress of concrete in the two–way slab is assumed uniaxial; however, normal stresses in a two–way slab are varied in both directions so that the state of stress at any point is a biaxial one. It was justified that there is not a profound effect due to considering the biaxial state of stress of concrete in compression (Broms, 1990). In the current model, the suggested stress–strain relationship of concrete considers the biaxial state of stress of concrete as well as the tensile properties of concrete.

7.3 Strengthening Technique of Two–Way Slabs

In Chapter 4, the results of centrally loaded two–way slabs strengthened with steel plates and bolts were presented. The strengthening steel plates are extended to twice the slab depth around the column and act as a drop panel. Full interaction between

the steel plates and concrete is ensured using epoxy adhesive as well as the steel bolts. The bolts are subjected to a specified tensile strain. Consequently, the bolts apply a pressure on the steel plates causing the steel plates to be in a continuous interaction with the concrete surface. Figure 7.3 shows details of a typical strengthened slab using that recommended technique.

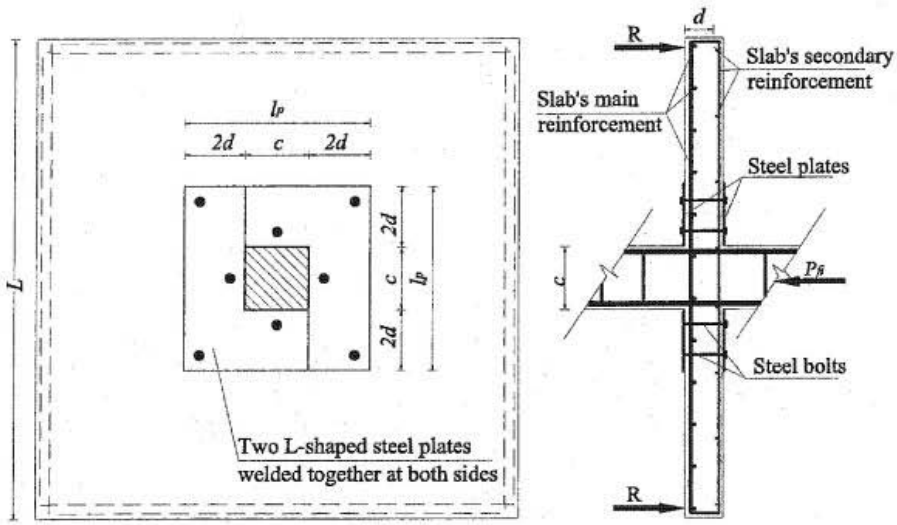

Figure 7.3: Strengthening and reinforcement details of a typical strengthened specimen

Generally, in a two–way slab system, two possible modes of failure are expected. These two possible modes are flexural failure mode and punching–shear failure mode. The reinforcement ratio contributes, at large, to the domination of a certain mode of failure (Marzouk and Hussein, 1991a). The flexural failure mode of slabs is normally developed for slabs with low reinforcement ratios. On the other hand, the punching–shear failure is generally associated with high reinforcement ratios. Flexural failure is more desirable in two–way slabs, since it is a ductile failure that gives enough warning by utilizing the steel reinforcement. Unlike flexural failure, punching–shear failure has

a sudden nature that makes it undesirable. In order to categorize the failure as flexural failure, the tensile flexural reinforcement must yield. In case of high reinforcement ratio, the steel reinforcement might not reach the yield limit before punching–shear capacity of the slab is reached. Consequently, relatively lower deflection values are expected in the latter and the failure can be classified as punching–shear failure.

7.4 Mechanical Model

As the flexural central concentrated load, P_{fi}, is applied increasingly, the section around the column is strained in the radial direction. For a unit width of the critical cross section at the column face, the strain distribution along the thickness of the section is assumed linear. Hence, internal stresses corresponding to that distribution are induced in the materials. The correlation between stresses and strains are defined using the appropriate relationship for each individual material. Due to the presence of the epoxy adhesive as well as the steel bolts in case of the strengthened slabs, full interaction between concrete and steel plates is assumed. Using the concept of balancing internal and external forces applied to the critical section, the resisting moment is evaluated. The resisting moment is equal to the external moment caused by the flexural central concentrated load as shown in Figure 7.4. Hence, a complete M_{ri}–ϕ_i (moment–curvature) relationship is developed for the two–way slab in the radial direction at each load increment, i. Consequently, using the M_{ri}–ϕ_i relationship, an expression for the varied stiffness of the slab at any load increment, i, can be derived. Hence, the slab deflection, δ_i, at the center of the two–way slab for each load increment, i, can be evaluated.

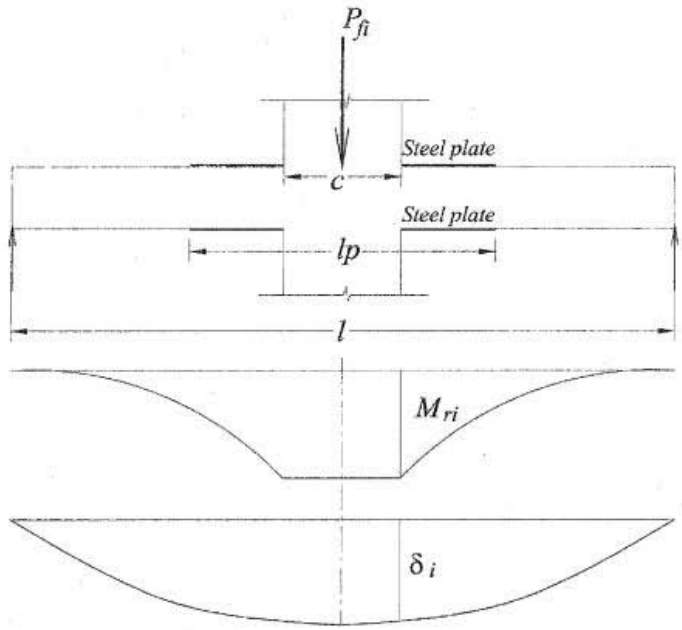

Figure 7.4: Moment and deflection distribution of a two-way slab

7.4.1 Compressive Stress–Strain Relationship for Concrete

An equal–biaxial state of stress ($\sigma_I = \sigma_{II}$) is considered in the current model. Considering the biaxial stress envelopes of concrete as shown in Figure 7.5.a, it is clear that along the compression surfaces, the combination of the in-plane stresses, σ_I and σ_{II}, leads to a different value of the actual compressive strength of concrete. For the failure surface envelope as shown in Figure 7.5.b, there are upper and lower limits of the actual concrete compressive strength, based on the ratio between σ_I and σ_{II}. The lower limit is the uniaxial state of stresses and the upper is at the state of stresses when the ratio σ_I / σ_{II} is equal to about 0.5. Considering the lower limit case, the actual compressive strength values will be underestimated and will not represent the

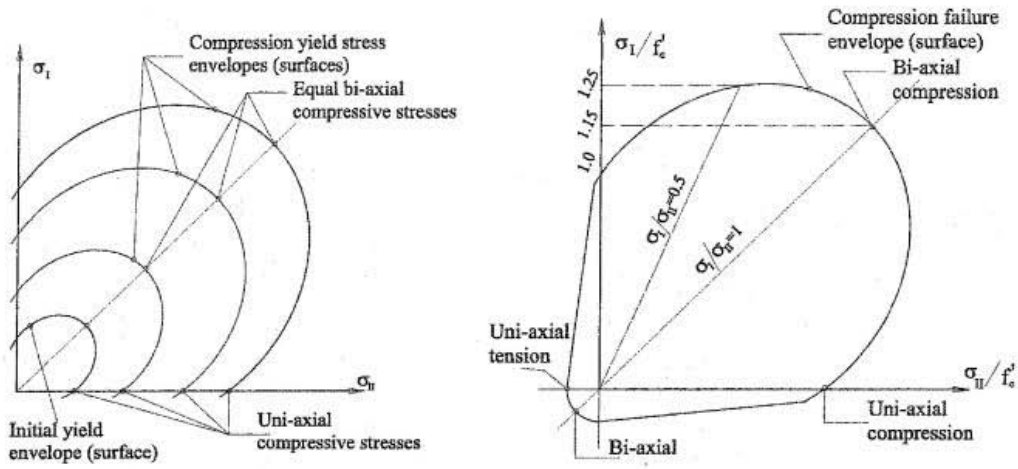

(a) biaxial Plane stress envelops

(b) biaxial stress failure envelope

Figure 7.5: biaxial behaviour of concrete

actual state of stress in a two–way slab. In case of the upper limit, the ultimate biaxial compressive stress is about 25% more than the uniaxial value. For the equal biaxial state of stress, σ_I / σ_{II} is unity, the actual compressive strength is about 19% and 14% more than that of the uniaxial compressive strength in the case of the normal strength and high strength concrete, respectively (Hussein and Marzouk, 1998). Based on Kupfer's work the increase in the compressive strength is 15% in case of equal biaxial state of stress.

The concept of an equivalent uniaxial model for concrete structural elements that best described using a biaxial model, as in the case of the state of stress in a two–way slabs, was suggested by many researchers (Floegl and Mang, 1982; Chen and Ting, 1980). Such expressions for the equivalent uniaxial models were always based on best fitting the available experimental results of biaxial tests. A stiffer behaviour of concrete is achieved in the case of biaxial state of stress compared to the case of

uniaxial state of stress. The stress–strain relationships for the uniaxial and the equal biaxial states of stress have the same trend with an accumulated shift (Kupfer et al., 1969; Hussein and Marzouk, 1998).

In this study, a modified uniaxial model for concrete is derived based on best fitting of available reliable results of comprehensive biaxial tests on concrete (Hussein and Marzouk, 1998). A multiplier function, $f(\varepsilon)$, is developed to transform the uniaxial stress–strain relationship to a biaxial one. This function, $f(\varepsilon)$, if multiplied by the uniaxial curve will result in the biaxial curve. Hence, the uniaxial stress–strain relation is magnified using the multiplier function, $f(\varepsilon)$.

$$f(\varepsilon) = c_1 e^{c_2 \varepsilon} \tag{7.4.1}$$

In Equation 7.4.1, c_1 and c_2 are 1.36 and -58.18 for normal strength concrete and 1.40 and -40.36 for high strength concrete, respectively.

7.4.2 Confinement Effect

When the steel bolts are strained as the nuts are tightened up, the steel plates are pushed against the concrete surfaces causing the strengthened part of concrete to be under a confinement pressure. Concrete is more confined at locations closer to the steel bolts than at locations between bolts due to the relative flexibility of the steel plates compared to the concrete slab. However, it is assumed that the strengthened part of concrete is subjected to a uniform confining pressure by neglecting the internal deformations of the steel plates that occur due to the installation of the steel bolts. The effect of out–of–plane stresses caused by tightening the steel bolts, is, at best, included by treating the state of stress as a tri–axial state of stress. However, adopting such a treatment complicates the mechanical model. A simpler approach is used

in this study to consider the confinement effect on the compression stress–strain relationship of concrete. This approach is based on utilizing a magnification factor, K.

Kent-Park and Scott Models

The compressive stress can be evaluated as follows using this model (Kent and Park, 1971):

For the ascending part of the stress–strain relationship;

$$f = f_c'\left[\frac{2\varepsilon}{0.002} - \left(\frac{\varepsilon}{0.002}\right)^2\right] \tag{7.4.2}$$

For the descending part of the curve;

$$f = f_c'[1 - Z_m(\varepsilon_c - 0.002)] \geq f_{res} \tag{7.4.3}$$

The residual stress;

$$f_{res} = 0.2f_c' \tag{7.4.4}$$

One of the most famous and widely acceptable models for confined concrete is Scott model (Scott et al., 1982). Scott's model was applied primarily in the case of the confined normal reinforced concrete columns. A modification was made on the original model so that it could be used for high strength concrete columns (Mendis et al., 2000). In the current investigation, the original model is modified further so that it can be used for steel plates strengthened two–way slabs.

For the ascending part of the concrete uniaxial stress strain curve in Figure 7.6, the stress–strain relationship is parabolic in shape according to the following expression:

for $\varepsilon < 0.002K$

$$f = Kf_c^{'}\left[\frac{2\varepsilon}{0.002K} - \left(\frac{\varepsilon}{0.002K}\right)^2\right] \tag{7.4.5}$$

The post peak behaviour of the concrete in compression is divided into two zones. The first zone is assumed linearly descended using the following expression:

for $\varepsilon > 0.002K$

$$f = Kf_c^{'}[1 - Z_m(\varepsilon_c - 0.002K)] \geq f_{res} \tag{7.4.6}$$

The second part of the compression post peak relationship is a flat part at a constant value of the residual stress, f_{res}, that is given by:

$$f_{res} = 0.2\ K\ f_c^{'} \tag{7.4.7}$$

where

$$K = 1 + \frac{\rho_{sh}\ f_{yh}}{f_c^{'}} \tag{7.4.8}$$

where ρ_{sh} is the volumetric ratio of hoop reinforcement to the concrete core.

Also

$$Z_m = \frac{0.5}{\frac{3 + 0.29f_c^{'}}{145f_c^{'} - 1000}} + \frac{3}{4}\rho_{sh}\sqrt{\frac{h^{''}}{s} - 0.002K} \tag{7.4.9}$$

where $h^{''}$ is the width of the concrete core between the outside of the ties; and s is the spacing between ties.

7.4.3 Confined Concrete Stress Strain Relationship

Based on the revised models for unconfined and confined concrete proposed by Kent-Park and Scott et al., respectively, the stress–strain relationship of concrete under compression can be idealized for two–way slabs subjected to a confinement pressure.

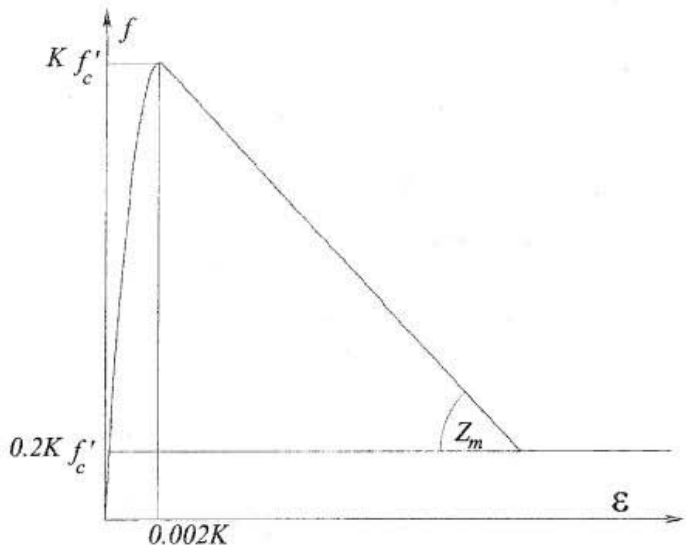

Figure 7.6: Compression stress strain relationship of concrete

Referring to Figure 7.6 that shows a hypothetical representation of the suggested compressive model of concrete used (Scott et al., 1982) and adopted herein:

For the ascending part of the relationship;

For $\varepsilon < 0.002K$

$$f = Kc_1 e^{\varepsilon c_2} f_c' \left[\frac{2\varepsilon}{0.002K} - \left(\frac{\varepsilon}{0.002K} \right)^2 \right] \tag{7.4.10}$$

For the descending part of the curve;

$$f = Kc_1 e^{.002Kc_2} f_c' [1 - Z_m (\varepsilon_c - 0.002K)] \geq f_{res} \tag{7.4.11}$$

The residual stress;

$$f_{res} = 0.2K f_c' \tag{7.4.12}$$

The value of K gives the ratio between confined and unconfined concrete compressive strengths. A simple expression is proposed by Scott et al. (Scott et al., 1982) and

employed herein; $K = 1 + A\frac{f_l}{f_c'}$ for confined concrete and $K = 1$ for unconfined concrete. The value of A is set as 2.00 for the normal strength concrete as recommended in Scott's model and varied from 3.00 to 5.00 for the high strength concrete (Mendis et al., 2000). The value of K is correlated to the volumetric ratio of the steel stirrups in Scott's model. In the current model the confinement effect of steel bolts along with part of the steel plates between bolts can provide a similar effect to that of the closed stirrups in the original confined concrete model.

7.4.4 Evaluation of the Confining Pressure, f_l

The steel bolts are strained as tightened up. The confining pressure of the steel plates on the concrete slab is evaluated using the following expression:

$$f_l = \frac{\varepsilon_{bolt}\, E_{sb}\, N_B\, \pi\, \phi^2}{4\left(l_p^2 - c^2\right)} \tag{7.4.13}$$

where, N_B is the number of bolts; ε_{bolt} is the strain induced in the bolt due to the applied torque; E_{sb} is the elastic modulus of the material of the bolts, and ϕ is the diameter of the bolts.

An equivalent expression to Z_m in Scott model is introduced in the current model taking into consideration the dimensions of the steel plates and the number of bolts.

$$Z_m = \frac{0.5}{\frac{3 + 0.29 f_c'}{145 f_c' - 1000} + \frac{3 f_l}{2 f_y}\sqrt{\frac{l_p - c}{4\sqrt{2}\,h^2 + 0.25c^2 + hc}} - 0.002K} \tag{7.4.14}$$

For unconfined concrete Z_m is evaluated according to the following expression (Mendis et al., 2000):

$$Z_m = \frac{0.5\left(.018\, f_c' + 0.55\right)}{\left(\frac{3 + 0.29 f_c'}{145 f_c' - 1000} - \varepsilon_c\right)} \tag{7.4.15}$$

7.4.5 Tensile Stress–Strain Relationship of Concrete

Many research works have investigated a complete stress–deformation relationship for normal concrete in tension (Guo and Zhang, 1987; Hilleborg, 1985; Gopalaratnam and Shah, 1985). One of the simplest expressions (Hurlbut, 1983) was adopted in Etse and Willam model (Etse and Willam, 1994). That expression correlates the post–peak normalized tensile stress σ_t/σ_t^u and the normalized crack opening displacement, u_t/u_{t0} using the following formula:

$$\sigma_t/\sigma_t^u = e^{-5\,u_t/u_{t0}} \tag{7.4.16}$$

More recently, a research investigation of the direct tension and fracture energy of high strength concrete was conducted (Marzouk and Chen, 1995). The following expression was adopted in the current analysis.

For pre-peak softening relationship ($\varepsilon_t \leq \varepsilon_{t0}$)

$$\sigma_t = \sigma_t^u \left(2\frac{\varepsilon_t}{\varepsilon_{t0}} - \frac{\varepsilon_t^2}{\varepsilon_{t0}^2} \right) \tag{7.4.17}$$

For post-peak stiffening relationship ($\varepsilon_t \geq \varepsilon_{t0}$)

$$\sigma_t = \sigma_t^u \left(\frac{\varepsilon_t/\varepsilon_{t0}}{\alpha\,(\varepsilon_t/\varepsilon_{t0} - 1)^{\beta} + \varepsilon_t/\varepsilon_{t0}} \right) \tag{7.4.18}$$

where:

$$\alpha = c_3\sigma_t^u \tag{7.4.19}$$

The value of c_3 is 0.31 for normal strength concrete (Guo and Zhang, 1987) and modified to 0.28 for high strength concrete (Marzouk and Chen, 1995). Also, β is equal to 1.70 for normal strength concrete and 1.67 for high strength concrete. Concrete tensile strength is taken as 0.08 and 0.05 times the uniaxial compressive

strength of normal and high strength concrete, respectively (Marzouk and Chen, 1995).

7.4.6 Stress Strain Relationship for Steel Reinforcement and Steel Plates

The definition of the stress strain relationship for steel reinforcement and steel plate is shown to be similar to that shown in Figure 7.7 considering the appropriate notations for the steel reinforcement and steel plates. The stress–strain relations in both compression and tension are the same. The stress strain relationship for steel reinforcement or steel plates can be expressed as follows:

$$f_s = \begin{cases} 210000\varepsilon_s & 0 < \varepsilon_s < \dfrac{f_y}{210000}, \\ f_y & \dfrac{f_y}{210000} < \varepsilon_s < 0.006, \\ f_y\left(-26.57\varepsilon_s^2 + 7.4388\varepsilon_s + 0.99\right) & 0.006 < \varepsilon_s < 0.1, \\ 0 & \varepsilon_s > 0.1. \end{cases} \tag{7.4.20}$$

where:

$$f_s = \begin{cases} f_{s,t} & \text{for tension steel reinforcement,} \\ f_{s,c} & \text{for compression steel reinforcement,} \\ f_{sp,t} & \text{for steel plates at the tension side of the slab,} \\ f_{sp,c} & \text{for steel plates at the compression side of the slab,} \end{cases}$$

and

$$\varepsilon_s = \begin{cases} \varepsilon_{s,t} & \text{for tension steel reinforcement,} \\ \varepsilon_{s,c} & \text{for compression steel reinforcement,} \\ \varepsilon_{sp,t} & \text{for steel plates at the tension side of the slab,} \\ \varepsilon_{sp,c} & \text{for steel plates at the compression side of the slab.} \end{cases}$$

The yield stress is equal to f_y in the case of steel reinforcement and is equal to f_{yp} in the case of steel plates.

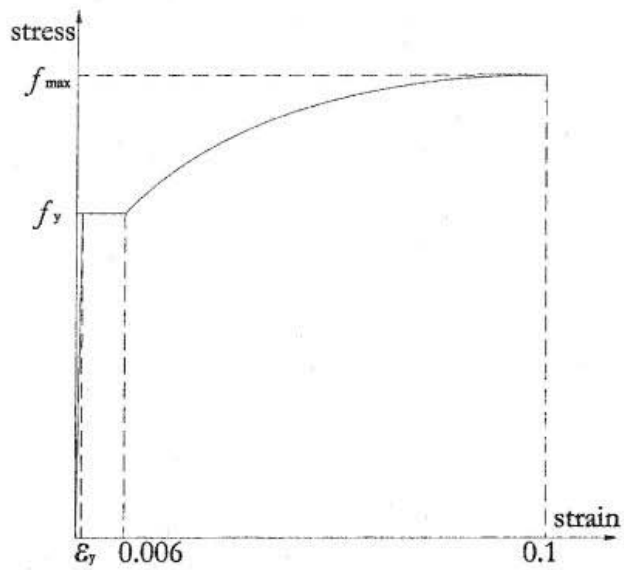

Figure 7.7: Stress strain relationship in both compression and tension for steel reinforcement and steel plates.

7.4.7 Computational Algorithm

The cross section at the slab to column connection of a unit width of a slab is subdivided to N number of divisions through the thickness of the slab. At the beginning of the analysis, two values of upper fibre concrete strain, $\varepsilon_{top,i}$, and lower fibre concrete strain, $\varepsilon_{bot,i}$, are interactively specified. The procedure also allows the user to define a range of $\varepsilon_{top,i}$and $\varepsilon_{bot,i}$. The upper and lower ranges of $\varepsilon_{top,i}$ and $\varepsilon_{bot,i}$ are divided into Q and M subdivisions, respectively. Each value of the lower subdivisions, $\varepsilon_{bot,i}$, is coupled with all the upper subdivisions in a successful manner to formulate M times

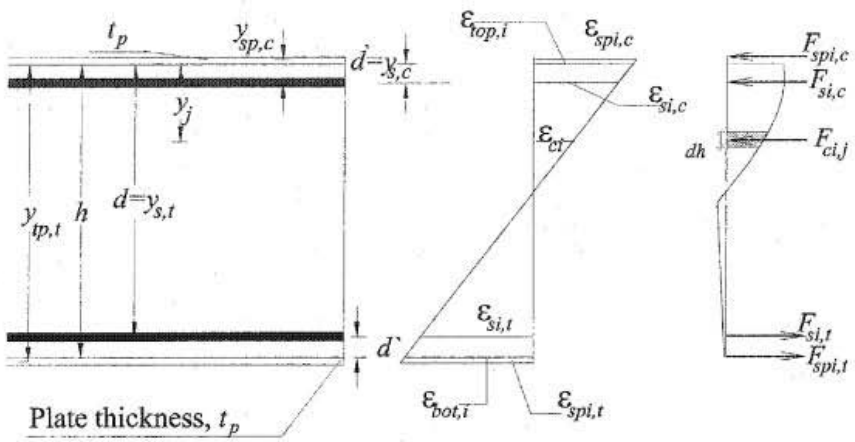

Figure 7.8: Calculation of the internal moment, M_{ri}.

of strain distribution profiles for each division of Q. Only one strain distribution profile, if any, is specified as a "true" strain distribution at which the internal equilibrium of the internal forces occur. The condition of a true distribution is achieved where the sum of the internal forces equals zero or equals acceptable tolerance, $O(F)$. Once the whole values of different strain profiles across the overall thickness of slab cross section for an assumed strain range are examined, another range of strain is automatically assumed for new strain profiles and new equilibrium positions, etc. The computer mechanical model intelligently defines the upper and lower ranges for each successive run to estimate the strain distribution profiles as they change with the load. The calculations of the internal forces at an arbitrary strain distribution profile is shown in Figure 7.8.

At any iteration, i, the internal forces generated in the concrete, steel reinforcement, and steel plates are calculated. These forces are associated with a certain strain distribution. For a true strain distribution, the sum of the internal forces,

$\sum F_i$, should equal to zero or to an acceptable tolerance.

$$\sum F_i = \sum_{j=1}^{N} F_{ci,j} + F_{si,t} + F_{si,c} + F_{spi,t} + F_{spi,c} \tag{7.4.21}$$

where, $\sum_{j=1}^{N} F_{ci,j}$ is the sum of the internal forces generated in concrete at iteration, i, along the section divisions, j_s. The value of $F_{ci,j}$ is the concrete force at section division j and load level i and is calculated from the following relation

$$F_{ci,j} = (f_{ci,j} + f_{ci,j+1})\ dh \tag{7.4.22}$$

Also $F_{si,t}$, $F_{si,c}$are the forces generated in the tension steel, compression reinforcement,

$$F_{si,t} = f_{si,t}\ \rho d \tag{7.4.23}$$

$$F_{si,c} = f_{si,c}\ \rho^{'} d \tag{7.4.24}$$

The steel plate length, l_p, is less than the slab length, L. Therefore, the total force in the tension and compression steel plates is reduced by a factor μ; where:

$$\mu = 0.85\frac{l_p - c}{L} \tag{7.4.25}$$

Hence, the forces generated in the tension and compression plates respectively are:

$$F_{spi,t} = t_p \mu\ f_{spi,t} \tag{7.4.26}$$

and;

$$F_{spi,c} = t_p \mu\ f_{spi,c} \tag{7.4.27}$$

Accordingly, the internal moment of the section around the upper concrete fibres–that is equal to the external moment caused by the flexural central concentrated load–can be calculated as;

$$M_{ri} = \sum_{j=1}^{N} f_{ci,j}\, dh\, y_j + \rho\, f_{si,t}\, d\, y_{si,t} + \rho'\, f_{si,c}\, d\, y_{si,c} + t_p\, \mu\, (f_{spi,t}\, y_{spi,t} + f_{spi,c}\, y_{spi,c}) \tag{7.4.28}$$

The flow chart shown in Figure 7.9 shows the computer algorithm used in the current analysis.

7.5 Ultimate load carrying capacity of Slabs

The radial bending moment for a plate under a central concentrated load according to the theory of elasticity can be written as:

$$M_{ri} = \frac{P_{fi}}{4\pi}\left[\ln\frac{L}{c} + \frac{1}{2}\left(1 - \frac{c^2}{L^2}\right)\right] \tag{7.5.1}$$

Therefore, the associated concentrated load that causes a value of internal moment of M_{ri} (Broms, 1990) is;

$$P_{fi} = \frac{4\pi M_{ri}}{\left[\ln\frac{L}{c} + \frac{1}{2}\left(1 - \frac{c^2}{L^2}\right)\right]} \tag{7.5.2}$$

The curvature of the slab cross section of unit width of the slab at the column location is;

$$\phi_i = \frac{\varepsilon_{top,i} + \varepsilon_{si,t,i}}{d} \tag{7.5.3}$$

The stiffness of the slab at any load increment, i, is:

$$D_i = \frac{M_{ri}}{\phi_i} \tag{7.5.4}$$

The following approximate expression is used to evaluate the deflection at a slab center;

$$\delta_i \cong \frac{P_{fi}}{64\, D_i L}\left(L^2 - c^2\right)(L - c) \tag{7.5.5}$$

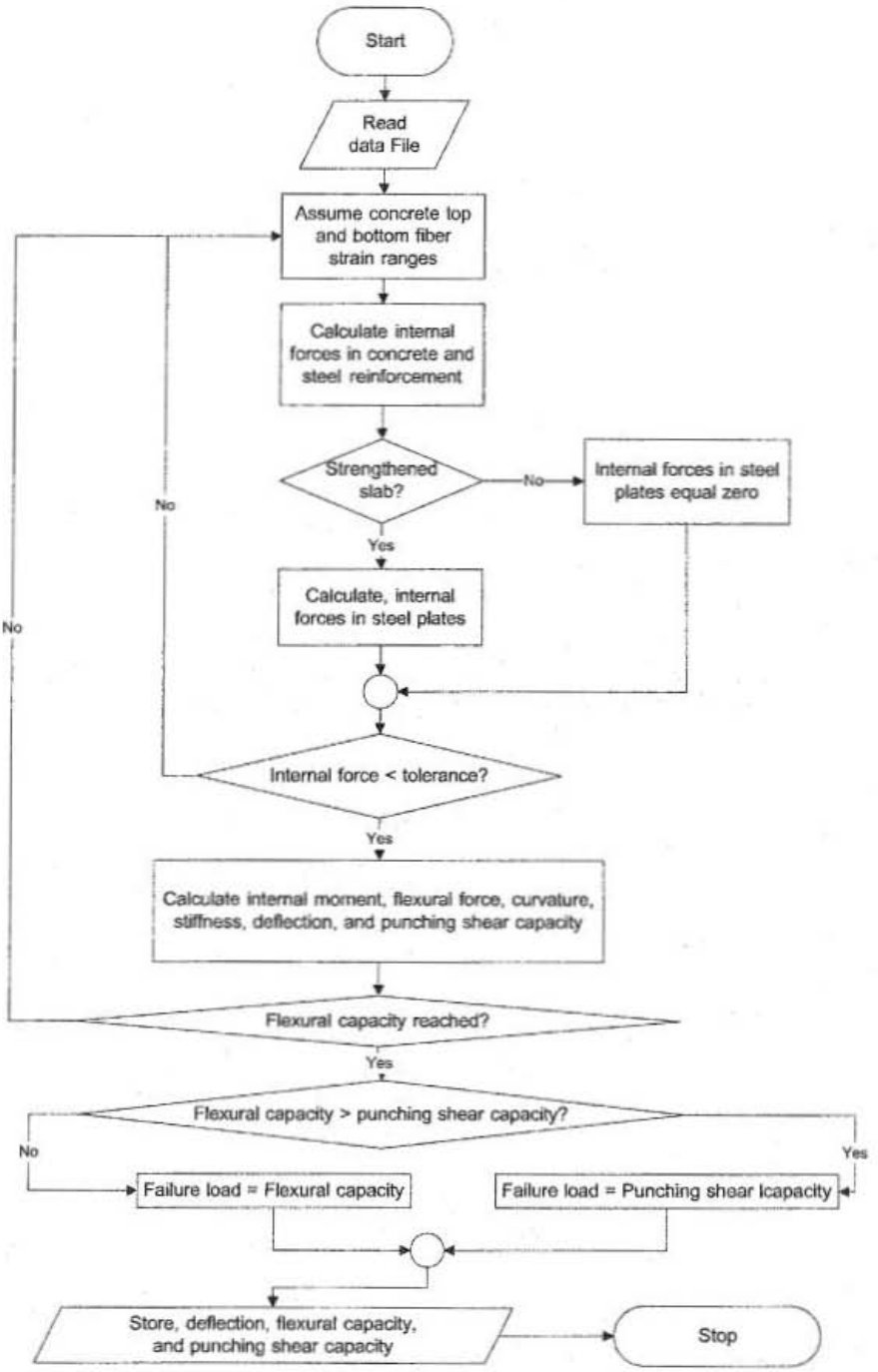

Figure 7.9: The computational algorithm flow chart

The punching–shear capacity of a square strengthened two–way slab can be calculated using the following expression:

In the case of unstrengthened specimens:

$$V_c = 0.4[4\,d\,(d+c)]\sqrt{f_c'} \tag{7.5.6}$$

In the case of strengthened specimens:

$$V_c = 0.4[4\left(d+\frac{E_s}{E_c}t_p\right)\left(d+\frac{E_s}{E_c}t_p+c\right)]\sqrt{f_c'} \tag{7.5.7}$$

Failure is assumed to occur according to two criteria, namely flexural criterion or punching–shear criterion. Hence, the slab failure is assumed to occur when one of the these two criteria is satisfied:

1. if the tensile strain at the location of the tensile steel reinforcement reaches a value of 0.01 or if the maximum compressive strain of concrete reaches a value of 0.0035. This case represents the flexural failure.

2. if V_c, the maximum shear is reached. This case represents the punching–shear failure.

7.5.1 Verification of the Proposed Model

The results of the mechanical model shows a good agreement with available experimental data, for both the strengthened and unstrengthened two–way concrete slabs. The model is verified against data of specimens Ref–P–1.0%, Ref–P–0.5%, Steel–P2–1.0%, Steel–P3–1.0%, and Steel–P4–1.0% as presented Chapter 4. Figure 7.11 shows a comparison between the experimental and theoretical results in terms of the load–deflection relationships of the slabs Steel–P3–1.0% and Steel–P4–1.0%. The developed model overestimates the initial stiffness of the slabs. The overestimation can

be attributed to the fact that the original slabs were subjected to pre-loading and pre-strengthening process of drilling, hammering, and roughening. Such factors were not considered in the current model. The model is verified further against some of other researchers experimental data of unstrengthened specimens (Marzouk and Hussein, 1991b; Elstner and Hognested, 1956). The verification of the suggested model shows a good agreement with these experimental data in terms of the ultimate load carrying capacity as shown in Figure 7.12. Tables 7.1 to 7.3 show a comparison between the theoretical and experimental results and indicate that the mean value of the ratio between the calculated load carrying capacity using the suggested model, P_{cal}, and that obtained experimentally, P_{exp}, is about 0.979.

Table 7.1: Comparison with experimental results

Title	f_c', MPa	ρ,%	No. of Bolts	P_{exp}, kN	P_{cal}, kN	P_{cal}/P_{exp}
Ref–P–1.0%	36	1.00	—	420	406	0.97
Ref–P–0.5%	35	0.50	—	314	276	0.88
Steel–P2–1.0%	32	1.00	8	645	649	1.01
Steel–P3–1.0%	34	1.00	12	650	650	1.00
Steel–P4–1.0%	33	1.00	18	678	654	0.96

Table 7.2: Comparison with experimental results (Marzouk and Hussein, 1991a)

Title	f_c', MPa	h, mm	c, mm	ρ,%	L, mm	P_{exp}, kN	P_{cal}, kN	P_{cal}/P_{exp}
NS1	42	120	150	1.474	1500	320	329	1.03
NS2	30	150	150	0.944	1500	400	359	0.90
HS1	67	120	150	0.491	1500	178	192	1.08
HS2	70	120	150	0.842	1500	249	239	0.96
HS3	69	120	150	1.474	1500	356	321	0.90
HS4	66	120	150	2.370	1500	418	421	1.01
HS5	68	150	150	0.640	1500	365	373	1.02
HS6	70	150	150	0.944	1500	489	522	1.07
HS7	74	120	150	1.193	1500	356	350	0.98

Table 7.3: Comparison with experimental results (Elstner and Hognested, 1956)

Title	f_c', MPa	h, mm	c, mm	ρ,%	L, mm	P_{exp}, kN	P_{cal}, kN	P_{cal}/P_{exp}
E&H-1	14.1	130	254	1.15	1780	302	295	0.98
E&H-2	25.2	130	254	1.15	1780	365	300	0.82
E&H-3	13.7	127	254	2.47	1780	334	358	1.07
E&H-4	12.8	127	254	3.70	1780	356	346	0.97
E&H-5	26.2	130	356	1.15	1780	400	390	0.98

7.6 Conclusion

It can be concluded that the mechanical model predicts the ultimate load carrying capacity of the strengthened and unstrengthened two–way slabs fairly accurately. The verification of the model against some experimental data showed a good agreement with respect to the deformational characteristics the steel–strengthened specimens. The proposed concrete model can successfully integrate the equal-biaxial state of stress of normal and high strength concrete in two–way slabs. The contribution of steel plates and bolts on the compressive stress–strain relationship is also considered in the model. The steel bolts confinement effect is considered in developing the model by modifying the stress–strain relationship of concrete in compression. A full tensile stress-deformation relationship of concrete is imposed in the model including both the pre-peak and post-peak properties of concrete.

An overall evaluation of the mechanical model indicates that it estimates the values of the ultimate loading capacity with an overestimation average ratio of about 6%, based on the 19 examined specimens. The ability of this model in evaluating the deflection of the two–way slabs, as well as the ultimate load carrying capacity makes it useful on the academic and industrial level.

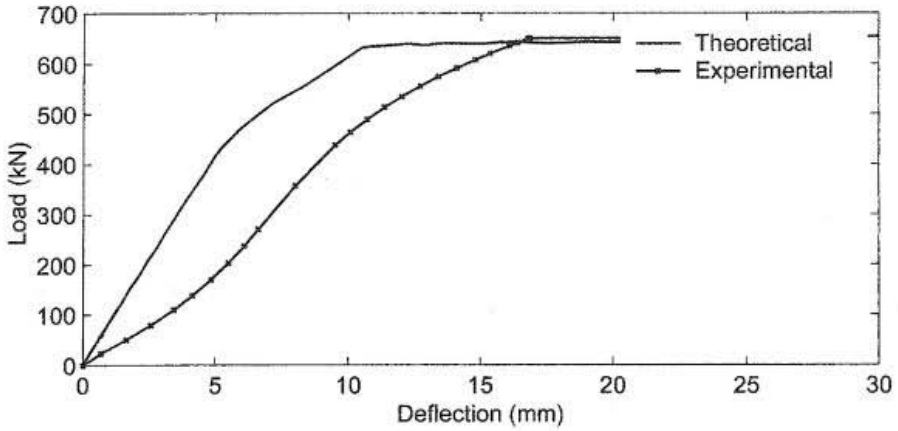

(a) Specimen Steel-P2-1.0%

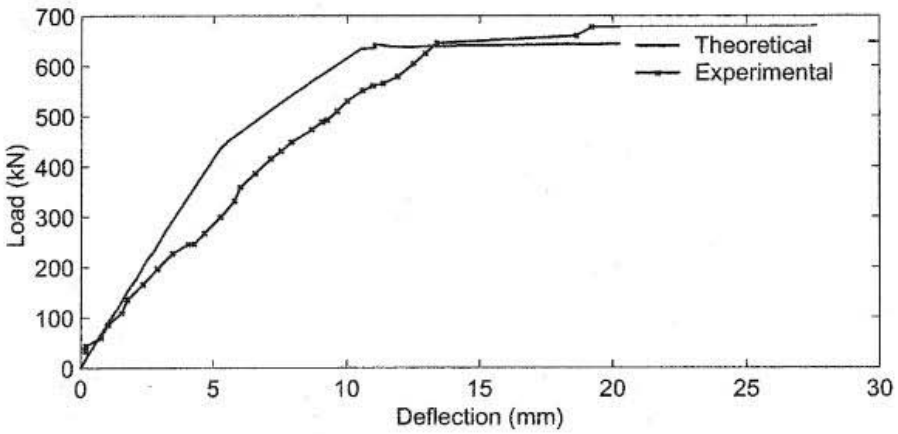

(b) Specimen Steel-P4-1.0%

Figure 7.10: Load–deflection relationship of selected specimens

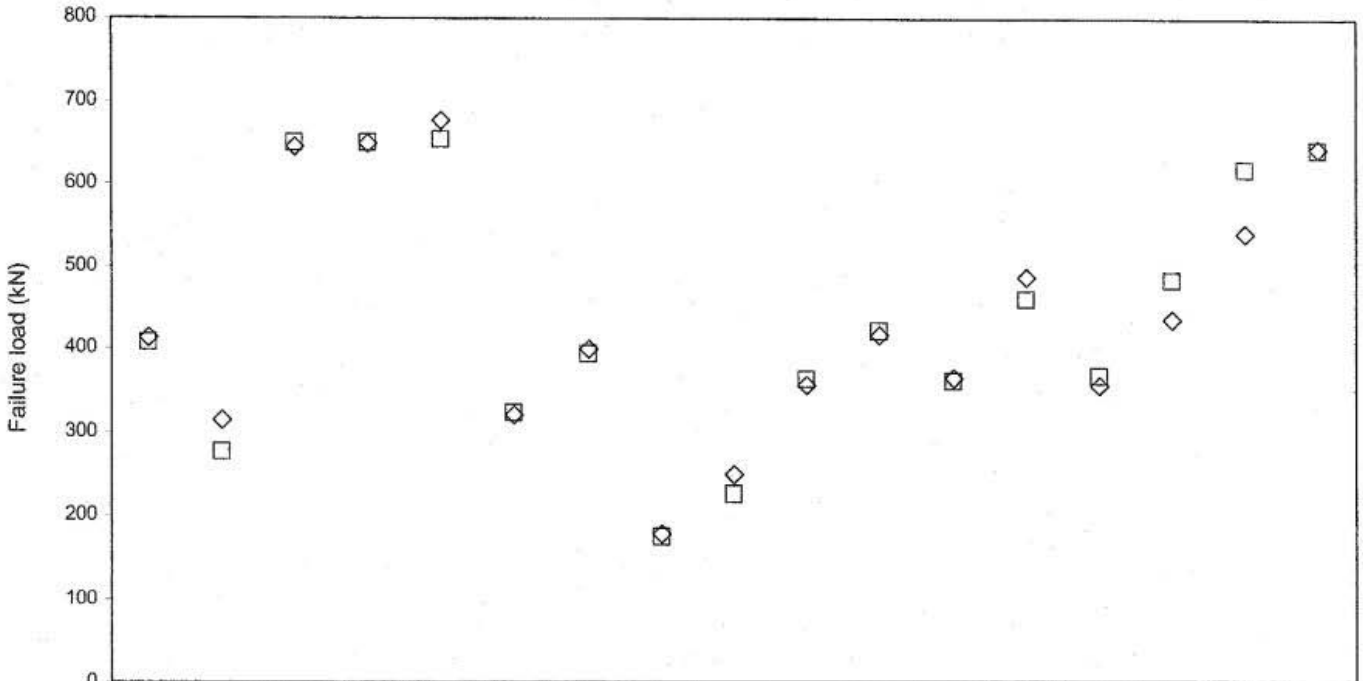

	Ref-P-1.0%	Ref-P-0.5%	Steel-P3-1.0%	Steel-P2-1.0%	Steel-P1-1.0%	NS1	NS2	HS1	HS2	HS3	HS4	HS5	HS6	HS7	HS8	HS9	HS10
◇ Exp.	412	314	645	650	678	320	400	178	249	356	418	365	489	356	436	543	645
□ Cal.	406	276	649	650	654	322	394	175	226	364	421	362	461	368	484	619	643

Figure 7.11: Verification of the mechanical model (Exp. =Experimental, Cal. = Model prediction)

Chapter 8

Finite Element and Numerical Analyses of FRP–strengthened Two–Way Slabs

8.1 General

The research work on strengthening two–way slabs is scarce. A few research works have dealt experimentally with the strengthening two–way slabs (Ebead and Marzouk, 2002a; Ebead and Marzouk, 2002b; Farhey et al., 1995). Consequently, and to the best of the authors knowledge, there is no research work on the finite element analysis (FEA) of strengthened two–way slabs. In the literature, there are research works on the finite element analysis of unstrengthened two–way slabs (Marzouk et al., 1998b; Marzouk and Jiang, 1997; Megally and Ghali, 2000; Marzouk and Chen, 1993).

In the experimental investigation presented in Chapter 6, the results of the study on strengthening two–way slabs using CFRP strips and GFRP laminates was presented. It was concluded that CFRP strips and GFRP laminates could be recommended for strengthening two–way slabs subject to flexural failure. The FRP laminates and strips could be used for strengthening slabs with reinforcement ratio less

than 1.0% that normally fail in a flexural mode.

Although the finite element method provides an accurate analysis for a single case, it does not provide a design guide or equations. The design equation should consider certain input parameters to achieve certain output responses. The response surface methodology (RSM) is an important statistical method used to pre–design cases of study or computer runs, which can be conducted in a laboratory or implemented using a finite element package. Based on the data results of the pre–designed runs, the RSM can be used to provide design equations that correlate the output responses to the input parameters.

This Chapter includes FEA of the flexural FRP–strengthened two–way slabs presented experimentally in Chapter 6. The experimental results of the strengthened slabs were used to calibrate the finite element model based on the ultimate load carrying capacity. The FEA is used to generate data for cases that were not included in the experimental program presented in Chapter 6.

Part of this numerical evaluation is aimed at proposing a tension stiffening model that considers the effect of the FRP strengthening materials. In addition, the numerical evaluation includes proposing a simple equation for the ultimate load carrying capacity of the FRP–strengthened two–way slabs to be available for the design engineer.

The FEA presented herein is divided into two main stages of study: a calibration study and a parametric study. In the first stage, the finite element model is calibrated for the available experimental results presented in Chapter 6. In the parametric study, the effect of certain parameters on certain responses is investigated. These parameters are the slab size represented by the slab thickness and the span, the

tensile reinforcement ratio, and the width of the FRP–strengthening material. On the other hand, the output responses are represented by the actual tensile behaviour and the ultimate load carrying capacity of the strengthened slabs. In the second stage, the RSM is used to pre-design a number of finite element runs to be implemented using the FEA to develop a model for the tensile stress–strain relationship for FRP–strengthened concrete and a simple equation for the ultimate load carrying capacity of FRP–strengthened two–way slabs.

8.2 Concrete Constitutive model

Several constitutive models have been developed to describe the behaviour of plain concrete. These constitutive models differ from one to another regarding the degree of complexity in describing concrete behaviour. The concrete model used in this study is plasticity–based constitutive model that utilizes the classical aspects of the theory of plasticity (ABAQUS, 2001). A complete representation of the model is defined by considering the following concepts: strain rate decomposition into elastic and inelastic strain rates; elasticity; yield; flow; and hardening. The model uses a crack detection surface to determine the cracking onset.

8.2.1 Behaviour of Concrete in Compression

Concrete model in compression is elastic until the initial yield surface limit is reached as shown in Figure 8.1.a. Figure 8.1.b shows the compression surface in the $p - q$ plane. The initial yield surface defines the elastic limit at which the linear–elastic constitutive relationships are valid. Further stresses of concrete cause an expansion of the initial yield surface so that new yield surfaces are developed. Moreover, stresses

beyond the initial yield surface formation cause further "irrecoverable" strain. The strain rate is then decomposed into elastic strain rate and plastic strain rate. The strain rate decomposition is governed by this simple equation:

$$d\varepsilon_c = d\varepsilon_c^{el} + d\varepsilon_c^{pl} \tag{8.2.1}$$

where $d\varepsilon_c$ is the total compressive strain rate, $d\varepsilon_c^{el}$ is the compressive elastic strain rate, and $d\varepsilon_c^{pl}$ is the compressive plastic strain rate.

The yield stage is followed by flowing of the material, as if it is a metal, and then hardening. The main equation of the compression surface is defined using the following relationship;

$$f_c = q - 3\left(\frac{1-\bar{f}_{bc}}{1-2\bar{f}_{bc}}\right)p - \sqrt{3}\tau_c = 0 \tag{8.2.2}$$

The compression stress in concrete is expressed in terms of the effective pressure stress, p, the Mises equivalent deviatoric stress, q, and a hardening parameter, τ_c. The effective pressure stress, p is expressed as:

$$p = -\frac{1}{3}(\sigma_1 + \sigma_2 + \sigma_3) \tag{8.2.3}$$

where σ_1, σ_2, and σ_3 are the principal normal stresses.

Also the Mises deviatoric stress, q is expressed as:

$$q = \sqrt{\tfrac{3}{2}\left(\tfrac{1}{3}\right)\left(S_1^2 + S_2^2 + S_3^2\right)} \tag{8.2.4}$$

where S_1, S_2, and S_3 are the principal stress deviators. Hence the amount q^2 is equivalent to 3/2 times the mean of the square of principal-stress deviations. The deviatoric stress components, S_{ij}, are correlated to the normal stresses components,

σ_{ij}, using the following formula:

$$S_{ij} = \sigma_{ij} + p\,\delta_{ij} \tag{8.2.5}$$

where δ_{ij} is equal to:

$$\delta_{ij} = \begin{bmatrix} 1 & 0 & 0 \\ 0 & 1 & 0 \\ 0 & 0 & 1 \end{bmatrix} \tag{8.2.6}$$

The factor $\bar{f}'_{bc}$ in Equation 8.2.2 defines the ratio between the equal biaxial compressive strength, f'_{bc}, and the uniaxial compressive cylinder strength, f'_c, through the equation:

$$\bar{f}'_{bc} = \frac{f'_{bc}}{f'_c}, \left(f'_c > 0\right) \tag{8.2.7}$$

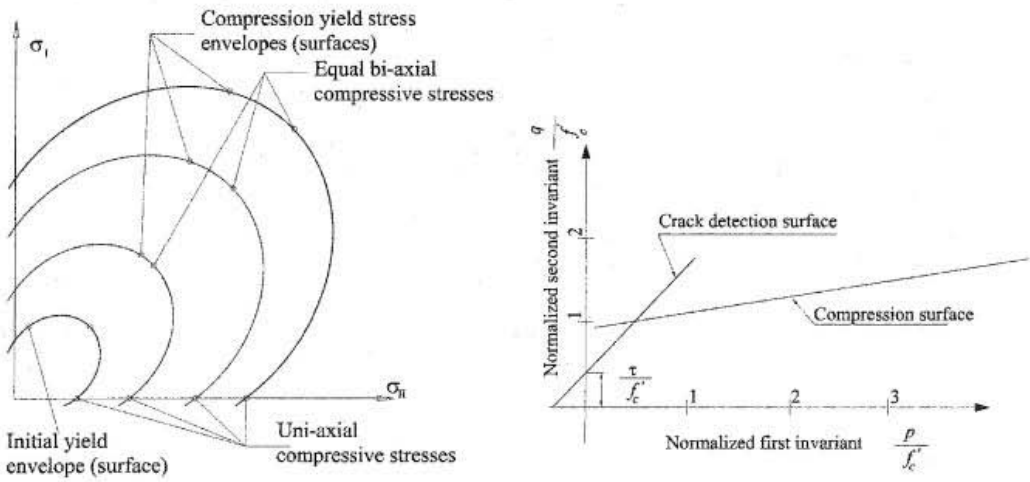

(a) biaxial Plane stress envelops

(b) Failure surface in the $p-q$ plane

Figure 8.1: Concrete behaviour in compression

In Equation 8.2.2, $\tau_c\left(\lambda_c\right)$ is the hardening relationship as a function of the hardening parameter, λ_c, that is used to define the hardening component in the compressive

constitutive model of concrete. τ_c is the yield stress in a state of pure shear stress when all the components of σ_{ij} vanish except $\sigma_{12} = \sigma_{21} = \tau_c$ due to the equilibrium of an infinitesimal element of the concrete material. Hence, τ_c is the size of the yield surface on the q axis at zero value of p in Figure 8.1.b. In the case of the uniaxial state of compressive stress:

$$\tau_c = \frac{1}{\sqrt{3}}\sigma_c \left(1 - \frac{1 - \vec{f}_{bc}}{1 - 2\vec{f}_{bc}}\right) \tag{8.2.8}$$

In the case of the biaxial state of compressive stress:

$$\tau_c = \frac{2}{\sqrt{3}}\sigma_{bc} \left(\frac{1}{2} - \frac{1 - \vec{f}_{bc}}{1 - 2\vec{f}_{bc}}\right) \tag{8.2.9}$$

where, σ_c and σ_{bc} are the stress magnitude in case of uniaxial stress state and the magnitude of each nonzero principal stress in biaxial state of stress, respectively.

The associated flow rule assumption is used to determine the flow component in the elastic–plastic model in concrete under compression. The associated flow rule assumptions are threefold (Chen and Ting, 1980):

1. Perfectly plastic behaviour of concrete after the maximum carrying capacity has been reached.

2. The failure surface is taken directly as the fixed yield surface in stress space.

3. The plastic strain increment vector is assumed to be normal to the yield surface in the current stress space.

In the general case of nine-dimensional stress space, the plastic–strain increment

vector, $d\varepsilon_{ij}^{pl}$, is correlated to the plastic–potential function, $g(\sigma_{ij})$, through the equations of plastic flow in the form:

$$d\varepsilon_{ij}^{pl} = d\lambda_c \left(1 + c_0 \left(\frac{p}{\sigma_c}\right)^2\right) \frac{\partial g}{\partial \sigma_{ij}} \tag{8.2.10}$$

If the yield function, f_c, and the plastic–potential function, g, coincide, i.e.:

$$f_c = g \tag{8.2.11}$$

Equation 8.2.10 can be modified as:

$$d\varepsilon_{ij}^{pl} = d\lambda_c \left(1 + c_0 \left(\frac{p}{\sigma_c}\right)^2\right) \frac{\partial f_c}{\partial \sigma_{ij}} \tag{8.2.12}$$

In Equations 8.2.10 and 8.2.12, c_0 is a constant that determines the ratio between the plastic strain in a monotonically loaded biaxial compression test and the plastic strain in a monotonically loaded uniaxial test. Equation 8.2.10 is valid as long as $f_c = 0$ and $d\lambda_c$ is a positive scalar factor, otherwise $d\varepsilon_{ij}^{pl} = 0$. It is worth mentioning that if Equation 8.2.11 is not satisfied; Equation 8.2.10 refers to the non–associated flow rule.

8.2.2 Behaviour of Concrete in Tension

When addressing the tensile behaviour of concrete, several aspects are considered. These aspects are cracking, shear modulus degradation, fracture energy, and tension stiffening.

Cracking is considered the most significant factor of the material behaviour in tension. Generally, cracks in the finite element simulation may be defined as smeared, discrete, or fracture cracks. Cracking is assumed to occur when the stresses reach crack detection surface that is defined by the Coulomb line written in the first two

stress invariants p and q. Crack occurrence is determined using the crack detection plasticity surface in stress space. In the crack detection model, the strain rate decomposition in tension is governed by the simple equation:

$$d\varepsilon_t = d\varepsilon_t^{el} + d\varepsilon_t^{pl} \tag{8.2.13}$$

where $d\varepsilon_t$ is the total tensile strain rate for the crack detection problem, $d\varepsilon_t^{el}$ is the tensile elastic strain rate, and $d\varepsilon_t^{pl}$ is the tensile plastic strain rate associated with the crack detection surface. The main equation of the crack detection surface is the Coulomb line as follows:

$$f_t = \hat{q} - \left(3 - b_0 \frac{\sigma_t}{\sigma_t^u}\right)\hat{p} - \left(2 - \frac{b_0}{3}\frac{\sigma_t}{\sigma_t^u}\right)\sigma_t = 0 \tag{8.2.14}$$

where σ_t^u is the uniaxial tensile strength of concrete. The factor b_0 is used to define the ratio between the biaxial and uniaxial tensile strengths. In Equation 8.2.14, σ_t is the equivalent uniaxial tensile stress. The crack detection model uses the associated flow rule assumption that states:

$$d\varepsilon_t^{pl} = \begin{cases} d\lambda_t \frac{\partial \sigma_t}{\partial \sigma} & \sigma_t = 0 \text{ and } d\lambda_t > 0, \\ 0 & \text{otherwise.} \end{cases} \tag{8.2.15}$$

where λ_t is a factor to measure the hardening.

Cracks in concrete reduce the shear modulus of concrete linearly as the crack opening increases. The shear modulus of concrete is reduced using the following set of equations as adopted earlier (Marzouk and Chen, 1993):

$$G = \phi\, G_0 \tag{8.2.16}$$

$$\phi = \begin{cases} \left(1 - \frac{\bar{\varepsilon}_t}{\varepsilon_{sr}}\right) & \varepsilon_t < \varepsilon_{sr}, \\ 0 & \text{otherwise.} \end{cases} \tag{8.2.17}$$

$$\varepsilon_{sr} = \varepsilon_{st}^{u} - \varepsilon_{t0} \tag{8.2.18}$$

$$\bar{\varepsilon}_t = \varepsilon_t - \varepsilon_{t0} \tag{8.2.19}$$

where G_0 is the shear modulus of the uncracked concrete, ϕ is the linear degradation function of shear modulus, and $\bar{\varepsilon}_t$ is the average crack opening strain across the crack. ε_{sr} and $\bar{\varepsilon}_{sr}$ are the total average shear effective strain and the ultimate shear effective strain at which concrete shear stiffness vanishes.

In the case of plain concrete, fracture energy, G_f, is defined as the energy required to form a unit area of crack surface. Fracture energy is considered a material property based on the brittle fracture concept of (Hilleborg, 1985). The fracture energy, G_f, is estimated as the numerical integration of the function between the tensile stress, σ_t, and the "crack width" or displacement, u_t as shown in Figure 8.2, i.e.:

$$G_f = \int \sigma_t \, du \tag{8.2.20}$$

Cracks exist in reinforced concrete subjected to tensile stresses along with the steel

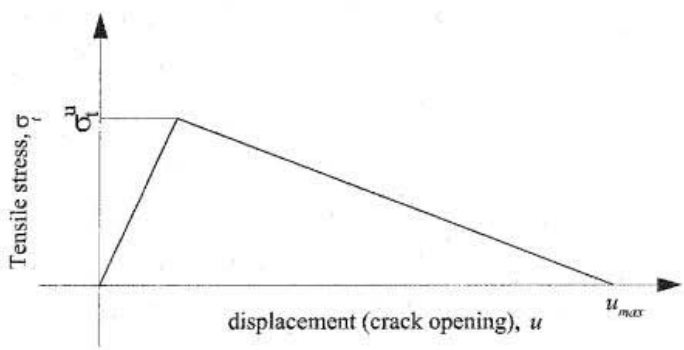

Figure 8.2: Fracture energy and cracking model of concrete

reinforcement. Subsequently, interfacial shear stresses between concrete and the reinforcement are transmitted to concrete between cracks as tensile stresses. Hence,

concrete bonded to the reinforcement is loaded with tensile stresses causing an increase of the overall stiffness. This phenomenon is called *Tension Stiffening*. In the case of reinforced or strengthened concrete, the calculations are made based on the assumption of smeared crack approach. In this case the tensile behaviour of concrete is represented using the tension stiffening that is expressed as the tensile stress–strain (σ_t–ε_t) relationship rather than stress–displacement. The numerical integration of the σ_t–ε_t curve can be referred to as the fracture energy density, W_f (Marzouk and Chen, 1993).

Based on some experimental evidence on high strength concrete (Marzouk and Chen, 1995), it was found that the post–peak relationship may be defined according to the following relationship:

For ($\varepsilon_t \geq \varepsilon_{t0}$)

$$\sigma_t = \sigma_t^u \left(\frac{\varepsilon_t/\varepsilon_{t0}}{\alpha \left(\varepsilon_t/\varepsilon_{t0} - 1\right)^{\beta} + \varepsilon_t/\varepsilon_{t0}} \right) \tag{8.2.21}$$

where:

$$\alpha = c_3 \sigma_t^u \tag{8.2.22}$$

where ε_t is the concrete tensile strain and ε_{t0} is the concrete tensile strain at $\sigma_t = \sigma_t^u$. In addition, the value of c_3 is 0.31 for normal strength concrete (Guo and Zhang, 1987) and modified to 0.28 for high strength concrete (Marzouk and Chen, 1995). Also, β is equal to 1.70 for normal strength concrete and 1.67 for high strength concrete.

The post–peak zone can be define using broken line segments such as lines AB, BC, and CD in Figure 8.3. It has been decided to define the tension stiffening of concrete by considering only two points on the post–peak zone of the σ_t–ε_t relationship as shown in Figure 8.4.

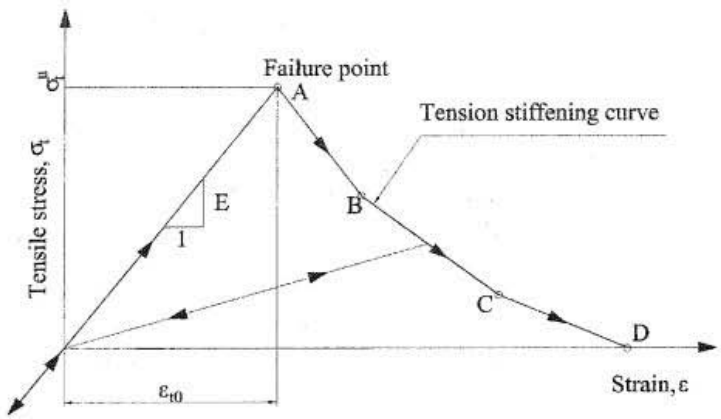

Figure 8.3: Tension stiffening model

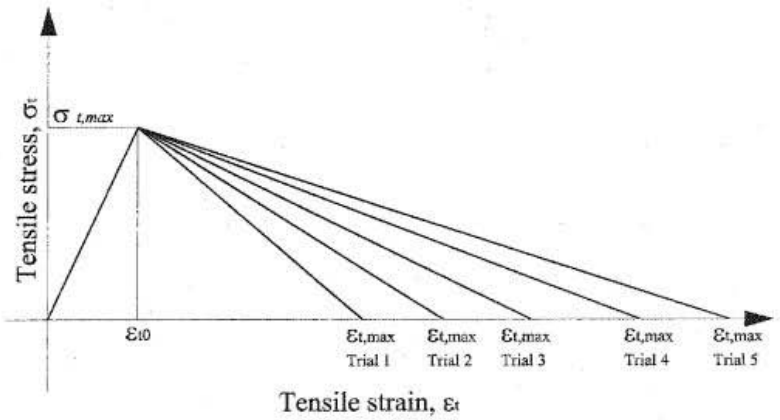

Figure 8.4: Tension stiffening calibration for strengthened concrete slabs

The interaction of FRPs with concrete is assumed similar to that of steel reinforcing bars. A similar effect to steel rebars is recognized when concrete interacts with FRP materials. Hence, FRP materials are defined as smeared external reinforcement located at the tension side of the slab. It is expected that there is a difference in the tensile behaviour of the strengthened and the unstrengthened concrete.

8.3 Finite Element Calibration Study

It is intended to investigate the effect of certain parameters on FRP strengthened concrete tensile behaviour and the load carrying capacity of strengthened two–way slabs. The following parameters are investigated:

1. FRP strengthening width ratio, w_r.
2. The original steel reinforcement ratio, ρ.
3. The slab length ratio, l_r.
4. The slab thickness ratio, t_r

The FRP strengthening width ratio, w_r, is the ratio between the width of the FRP material and the slab length, L. The original steel reinforcement ratio, ρ, is the tension reinforcement ratio of the slab. The slab length ratio, l_r, is the normalized slab length with respect to a test specimen's length of 1830 mm. Finally, the slab thickness ratio, t_r, is the normalized slab thickness with respect to a test specimen's thickness of 150 mm. The length of 1830 mm and the thickness 150 mm are the typical length and thickness of the specimens tested experimentally in Chapter 6.

In this stage of the FEA study, the σ_t–ε_t relationship, and hence the fracture energy density are calibrated. The calibration is based on the agreement of the FEA

results and the available experimental results from Chapter 6. This calibration is conducted with respect to the ultimate load carrying capacity of the slabs. Six finite element cases are implemented and compared to the available experimental results of the flexural–strengthening specimens. The cases implemented in the calibration study are for the reference specimens Ref–P–0.35% and Ref–P–0.5% to represent the flexural reference specimens; specimens CFRP–F–0.35% and CFRP–F–0.5% to represent the flexural strengthening specimens using CFRP strips; and specimens GFRP–F–0.35% and GFRP–F–0.5% to represent the flexural strengthening specimens using GFRP laminates. The FRP width ratio of the reference and strengthened specimens is zero and 0.164, respectively. Both the slab length ratio, l_r, and the slab thickness ratio, t_r, are equal to the unity. The original steel reinforcement ratio, ρ, for two–way slab specimens is either 0.35% or 0.5% as listed in Table 8.1. Figure 8.5 shows a schematic representation of a strengthened specimen of the calibration study.

Table 8.1: Ranges of the studied parameters of the calibration study specimens

Title	w_r	ρ	t_r	l_r
Ref–P–0.35%	0	0.35	1.0	1.0
Ref–P–0.5%	0	0.50	1.0	1.0
CFRP–F–0.35%	0.164	0.35	1.0	1.0
GFRP–F–0.35%	0.164	0.35	1.0	1.0
CFRP–F–0.5%	0.164	0.50	1.0	1.0
GFRP–F–0.5%	0.164	0.50	1.0	1.0

For each set of implementations, the fracture energy density of concrete strengthened with FRP materials is calculated as follows:

$$W_f = \int_0^{\varepsilon_{t,max}} \sigma_t \, d\varepsilon_t \tag{8.3.1}$$

Based on the approach considered in Figure 8.4, the fracture energy density can be calculated as follows:

$$W_f = 1/2\, \varepsilon_{t,max}\, \sigma_t^u \tag{8.3.2}$$

8.3.1 Material Properties

The properties of materials are known based on experimental testing and/or as given by the manufacturer's specifications to be used in the finite element materials simulation. The uniaxial compressive strength of concrete, $f_c^{'}$, is assumed 35 MPa to represent the normal strength concrete class. The modulus of elasticity of concrete, E_c, is calculated as 26600 MPa (ACI-318, 1999). The equal biaxial strength of concrete is assumed 1.16 times that of the uniaxial strength of concrete as 40.6 MPa (Hussein and Marzouk, 1998). The yield stress of concrete is assumed 20 MPa. The tensile strength of concrete, σ_t^u, is assumed 0.08 times the uniaxial strength of concrete that is equal to 2.8 MPa (Marzouk and Chen, 1995). The post-peak σ_t-ε_t relationship of strengthened or unstrengthened concrete is assumed linear descending to zero tensile stress at maximum strain $\varepsilon_{t,max}$ as shown in Figure 8.4.

A calibration concept is adopted by assuming the values of the tensile strain at zero tensile stresses, $\varepsilon_{t,max}$ from which the values of the fracture energy density of the strengthened concrete, W_f, can be evaluated according to Equation 8.3.1. The calibration attempts are implemented so that the FEA results will yield close results to the experimental results in terms of the ultimate load carrying capacity of the slabs. Each implementation in the calibration study leads to a better assumption of the maximum strain, $\varepsilon_{t,max}$, and hence the fracture energy density, W_f. Table 8.2 shows a sample of a case of calibration in this study. Three attempts are sufficient to

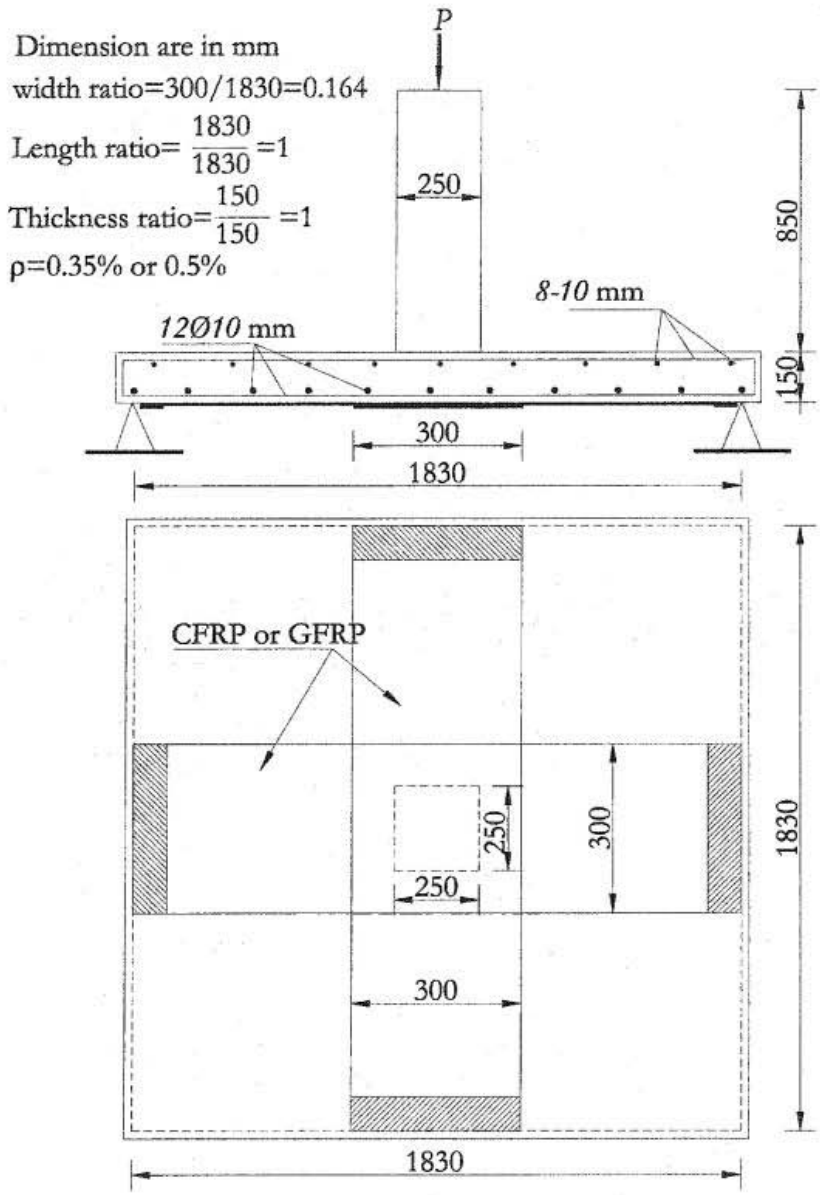

Figure 8.5: Strengthened specimen configuration and reinforcing details

achieve satisfying results. The satisfying values of the maximum strain, $\varepsilon_{t,max}$, and the fracture energy density, W_f, are used in the finite element parametric study.

Table 8.2: A sample of the FEA calibration-runs

Specimen	$\varepsilon_{t,max}, \mu\varepsilon$	W_f,MPa. $\mu\varepsilon$	V_{test}, kN	V_{FEA}, kN	V_{FEA}/V_{test}
Ref–P–0.35%	400	560	250	227.6	0.910
Ref–P–0.5%	600	840	330	320.8	0.972
CFRP–F–0.35%	1600	2240	361	329.6	0.913
GFRP–F–0.35%	800	1120	345	300.0	0.870
CFRP–F–0.5%	2400	3360	450	399.2	0.887
GFRP–F–0.5%	1200	1680	415	412.0	0.993

The steel reinforcement is assumed to have a yield stress as 440 MPa and a modulus of elasticity of 210 GPa. CFRP strips and GFRP laminates are defined as elastic material until breaking points. Both tensile strength and the modulus of elasticity of the FRP strengthening materials are defined as per the manufacturer specifications. One layer of the CFRP strips is 1.2 mm thick having a tensile strength of 2800 MPa and a modulus of elasticity of 170 GPa. Two layers of the GFRP are used in each direction with a thickness of 1.0 mm per layer. The tensile strength of the GFRP is 600 MPa and the modulus of elasticity is 26.16 GPa. The properties of the CFRP strips and the GFRP laminates are summarized in Table 8.3. The assumption of the full bond between FRP materials and concrete is inherited by the definition of these materials as smeared reinforcing layers located at the tension side of the concrete slabs.

Table 8.3: Properties of a layer of the FRP materials

FRP	Cured thickness, mm	Tensile strength, MPa	Elastic modulus, GPa	Elongation at break ,%
CFRP strips	1.2	2800	170	>1.7
GRFP laminates	1.0	600	26.13	2.24

8.3.2 Geometric Modelling

One quarter of the slab is modeled due to the geometrical and loading symmetry using a 5 × 5 mesh. Modelling only one quarter of the slabs is essential to save the computational time and running cost. The general layout of the finite element model is shown in Figure 8.6.

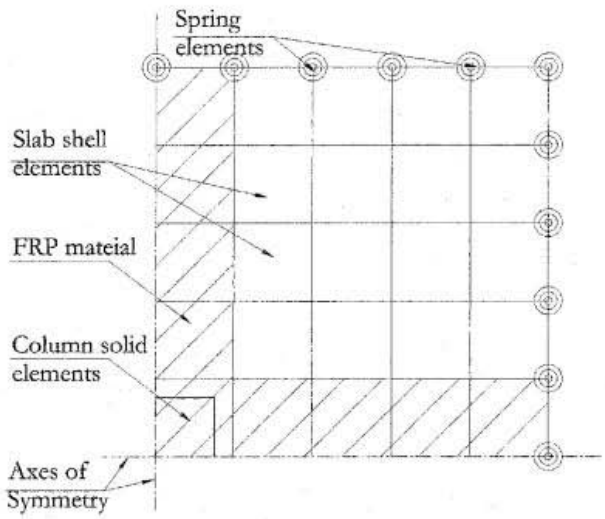

Figure 8.6: Finite element mesh layout for the calibration specimens

Degenerated 8–node quadrilateral shear–flexible shell elements with six degrees of freedom at each node are used for modelling the slab. The degrees of freedom are three translations and three rotations. This permits the transverse shear deformation to be accounted for. Nine Simpson–type integration points are used along the thickness of each shell element. In addition, a reduced 2 × 2 Gaussian integration rule is used over the X–Y plane of the elements. Eight–node brick elements are used to represent the column stub through which the load is applied. The brick element has three translational degrees of freedom per node in the X, Y, and Z directions. The

discrepancy between the degrees of freedom of the column stub brick element and the panel shell elements is overcome using the Multi Point Constraints (MPC) technique. MPC technique allows constraints to be imposed between different degrees of freedom in the model.

8.3.3 Steel Reinforcement and FRP Representation

Steel reinforcement in either the tension or compression side of the panel in each direction is treated as smeared unidirectional layers. These layers are embedded in concrete and located at the center line of the actual reinforcing bars in the slabs. The layers are smeared with a constant thickness that is equal to the area of each reinforcing bar divided by the reinforcing bars spacing. CFRP strips and GFRP laminates are represented in a similar way to the rebars. FRP materials are treated as smeared unidirectional layers located at the tension surface of concrete. The definition of FRP materials as smeared reinforcement inherits the assumption of full bond with the concrete surface. In addition, the impact of steel reinforcement and FRP materials on tensile properties of plain concrete is modeled through the developed tension stiffening relationship for the FRP strengthened portions of the slab. For the unstrengthened portions of the slab, the tension stiffening model is used as was recommended (Marzouk and Chen, 1993).

8.3.4 Boundary Conditions

The simply supported slabs are free to lift at corners. Non-linear spring elements are defined in the transverse direction at slab edges as shown in Figure 8.6. The stiffness values of the springs are set to very high values as long as the spring is under compression, and are set to very low values as long as the spring is under tension to

simulate the actual boundary condition of the tested slabs.

8.3.5 Solution Strategy

The modified Riks algorithm type of analysis is used in the current analysis. Modified Riks algorithm is generally used to find solutions of problems that involve unstable, geometrically nonlinear collapse of a structure, and/or nonlinear materials and boundary conditions. Hence, modified Riks algorithm is suitable for this analysis to deal effectively with the instability during the analysis caused by the initiation of concrete cracking in tension, concrete crushing in compression, and/or steel reinforcement yielding. The Riks method uses the load magnitude as an additional unknown and it solves simultaneously for loads and displacements.

8.4 Results of the Calibration Study

The results of the FEA of the calibration study in terms of the actual tensile stress strain relationships, load carrying capacity, and load–deflection relationships and discussed.

8.4.1 Stress–Strain Relationships and Contours

Figures 8.7 and 8.8 show the actual tensile stress–strain relationships for specimens of the calibration study at the slab center. It is clear that due to the contribution of FRP strengthening materials, the post–peak behaviour of slabs is stiffened. The slope of the tensile stress-tensile strain is decreased at the post–peak zone indicating the contribution of the FRP strengthening materials in increasing the post–peak stiffness of concrete in tension. The tensile post–peak behaviour is drastically changed due to the strengthening. A stiffer post–peak for strengthened concrete is recognized. A

suggested profile for the tensile stress–strain has emerged to account for the effect of FRP strengthening process.

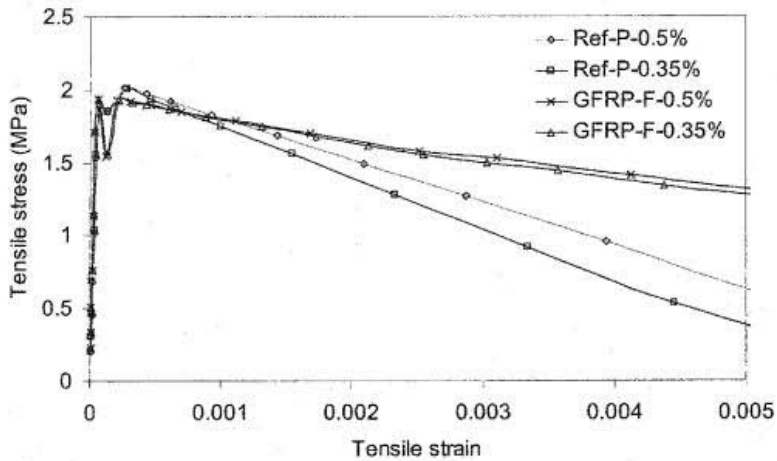

Figure 8.7: Tensile stress–strain at slab center relationships for GFRP–strengthened slabs

The FEA results in terms of the normal stresses, σ_{11}, and normal strains, ε_{11}, contours at the tension side of selected specimens are shown in Figure 8.9. For the unstrengthened specimens, the contours are smooth and continuous as shown in Figure 8.9.b. It is evident that due to the geometrical and loading symmetry along the diagonal axis, the stresses and strain are also distributed symmetrically. In the case of the strengthened specimens, there is a clear dis–continuous distribution of the stresses and strains contours as shown in Figures 8.9.c to 8.9.f. It was obvious that the values of stresses were corresponding to lower values of strains at the strengthened locations. It is clear that the values of stresses are corresponding to lower values of strains at the strengthened locations. Moreover, the unstrengthened portions in the strengthened specimens have different stresses and strains distributions compared to those of the

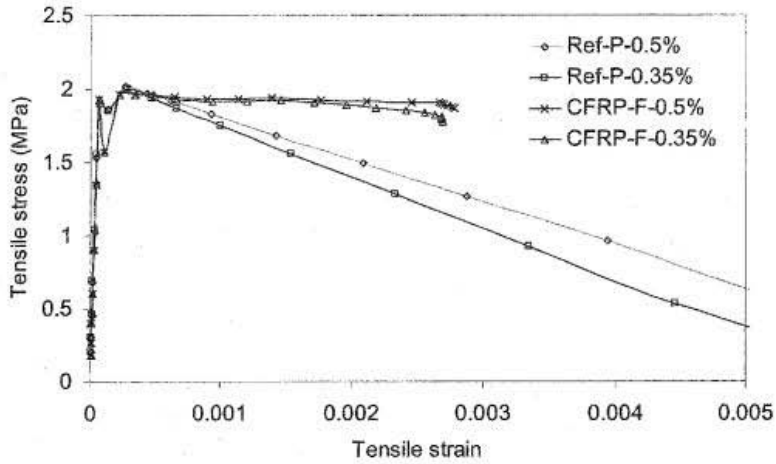

Figure 8.8: Tensile stress–strain at slab center relationships for CFRP–strengthened slabs

associated unstrengthened specimens at the same locations. This indicates that the effect of the strengthening is not local but it affects the stress and strain distributions of the entire slab.

8.4.2 Load Carrying Capacity and Deformations

Values of the load carrying capacity of the six specimens investigated in the calibration study shows a good match to those tested experimentally. As shown in Table 8.2, the initial assumptions of the strengthening energy, W_f, lead to a good agreement between the FEA and the experimental results in terms of the load carrying capacity.

The FEA underestimated the values of the central deflections for either the strengthened and unstrengthened specimens. Figures 8.10 and 8.11 show the load deflection relationships of the specimens. The FEA gave a stiffer deformational behaviour compared to the experimental results presented in Chapter 6. Many factors may contribute to this discrepancy. These factors include the pre–loading effect that does

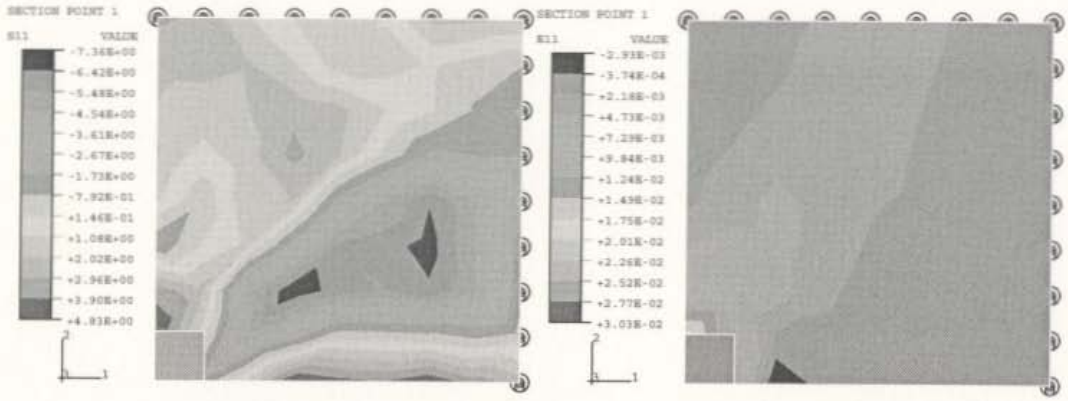

(a) Ref–P-0.35%(σ_{11}) (b) Ref–P-0.35%(ε_{11})

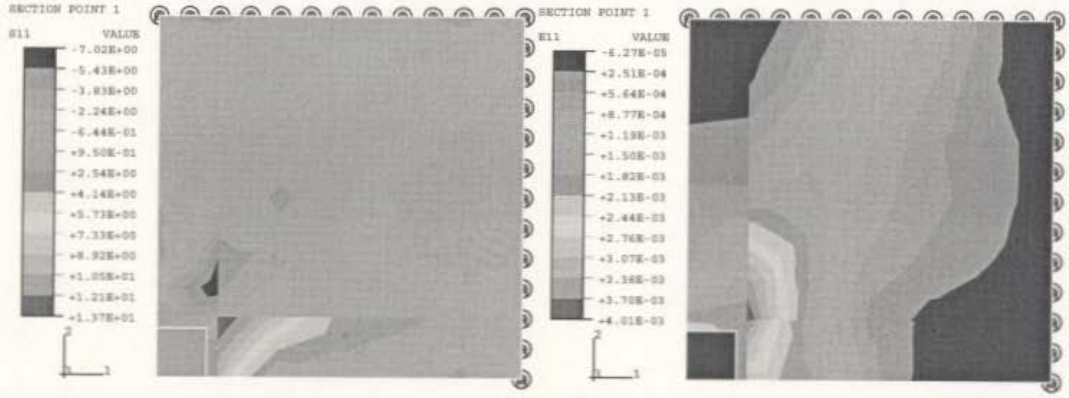

(c) CFRP–F–0.35%(σ_{11}) (d) CFRP–F–0.35%(ε_{11})

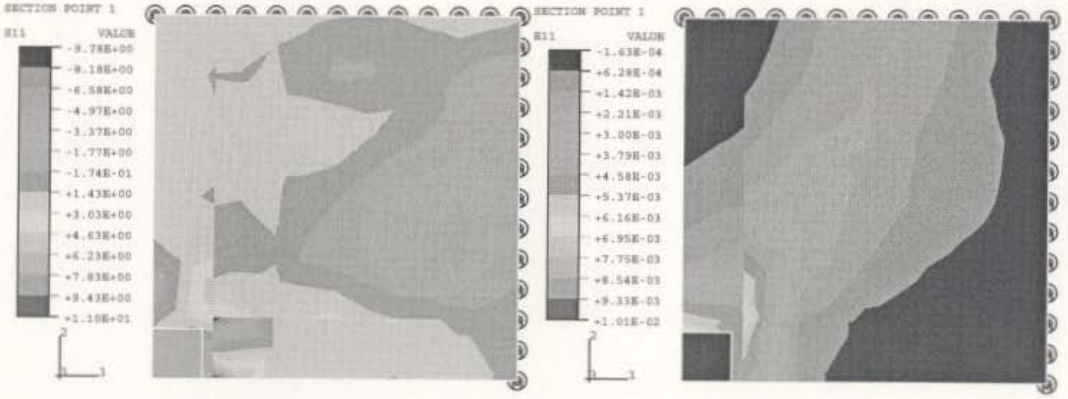

(e) GFRP–F–0.35%(σ_{11}) (f) GFRP–F–0.35%(ε_{11})

Figure 8.9: Stresses, σ_{11} and strains, ε_{11}, at maximum load at the tension side

not affect the ultimate load carrying capacity but cause permanent (plastic) deformation (Ebead, 1998; Al-Sulaimani et al., 1994). In addition, there is an initial deformation associated with the imperfect fit of the slab on the loading frame. For the strengthened specimens, a possible reason for that discrepancy is the full bond assumption.

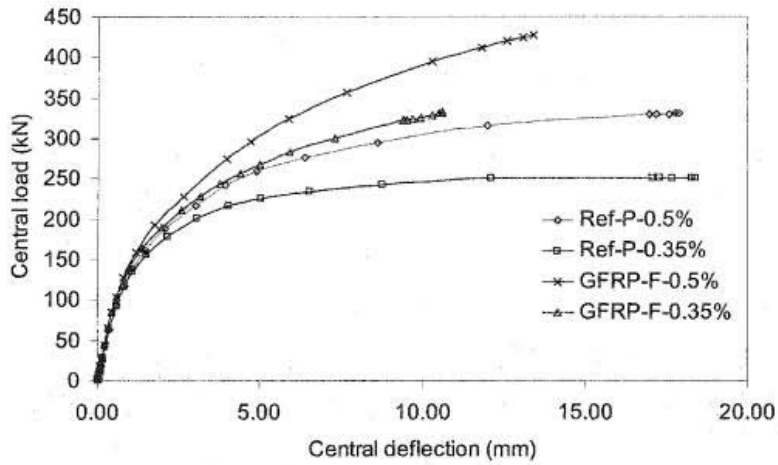

Figure 8.10: Central load–deflection relationships for GFRP–strengthened slabs

8.5 Numerical Analysis Based on the RSM

8.5.1 Introduction

There is a difference between data such as experimental or finite element analysis results; and information such as mathematical models. The information can be extracted from data by making assumptions about the whole system through which the data is generated to develop a mathematical model of that system. In general, the mathematical models contain some unknown constants. Experimentation is a way

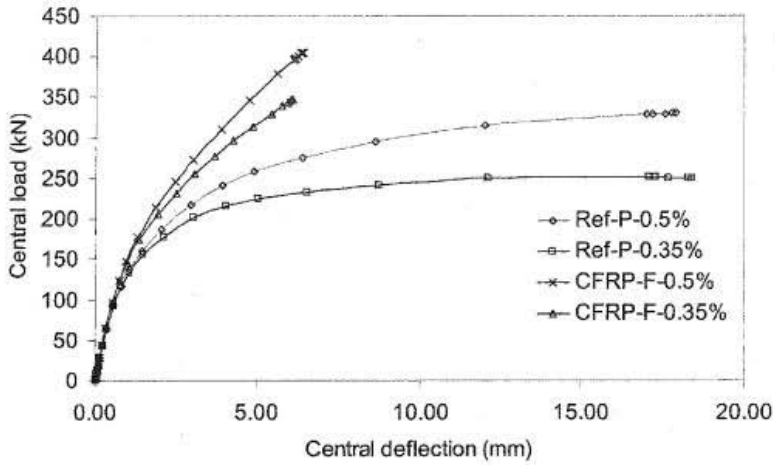

Figure 8.11: Central load–deflection relationships for CFRP–strengthened slabs

that used to acquire the data that enables determining these constants included in these mathematical models.

Hence, the experimentation provides the data needed for creating a successful mathematical model. The data can be collected from laboratory experimentation or running finite element package. For a successful mathematical model, the experiments have to be designed. The number of experiments depends on the number of variables and factors (inputs) to be considered and on the number of responses "outputs" to be achieved. The main role of the mathematical model is to identify the reasons for changes in the output response with the change in the input variables.

8.5.2 Response Surface Methodology

There are several different strategies of experimentation. Three of those are the *Best Guess* approach, the *One Factor At a Time* (OFAT) approach, and the *Factorial* approach.

The most efficient approach ever developed is the Factorial approach. This approach is capable of handling large models very efficiently. It pre-determines the number of experiments based on the available input variables and the required output responses. There are three major classes of the factorial design approach those are 1) the 2-level full factorial, 2) the fractional factorial, and 3) the response surface methodology (RSM). In the current analysis the RSM was selected to develop the mathematical models involved in this study.

The RSM is a collection of mathematical and statistical techniques used for modelling and analysis in applications where a response of interest is influenced by several variables (Myers and Montgomery, 1995). Suppose there are two factors x_1 and x_2, the surface represented using the function $f(x_1, x_2)$ is called the Response Surface. If there is another amount Y that represents the response, then $Y = f(x_1, x_2) + \eta$; where η is a constant.

In this study, a face-centered central composite response surface design was used to carry out the parametric study. The central composite design (CCD) is the most popular response surface method (RSM) design. The factors and their ranges of interest are shown in Table 8.3. For $k = 4$ factors, the design requires 25 $(2k+2k+1)$ FEA runs; where k is the number of parameters. For the case of CFRP and GFRP strengthened slabs.

8.6 Parametric Study

8.6.1 Generation of Finite Element Data

In the parametric study stage, the four aforementioned factors or parameters are considered as listed in Table 8.4. The FRP width ratio, w_r, ranges from 0.0 to 1.0;

the original steel reinforcement ratio, ρ, ranges from 0.35% to 0.80%; the slab length ratio, l_r, ranges from 0.8 to 2.0; and finally the slab thickness ratio, t_r, ranges from 0.8 to 1.2. The rest of the materials properties, geometric modelling, element type, steel reinforcement representation, strengthening materials representation, boundary conditions, and solution strategy are the same as for the calibration study.

Table 8.4: Factors and ranges for the parametric study

Parameter	Name	Low	Medium			High
			Mid1	Mid2	Mid3	
w_r	FRP Width ratio	0.000	0.250	0.500	0.750	1.000
ρ	Reinforcement ratio	0.350	0.463	0.575	0.688	0.800
t_r	Thickness ratio	0.800	0.900	1.000	1.100	1.200
l_r	Slab length ratio	0.800	1.100	1.400	1.700	2.000

Altering the mesh has to be made to accommodate widths of FRP strengthening materials and different slab spans. An investigation of the mesh sensitivity effect is carried out using three specimens of the same slab length and with different mesh sizes. A minor increase in the load carrying capacity within 5.0% resulted when using 50% coarser mesh size. Figure 8.12 shows the load deflection curves of specimen Ref–P–0.35% using three different mesh sizes. The mesh sizes are 232 mm, 186 mm, and 155 mm for 4×4, 5×5, and 6×6 meshes, respectively. Based on this investigation, there is not a considerable effect of the mesh size on the FEA results.

The statistical approach of the RSM is used in this study to pre-design the finite element runs. This methodology is capable of handling large models efficiently. It pre-determines the number of runs based on the available input variables and the required output responses. In this study, a face-centered central composite response surface design method is used to carry out the parametric study. The selected finite

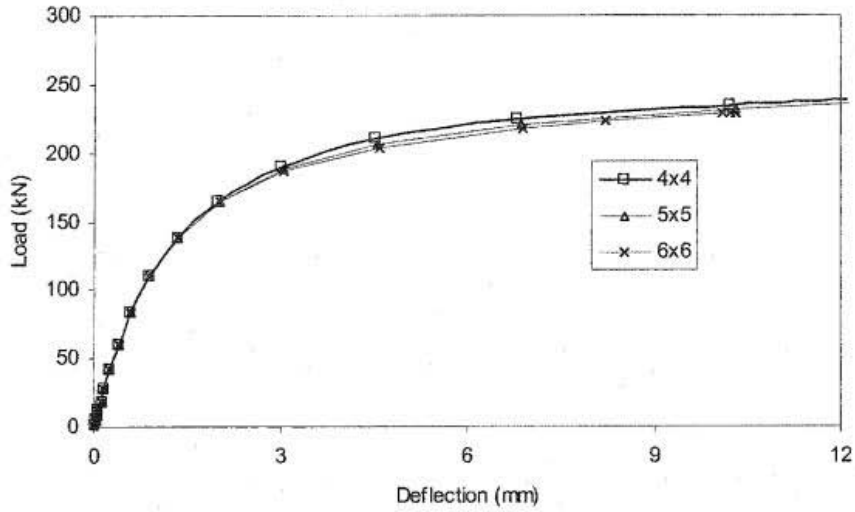

Figure 8.12: Mesh sensibility effect on the load history

element runs are designed based on the RSM using a statistical software (Design-Expert, 2001). The statistical technique of the RSM minimizes the number of finite element runs; however, it permits efficiency and economy.

The finite element runs are designed as 25 runs for each case of CFRP strips and GFRP laminates strengthening. The total number of the finite element runs is 41 runs since there are nine (9) duplicated runs for the unstrengthened slabs. The values of the studied parameters for the parametric study along with the actual value of the length, L, for both CFRP strips and GFRP laminates strengthening specimens are listed in Table 8.5. The results of the parametric study are tabulated in Table 8.6. The ultimate load carrying capacities, P_{max}, are shown for both CFRP strips and GFRP laminates strengthened specimens.

Table 8.5: The studied parameters and variables

Run	w_r	ρ,%	t_r	l_r	S, mm	Strengthened				Unstrengthened	
						CFRP		GFRP			
						$\varepsilon_{t,max}$, $\mu\varepsilon$	W_f, MPa.$\mu\varepsilon$	$\varepsilon_{t,max}$, $\mu\varepsilon$	W_f, MPa.$\mu\varepsilon$	$\varepsilon_{t,max}$, $\mu\varepsilon$	W_f, MPa.$\mu\varepsilon$
1	0.0	0.35	0.8	0.8	1464	NA	NA	NA	NA	575	805
2	1.0	0.35	0.8	0.8	1464	2111	2955	1030	1442	NA	NA
3	0.0	0.80	0.8	0.8	1464	NA	NA	NA	NA	962	1346
4	1.0	0.80	0.8	0.8	1464	4340	6076	1390	1946	NA	NA
5	0.0	0.35	1.2	0.8	1464	NA	NA	NA	NA	575	805
6	1.0	0.35	1.2	0.8	1464	2111	2955	1030	1442	NA	NA
7	0.0	0.80	1.2	0.8	1464	NA	NA	NA	NA	962	1346
8	1.0	0.80	1.2	0.8	1464	4340	6076	1390	1946	NA	NA
9	0.0	0.35	0.8	2.0	3660	NA	NA	NA	NA	575	805
10	1.0	0.35	0.8	2.0	3660	2111	2955	1030	1442	NA	NA
11	0.0	0.80	0.8	2.0	3660	NA	NA	NA	NA	962	1346
12	1.0	0.80	0.8	2.0	3660	4340	6076	1390	1946	NA	NA
13	0.0	0.35	1.2	2.0	3660	NA	NA	NA	NA	575	805
14	1.0	0.35	1.2	2.0	3660	2111	2955	1030	1442	NA	NA
15	0.0	0.80	1.2	2.0	3660	NA	NA	NA	NA	962	1346
16	1.0	0.80	1.2	2.0	3660	4340	6076	1390	1946	NA	NA
17	0.0	0.57	1.0	1.4	2562	NA	NA	NA	NA	768	1075
18	1.0	0.58	1.0	1.4	2562	3475	4865	1210	1694	768	1075.9
19	0.5	0.35	1.0	1.4	2562	2111	2955	1030	1442	575	805
20	0.5	0.80	1.0	1.4	2562	4340	6076	1390	1946	962	1346
21	0.5	0.58	0.8	1.4	2562	3475	4865	1210	1694	768	1075.9
22	0.5	0.58	1.2	1.4	2562	3475	4865	1210	1694	768	1075
23	0.5	0.58	1.0	0.8	1464	3475	4865	1210	1694	768	1075
24	0.5	0.58	1.0	2.0	3660	3475	4865	1210	1694	768	1075
25	0.5	0.58	1.0	1.4	2562	3475	4865	1210	1694	768	1075

Table 8.6: FEA parameters and responses

No	Parameters				GFRP specimens responses					CFRP specimens responses				
	w_r	ρ, %	t_r	l_r	P_{max}, kN	ε_{t0}, $\mu\varepsilon$	σ_t^u, MPa	a_1	a_2	P_{max}, kN	ε_{t0}, $\mu\varepsilon$	σ_t^u, MPa	a_1	a_2
1	0.00	0.35	0.80	0.80	164.7	163	1.902	0.526	-0.0081	164.8	237	1.868	0.542	-0.029
2	1.00	0.35	0.80	0.80	396.6	199	1.904	0.542	-0.0059	595.2	274	2.062	0.489	-0.012
3	0.00	0.80	0.80	0.80	347.4	258	1.905	0.548	-0.0133	347.5	194	1.863	0.585	-0.046
4	1.00	0.80	0.80	0.80	436.4	351	2.075	0.472	-0.0045	623.2	255	2.093	0.479	-0.006
5	0.00	0.35	1.20	0.80	357.0	341	1.983	0.685	-0.1435	357.1	341	1.983	0.685	-0.144
6	1.00	0.35	1.20	0.80	836.8	286	2.032	0.556	-0.0501	1096.4	215	2.052	0.500	-0.014
7	0.00	0.80	1.20	0.80	609.2	281	2.021	0.541	-0.0493	609.6	281	2.021	0.541	-0.049
8	1.00	0.80	1.20	0.80	917.6	252	2.036	0.635	-0.0636	1097.2	198	2.050	0.500	-0.009
9	0.00	0.35	0.80	2.00	158.4	146	2.113	0.474	-0.0005	158.0	271	2.009	0.661	-0.117
10	1.00	0.35	0.80	2.00	371.9	239	2.042	0.679	-0.0687	580.4	176	2.052	0.490	-0.008
11	0.00	0.80	0.80	2.00	318.8	232	2.040	0.580	-0.0518	318.9	231	2.040	0.579	-0.051
12	1.00	0.80	0.80	2.00	438.8	221	2.050	0.512	-0.0231	602.4	169	2.057	0.489	-0.005
13	0.00	0.35	1.20	2.00	343.2	300	2.004	0.582	-0.0865	343.2	300	2.004	0.582	-0.087
14	1.00	0.35	1.20	2.00	718.0	274	2.042	0.850	-0.3745	1088.4	226	2.059	0.500	-0.014
15	0.00	0.80	1.20	2.00	605.2	274	2.038	0.540	-0.0441	607.2	274	2.038	0.681	-0.082
16	1.00	0.80	1.20	2.00	872.8	249	2.042	0.710	-0.0718	1089.6	213	2.063	0.497	-0.007
17	0.00	0.58	1.00	1.40	342.2	262	2.027	0.526	-0.0484	342.5	262	2.027	0.562	-0.063
18	1.00	0.58	1.00	1.40	612.0	232	2.054	0.511	-0.0203	858.0	178	2.056	0.485	-0.004
19	0.50	0.35	1.00	1.40	526.4	243	2.033	0.521	-0.0375	774.4	192	2.082	0.473	-0.007
20	0.50	0.80	1.00	1.40	661.2	224	2.048	0.555	-0.0322	865.2	174	2.056	0.489	-0.004
21	0.50	0.58	0.80	1.40	408.4	243	2.033	0.521	-0.0375	571.2	167	2.055	0.483	-0.003
22	0.50	0.58	1.20	1.40	715.2	282	2.057	0.609	-0.0504	1092.4	228	2.063	0.495	-0.009
23	0.50	0.58	1.00	0.80	631.2	212	2.055	0.495	-0.0086	880.8	324	2.068	0.481	-0.007
24	0.50	0.58	1.00	2.00	593.2	232	2.055	0.518	-0.0221	827.6	182	2.058	0.484	-0.004
25	0.50	0.58	1.00	1.40	599.6	233	2.054	0.528	-0.0219	832.4	180	2.057	0.484	-0.004

8.6.2 Proposed FRP Tension Stiffening Model

Based on the generated finite element data, a suggested model for the tensile stress–strain for concrete is developed. This model was according to the following suggested form:

For the pre–peak portion of the relationship:

$$\sigma_t = [\sigma_t^u / \varepsilon_{t0}]\, \varepsilon_t \tag{8.6.1}$$

For the post–peak portion of the relationship:

$$\sigma_t / \sigma_t^u = a_1\, e^{a_2\, \varepsilon_t / \varepsilon_{t0}} \tag{8.6.2}$$

The tensile stress–strain relationship presented in Equations 8.6.1 and 8.6.2 can be completely defined by determining the values of the maximum tensile stress, σ_t^u, the associated tensile strain, ε_{t0}, and the constants a_1 and a_2. For all of the finite element runs, the values of σ_t^u and ε_{t0} can be easily determined. A study based on the best fitting of the post–peak relationship of each case study (run) is conducted to determine the values of the constants a_1 and a_2. These two constants along with the values of the maximum tensile stress, σ_t^u and the associated tensile strain, ε_{t0}, are needed for a complete representation of the tensile post–peak relationship. The quantities σ_t^u, ε_{t0}, a_1, and a_2 are tabulated in Table 8.6.

Considering the FEA results in Table 8.6, one can notice that the impact of the studied parameters on the actual maximum tensile stress, ${\sigma_t}^u$, and the corresponding tensile strain, ε_{t0}, is either random or minor. Due to FRP strengthening there is a drastic change in the post–peak behaviour of strengthened concrete compared to that of the unstrengthened concrete. Bonded FRP materials delay the initiation of cracks and then control the propagation of cracks for a higher load. This is clear due to the

stiffer post–peak part of the tensile stress–strain relationship as shown in Figures 8.7 and 8.8.

The actual tensile stress–strain relationship of the FRP strengthened concrete can be modified to take into consideration the effect of the FRP strengthening materials. Hence, it is decided to develop an expression for the descending portion of the tensile stress–strain relationship of concrete. The model is developed mainly to describe the post–peak behaviour of concrete slabs strengthened for flexure using FRP materials.

By analyzing the results presented in Table 8.6, it is obvious that the best fit of both the maximum tensile stress, σ_t^u, and the associated tensile strain, ε_{t0}, is the mean value of the data for these two quantities. Hence, for the CFRP and GFRP specimens, the tensile pre–peak behaviour of concrete can be represented using Equation 8.6.1 using the quantities σ_t^u and ε_{t0} as 2.03 MPa and 247.5 $\mu\varepsilon$, respectively.

The proposed model of post–peak relationship is in the form of Equation 8.6.2 that contains the four quantities: the maximum tensile stress,σ_t^u, the associated tensile strain, ε_{t0}, the constant a_1, and the constant a_2. The quantities a_1 and a_2 are required for representing the relationship. In particular, a_2 determines the slope of the descending portion of the post–peak relationship. These two quantities are dependent on the aforementioned parameters.

For CFRP specimens, a_1 and a_2 can be evaluated using Equations 8.6.3 and 8.6.4.

$$a_1 = 0.528 + 0.093\, w_r - 0.143\, \rho + 0.427\, t_r + 0.0744\, l_r \tag{8.6.3}$$

$$a_2 = 0.153 - 0.026\, w_r + 0.104\, \rho - 0.200\, t_r - 0.0367\, l_r \tag{8.6.4}$$

Similarly, for the GFRP specimens, the quantities, a_1 and a_2 can be calculated using Equations 8.6.5 and 8.6.6.

$$a_1 = 0.945 - 0.198\, w_r - 0.037\, \rho + .091\, t_r + .027\, l_r \tag{8.6.5}$$

$$a_2 = -0.043 + 0.065\, w_r + 0.042\, \rho - 0.038\, t_r - 0.006\, l_r \tag{8.6.6}$$

Researchers and design engineers may find the model to be useful. The model is simple to be applied although many parameters are considered. The proposed model (Equation 8.6.2) can either be used to define the post–peak behaviour of concrete, strengthened with FRP, in a finite element package or in a classical concrete mechanical model. This equation is limited to the configuration and of the studied parameters presented in this study.

This model is verified against the available finite element results of the calibration study specimens as shown in Figure 8.13. The comparison between the FEA results and the RSM regression models shows a good agreement for the reference specimens as shown in Figures 8.13.a and 8.13.b. Figures 8.13.c and 8.13.d show an acceptable level of agreement between the FEA and RSM results for specimens strengthened using GFRP materials. Finally, the RSM results show an overestimated behaviour of the post–peak stiffness compared to the FEA results for CFRP strengthened specimens.

8.6.3 Load Prediction Using RSM

The finite element data are used as input data for the RSM procedure. Using a step–wise regression procedure, the following expression is obtained for FRP strengthened two–way slabs. For specimens made of concrete of strength up to 35 MPa and strengthened using CFRP strips type Sika CarboDur of Young's Modulus of 170 GPa , the regression expression for the ultimate load carrying capacity in terms of the studied parameters is expressed as follows:

$$P_{\max} = [-4.59 + 31.7\, w_r + 12.4\, \rho + 16.0\, t_r - 20.3\, w_r^2 - 12.2\, w_r\, \rho + 5.87\, w_r t_r]^2 \tag{8.6.7}$$

Similarly, for For specimens made of concrete of strength up to 35 MPa and strengthened using CFRP laminates type Sika Wrap of Young's Modulus of 26.13

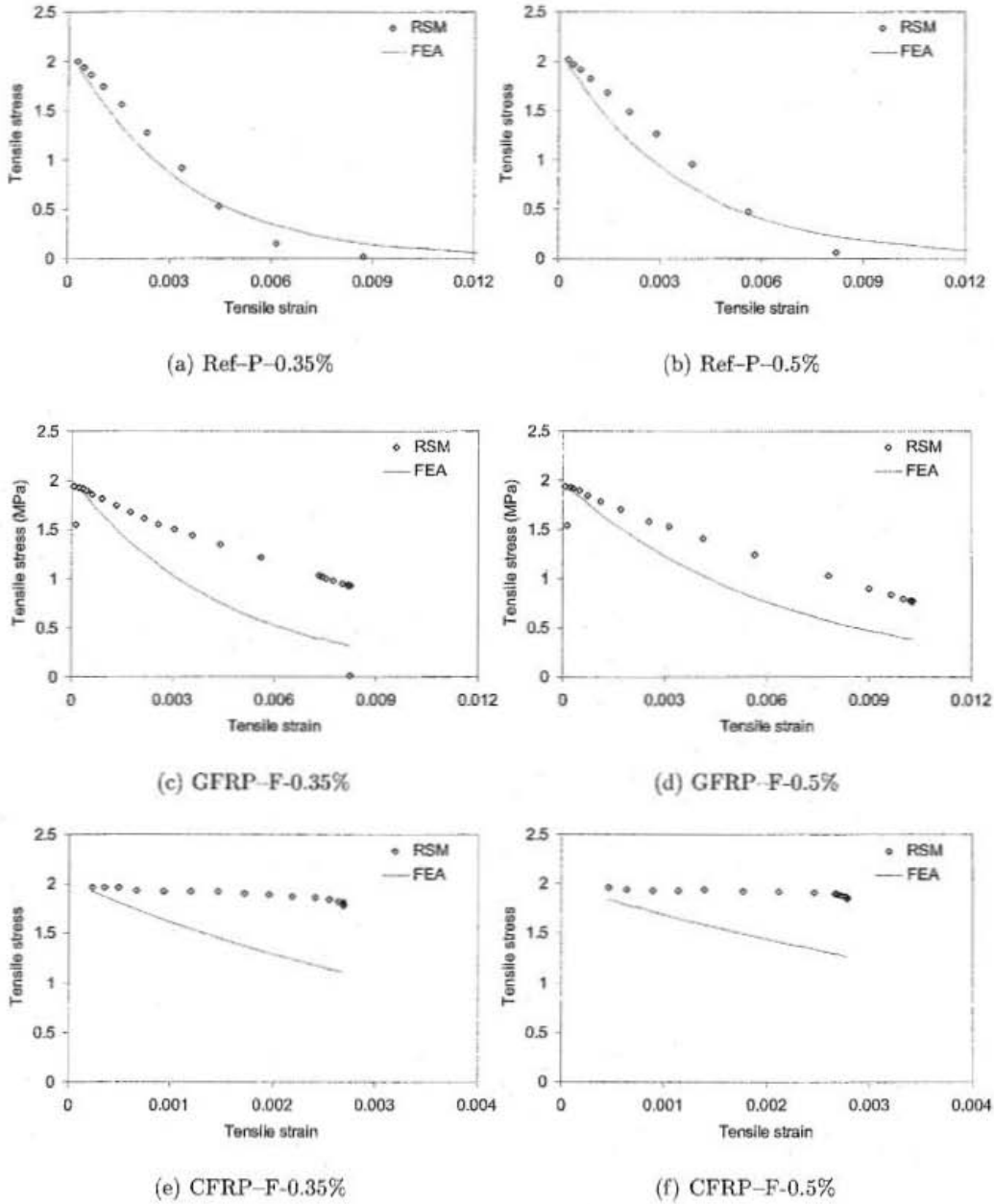

(a) Ref–P–0.35%

(b) Ref–P–0.5%

(c) GFRP–F-0.35%

(d) GFRP–F-0.5%

(e) CFRP–F-0.35%

(f) CFRP–F-0.5%

Figure 8.13: Comparison between FEA and RSM regarding the tensile post–peak response of concrete

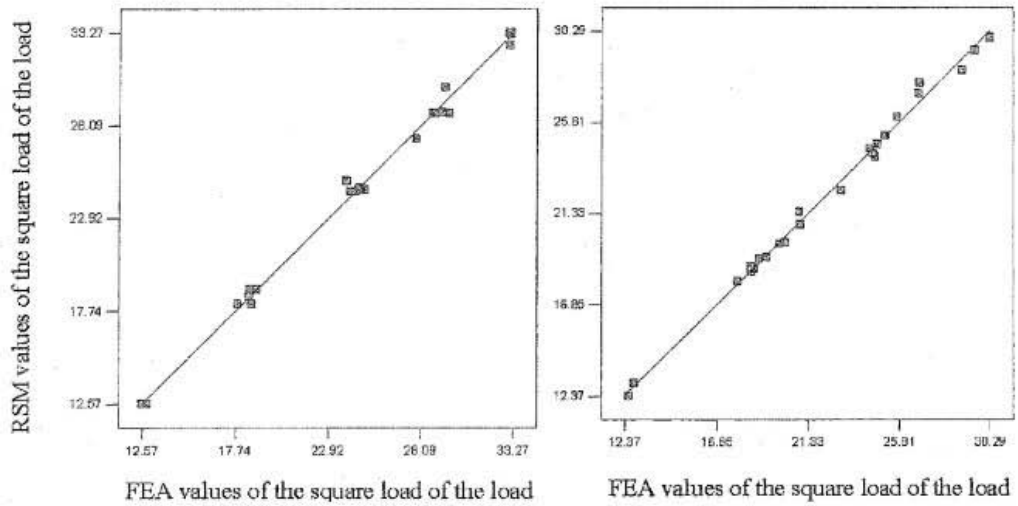

(a) CFRP specimens

(b) GFRP specimens

Figure 8.14: Comparison between FEA and RSM load response for CFRP and GFRP runs

GPa, the regression expression for the ultimate load carrying capacity of these specimens in terms of studied parameters is expressed as:

$$\begin{aligned} P_{\max} = [& -17.5 + 15.3\, w_r + 12.5\, \rho + 50.4\, t_r - 4.89\, l_r \\ & -10.2\, w_r^2 - 17.6\, t_r^2 + 1.56\, l_r^2 - 8.99\, w_r \rho + 6.08\, w_r t_r]^2 \end{aligned} \tag{8.6.8}$$

It is clear that the slab length ratio, l_r, has a small effect on the load response for both the CFRP and GFRP specimens. The regression correlation coefficient, R^2, is 0.9926 and 0.9915 for CFRP and the GFRP strengthened specimens, respectively. This indicates good fit and prediction accuracy. Figure 8.14 shows a comparison between the predicted maximum load using the RSM and the actual finite element results of specimens strengthened using CFRP specimens and GFRP specimens. Figure 8.14 indicates a good fit between the predicted and actual maximum loads.

Effect of the different parameters on the load carrying capacity

The RSM provides an outstanding statistical evaluation of the results such as the effect of each parameter at a time on the responses and the correlation coefficient. Moreover, the combination effect of two parameters on a single response can be discussed on one graph. From Figure 8.15 and from the regression expressions in Equations 8.6.7 and 8.6.8, one can see that there is a clear w_r/t_r, and w_r/ρ interactions. Figures 8.15.a and 8.15.b show w_r/ρ and w_r/t_r interaction graphs for CFRP and GFRP specimens, respectively. Regarding the effect of the FRP width ratio, w_r, it is evident that there is a clear second order effect as shown in Figures 8.15.a and 8.15.b. In addition, there is an optimum value of w_r that is almost 0.75 at which the load is maximum and beyond which the square root of the ultimate load carrying capacity decreases. The interaction diagram in Figure 8.15.a converges indicating that increasing both FRP width ratio, w_r, and the reinforcement ratio, ρ, leads to a lower load response, P_{max}. On the other hand, the diagram in Figure 8.15.b diverges indicating that increasing both the FRP width ratio, w_r, and the slab thickness ratio, t_r, leads to a higher load response.

8.7 Summary and Conclusions

In this chapter a finite element analysis analysis complimented with a statistical approach was presented. The full bond between either the steel reinforcement or FRP materials and concrete was assumed.

A calibration study is conducted on a finite element model and is used to analyze strengthened two-way slabs. The finite element results are calibrated with the experimental results. A parametric study is carried out to generate finite element data. A

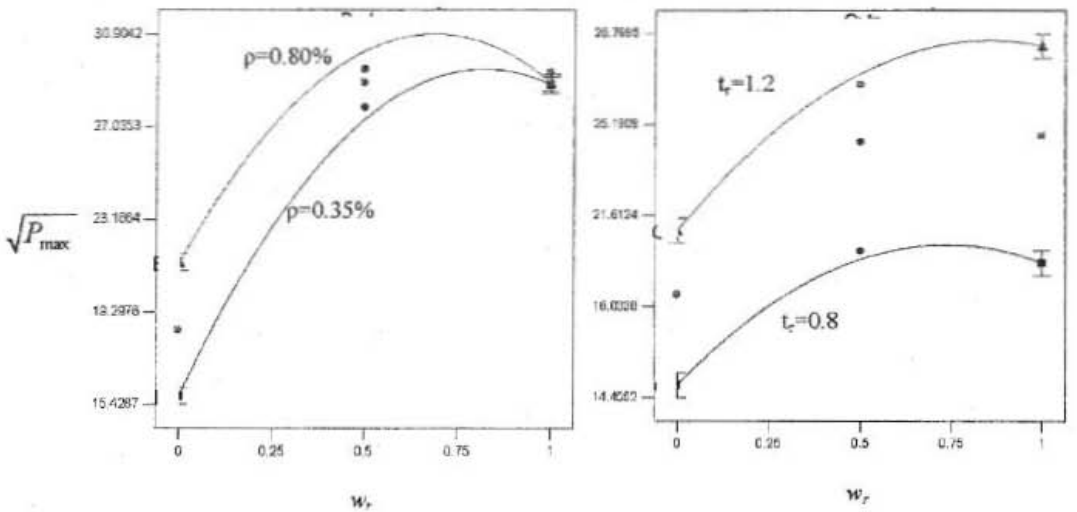

(a) CFRP specimens(w_r–ρ) (b) GFRP specimens(w_r–t_r)

Figure 8.15: Interaction effect of the different parameters on the load

total of 25 runs are implemented for each of the CFRP strips and GFRP laminates strengthened specimens.

An FRP tension stiffening model is recommended to predict the complete behaviour of concrete in tension. The recommended model describes the tensile behaviour of concrete slabs strengthened using FRP materials. The parameters of the model are derived based on the statistical analysis using the Response Surface Methodology and modified to obtain a better fit. The comparison between the predicted post–peak concrete model and the actual post–peak behaviour shows an acceptable agreement. The model is useful as an input in finite element packages and useful for classical approaches. The restriction to the model is that concrete has to be normal strength concrete and the configuration of the tested slab has to be within the values of the studied parameters.

A simple equation is developed to provide a simple design guide for engineers to predict the ultimate load carrying capacity of CFRP or GFRP strengthened two-way slabs. The correlation coefficient of the developed expression is close to unity indicating that the models can predict the ultimate loads extremely well.

Chapter 9

Conclusions

9.1 Summary

A comprehensive experimental and theoretical study on different strengthening techniques of two–way slabs are presented. The research work is divided into two main phases: experimental and theoretical. The experimental work includes investigating the effectiveness of using steel as a traditional strengthening material. The combined effect of steel bolts as vertical shear reinforcement and steel plates as horizontal reinforcement is studied experimentally. The strengthening technique using steel plates and bolts noticeably increases the load carrying capacity and enhances the deformational characteristics of the strengthened slabs. An average increase of the ultimate load carrying capacity of about 50% is achieved.

In addition, the experimental work included investigating the validity of using Carbon Fibre Reinforced Polymer (CFRP) strips and Glass Fibre reinforced polymer (GFRP) laminates as flexural–strengthening of two–way slabs. Although specimens showed a greater brittle behaviour, the load capacity can be increased up to about 36%.

The theoretical work includes an iterative–incremental–mechanical model suitable

for slabs strengthened with steel plates. This model can analyze two–way slabs made of normal or high–strength concrete.

Moreover, the theoretical work includes a finite element analysis of FRP flexural–strengthened two–way slabs. The finite element model is calibrated with the available experimental data and showed a good agreement. A tension stiffening model for concrete portions strengthened using FRP is suggested. This model accounts for the effect of FRP–strengthening material. In addition, a mathematical regression model is suggested to evaluate the ultimate load carrying capacity of FRP–strengthened two–way slabs. The suggested model predicts the ultimate load carrying capacity of FRP–strengthened two–way slabs accurately.

9.2 Steel Strengthened Centrally Loaded Slabs

The effectiveness of two different configurations of steel plates and four different arrangements of steel bolts is investigated. The strengthening steel plates are extended to twice the slab depth around the column and act as drop panels of an equivalent concrete depth. The minimum number of eight 19–mm diameter steel bolts is sufficient to transfer the horizontal forces from the steel plates to concrete and to confine concrete between the steel plates.

The recommended dimensions of the strengthening steel plates and the number of the steel bolts are sufficient to achieve positive results. The steel plate side dimension should equal the column size plus four times the slab depth. A minimum of eight bolts are recommended with four bolts on the outer perimeter of the steel plate and four bolts on the inner perimeter of the steel plate near the column.

The strengthening technique contributed to an increase of the yield and ultimate

load of the slabs. For specimens with 1.0% reinforcement ratio, an average increase of the yield load of 50% compared to that of the reference specimen is achieved. Moreover, the average increase of the ultimate load of 53% is achieved. The increase of the ultimate load of the specimens with separate steel plates is evaluated at 36%. For the specimen with a reinforcement ratio of 0.5%, the strengthening contributes to increase the ultimate load by 45.19%.

It is concluded that the minimum number of steel bolts needed to ensure full interaction between steel plates and slab is eight bolts. In addition, the steel plates with the suggested dimensions and steel bolts with the suggested configuration are well utilized. The strain in the steel plates and bolts indicates a complete composite interaction between concrete and steel plates.

The strengthened specimens show stiffer behaviour than that of the reference specimen. Moreover, the average ductility of the strengthened specimens is about 29% more than the ductility of the reference specimens. The energy absorption of the strengthened specimens is greatly increased due to the strengthening process. The average increase of the energy absorption of the strengthened specimens over that of the reference specimen is about 100%.

9.3 Steel Strengthened Two–Way Slabs under Different Types of Loading

The applications of the steel strengthening technique was extended to cases of two–way slabs loaded with different loading types and reinforced with different reinforcement ratios. Specimens were loaded centrally plus either monotonic or cyclic moments. The specimens were reinforced with either 0.5% or 1.0% reinforcement ratio.

The strengthened specimen with a reinforcement ratio of 0.5% and subjected to central load plus monotonic moment showed more than twice the ultimate capacity of the associated reference specimen. Moreover, the gain of the ultimate capacity for specimen with reinforcement ratio of 1.0% subjected to central load plus moment was greater than that of the associated reference specimens by about of 88%.

It was evident that the strengthened slabs subjected to central load plus monotonic moment showed an increase of the stiffness over that of the reference slabs. The strengthened specimens showed about an average of 72% increase in the initial stiffness over that of the reference specimens. In addition, a considerable increase in the energy absorption values was observed over that of the reference specimens. Specimen with reinforcement ratio of 0.5% showed energy absorption of about 8.4 times that of the reference specimen.

For specimens subjected to central load plus cyclic moment , the unbalanced cyclic moment resistance of the strengthened was about 15% higher than that of the reference specimen, regardless the reinforcement ratio. Furthermore, strengthened slabs can undergo a lateral drift capacity 76% higher than that of the associated reference specimen. Moreover, the strengthened specimens had more drift cycles than that of the reference specimens.

9.4 FRP–Strengthened Slabs

It was concluded that CFRP strips and GFRP laminates were sufficient to achieve positive results for the FRP flexural–strengthening for two–way slabs. Flexural–strengthening specimens using CFRP strips showed an average gain in load capacity of about 36% over that of the reference specimens. In addition, flexural–strengthening

specimens using GFRP laminates showed an average gain in load capacity of about 31% over that of the reference specimens.

The flexural–strengthening specimens showed a stiffer behaviour than that of the reference specimens. However, a decrease in ductility and energy absorption was recorded due to the brittle nature of the FRP materials. The average decrease of the energy absorption of the strengthened specimens over that of the reference specimens was about 37.5% for flexural–strengthening specimens using CFRP strips. The ratio was 24% in case of GFRP laminates. For the suggested flexural–strengthening technique, debonding between FRP materials and concrete was the main cause of failure. None of the strengthening materials experienced rupture.

On the other hand, a small average increase within 10% was achieved for punching–shear–strengthening. In addition, the strengthened specimens failed under sudden undesirable punching–shear failure mode. Therefore, it is not recommended to use CFRP strips or GFRP laminates for punching–shear–strengthening two–way system for specimens with steel reinforcement ratios of 1.0% or more.

9.5 Mechanical Model for Steel Strengthened Slabs

The mechanical model analyzes steel strengthened and unstrengthened two–way slabs fairly accurately. The verification of the new model for 19 specimens showed a good agreement with respect to the ultimate load carrying capacity. The proposed concrete model successfully integrates the equal–biaxial state of stress of normal and high strength concrete in two–way slabs. The contribution of steel plates and bolts as well as the confinement effect on the concrete compressive stress–strain relationship are considered in the model. A complete tensile stress-strain relationship of concrete is

imposed in the model that includes both the pre-cracking and post-cracking properties of concrete in tension.

An overall evaluation of the mechanical model indicated estimation of the ultimate loading capacity. The ability of this model to evaluate the deflection of the two-way slabs, as well as the ultimate load carrying capacity makes it useful on the academic and industrial level.

9.6 FEA of FRP Flexural Strengthened Slabs

A finite element analysis of FRP strengthened two-way slabs is presented. The finite element analysis is calibrated with available experimental results with respect to the ultimate load carrying capacity of the slabs. The calibration study leads to a successful modelling of different aspects of the finite element analysis so that a good agreement between the finite element analysis and the available experimental results is achieved. This calibration finite element analysis is followed by a parametric study to generate several pre-designed cases of FRP strengthened slabs. The data generated of these cases are pre-designed using the Response Surface Methodology (RSM) statistical approach.

The impact of four parameters on the output responses was investigated. The studied parameters were the strengthening width ratio, the original slab reinforcement ratio, the slab thickness ratio, and the slab length ratio. The output responses were the ultimate capacity of the slabs and the actual tensile post-peak behaviour of concrete.

The RSM is used to develop a model for the tensile stress-strain relationship of FRP strengthened concrete. The developed model is referred to as FRP tension

stiffening model. The model is useful in a finite element analysis input or for classical mechanical model of FRP strengthened two–way slabs. In addition, the RSM is used to develop a simple design regression equation to predict the ultimate load carrying capacity of CFRP and GFRP strengthened two–way slabs. The regression equation can be very useful for design engineers to predict the ultimate load carrying capacity of FRP strengthened two–way slabs accurately.

9.7 Author's Contribution

1. The research was focused on different strengthening techniques of two–way slabs with different loading types and reinforcement ratios. The strengthening techniques were evaluated in cases where slabs were subjected to central load only, central load plus monotonic moment, or central load plus cyclic moment. In addition, specimens with reinforcement ratios ranged from 0.35% to 1.0% were investigated. Hence, the presented research will benefit the researchers and design engineers with such a comprehensive data on a subject that is rarely investigated; that it the strengthening of two–way slabs.

2. A new strengthening technique is recommended using an innovative idea of using the integration of steel plate and steel bolts. This technique is technically viable and sound. It is successful and can be applied in the field without installation difficulties.

3. Unlike the several mechanical models that analyze two–way slabs, a mechanical model was suggested in this study able to keep track of the load–deflection relationship of two–way slabs. In addition, the suggested model is the first of its kind that analyzes the strengthened two–way slabs.

4. A finite element analysis is presented to analyze FRP–strengthened two–way slabs. A tension stiffening model for concrete strengthened with FRP is recommended for concrete two–way slabs. The tension stiffening model accounts for the effect of FRP–strengthening material. It is useful when defining the concrete tensile post–peak stress–strain relationship in the case of FRP strengthened slabs. In addition, a regression model is recommended to estimate the ultimate load carrying capacity of FRP strengthened two–way slabs.

9.8 Recommendation for Further Research

1. The author suggests that a numerical analysis based on the RSM be used for similar research work where certain other parameters need to be investigated, for instance, FRP–strengthened beams or columns. It would be beneficial to obtain the equivalent formula for concrete tensile stress–strain relationship in the case strengthened beams and columns as an attempt to develop a unified formula.

2. The author suggests that the finite element analysis be carried out without the assumption of the full bond. A comparison between the potential results and those presented in this research will greatly benefit the research.

Bibliography

ABAQUS (2001). *"ABAQUS Users Manual"*. Hibbitt, Kalrsson and Sorensen Inc., Providence, R. I., version 6.2 edition.

Aboutaha, R. S., Engelhardt, M. D., Jirsa, J. O., and Kreger, M. E. (1999). "Rehabilitation of Shear Critical Concrete Columns by Use of Rectangular Steel Jackets". *ACI Structural Journal*, 96(1):68–78.

ACI–318 (1999). "Building Code Requirements for Structural Concrete". Detriot, USA.

Al-Sulaimani, G. J., Sherif, A., Basunbul, I. A., Blunch, M. H., and Ghalab, B. N. (1994). "Shear Repair for Concrete by Fiberglass Plate Bonding". *ACI Structural Journal*, 92(3):458–464.

Alcocer, S. M. and Jirsa, J. O. (1993). "Strength of Reinforced Concrete Frame Connections Rehabilitated by Jacking". *ACI Structural Journal*, 90(3):249–261.

Arduini, M., D'Amrisi, A., and Tommaso, A. D. (1994). "Shear Failure of Concrete Beams Reinforced with FRP Plates". In *Proceedings, Infrastructure: A New Materials and Methods of Repair, Proceedings of the Third Materials Engineering Conference*, pages 123–130, San Diego, CA, USA.

ASTM (1995). *"Standard Specification for High Strength Bolts for Structural Steel Joints"*, chapter Standard A325M-93–93. American Society for Testing and Material, West Conshohocken, PA. USA.

ASTM-C192-88 (1993). *Annual Book of ASTM Standards*, volume 04.02, chapter Standard Practice for Making and Curing Concrete Test Specimens in the Laboratory, pages 188–189. American Society for Testing and Materials, West Conshohocken, PA. USA.

Ballinger, C. A. (1997). "Strengthening of Engineering Structures with Carbon Fiber Reinforced Plastics-An Overview of History and Current Worldwide Usage". In *Proceedings of the 1997 42nd International SAMPE Symposium and Exhibition*, pages 927–932, Anaheim, CA, USA. AMPE, Covina, CA, USA.

Benmokrane, B., Rahman, H., Mukhopadhyaya, P., and Radhouane, C. (1998). "Use of Fiber Reinforced Polymer Reinforcement Integrated with Fiber Optic Sensors for Concrete Bridge Deck Slab Construction". *Canadian Journal for Civil Engineering*, 27(5):928–940.

Benmokrane, B., Theriault, M., Masmoudi, R., and Rizkalla, S. (1997a). "Effect of Reinforcement Ratio on Concrete Members Reinforced with FRP Bars". In *Proceedings of the 1997 42nd International SAMPE Symposium and Exhibition*, pages 87–98, Anaheim, CA, USA. SAMPE, Covina, CA, USA.

Benmokrane, B., Tighiouart, B., and Theriault, M. (1997b). "Bond Strength of Fiber Reinforced Plastic (FRP) Bars Embedded in Concrete Beams". In *Annual Conference of the Canadian Society for Civil Engineering*, volume 6, pages 111–120, Montréal, Québec, Canana. Canadian Society for Civil Engineering.

Bonacci, J., Thomas, M., Hearn, N., Lee, C., Maalej, M., and Pantazopoulou, M. S. (1998). "Laboratory Simulation of Corrosion in Reinforced Concrete and Repairwith CFRP Wraps". In *Annual Conference of the Canadian Society for Civil Engineering*, pages 653–663, Halifax, Nova Scotia, Canada.

Bonacci, J. F. (1996). "Faiure mode and Deformability of Concrete Beams Strengthened Eternally with Advanced Composites". In El-Badri, M. M., editor, *Advanced Composite Materials in Bridges and Structures*, pages 419–426, Montréal, Québec, Canada. Canadian Society for Civil Engineering, Elsevier Science Publishers B.V.

Bortolotti, L. (1990). "Punching Shear Strength in Concrete Slabs". *ACI Structural Journal*, 87(2):208–219.

Broms, C. E. (1990). "Punching of Flat Plates – A Question of Concrete Properties in Bi–axial Compression and Size Effect". *ACI Structural Journal*, 87(3):292–304.

Broms, C. E. (2000). "Elimination of Flat Plate Punching Failure Mode". *ACI Structural Journal*, 97(1):94–101.

Brotchie, J. F. (1978). "Some Australian Research on Flat Plate Structures". *ACI Journal, Technical Paper*, 77(1):2–11.

BS 8110 (1985). "Structural Use of Concrete, Part1: Code of Practice for Design and Construction". British Standards Institute, London, UK, 126p.

CEB–FIP (1990). "Model Code for Concrete Structures". In *Comité Euro–Internationale de Beton/Federation Internationale de la Procontrainte*. Lausanne, Switzerland.

Cerruti, L. M. and Marti, P. (1987). "Staggered Shear Design of Concrete Beams: Large Scale Tests". *Canadian Journal for Civil Engineering*, 14(2):257–268.

Chaallal, O., Nollet, M., and Perraton, D. (1998). "Strengthening of Reinforced Concrete Beams with Externally Bonded Reinforced Plastic Plates: Design Guidelines for Shear and Flexure". *Canadian Journal for Civil Engineering*, 25:692–704.

Chai, Y., Priestly, M., and Seible, F. (1990). "Retrofit of Bridge Column for Enhanced Seismic Performance". In *Joint US/Japan Workshop on Seismic Retrofit of Bridges*, pages 157–180, Tsukuba, Japan.

Chajes, M. J., Thomson, T. A., Januszka, T. F., and Finch, W. (1994). "Flexural–Strengthening of Concrete Beams Using Externally Bonded Composite Materials". *Construction and Building Materials*, 8(3):191–201.

Chajes, M. J., Thomson, T. A., and Tarantino, B. (1995). "Reinforcement of Concrete Structures Using Externally Bonded Composite Materials". In Taerwe, L., editor, *International RILEM Symposium, Non-Metallic (FRP)Reinforcement for Concrete Structures*, 2–6 Boundary Row, SE1 8HN, London, UK. E & FN Spon.

Chen, W. F. and Ting, E. C. (1980). "Constitutive Models for Concrete Structures". *Journal of the Engineering Mechanics Division, ASCE*, 106(EM1, Proc. Paper 15463):1–21.

Corley, W. g. and Hawkins, N. M. (1968). "Shear Head Reinforcement for Slabs". *ACI Journal, Proceedings*, 65(10):811–823.

CSA–A23.3 (1994). "Design of Concrete Structures for Buildings". Rexdale, Ontario, Canada.

De Lorenzis, L., Nanni, A., and Tegola, A. L. (2000). "Flexural and Shear Strengthening of Reinforced Concrete Structures with Near Surface Mounted FRP Rods". In Humar, J. and Razaqpur, A., editors, *3rd International Conference on Advanced Composite Materials in Bridges and Structures*, pages 521–5 g28, Ottawa, Canada.

Demers, M., Hebert, D., Gauthier, P., and Neale, K. W. (1996). "The Strengthening of Structural Concrete with an Aramid Woven Fiber/Epoxy Resin Composite".

In El-Badri, M. M., editor, *Advanced Composite Materials in Bridges and Structures*, pages 435–442, Montréal, Québec, Canada. Canadian Society for Civil Engineering, Elsevier Science Publishers B.V.

Design-Expert (2001). *"Software for experiment design"*. Stat-Ease, Inc., Minneapolis, MN 55413-2726, USA, version 6 edition.

Di Stasio, J. S. and Van Buren, M. P. (1960). "Transfer of Bending Moment Between Flat Plate Floor and Column". *Journal of the Ameican Concrete Institute*, 57(3):299–314.

Dilger, W. and Ghali, A. (1981). "Shear Reinforcement for Concrete Slabs". *Journal of the Structural Division, Proceedings of the American Society of Civil Engineering, ASCE*, 107(ST12):2403–2420.

Ebead, U. (1998). "Repair of Partialy Loaded Reinforced Concrete Beams Using Ferrocement". Master's thesis, Faculty of Engineering, Helwan University, Cairo, Egypt. 227p.

Ebead, U. and Marzouk, H. (2002a). "Strengthening of Two–Way Slabs Subjected to Moment and Cyclic Loading". *ACI Structural Journal*, 99(4):435–444.

Ebead, U. and Marzouk, H. (2002b). "Strengthening of Two–Way Slabs Using Steel Plates". *ACI Structural Journal*, 99(1):16–21.

El-Salakawy, E. F., Polak, M. A., and Soliman, M. H. (1998). "Slab–Column Connections Subjected to High Moments". *Canadian Journal for Civil Engineering*, 25:526–538.

Elgabry, A. A. and Ghali, A. (1996a). "Moment Transfer by Shear in Slab–Column connections". *ACI Structural Journal*, 93(2):187–196.

Elgabry, A. A. and Ghali, A. (1996b). "Transfer of Moments Between Columns and Slabs: Proposed Code Revisions". *ACI Structural Journal*, 93(1):56–61.

Elstner, R. C. and Hognested, E. (1956). "Shearing Strength of Reinforced Concrete Slabs". *ACI Journal, Proceedings*, 53(1):29–58.

Emam, M., Marzouk, H., and Hilal, M. S. (1997). "Seismic Response of Slab–Column Connections Constructed with High–Strength Concrete". *ACI Structural Journal*, 94(2):197–205.

Erki, M. A. and Hehhernan, P. J. (1995). "Reinforced Concrete Slabs Externally Strengthened with Fibre-Reinforced Plastic Materials". In Taerwe, L., editor, *International RILEM Symposium, Non-Metallic (FRP) Reinforcement for Concrete Structures*, 2–6 Boundary Row, SE1 8HN, London, UK. E & FN Spon.

Etse, G. and Willam, K. (1994). "Fracture Energy Formulation for Inelastic Behavior of Plain Concrete". *Journal of Engineering Mechanics, ASCE*, 120(9):1983–2011.

Farhey, D. N., Adin, M. A., and Yankelesky, D. Z. (1995). "Repaired RC Flat Slab–Column Connection Subassemplages under Lateral Loading". *Journal of Structural Engineering, ASCE*, 121(11):1710–1720.

Floegl, H. and Mang, H. A. (1982). "Tension Stiffening Concept Based on Bond Slip". *Journal of Structural Division, Proceedings of the American Society of civil Engineers*, 108(ST12):2681–2701.

GangaRao, H. V. S. and Vijay, P. V. (1998). "Bending Behavior of Concrete Beams Wrapped with Carbon Fabric". *Journal of Structural Engineering*, 124(1):3–10.

Gardner, N. J. and Shao, X. (1996). "Punching Shear of Continuous Flat Reinforced Concrete Slabs". *ACI Structural Journal*, 93(2):218–228.

Geng, Z., Chanjes, M. J., Chou, T., and Pan, D. (1998). "The Retrofitting of Reinforced Concrete Column–to–Beam Connections". *Composites Science and Technology*, 58:1297–1305.

Ghali, A., Elmasri, M. Z., and Dilger, W. (1976). "Punching of Flat Plates under Static and Dynamic Horizontal Forces". *ACI Journal, Proceedings*, 73(10):566–572.

Ghali, A. and Megally, S. (1999). "Design for Punching Shear Strength with ACI 318-95". *ACI Structural Journal*, 96(4):539–548.

Ghobarah, A., Aziz, T. S., and Biddah, A. (1997). "Rehabilitation of Reinforced Concrete Frame Connections Using Corregated Steel Jacketing". *ACI Structural Journal*, 94(3):283–294.

Gopalaratnam, V. S. and Shah, S. P. (1985). "Softening Response of Plain Concrete in Direct Tension". *ACI Journal, Proceedings*, 82(3):310–323.

Guo, Z. and Zhang, X. (1987). "Investigation of Complete Stress–Deformation Curves for Concrete in Tension". *ACI Materials Journal*, 84(4):278–285.

Hawkins, N. M. and Corley, W. G. (1989). "Moment Transfer From Concrete Slabs to Columns". *ACI Structural Journal*, 86(6):705–716.

Hewitt, B. E. and Batchelor, B. (1975). "Punching Shear Strength of Restrained Slabs". *Journal of Structural Division, Proceedings of the American Society of civil Engineers*, 101(ST9):1837–1853.

Hilleborg, A. (1985). "Numerical Methods to Simulate Softening and Fracture of Concrete". *Fracture Mechanics of Concrete*, pages 141–170.

Hormann, M., Menrah, H., Ramm, E., and Seible, F. (1999). "Finite Element Investigation of Concrete Slabs Post Strengthened by Fiber Reinforced Polymers".

In Avent, R. and Alawady, M., editors, *Structural Engineering in the 21st Century: Proceedings of the 1999 Structures Congress.*, pages 174–178, New Orleans, Louisiana, US. Structural Engineering Institute of ASCE., Reston, VA : Amerivcan Society of Civil Engineers.

Hurlbut, B. (1983). "Experimental and Computation Investigtion of Strain–Softening in Concrete". M.sc., University of Colorado, Boulder, USA. 128p.

Hussein, A. and Marzouk, H. (1998). "Behavior of High Strength Concrete under Biaxial Stresses". *ACI Structural Journal*, 97(1):27–36.

Islam, S. and Park, R. (1976). "Tests on Slab–Column Connections with Shear and Un-Balanced Flexure". *Proceedings, ASCE*, 102(ST3):549–568.

Jiang, D. and Shen, J. (1986). "Strength of Concrete Slabs in Punching Shear". *Journal of Structural Engineering, ASCE*, 112(12):2578–2591.

Jin, L., Saadatmanesh, H., and Ehsani, M. R. (1994). "Seismic Retrofit of Existing Reinforced Concrete Columns by Glass–Fiber Composites". In *Proceedings, Infrastructure: A New Materials and Methods of Repair, Proceedings of the Third Materials Engineering Conference*, pages 758–763, San Diego, CA, USA.

Karbhari, V. M., Seible, F., Seim, W., and Vasquez, A. (1994). "Post–Strengthening of Concrete Slabs". In *Proceedings, Infrastructure: A New Materials and Methods of Repair, Proceedings of the Third Materials Engineering Conference*, pages 1163–1172, San Diego, CA, USA.

Kent, D. C. and Park, R. (1971). "Flexural Members with Confined Concrete". *Journal of the Structural Division, Proceedings of the American Society of Civil Engineering*, 97(ST7):1969–1990.

Kikukawa, K., Mutoh, K., Ohya, H., Ohyama, Y., and Tanaka, H. (1998). "Flexural Reinforcement of Concrete Floor Slabs by Carbon Fiber Textiles". *Composite Interfaces*, 5(5):469–478.

Kinnunen, S. and Nylander, H. (1960). "Punching of Concrete Slabs without Shear Reinforcement". Transaction, Royal Institute of Technology, Stokholm.

Kupfer, H., Hilsdorf, H. K., and Rusch, H. (1969). "Behavior of Concrete under Bi–Axial Stresses". *ACI Journal, Proceedings*, 114(8):1804–1826.

Lorenzis, D. and Nanni, A. (2002). "Bond Between Near Surface Mounted FRP Rods and Concrete in Structural Strengthening". *ACI Structural Journal*, 99(2):123–133.

Lorenzis, L. and Nanni, A. (2001). "Characterization of FRP Rods as Near-Surface Mounted ReinforcemenT". *Journal of Composites for Construction, ASCE*, 5(2):114–124.

Maalej, M. and Bonacci, J. F. (1998). "Repair and Strengthening of RC Beams Using FRP Reinforcement". In *Proceedings, Annual Conference of the Canadian Society for Civil Engineering*, pages 643–652, Halifax, Nova Scotia, Canada. Engineers' Soc. of Western Pennsylvania.

Malek, A. M., Saadatmanesh, H., and Ehsani, M. R. (1998). "Pridiction of Failure Load of R/C Beams Strengthened with FRP Plate Due to Stress Concentration at the Plate End". *ACI Structural Journal*, 95(1):142–152.

Marti, P. (1986). "Staggered Shear Design of Simply Supported Concrete Beams". *ACI Journal, Proceedings*, 83(1):36–42.

Marti, P. (1990). "Design of Concrete Slabs for Transverse Shear". *ACI Structural Journal*, 87(2):180–190.

Marzouk, H. and Chen, Z. (1993). "Finite Element Analysis of High Strength Concrete Slabs". *ACI Structural Journal*, 90(5):505–513.

Marzouk, H. and Chen, Z. M. (1995). "Fracture Energy and Tension Properties of High Strength Concrete". *Journal of Materials in Civil Engineering*, 7(2):108–116.

Marzouk, H., Emam, H., and Hilal, M. S. (1996). "Effect of High Strength Concrete Columns on the Behavior of Slab–Column Connections". *ACI Structural Journal*, 93(5):545–563.

Marzouk, H., Emam, H., and Hilal, M. S. (1998a). "Effect of High Strength Concrete Slabs on the Behavior of Slab–Column Connections". *ACI Structural Journal*, 95(3):227–237.

Marzouk, H., Emam, M., and Hillal, M. (1998b). "Sensitivity of Shear Strength to Fracture Energy of High–Strength Concrete Slabs". *Canadian Journal for Civil Engineering*, 25:40–50.

Marzouk, H. and Hussein, A. (1991a). "Experimental Investigation on the Behavior of High Strength Concrete Slabs". *ACI Structural Journal*, 88(6):701–713.

Marzouk, H. and Hussein, A. (1991b). "Punching Shear Analysis of Reinforced High–Strength Concrete Slabs". *Canadian Journal for Civil Engineering*, 18:954–963.

Marzouk, H. and Jiang, D. (1996). "Finite Element Evaluation of Shear Enhancement for High Strength Concrete Plates". *ACI Structural Journal*, 93(6):667–673.

Marzouk, H. and Jiang, D. (1997). "Experimental Investigation on Shear Enhancement Types for High Strength Concrete Plates". *ACI Structural Journal*, 94(1):701–713.

Marzouk, H., Osman, M., and Helmy, S. (2000a). "Behavior of High–Strength Lightweight Aggregate Concrete Slabs under Column Load and Un-Balanced Moment". *ACI Structural Journal*, 97(6):860–866.

Marzouk, H., Osman, M., and Hussein, A. (2000b). "Punching Shear of Slabs: Crack Size and Size Effects". *Magazine of Concrete Research*, 54(1):13–21.

Marzouk, H., Osman, M., and Hussein, A. (2001). "Cyclic Loading of High–Strength Lightweight Concrete Slabs". *ACI Structural Journal*, 98(2):207–214.

Masmoudi, R., Theriault, M., and Benmokrane, B. (1998). "Flexural Behavior of Concrete Beams Reinforced with Deformed Fiber Reinforced Plastic Reinforcing Rods". *ACI Structural Journal*, 95(6):665–675.

Matthys, S. and Taerwe, L. (2000a). "Concrete Slabs Reinforced with FRP Grids. I: One–Way Bending". *Journal of Composites for Construction*, 4(3):145–153.

Matthys, S. and Taerwe, L. (2000b). "Concrete Slabs Reinforced with FRP Grids II: Punching Resistance". *Journal of Composites for Construction*, 4(3):154–161.

Megally, S. and Ghali, A. (2000). "Punching of Concrete Slabs Due to Column Moment Transfer". *Jornal of Structural Engineering*, 126(2):180–189.

Meier, U., Deuring, M., Meier, H., and Schwegler, G. (1993). "CFRP Bonded Sheets". In Nanni, A., editor, *Fiber–Reinforced–Plastic(FRP) Reinforcement for Concrete Structures: Properties and Applications*, pages 423–434, CH–8600 Duebendof, Switzerland. Swiss Federal Laboratories for Materials Testing and Research(EMPA), Elsevier Science Publishers B. v.

Mendis, P., Pendyala, R., and Setunge, S. (2000). "Stress–Strain Model to Predict the Full–Rage Moment Curvature behavior of High–Strain Rates". *Magazine of Concrete Research*, 52(4):227–234.

Michaluk, C., Rizkalla, S., Tadros, G., and Benmokrane, B. (1998). "Flexural Behavior of One–Way Concrete Slabs Reinforced by Fiber Reinforced Plastic Reinforcements". *ACI Structural Journal*, 95(3):353–365.

Moe, J. (1961). "Shearing Strength of Reinforced Concrete Slabs and Footing under Concentrated Loads". Development Bulletin D47, Portland Association, Skokie, ILL, USA.

Mokhtar, A. S., Ghali, A., and Dilger, W. (1986). "Stud Shear Reinforcement for Flat Concrete Plates". *ACI Structural Journal*, 82(5):676–683.

Mortin, J. D. and Ghali, A. (1991). "Connection of Flat Plates to Edge Columns". *ACI Structural Journal*, 88(2):191–198.

Myers, R. H. and Montgomery, D. C. (1995). *Response Surface Methdoogy: Process and Product*. John Wiley and Sons.

Nanni, A. (1993). "FRP Reinforcement for Prestressed and Non–Prestressed Concrete Structures". In Nanni, A., editor, *Fiber Reinforced Plastic(FRP) Reinforcement for Concrete Structures: Properties and Applications*, pages 3–12, Amsterdam, The Netherlands. Elsevier Science Publishers B.V.

Osman, M., Marzouk, H., and Helmy, S. (1998). "Behavior of High-Strength Lightweight Concrete Interior Slab Connections under Static and Cyclic Loading". Technical Report 98002, Faculty of Engineering and Applied Science, Memorial University of Newfoundland, St. John's, Newfoundland, Canada.

Pan, A. and Moehle, J. P. (1989). "Lateral Displacement Ductility of Reinforced Concrete Flat Plates". *ACI Structural Journal*, 86(3):250–258.

Paramasivam, P., Ong, K. C. G., and L., L. S. (1995). "Performance of Repaired Reinforced Concrete Slabs under Static and Cyclic Loadings". *Cement and Concrete Composites*, 17:37–45.

Priestley, M. J. N., Seible, F., Xiao, Y., and Verma, R. (1994). "Steel Jacket Retrofitting of Reinforced Concrete Bridge Columns for Enhanced Shear Strength–Part 1: Theoretical Considerations and Test Design". *ACI Structural Journal*, 91(4):394–405.

Rankin, G. I. B. and Long, A. E. (1987). "Predicting the Punching Strength of Conventional Slab – Column Specimen". In *Proceedings, Part1: Design and Construction*, volume 82, pages 327–346. The Institution of Civil Engineers.

Regan, P. E. (1981). "Behavoir of Reinforced Concrete Flat Slabs". *Construction Industry Research and Information Association, London, UK*, 87(3):292–304.

Ritchie, P. A., Thomas, D. A., Lu, L., and Connelly, G. M. (1991). "External Reinforcement of Concrete Beams Using Fiber Reinforced Plastics". *ACI Structural Journal*, 88(6):490–500.

Robertson, I. N. and Durrani, A. J. (1992). "Gravity Load Effect on Seismic Behavior of Interior Slab–Column Connections". *ACI Structural Journal*, 89(1):37–45.

Saatcioglu, M. and Baingo, D. (1999). "Circular High-Strength Concrete Columns under Simulated Seismic Loading". *Journal of Structural Engineering, ASCE*, 125(3):272–280.

Scott, B. D., Park, R., and Priestley, N. (1982). "Stress–Strain Behavior of Concrete Confined by Overlapping Hoops at Low and High Strain Rates". *ACI Journal, Proceedings*, 79(1):13–27.

Seible, F., Ghali, A., and Dilger, W. H. (1980). "Preassempled Shear Reinforcement Units for Flat Plates". *ACI Structural Journal*, 77(1):28–35.

Seim, W., Hormann, M., and Karbhari, V. (2001). "External FRP Poststrengthening of Scaled Concrete Slabs". *Journal of Composites for Construction*, 4(3):145–153.

Sharif, A., Al-Sulaimani, G. J., Basunbul, I. A., Baluch, M. H., and Ghalab, B. N. (1994). "Strengthening of Initially Loaded Reinforced Concrete Beams Using FRP Plates". *ACI Structural Journal*, 91(2):160–168.

Soudki, K. A. and Green, M. F. (1996). "Performance of CFRP Retrofitted Concrete Columns at Low Temperature". In El-Badri, M. M., editor, *Advanced Composite Materials in Bridges and Structures*, pages 427–434, Montréal, Québec, Canada. Canadian Society for Civil Engineering, Elsevier Science Publishers B.V.

Sozen, M, A. and Seiss, C. P. (1963). "Investigation of Multiple Panel Reinforced Concrete Floor Slabs: Design Methods- Their Evelauation and Comparison". *ACI Journal, Proceedings*, 60(8):999–1027.

Theriault, M. and Benmokrane, B. (1997). "Theoretical and Experimental Investigation on Crack Width, Deflection and Deformability of Concrete Beams Reinforced with FRP Rebars". In *Annual Conference of the Canadian Society for Civil Engineering*, volume 6, pages 151–160, Montréal, Québec, Canana. Canadian Society for Civil Engineering.

Theriault, M. and Benmokrane, B. (2001). "Effects of FRP Reinforcement Ratio and Concrete Strength on Flexural Behavior of Concrete Beams". *Journal of Composites for Construction*, 2(1):7–16.

Toutanji, T. C. (1999). "Stress–Strain Characteristics of Concrete Columns Externally Confined with Advanced Fiber Composite Sheets". *ACI Structural Journal*, 96(3):393–404.

Triantafillou, T. C. (1998). "Shear–Strengthening of Reinforced Concrete Beams Using Epoxy–Bonded FRP Composites". *ACI Structural Journal*, 95(2):107–115.

Yamada, T., Nanni, A., and Endo, K. (1992). "Punching Shear Resistance of Flat Slabs: Influence of Reinforcement Type and Ratio". *ACI Structural Journal*, 89(5):555–562.

Zdenek, D. and Shen, J. (1985). "Strength of Concrete Slabs in Punching Shear". *Journal of Structural Engineering, ASCE*, 112(12):2578–2591.